Pathology & Oncology Research

Liquid Biopsy - A Great Hope or Just Hype?

Issue Editor

Ales Ryska
Charles University, Czechia

frontiers | Publishing Partnerships

Pathology & Oncology Research

Liquid Biopsy - A Great Hope or Just Hype?

ISSN 1532-2807
ISBN 978-2-83252-182-3
DOI 10.3389/978-2-83252-182-3

This Special Issue is lead by Prof. Ales Ryska, President Elect of the European Society of Pathology. Prof. Ryska's research interests focus on the diagnostics of lesions of the breast, thyroid and salivary glands - cytology, histology and special methods, such as immunohistochemistry and molecular biology.

The current development of our understanding of tumor biology, role of individual driver mutations and activation of signaling pathways is reflected in rapid implementation of targeted therapy of tumors. To identify patients, who are the best candidates of such treatment, requires use of up-to-date molecular testing of tumor tissue. However, use of molecular techniques is sometimes precluded by limited tissue specimens (insufficient neoplastic cell content, poor quality of nucleic acids, etc.). For the last 10 years, so-called liquid biopsy - testing of cell free tumor DNA or circulating tumor cells isolated from the patients' blood - has been demonstrated as a feasible alternative solution. This approach shows many additional promising applications, such as control of minimal residual disease, early detection of tumor recurrence or detection of development of resistant clones. This resulted in huge clinical expectations which, however, cannot be always fulfilled.

So, what is the current position of liquid biopsy in routine clinical practice? Is it a real game changer or rather a highly sophisticated laboratory test with limited clinical use?

Pathology & Oncology Research

Table of contents

04 Editorial: Liquid biopsy—A great hope or just hype?
Aleš Ryška

07 Detection and Quantification of ctDNA for Longitudinal Monitoring of Treatment in Non-Small Cell Lung Cancer Patients Using a Universal Mutant Detection Assay by Denaturing Capillary Electrophoresis
Lucie Benesova, Renata Ptackova, Tereza Halkova, Anastasiya Semyakina, Martin Svaton, Ondrej Fiala, Milos Pesek and Marek Minarik

17 EGFR T790M Mutation Detection in Patients With Non-Small Cell Lung Cancer After First Line EGFR TKI Therapy: Summary of Results in a Three-Year Period and a Comparison of Commercially Available Detection Kits
Eszter Bencze, Krisztina Bogos, Andrea Kohánka, László Báthory-Fülöp, Veronika Sárosi, Erzsébet Csernák, Nóra Bittner, Zsombor Melegh and Erika Tóth

23 Methodological Challenges of Digital PCR Detection of the Histone *H3* K27M Somatic Variant in Cerebrospinal Fluid
Margarita Zaytseva, Natalia Usman, Ekaterina Salnikova, Agunda Sanakoeva, Andge Valiakhmetova, Almira Chervova, Ludmila Papusha, Galina Novichkova and Alexander Druy

36 Blood, Toil, and Taxoteres: Biological Determinants of Treatment-Induced ctDNA Dynamics for Interpreting Tumor Response
Christopher T. Boniface and Paul T. Spellman

48 Single-Cell Transcriptome Profiling Signatures and Alterations of Microglia Associated With Glioblastoma Associate Microglia Contribution to Tumor Formation
Hailong Xia, Lei Deng, Shu Meng, Xipeng Liu and Chao Zheng

58 Identification of Diagnostic Exosomal LncRNA-miRNA-mRNA Biomarkers in Colorectal Cancer Based on the ceRNA Network
Yajing Zhao, Xingguo Song, Xianrang Song and Li Xie

69 Plasma Exosomal hsa_circ_0015286 as a Potential Diagnostic and Prognostic Biomarker for Gastric Cancer
Peiming Zheng, Huijie Gao, Xuanhu Xie and Peipei Lu

77 Co-Detection of VEGF-A and Its Regulator, microRNA-181a, May Indicate Central Nervous System Involvement in Pediatric Leukemia
Bálint Egyed, Anna Horváth, Ágnes F. Semsei, Csaba Szalai, Judit Müller, Dániel J. Erdélyi and Gábor T. Kovács

Pathology & Oncology Research | frontiers

TYPE Special Issue Editorial
PUBLISHED 28 March 2023
DOI 10.3389/pore.2023.1611170

OPEN ACCESS

EDITED BY
József Tímár,
Semmelweis University, Hungary

*CORRESPONDENCE
Aleš Ryška,
ryskaale@gmail.com

RECEIVED 09 March 2023
ACCEPTED 20 March 2023
PUBLISHED 28 March 2023

CITATION
Ryška A (2023), Editorial: Liquid biopsy—A great hope or just hype? *Pathol. Oncol. Res.* 29:1611170. doi: 10.3389/pore.2023.1611170

Editorial: Liquid biopsy—A great hope or just hype?

Aleš Ryška*

The Fingerland Department of Pathology, Charles University Medical Faculty, Hradec Králové, Czechia

KEYWORDS

liquid biopsy, ctDNA, circulating tumor cells, exosomes, monitoring

Editorial on the Special Issue
Liquid biopsy—A great hope or just hype?

Introduction

Liquid biopsy is a term which gained in last decade a lot of attention from both clinicians (namely oncologists) and pathologists/scientists. It became one of the fancy buzzwords, creating a lot of expectations, sometimes without sufficient knowledge about its full potential, but more importantly (and certainly more frequently) about its limitations. Already the term liquid biopsy is quite misleading, as it covers several entirely different ways of detection of various genomic alterations in humans. Two most important—and mostly clinically used—modes are detection of circulating tumors cells (CTCs) and circulating cell free tumoral DNA (ctDNA). While the detection of genomic alterations in CTCs sounds more based on the tumor biology (we are detecting the changes in DNA in the cells, which are certainly neoplastic, are potential source of metastatic dissemination of the tumor and have survived at least the initial interaction with antitumor immunity), it turned out that this approach has so far only limited clinical application. The main reason are the technical/methodological challenges during the isolation of the CTCs as well as their limited number used for genomic testing. Considering the fact, that vast majority of them do not belong to the subgroup of tumor progenitor cells, which are the crucial players in tumor growth, we can easily detect the noise (mutations in cells which can represent merely a bystander information) dominating over the biologically/clinically important signal (genomic profile in tumor progenitor cells).

Detection of ctDNA, on the other hand, has been demonstrated to be sufficiently robust to be incorporated into everyday routine practice. The total amount of ctDNA statistically correlates with total tumor burden, represents genotype of neoplastic cells from multiple metastatic foci (and provides therefore more complex information about the tumor genotype), levels of ctDNA generally correlate well with response of tumor population to treatment and provide us with prognostic information. However,

as devil is hiding in the detail, the two very important words in the lines above are "statistically" and "generally." Multiple studies have demonstrated that ctDNA testing has several critical limitations, which are partially solvable and partially intrinsic. The solvable ones are the limited sensitivity of currently used methods and their costs. We see how much the technical and scientific progress improves the molecular genetic methods while the financial cost is dramatically decreasing every year. Thus, it is just question of time (at least this is what the author of this editorial believes) when the methods will reach such laboratory sensitivity and sufficiently low price which will be not anymore limiting their use in everyday practice. The other issue, however, are the inherent limitations, which cannot be solved by mere technological development. It is the well-known and repeatedly demonstrated fact that shedding of the ctDNA is not the same by all cancer types, differs (sometimes by order of several magnitudes) even in one diagnosis from patient to patient. Thus, the sensitivity of liquid biopsy is in most situations significantly lower than testing of the tumor tissue, irrespective of the fact, how sensitive method is used. On the other hand, with increasing the sensitivity of the method, we must face the other side of the coin (for long not the expected one)—the false positivity—which is the result of identification of mutations in cfDNA originating from elements of clonal hematopoesis.

The above statements should not demonstrate the skepticism of the author of this text, but rather the need for critical thinking and awareness of both pros but also cons of liquid biopsy.

Nevertheless, already today, liquid biopsy has found a way to routine clinical use in several settings and its potential is further massively investigated. To demonstrate how much has this term set in everyday medical practice, I tried to test (for the first time in my life) the publicly available system of artificial intelligence—ChatGPT (https://openai.com/blog/chatgpt/).

My question was very simple: What are the main pros and cons of liquid biopsy in testing genomic alterations of different types of cancer?

Here is the (rather complex and comprehensive) answer:

Liquid biopsy is a technique that involves the analysis of circulating tumor cells (CTCs), cell-free DNA (cfDNA), or exosomes, which are shed by tumors into the bloodstream. Liquid biopsy is a non-invasive method that allows for the detection of genomic alterations in cancer cells, which can provide important diagnostic and prognostic information, as well as help guide treatment decisions. Here are some of the main pros and cons of liquid biopsy in testing genomic alterations of different types of cancer.

Pros

Non-invasive: Liquid biopsy is a non-invasive method that can be performed on a simple blood sample, which eliminates the need for invasive tissue biopsies.

Detection of genetic heterogeneity: Liquid biopsy can detect multiple genomic alterations in different regions of a tumor, which can help identify genetic heterogeneity within the tumor and guide treatment decisions.

Early detection: Liquid biopsy can detect cancer at an earlier stage than traditional imaging methods, which can lead to earlier treatment and better outcomes.

Monitoring disease progression: Liquid biopsy can be used to monitor disease progression and treatment response over time, which can help guide treatment decisions and identify resistance mechanisms.

Cons

Sensitivity and specificity: Liquid biopsy may not always detect all genomic alterations present in the tumor due to limitations in sensitivity and specificity, which can result in false negatives or false positives.

Variability: The amount and quality of circulating tumor DNA can vary depending on the type and stage of cancer, as well as other factors, which can affect the accuracy of liquid biopsy results.

Cost: Liquid biopsy can be expensive, and may not be covered by all insurance plans.

Limited availability: Liquid biopsy testing may not be widely available, which can limit access to this technology for some patients.

In summary, liquid biopsy is a promising technique for the detection of genomic alterations in cancer, but it has limitations that need to be considered when interpreting the results. Further research is needed to optimize the sensitivity and specificity of liquid biopsy, as well as to establish its clinical utility in different types of cancer.

Not bad, right?

In this special issue of Pathology, Oncology and Research you find 8 articles focused on various aspects of liquid biopsy—from paper reporting routine implementation of LB in monitoring of the disease, as described by Benesova et al., through comparison of different commercially available detection kits in paper from Bencze et al. up to the experience with methodological challenges in detection of histone H3 K27M in cerebrospinal fluid as reported by Zaytseva et al. The article from Boniface and Spellman

summarizes various factors (namely effect of treatment) responsible for variability of dynamics in ctDNA blood levels. Other papers are more oriented on future development—such as paper by Xia et al. describing single-cell transcriptome profiling signatures and alterations of microglia associated with glioblastoma multiforme or two papers focused on exploitation of exosomes as carriers of different subtypes of RNA (by Zhao et al. and by Zheng et al.). Finally, you will find very interesting data on potential use of detection of microRNA-181a combined with measurement of VEGF-A as an indicator as CNS involvement in children with leukemia. Enjoy reading this special issue!

Author contributions

The author confirms being the sole contributor of this work and has approved it for publication.

Conflict of interest

The author declares that the research was conducted in the absence of any commercial or financial relationships that could be construed as a potential conflict of interest.

Pathology & Oncology Research

frontiers

ORIGINAL RESEARCH
published: 28 June 2022
doi: 10.3389/pore.2022.1610308

Detection and Quantification of ctDNA for Longitudinal Monitoring of Treatment in Non-Small Cell Lung Cancer Patients Using a Universal Mutant Detection Assay by Denaturing Capillary Electrophoresis

Lucie Benesova[1], *Renata Ptackova*[1], *Tereza Halkova*[1], *Anastasiya Semyakina*[1], *Martin Svaton*[2], *Ondrej Fiala*[3,4], *Milos Pesek*[2] *and Marek Minarik*[5,6]*

[1]*Center for Applied Genomics of Solid Tumors, Genomac Research Institute, Prague, Czechia,* [2]*Department of Pneumology and Phtiseology, Faculty of Medicine and University Hospital in Pilsen, Charles University, Pilsen, Czechia,* [3]*Laboratory of Cancer Treatment and Tissue Regeneration, Biomedical Center, Faculty of Medicine in Pilsen, Charles University, Pilsen, Czechia,* [4]*Department of Oncology and Radiotherapeutics, Faculty of Medicine and University Hospital in Pilsen, Charles University, Pilsen, Czechia,* [5]*Elphogene, Prague, Czechia,* [6]*Department of Analytical Chemistry, Faculty of Science, Charles University, Prague, Czechia*

Background: Observation of anticancer therapy effect by monitoring of minimal residual disease (MRD) is becoming an important tool in management of non-small cell lung cancer (NSCLC). The approach is based on periodic detection and quantification of tumor-specific somatic DNA mutation in circulating tumor DNA (ctDNA) extracted from patient plasma. For such repetitive testing, complex liquid-biopsy techniques relying on ultra-deep NGS sequencing are impractical. There are other, cost-effective, methods for ctDNA analysis, typically based on quantitative PCR or digital PCR, which are applicable for detecting specific individual mutations in hotspots. While such methods are routinely used in NSCLC therapy prediction, however, extension to cover broader spectrum of mutations (e.g., in tumor suppressor genes) is required for universal longitudinal MRD monitoring.

Methods: For a set of tissue samples from 81 NSCLC patients we have applied a denaturing capillary electrophoresis (DCE) for initial detection of somatic mutations within 8 predesigned PCR amplicons covering oncogenes and tumor suppressor genes. Mutation-negative samples were then subjected to a large panel NGS sequencing. For each patient mutation found in tissue was then traced over time in ctDNA by DCE.

Results: In total we have detected a somatic mutation in tissue of 63 patients. For those we have then prospectively analyzed ctDNA from collected plasma samples over a period of up to 2 years. The dynamics of ctDNA during the initial chemotherapy therapy cycles as well as in the long-term follow-up matched the clinically observed response.

Conclusion: Detection and quantification of tumor-specific mutations in ctDNA represents a viable complement to MRD monitoring during therapy of NSCLC patients. The presented approach relying on initial tissue mutation detection by DCE combined with

OPEN ACCESS

Edited by:
József Tímár,
Semmelweis University, Hungary

***Correspondence:**
Marek Minarik
mminarik@elphogene.cz

Received: *07 January 2022*
Accepted: *17 May 2022*
Published: *28 June 2022*

Citation:
Benesova L, Ptackova R, Halkova T, Semyakina A, Svaton M, Fiala O, Pesek M and Minarik M (2022) Detection and Quantification of ctDNA for Longitudinal Monitoring of Treatment in Non-Small Cell Lung Cancer Patients Using a Universal Mutant Detection Assay by Denaturing Capillary Electrophoresis. Pathol. Oncol. Res. 28:1610308. doi: 10.3389/pore.2022.1610308

NGS and a subsequent ctDNA mutation testing by DCE only represents a cost-effective approach for its routine implementation.

Keywords: liquid biopsy, NSCLC, ctDNA, KRAS mutations, minimal residual disease, capillary electrophoresis, TP53 mutations

INTRODUCTION

Lung cancer is the most commonly diagnosed cancer globally, with the highest mortality rate (18.4% of total cancer deaths) [1]. The treatment of lung cancer depends on the histological type, the stage of the disease and the overall physical condition of the patient. Over the past 2 decades the conventional treatment options including surgery, chemotherapy and/or radiotherapy have been supplemented by therapy targeted at tumor-specific aberrations [2]. Furthermore, a notable impact on patient survival has been achieved by introduction of immunotherapy using CTLA-4 or PDL inhibitors [3]. The initial diagnosis relying on histopathology/cytology processing of tumor tissue has been extensively complemented by testing for a presence of molecular markers. The tumor-specific DNA markers including point mutations in *EGFR* or *BRAF* genes, rearrangements involving *ALK* or *ROS1* genes and fusions of *NTRK1/2/3* genes along with tumor mutation burden (TMB) and PDL-1 RNA expression serve as guides in proper therapy selection. In the event of marker absence patients were so far treated by non-targeted chemotherapy, often using anti-angiogenic agents [2].

In an established routine practice, appropriate selection of targeted treatment by molecular tumor profiling results in a significant improvement of fundamental clinical parameters including extended time to disease progression and overall survival time [4]. The therapy efficacy is further enhanced when the initial proper selection is complemented by close monitoring allowing for timely decisions of interventions in case of emergent therapy resistance. The observation of therapy is primarily relying on imaging techniques including CT or hybrid PET/CT directed at evaluation of tumor morphology (dimensions and volume) and, more recently, also functional parameters including the metabolic activity, tumor vascularization etc. [5].

Use of circulating tumor DNA (ctDNA) has recently demonstrated viability for monitoring of the response to treatment in various solid tumors, including non-small cell lung cancer (NSCLC) [6]. ctDNA is detectable in a form of short DNA fragments released into the bloodstream from the decomposing tumor mass. Due to its exclusive origin in cancerous tissue, ctDNA inherently reflects genetic profile of any present tumor bearing cancer specific DNA mutations [7, 8]. This is used in the methodology of ctDNA monitoring, which is typically directed at detection and quantification of tumor-specific DNA mutations in patient plasma. In a simplified view the ctDNA level (e.g., the number of mutated DNA alleles) reflects the actual volume of tumor mass present in the patient's body, often referred to as a minimal residual disease (MRD) [9]. MRD monitoring by repeated plasma evaluation in short intervals enables early response by changing or tailoring the treatment for a specific patient. ctDNA monitoring of MRD has been recently applied for anti-EGFR therapy. The typical resulting ctDNA curve showed a decay in ctDNA bearing activating *EGFR* mutation in a sign of initial positive response of the EGFR-sensitive clones followed by an emergence of ctDNA harboring *EGFR* T790M resistant mutation as the EGFR-resistant clone emerges [10–12]. An alternative result has been presented in which a non-targetable mutant (such as *BRAF; KRAS; TP53; STK11*) was tracked resulting in swing-like shape curves tracking the phases of subsequent remissions and progressions of the disease upon administration of multiple lines of systemic therapy [13–15].

The concentration of ctDNA in the circulation is low, typically in the orders of a few ng per mL of plasma [16]. Moreover, its detection is obstructed by an excess of highly similar short DNA fragments coming from non-cancerous body cells, mainly by necrosis due to inflammation or a spontaneous decay by apoptosis [17]. The fraction of ctDNA in a total non-mutated cell-free DNA (cfDNA) could span down to less than 0.05% of mutated (minor) allele fraction (MAF) [18]. Such low ctDNA abundance presents a challenge for detection methodology. Several approaches are currently in use for ctDNA detection. The most universal is indiscriminate comprehensive sequencing of all ctDNA fragments extracted from plasma. This approach, often termed a "liquid biopsy" is exclusively based on improved next-generation sequencing (NGS) technologies ensuring reduction of errors inherent to standard NGS [19]. The upmost advantage of this approach is in its use as surrogate for classic tissue biopsy. In clinical management of lung cancer this is particularly important in situations where specimens acquired by bronchoscopy are not available or do not yield reliable results. While clinically useful, the NGS-based liquid biopsy is very costly with current prices in the order of thousands of EUR per test rendering its use for longitudinal monitoring by repeated testing unfeasible.

Along with the NGS-based liquid biopsy another approach has been presented in which only a DNA mutation found in tumor tissue is subsequently searched for in plasma ctDNA [19]. This "tumor-informed" liquid biopsy is naturally not applicable for initial diagnosis, but with its relatively low cost it is well-suited for repeated testing of MRD. Currently used methods are mainly based on standard mutation detection by quantitative PCR (qPCR) or digital PCR (dPCR). In order to use these for ctDNA detection, the mutant sensitivity is typically enhanced by some means of mutant enrichment, mainly through artificial suppression of amplification of non-mutated (wild type) alleles [20, 21]. Both qPCR and dPCR are performed in an allele-specific format, which means that each such assay is designed to detect only a particular mutation at a particular sequence site. While

TABLE 1 | Clinicopathological characteristics of NSCLC patients with detected mutation.

Characteristics		Value
Number of patients		63
Age	mean (years)	64.6
	range (years)	40–80
Gender	male	42
	female	21
TNM stage	III	8
	IV	55
Number of metastatic organs	0–1	34
	2–4	29
ECOG Performance status	0	1
	1	53
	2	9
Smoking history	non-smokers	9
	former smokers	16
	smokers	38
First-line chemotherapy	carboplatin + paclitaxel (+ bevacizumab)	32
	cisplatin + pemetrexed	24
	carboplatin + paclitaxel (+ bevacizumab)	6
	cisplatin + vinorelbine	1
RECIST[a]	CR	1
	PR	15
	SD	30
	PD	14
	unknown	3

[a]*The response was evaluated after the 2nd cycle of chemotherapy. CHT, chemotherapy; CR, complete response; PR, partial response; SD, stable disease; PD, progressive disease.*

that is satisfactory for oncogenes, where somatic mutations are mainly localized at specific hotspots, the technique is not applicable for mutant detection in tumor-suppressor genes, whose mutations are typically dispersed across multiple exons [22, 23].

Denaturing capillary electrophoresis (DCE) has been used for routine mutation detection in a variety of solid cancers including colon and rectum [24–26], lung [27, 28], pancreas [29, 30] or brain [31]. The technique is based on heteroduplex formation with subsequent electrophoretic separation to visualize presence of mutant alleles in an abundance of nonmutated wildtype alleles [32]. The method is cost-effective and requires only a very low amount (tens of pg) of input DNA material [25, 31]. In the present work we have applied DCE for prospective monitoring of minimal residual disease in patients with advanced stage of NSCLC. We present a longitudinal observation with frequent sampling during the palliative treatment. We demonstrate clinical utility of the assay for assessment of therapy response as well as early detection of disease progression for use in management of NSCLC patients.

MATERIALS AND METHODS

Patient Inclusion and Clinical Evaluation

A total of 81 patients with histologically confirmed advanced NSCLC (stage III or IV) of adenocarcinoma subtype, treated with standard platinum-based chemotherapy, were eligible for inclusion in this exploratory prospective single center cohort study. Baseline characteristics for 63 patients eligible for ctDNA monitoring (mutation found in tumor tissue) were collected including gender, age, smoking history, ECOG Performance Status, TNM stage, localization of metastases, and chemotherapy regimen (see **Table 1**). Follow-up data included response to treatment, progression-free survival (PFS) and overall survival (OS) were also collected. Response to treatment was evaluated according to the Response Evaluation Criteria in Solid Tumors (RECIST) 1.1. as complete response (CR), partial response (PR), stable disease (SD) and progressive disease (PD) based on radiological examination [33]. PET/CT or CT scans were performed at the time of diagnosis, after approximately 6 weeks of treatment (after second therapy cycle) and further during the follow-up. PFS and OS were determined as the time elapsed between the initiation of treatment and first documented PD or date of death from any cause, respectively.

The study complied with the ethical standards of the World Medical Association's Declaration of Helsinki. The research plan was approved by the Ethical Committee of the Faculty of Medicine in Pilsen, Charles University and University Hospital in Pilsen (Pilsen, Czechia) and informed consent was obtained from all patients.

Tumor DNA and Plasma-Based ctDNA Extraction and Mutational Analysis

Tumor biopsy material, cytological smear or formalin-fixed paraffin-embedded tissue samples, were processed according to the standard procedures of participating clinical facilities and were obtained from all subjects at study entry. Whole blood samples were collected in stabilization blood collection tubes (Cell-Free DNA BCT, Streck, Inc., United States) before starting systemic therapy (sampling called "P0"—plasma 0, baseline), after approximately 3 weeks of therapy (P1, after first chemotherapy cycle), after second chemotherapy cycle (P2) and then at intervals according to the treatment schedule and/or radiological re-evaluation (P3–P10, follow-up). The plasma fraction was obtained by a two-step centrifugation of whole blood within 6–54 h after collection, and then immediately frozen at −20°C.

Tumor DNA was isolated from all available samples using the GenElute™ Mammalian Genomic DNA Miniprep Kit (Sigma Aldrich, USA) according to the instructions of the manufacturer for the respective tissue material. ctDNA was extracted from 650 µl of plasma collected at each sampling time-point using the QIAamp Circulating Nucleic Acid Kit (Qiagen, Germany) according to the instructions of the manufacturer.

Mutational analysis based on PCR with heteroduplex formation followed by separation by DCE was performed as described previously [31]. Using a tumor-informed approach, only somatic mutations detected in tumor tissue were evaluated in plasma by a personalized MRD assay and the MAF in the ctDNA-positive samples was further calculated. The tissue was initially subjected to mutation analysis using a small 8-amplicon DCE panel—a panel of 8 target regions from most frequently

TABLE 2 | DCE mutation testing panel used in the study.

Marker	Exon number	Target codons	Size of PCR product [bp]	LOD [%]	DCE separation temperature [°C]
EGFR	19	746–753	169	0.1	52
KRAS	2	12, 13	112	0.03	50
TP53	5	170–187	107	0.1	58
	6	187–224	169	0.5	52
	7	225–261	160	0.5	52
	8	262–307	151	0.03	56
PIK3CA	9	542	106	0.2	48
BRAF	15	600	230	0.05	48

Bp, Base pair; DCE, denaturing capillary electrophoresis; LOD, limit of detection.

mutated genes in NSCLC including *EGFR*, *KRAS, TP53*, *BRAF* and *PIK3CA*. Analytical sensitivity expressed as the limit of detection (LOD) was evaluated in terms of the minor-allele fraction (MAF) using DNA fragment peak intensities obtained from SeqStudio data using GeneMarker software (Softgenetics, State College, PA, United States) as described previously [31]:

$$MAF = I_{MUTHOMO} + 0.5\,(I_{HET1} + I_{HET2}) / (I_{WTHOMO} + I_{MUTHOMO} + I_{HET1} + I_{HET2})$$

where $I_{MUTHOMO}$ is the signal intensity of the mutant homoduplex peak, I_{WTHOMO} is the signal intensity of the wildtype homoduplex peak, and I_{HET1} and I_{HET2} are the respective signal intensities of the two heteroduplexes. The resulting LODs for each of the tested regions ranging from 0.03% to 0.5% depending on the actual mutation detected.

All details of the DCE panel markers are summarized in **Table 2**. DNA without any of the initially tested mutations meeting the concentration requirements for NGS testing were then subjected to Illumina MiSeq 67-gene sequencing by ArcherDx VariantPlex Solid Tumor panel (Invitae Corporation, USA). Based on the identified mutation, DCE primers were then designed for amplification of the region around the found mutation (typically 90–200 bp in a total length) followed by a brief optimization of PCR conditions (temperature gradient range 54–68°C) and DCE running temperature (typically within a range from 40 to 60°C). The details of the DCE primer design and running temperature optimization were also described previously [31, 34, 35]. For the DCE the Applied Biosystems SeqStudio Genetic Analyzer instrument (Thermo Fisher Scientific, United States) was used. CE analysis parameters are detailed in **Figure 3**.

RESULTS

Out of a total of 121 patients initially admitted, 81 met the study inclusion criteria (disease stage, histology subtype and therapy setting). The overview of the multi-tier mutation testing is shown in **Figure 1**. The initial analysis by an 8-amplicon DCE panel revealed somatic mutation in tissue specimens of 58 patients, which represents 72% from the cohort. Of the remaining 23 mutation-negative samples 19 were evaluated as suitable for NGS testing. Using the commercial 67-gene NGS panel additional 5 mutation-positive patients were identified. The spectrum of found mutations shown in **Figure 2** corresponds with the expected mutation frequencies with the dominating contribution of mutation in *KRAS* and *TP53* genes (54% in total) often in a combination with other mutations. In 9 patients, 2 mutations were found in the tumor tissue (see **Table 3**). It should be noted that just upon receiving the complete results from tissue testing, specific DCE primers were designed to allow for monitoring of additional mutations found by NGS. The newly designed DCE assays included *BRAF* Gly469Val, *GNAQ* Tyr101Ter, *MET* Leu971ProfsTer10, *NOTCH2* Trp1529Cys and *STK11* Glu57LysfsTer7 mutations. The DCE result data for selected newly designed *MET* mutation assay is shown in **Figure 3A** together with a typical example of a mutation detected in the tumor suppressor *TP53* (**Figure 3B**).

With the DCE assays optimized for all detected mutations, plasma samples for individual patients were prospectively tested. The baseline P0 samples revealed ctDNA positivity in 36 of the 63 patients. P2 plasma sample was available in 30 of these 36 patients, but MAF could not be determined in 2 patients. During the 6 weeks period upon administration of the first two chemotherapy cycles, the ctDNA levels have been significantly altered in 25 of 28 patients, of whom 23 showed a decrease corresponding to stabilization or remission and 2 an increase corresponding to progression. In 3 patients (1 with progression and 2 with stable disease), ctDNA levels remained virtually unchanged. Overall, changes in ctDNA levels in all patients studied well reflected the RECIST criteria (see **Figure 4**).

In 9 patients with two mutations found in the tumor tissue, both mutations were monitored and quantified in ctDNA (see **Table 3**). In individual plasma samples, occurrence of both mutations was very similar. Either always absent (patients 9, 14, 67, 105), or in sample P0 both present and in sample P1 both absent (sample 93), or always present (patients 70 and 110). Moreover, in those last two patients, we uniformly observed an increase (patient number 70) or decrease (patient 110) in the levels of both mutations during P0-P2 samples in response to ongoing chemotherapy. For the remaining 2 patients (26 and 102), a discrepancy in ctDNA detection is likely to occur because the *TP53* and *PIK3CA* mutations were below the LOD.

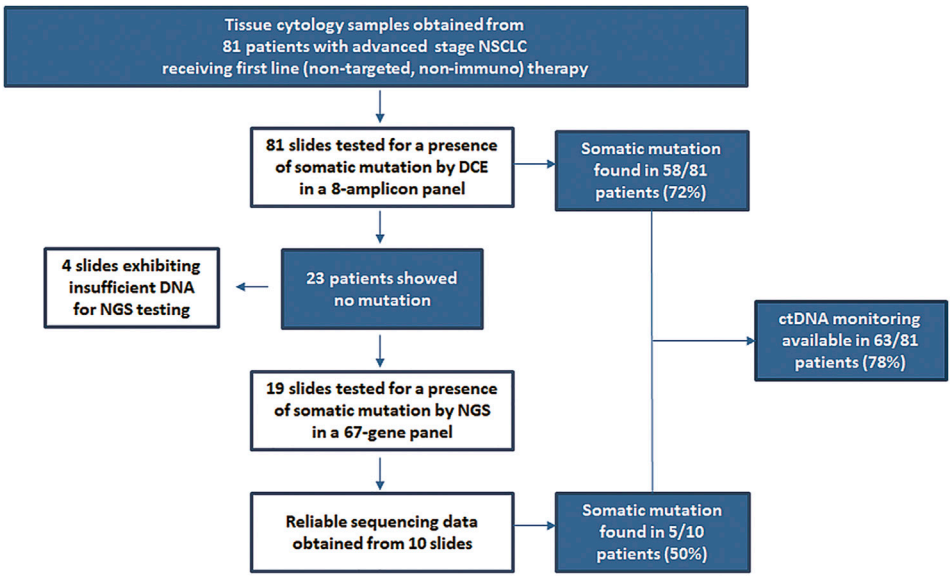

FIGURE 1 | Scheme of multi-tier mutation testing in tissue samples prior to ctDNA monitoring in plasma.

For most of the patient in the group the DCE assay was then repeatedly applied in a longitudinal monitoring of MRD as subsequent chemotherapy regimens were administered. In total 340 ctDNA detection analyses were performed among 63 monitored patients over the course of 2 years (follow-up time of individual patients 41–810 days). A clinically confirmed disease progression prompting either a change in regimen or a withdrawal of therapy after an interim partial or complete remission has been detected in 51 patients (mean time to progression 194 days, range 18–803 days). Examples of the long-term follow-up of a subgroup of 12 patients followed for more than half a year and having at least 7 plasma samples are illustrated in **Figure 5**.

All data acquired during this study is included in **Supplementary Table S1**.

DISCUSSION

The central point in the management of patients with advanced NSCLC is the ongoing assessment of the disease situation. This is primarily based on a recurring observation of tumor dynamics by imaging including CT or MRI. This universally accepted approach, however, exhibits certain disadvantages such as an exposure to ionizing radiation in case of CT or a spatial resolution limited to volume differences of several millimeters. A half a decade ago a groundbreaking work on ctDNA testing in NSCLC showed a significant link between changes in tumor volume and plasma ctDNA over time, which opened up prospects for the use of ctDNA in therapy monitoring [36]. The decrease or in some cases complete clearance of tumor specific mutation from ctDNA reflected a positive response to treatment, whereas the rise of ctDNA was directly related to disease progression, with several months lead over radiographic detection and clinical manifestation. In general, such approach is most efficiently applicable if identification of specific therapy-resistant clones is available during an ongoing targeted therapy such as those characterized by *EGFR* mutations T790M or C797S emerging in ctDNA during an ongoing antiEGFR targeted therapy (not applicable in presented patient group).

Over the recent years the most common plasma-based testing in NSCLC has been directed towards evaluation of *EGFR* mutation status as a direct alternative to tissue-based *EGFR* testing. While the ctDNA *EGFR* mutation assays have a stable position in routine diagnostics for prediction of therapy response or detection of therapy resistance, longitudinal monitoring of ctDNA mutations (including the non-targetable ones) has yet to find its full clinical utility. Consequently only a limited number of subsequent studies on longitudinal ctDNA monitoring of tumor-specific mutation in NSCLC has been published [13–15]. In first of them, median of 6 plasma samples from 13 patients with stage IV adenocarcinoma were analyzed during surveillance. Ten patients had *EGFR* sensitising mutations, two *BRAF* V600E mutation, and one patient had a combination of *KRAS*/*TP53*/*STK11* mutations [13]. In the second study, 13 baseline and post treatment ctDNA samples of patients in IV stage of NSCLC were analyzed for the occurrence of hot spot mutations in *EGFR*, *KRAS* and *BRAF* using dPCR [14]. In another study [15], 40 patients with one of the *EGFR*, *KRAS* or *BRAF* mutation was subjected to ctDNA analysis using dPCR at the time of enrollment and at least three follow-up blood samples were collected. The study group included patients in all stages of NSCLC who were treated with different types of treatment (targeted therapy, chemotherapy, immunotherapy, or their combination).

The plasma-based qPCR or dPCR assays typically used in the above mentioned reports were mainly directed at ctDNA detection of oncogenic mutations localized at distinct hotspots such as the relatively small exons 18–21 of *EGFR*, exon 2 of *KRAS*

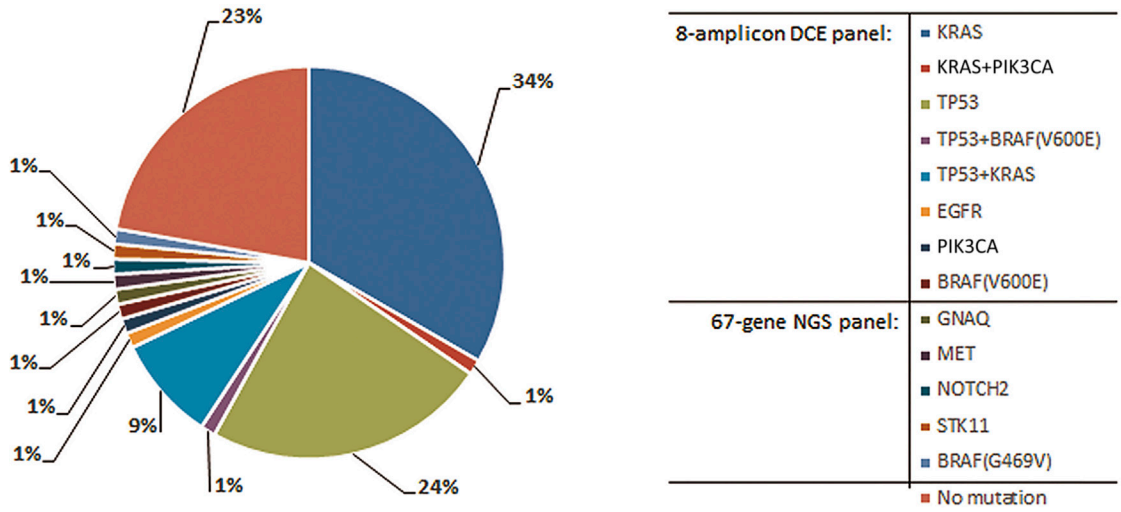

FIGURE 2 | Distribution of mutations found in tissue of 81 NSCLC patients. Specific primers were designed for the mutations identified by NGS to allow for subsequent ctDNA testing in plasma by the DCE method.

TABLE 3 | ctDNA quantification in patients having mutations in two different genes in tumor tissue.

Number of patient	Mutations traced in ctDNA	P0	MAF (%)	P1	MAF (%)	P2	MAF (%)
9	KRAS G12V / TP53ex5	O/O	-/-	O/O	-/-	O/O	-/-
14	KRAS G12C / TP53ex7	O/O	-/-	O/O	-/-	-/-	-/-
26	KRAS G12D / TP53ex5	**X/X**	21.6/6.9	**X**/O	3.9/-	**X**/O	2.1/-
67	KRAS G12D / TP53ex8	O/O	-/-	O/O	-/-	O/O	-/-
70	KRAS G12C / TP53ex8	**X/X**	4.1/<2	**X/X**	12.5/<2	**X/X**	57.3/29.6
93	KRAS G12C / TP53ex8	**X/X**	22.2/11.3	O/O	-/-	-/-	-/-
102	KRAS G12A / PIK3CAex9	**X**/O	15.7/-	**X**/O	6.8/-	**X**/O	7.1/-
105	KRAS G12C / TP53ex5	O/O	-/-	O/O	-/-	O/O	-/-
110	BRAF V600E / TP53ex8	**X/X**	40.2/44.9	**X/X**	4.1/3.5	**X/X**	4.6/2.6

MAF, mutant allele frequency; P0, plasma sample before starting systemic therapy; P1, plasma sample after first chemotherapy cycle; P2, plasma sample after second chemotherapy cycle; X, mutation found; O, no mutation found.

or exon 15 of *BRAF*. For longitudinal MRD monitoring this presents a significant limitation, since a large portion of the somatic DNA point mutations in NSCLC are in tumor suppressors, with absence of such hotspots. According to a recent report somatic mutations in *TP53* tumor suppressor alone account for over 50% of all mutation-positive cases in NSCLC with a strong correlation to tobacco smoke [37].

The DCE method used in this work presents a suitable alternative in targeted monitoring of oncogenic as well as tumor-suppressor mutations. In the current study, ctDNA was monitored in plasma of patients whose tumors were bearing mutations in *TP53*, *APC*, *NOTCH2*, *FGFR1* or *STK11*, among others. All these genes exhibit wide distributions of cancer-associated mutations spread across all coding sequence in a typical mark of a tumor suppressor [38]. Due to its relative simplicity the method can be applied to monitor virtually any ctDNA point mutation after just a very basic PCR amplification optimization. The combination of low noise with wide dynamic range of the SeqStudio detection system enables quantification of CE peak intensities across several orders of magnitude of relative fluorescence units. This allows for readout of the high signal for wildtype fragments next to a low signal for mutant fragments necessary for accurate calculation of MAFs.

In the present study we have evaluated therapy response from the relative change in ctDNA levels from P0 (baseline, prior to therapy) and P2 (after 2nd chemotherapy cycle) sampling. The results, illustrated by a waterfall plot in **Figure 4**, suggest that such testing may allow for prediction of therapy response already during the first 6 weeks of treatment.

Finally, we have applied the DCE method for repetitive longitudinal testing of patients that have or have not shown ctDNA in baseline sample. The monitoring was performed over the 0.5–2 years therapy period typically covering multiple chemotherapy regimens and in total acquiring from 7 to 11 samples for each patient. The clinical course of the disease was in all cases directly related to the ctDNA dynamics with patients experiencing a lasting remission or stabilization of the disease to those who, during the observation period, showed a disease

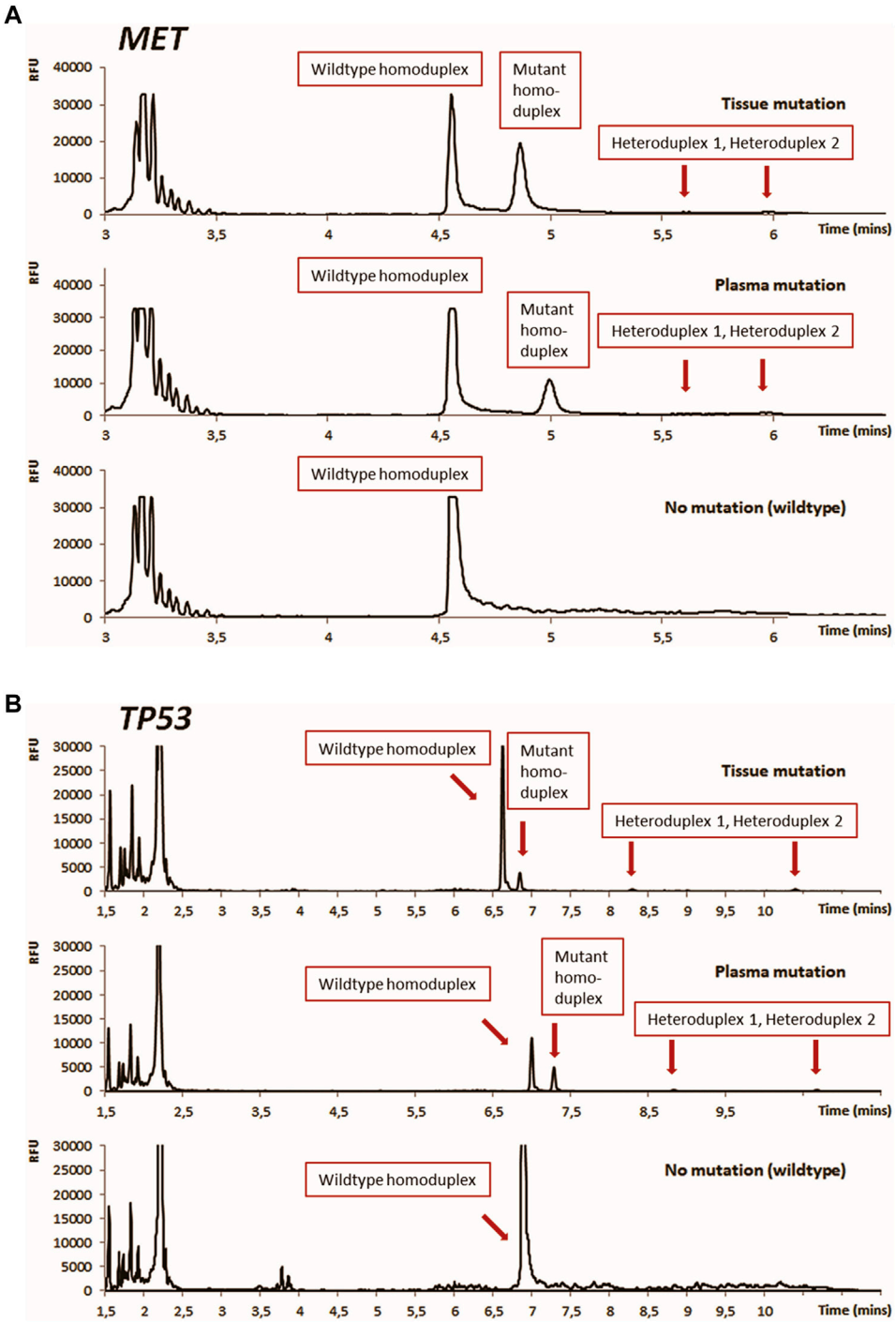

FIGURE 3 | Results of DCE mutation analysis for tissue and plasma illustrated for mutations found in tumor-suppressor genes *MET* **(A)** and *TP53* **(B)**. DCE conditions: Instrument: Applied Biosystems SeqStudio Genetic Analyzer, Injection: 1kV/10 s, Running voltage: 13 kV, Running temperature: 44°C [*MET*, Panel **A**], 54°C [*TP53*, Panel **B**].

progression with or without success of the subsequent therapy alterations. A variety of clinical developments could be observed across monitored patients as illustrated in **Figure 5**. In a subset of patients a continuing positive response to the therapy could be observed as their ctDNA was undetectable during weeks of monitoring (ID019, ID100 and ID051). A more frequently observed course of the disease was characterized by initial response (no ctDNA presence) followed by reappearance of

FIGURE 4 | Waterfall plot showing the treatment benefit in 28 patients according to relative change in ctDNA levels between the start of the first and the end of the second cycle of first-line chemotherapy. PD—progression (red), SD—stabilization (yellow), PR—partial + CR—complete response (green).

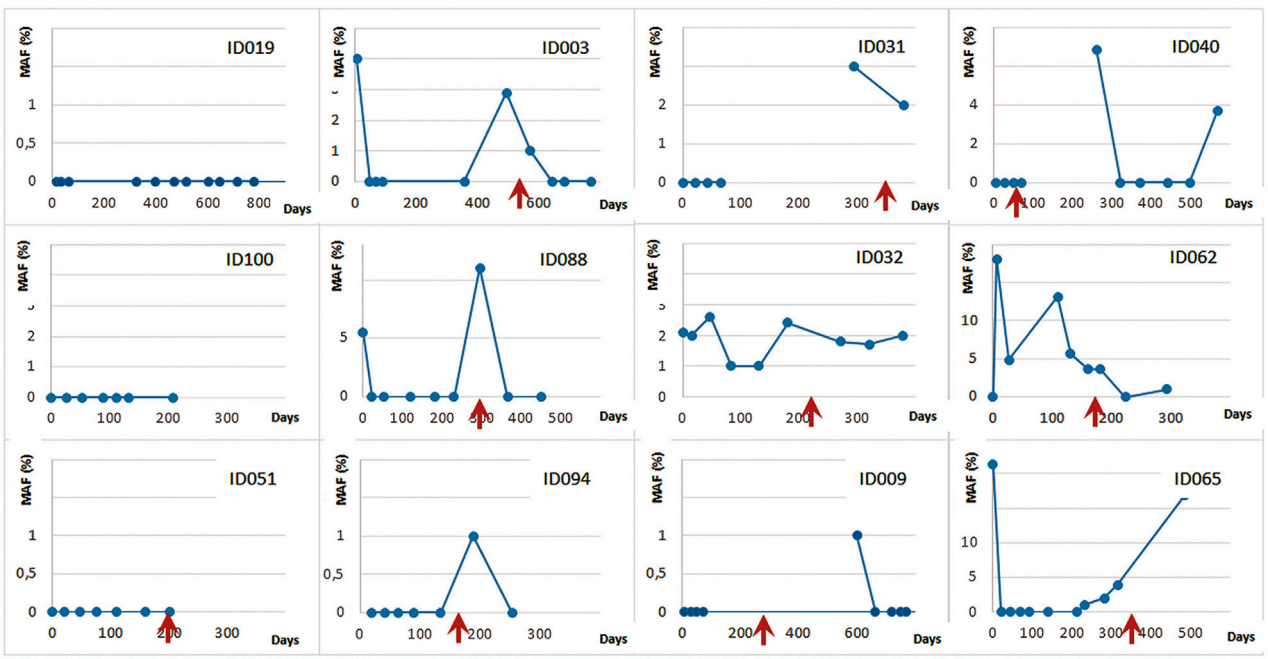

FIGURE 5 | DCE longitudinal MRD monitoring for advanced NSCLC patients undergoing chemotherapy (MAF—% of mutated minor allele fraction). The red arrows denote clinically confirmed disease progression.

ctDNA several months into the therapy. There a new regimens could either bring a positive effect seen as a reinstated ctDNA elimination (ID003, ID088, ID094, ID009, ID040) or a negative response by continuance of detectable ctDNA (ID032). Occasionally, a lasting progression regardless of the treatment applied could be seen as a slow rise in ctDNA (ID065).

In the current work somatic mutations were first detected in tumor tissue using a two-tier approach in which a small set of frequently mutated oncogenic hotspots was initially evaluated by a smaller DCE panel and the mutation-negative samples were then subjected to a large NGS panel sequencing. For each patient the DCE was then used to detect and quantify the tissue-specific mutation in ctDNA extracted from plasma. A total of 28 patients were subjected to such ctDNA evaluation resulting in a correlation of the ctDNA dynamics with the initial RECIST response approximately 6 weeks into the therapy. A longitudinal MRD monitoring of patients spanning for up to 24 months was also demonstrated. The lower cost of the DCE assay allowed for the ctDNA testing to be performed repeatedly

during treatment to monitor the effectiveness of chemotherapy and to detect tumor progression presenting a viable tool useable in routine clinical management on NSCLC. This described approach to MRD monitoring allows for cost-efficient detection of tumor response or, eventual progression before its clinical manifestations and detection by imaging methods.

DATA AVAILABILITY STATEMENT

The original contributions presented in the study are included in the article/**Supplementary Material**, further inquiries can be directed to the corresponding author.

ETHICS STATEMENT

The studies involving human participants were reviewed and approved by the Ethics Committee of the Faculty Hospital Pilsen, Pilsen, Czechia. The patients/participants provided their written informed consent to participate in this study.

AUTHOR CONTRIBUTIONS

MM, MP, LB, and MS designed the study. LB, RP, TH, AS, and MM performed planning and execution of mutation testing and ctDNA monitoring. MP, MS, and OF conducted the clinical part of the study. LB and MM wrote the manuscript with support from TH, RP, and AS.

FUNDING

This work was supported by Czech Ministry of Health project no. AZV NV17-30748A.

CONFLICT OF INTEREST

MM is employed by Elphogene company. Elphogene is currently providing oncoMonitor liquid biopsy/ctDNA test, which is in part utilizing the DCE mutation detection technology presented in this work.

The remaining authors declare that the research was conducted in the absence of any commercial or financial relationships that could be construed as a potential conflict of interest.

ACKNOWLEDGMENTS

Authors would like to thank Tomas Vanecek and Veronika Hajkova at Biopticka laborator in Pilsen, CZ for performing the NGS sequencing from submitted DNA samples.

SUPPLEMENTARY MATERIAL

The Supplementary Material for this article can be found online at: https://www.por-journal.com/articles/10.3389/pore.2022.1610308/full#supplementary-material

Supplementary Table S1 | Clinical and experimental data for all patients in the study.

REFERENCES

1. Bray F, Ferlay J, Soerjomataram I, Siegel RL, Torre LA, Jemal A. Global Cancer Statistics 2018: GLOBOCAN Estimates of Incidence and Mortality Worldwide for 36 Cancers in 185 Countries. *CA Cancer J Clin* (2018) 68(6):394–424. doi:10.3322/caac.21492
2. Ettinger DS, Wood DE, Aisner DL, Akerley W, Bauman JR, Bharat A, et al. NCCN Guidelines Insights: Non-Small Cell Lung Cancer, Version 2.2021. *J Natl Compr Canc Netw* (2021) 19(3):254–66. doi:10.6004/jnccn.2021.0013
3. Gubens MA, Davies M. NCCN Guidelines Updates: New Immunotherapy Strategies for Improving Outcomes in Non-Small Cell Lung Cancer. *J Natl Compr Canc Netw* (2019) 17:574–8. doi:10.6004/jnccn.2019.5005
4. Malone ER, Oliva M, Sabatini PJB, Stockley TL, Siu LL. Molecular Profiling for Precision Cancer Therapies. *Genome Med* (2020) 12(1):8. doi:10.1186/s13073-019-0703-1
5. Theodoropoulos AS, Gkiozos I, Kontopyrgias G, Charpidou A, Kotteas E, Kyrgias G, et al. Modern Radiopharmaceuticals for Lung Cancer Imaging with Positron Emission Tomography/Computed Tomography Scan: A Systematic Review. *SAGE Open Med* (2020) 8:205031212096159. doi:10.1177/2050312120961594
6. Boonstra PA, Wind TT, van Kruchten M, Schuuring E, Hospers GAP, van der Wekken AJ, et al. Clinical Utility of Circulating Tumor DNA as a Response and Follow-Up Marker in Cancer Therapy. *Cancer Metastasis Rev* (2020) 39(3):999–1013. doi:10.1007/s10555-020-09876-9
7. Schwarzenbach H, Hoon DSB, Pantel K. Cell-Free Nucleic Acids as Biomarkers in Cancer Patients. *Nat Rev Cancer* (2011) 11(6):426–37. doi:10.1038/nrc3066
8. Diaz LA, Bardelli A. Liquid Biopsies: Genotyping Circulating Tumor DNA. *J Clin Oncol* (2014) 32(6):579–86. doi:10.1200/JCO.2012.45.2011
9. Peng Y, Mei W, Ma K, Zeng C. Circulating Tumor DNA and Minimal Residual Disease (MRD) in Solid Tumors: Current Horizons and Future Perspectives. *Front Oncol* (2021) 11:763790. doi:10.3389/fonc.2021.763790
10. Zheng D, Ye X, Zhang MZ, Sun Y, Wang JY, Ni J, et al. Plasma EGFR T790M ctDNA Status is Associated with Clinical Outcome in Advanced NSCLC Patients with Acquired EGFR-TKI Resistance. *Sci Rep* (2016) 6:20913. doi:10.1038/srep20913
11. Karlovich C, Goldman JW, Sun J-M, Mann E, Sequist LV, Konopa K, et al. Assessment of EGFR Mutation Status in Matched Plasma and Tumor Tissue of NSCLC Patients from a Phase I Study of Rociletinib (CO-1686). *Clin Cancer Res* (2016) 22(10):2386–95. doi:10.1158/1078-0432.CCR-15-1260
12. Garrido P, Paz-Ares L, Majem M, Morán T, Trigo JM, Bosch-Barrera J, et al. LungBEAM: A Prospective Multicenter Study to Monitor Stage IV NSCLC Patients with EGFR Mutations Using BEAMing Technology. *Cancer Med* (2021) 10(17):5878–88. doi:10.1002/cam4.4135
13. Fernandes MGO, Sousa C, Pereira Reis J, Cruz-Martins N, Souto Moura C, Guimarães S, et al. Liquid Biopsy for Disease Monitoring in Non-Small Cell Lung Cancer: The Link Between Biology and the Clinic. *Cells* (2021) 10(8):1912. doi:10.3390/cells10081912
14. Metzenmacher M, Hegedüs B, Forster J, Schramm A, Horn PA, Klein CA, et al. Combined Multimodal ctDNA Analysis and Radiological Imaging for Tumor Surveillance in Non-Small Cell Lung Cancer. *Transl Oncol* (2022) 15(1):101279. doi:10.1016/j.tranon.2021.101279
15. de Kock R, Borne Bv. d., Soud MYE, Belderbos H, Stege G, de Saegher M, et al. Circulating Biomarkers for Monitoring Therapy Response and Detection of Disease Progression in Lung Cancer Patients. *Cancer Treat Res Commun* (2021) 28:100410. doi:10.1016/j.ctarc.2021.100410
16. Di Capua D, Bracken-Clarke D, Ronan K, Baird A-M, Finn S. The Liquid Biopsy for Lung Cancer: State of the Art, Limitations and Future Developments. *Cancers* (2021) 13(16):3923. doi:10.3390/cancers13163923

17. Thierry AR, El Messaoudi S, Gahan PB, Anker P, Stroun M. Origins, Structures, and Functions of Circulating DNA in Oncology. *Cancer Metastasis Rev* (2016) 35(3):347–76. doi:10.1007/s10555-016-9629-x
18. Diehl F, Li M, Dressman D, He Y, Shen D, Szabo S, et al. Detection and Quantification of Mutations in the Plasma of Patients with Colorectal Tumors. *Proc Natl Acad Sci U.S.A* (2005) 102(45):16368–73. doi:10.1073/pnas.0507904102
19. Elazezy M, Joosse SA. Techniques of Using Circulating Tumor DNA as a Liquid Biopsy Component in Cancer Management. *Comput Struct Biotechnol J* (2018) 16:370–8. doi:10.1016/j.csbj.2018.10.002
20. Sefrioui D, Mauger F, Leclere L, Beaussire L, Di Fiore F, Deleuze J-F, et al. Comparison of the Quantification of KRAS Mutations by Digital PCR and E-Ice-COLD-PCR in Circulating-Cell-Free DNA from Metastatic Colorectal Cancer Patients. *Clinica Chim Acta* (2017) 465:1–4. doi:10.1016/j.cca.2016.12.004
21. Chen H, Zhang J, Chen H-Y, Su B, Lu D. Establishment of Multiplex Allele-Specific Blocker PCR for Enrichment and Detection of 4 Common *EGFR* Mutations in Non-Small Cell Lung Cancer. *Ann Transl Med* (2020) 8(22):1509. doi:10.21037/atm-20-6754
22. Soussi T. The P53 Tumor Suppressor Gene: From Molecular Biology to Clinical Investigation. *Ann NY Acad Sci* (2000) 910:121–39. doi:10.1111/j.1749-6632.2000.tb06705.x
23. van Es JH, Giles RH, Clevers HC. The Many Faces of the Tumor Suppressor Gene APC. *Exp Cel Res* (2001) 264(1):126–34. doi:10.1006/excr.2000.5142
24. Minarikova P, Benesova L, Halkova T, Belsanova B, Suchanek S, Cyrany J, et al. Longitudinal Molecular Characterization of Endoscopic Specimens from Colorectal Lesions. *World J Gastroenterol* (2016) 22(20):4936–45. doi:10.3748/wjg.v22.i20.4936
25. Benešová L, Hálková T, Ptáčková R, Semyakina A, Menclová K, Pudil J, et al. Significance of Postoperative Follow-Up of Patients with Metastatic Colorectal Cancer Using Circulating Tumor DNA. *World J Gastroenterol* (2019) 25(48):6939–48. doi:10.3748/wjg.v25.i48.6939
26. Pazdirek F, Minarik M, Benesova L, Halkova T, Belsanova B, Macek M, et al. Monitoring of Early Changes of Circulating Tumor DNA in the Plasma of Rectal Cancer Patients Receiving Neoadjuvant Concomitant Chemoradiotherapy: Evaluation for Prognosis and Prediction of Therapeutic Response. *Front Oncol* (2020) 10:1028. doi:10.3389/fonc.2020.01028
27. Lian D-S, Zhao S-J. Capillary Electrophoresis Based on the Nucleic Acid Detection in the Application of Cancer Diagnosis and Therapy. *Analyst* (2014) 139(14):3492–506. doi:10.1039/c4an00400k
28. Fiala O, Pesek M, Finek J, Svaton M, Minarik M, Benesova L, et al. Pemetrexed versus Erlotinib in the Second-Line Treatment of Patients with Advanced-Stage Non-Squamous NSCLC Harboring Wild-Type EGFR Gene. *Anticancer Res* (2016) 36(1):447–53.
29. Bunganič B, Hálková T, Benešová L, Belšánová B, Laclav M, Hrůzová M, et al. KRAS Mutation Assay on EUS-FNA Specimens from Pacients with Pancreatic Mass. *Cas Lek Cesk* (2016) 155(1):48–51.
30. Benesova L, Halkova T, Bunganic B, Belsanova B, Zavoral M, Traboulsi E, et al. Comparison of Native Aspirates and Cytological Smears Obtained by EUS-Guided Biopsies for Effective DNA/RNA Marker Testing in Pancreatic Cancer. *Pathol Oncol Res* (2020) 26(1):379–85. doi:10.1007/s12253-018-0490-9
31. Benesova L, Belsanova B, Kramar F, Halkova T, Benes V, Minarik M. Application of Denaturing Capillary Electrophoresis for the Detection of Prognostic Mutations in Isocitrate Dehydrogenase 1 and Isocitrate Dehydrogenase 2 Genes in Brain Tumors. *J Sep Sci* (2018) 41(13):2819–27. doi:10.1002/jssc.201701473
32. Benesova L, Belsanova B, Suchanek S, Kopeckova M, Minarikova P, Lipska L, et al. Mutation-Based Detection and Monitoring of Cell-Free Tumor DNA in Peripheral Blood of Cancer Patients. *Anal Biochem* (2013) 433(2):227–34. doi:10.1016/j.ab.2012.06.018
33. Eisenhauer EA, Therasse P, Bogaerts J, Schwartz LH, Sargent D, Ford R, et al. New Response Evaluation Criteria in Solid Tumours: Revised RECIST Guideline (Version 1.1). *Eur J Cancer* (2009) 45(2):228–47. doi:10.1016/j.ejca.2008.10.026
34. Salek C, Minarikova P, Benesova L, Nosek V, Strnad R, Zavoral M, et al. Mutation Status of K-Ras, P53 and Allelic Losses at 9p and 18q are Not Prognostic Markers in Patients with Pancreatic Cancer. *Anticancer Res* (2009) 29:1803–10.
35. Bjørheim J, Minarik M, Gaudernack G, Ekstrøm PO. Mutation Detection in KRAS Exon 1 by Constant Denaturant Capillary Electrophoresis in 96 Parallel Capillaries. *Anal Biochem* (2002) 304(2):200–5. doi:10.1006/abio.2002.5629
36. Newman AM, Bratman SV, To J, Wynne JF, Eclov NCW, Modlin LA, et al. An Ultrasensitive Method for Quantitating Circulating Tumor DNA with Broad Patient Coverage. *Nat Med* (2014) 20(5):548–54. doi:10.1038/nm.3519
37. Mogi A, Kuwano H. TP53 Mutations in Nonsmall Cell Lung Cancer. *J Biomed Biotechnol* (2011) 2011:1–9. doi:10.1155/2011/583929
38. Baeissa H, Benstead-Hume G, Richardson CJ, Pearl FMG. Identification and Analysis of Mutational Hotspots in Oncogenes and Tumour Suppressors. *Oncotarget* (2017) 8(13):21290–304. doi:10.18632/oncotarget.15514

Pathology & Oncology Research

frontiers

ORIGINAL RESEARCH
published: 05 October 2022
doi: 10.3389/pore.2022.1610607

EGFR T790M Mutation Detection in Patients With Non-Small Cell Lung Cancer After First Line EGFR TKI Therapy: Summary of Results in a Three-Year Period and a Comparison of Commercially Available Detection Kits

*Eszter Bencze[1†], Krisztina Bogos[2†], Andrea Kohánka[1], László Báthory-Fülöp[1], Veronika Sárosi[3], Erzsébet Csernák[1], Nóra Bittner[4], Zsombor Melegh[1] and Erika Tóth[1]**

[1]Department of Surgical and Molecular Pathology, National Tumour Biology Laboratory, National Institute of Oncology, Budapest, Hungary, [2]National Koranyi Institute of Pulmonology, Budapest, Hungary, [3]Faculty of Medicine, University of Pécs, Pécs, Hungary, [4]Department of Oncology Faculty of Medicine, Semmelweis University, Budapest, Hungary

EGFR mutation in non-small cell lung cancer (NSCLC) offers a potential therapeutic target for tyrosine kinase inhibitor (TKI) therapy. The majority of these cases, however eventually develop therapy resistance, mainly by acquiring *EGFR* T790M mutation. Recently, third-generation TKIs have been introduced to overcome T790M mutation-related resistance. Cell free circulating tumor DNA (liquid biopsy) has emerged as a valuable alternative method for T790M mutation detection during patient follow up, when a tissue biopsy cannot be obtained for analysis. In this study, we summarized our experience with Super-ARMS EGFR Mutation Detection Kit (AmoyDx) on 401 samples of 242 NSCLC patients in a 3-year period in Hungary, comprising 364 plasma and 37 non-plasma samples. We also compared the performance of two commercially available detection kits, the cobas EGFR Mutation test v2 (Roche) and the Super-ARMS EGFR Mutation Detection Kit (AmoyDx). The same activating *EGFR* mutation was detected with the AmoyDx kit as in the primary tumor in 45.6% of the samples. T790M mutation was identified in 48.1% of the samples containing activating *EGFR* mutation. The detection rate of T790M mutation was not dependent on the DNA concentration of the plasma sample and there was no considerable improvement in mutation detection rate after a second, subsequent plasma sample. The concordance of *EGFR* activating mutation detection was 89% between the two methods, while this was 93% for T790M mutation detection. The AmoyDx kit, however showed an overall higher detection rate of T790M mutation compared to the cobas kit (p = 0.014). T790M mutation was detected at 29.8% of the patients if only plasma samples were available for analysis, while the detection rate was 70.2% in non-plasma samples. If the activating *EGFR* was detected in the plasma samples, the detection rate of T790M mutation was 42.4%. Although non-plasma samples provided a superior T790M mutation detection rate, we found that liquid

OPEN ACCESS

Edited by:
József Tímár,
Semmelweis University, Hungary

***Correspondence:**
Erika Tóth
dr.toth.erika@oncol.hu

†These authors have contributed equally to this work and share first authorship

Received: *19 May 2022*
Accepted: *22 September 2022*
Published: *05 October 2022*

Citation:
Bencze E, Bogos K, Kohánka A, Báthory-Fülöp L, Sárosi V, Csernák E, Bittner N, Melegh Z and Tóth E (2022) EGFR T790M Mutation Detection in Patients With Non-Small Cell Lung Cancer After First Line EGFR TKI Therapy: Summary of Results in a Three-Year Period and a Comparison of Commercially Available Detection Kits. Pathol. Oncol. Res. 28:1610607. doi: 10.3389/pore.2022.1610607

biopsy can offer a valuable tool for T790M mutation detection, when a tissue biopsy is not available. Alternatively, a liquid biopsy can be used as a screening test, when re-biopsy should be considered in case of wild-type results.

Keywords: liquid biopsy, NSCLC, ctDNA, EGFR T790M mutation, AmoyDx super-ARMS EGFR mutation detection kit, cobas EGFR test v2

INTRODUCTION

Lung cancer is one of the most common malignant tumors with high mortality rate. Hungary was reported to have one of the highest incidence and mortality rates of lung cancer worldwide (1). The majority of the patients are smokers. In European studies, mutation in the *EGFR* gene exon 18, 19, 20 or 21 can be detected in 12%–17% of non-small cell lung cancers (NSCLC). These patients are predominantly non-smokers with a diagnosis of adenocarcinoma (2). EGFR tyrosine kinase inhibitor (TKI) therapy proved to be highly effective in these cases. The most common activating mutations are the point mutation L858R and a subset of in-frame deletions involving exon 19 (3). While the first-generation TKIs, such as gefitinib and erlotinib reversibly bind to EGFR, the binding and inhibition are irreversible at second-generation inhibitors, such as afatinib and dacomitinib. Despite this difference in their tyrosine-kinase binding ability, there is a similar pattern of acquired resistance, which usually occurs after 9–14 months (4). The resistance mechanism mainly involves gatekeeper *EGFR* mutations, activation of alternative signaling pathways through *MET* and *ERBB2* amplifications or activation of downstream MAPK or PI3K pathways (5). Among secondary gatekeeper *EGFR* mutations, T790M substitution mutation in exon 20 has emerged as the most common mechanism of acquired resistance (6). Most recently, third-generation EGFR TKIs, such as osimertinib have been introduced to overcome therapy resistance, which can evade *EGFR* T790M mutation by irreversibly binding to the mutated protein (7). This emphasizes the necessity of identifying patients with *EGFR* T790M mutation, as they may benefit from third-generation TKI therapy.

Tumor tissue biopsy has been conventionally used for tumor sampling and mutation analysis. However, it is not always possible to obtain a tissue sample when the tumor is difficult to access or a biopsy is hindered by the impaired health of the patient. Therefore, a less invasive method may be preferred to obtain tumor DNA in these cases. Cell-free circulating tumor DNA (ctDNA) regularly appears in the blood as a consequence of tumor cell apoptosis and necrosis, and has been reported to faithfully mirror the DNA content of the primary tumor of the same patient (8). Furthermore, it may better reflect the genetic heterogeneity of the tumor than a tissue biopsy (9). Hence, obtaining ctDNA from peripheral blood plasma emerged as a promising alternative to invasive tissue biopsies. Despite this fact, there are various factors which make detection of ctDNA difficult: the heavily fragmented nature and short half-life of ctDNA, low and widely variable plasma concentration levels, and the presence of background normal plasma DNA (10). This emphasizes the importance of employing a highly sensitive, reliable and accurate detection method. There are multiple diagnostic assays developed to assess *EGFR* status in blood plasma samples, including a number of PCR based systems, mass spectrometry, and next-generation sequencing (11). In this study, we summarized our results with the Amoydx Super-ARMS EGFR Mutation Detection Kit (Amoy Diagnostics Co., Ltd., Xiamen, China) test and we also compared the performance of the AmoyDx and the cobas EGFR Mutation test v2 (cobasv2; Roche Molecular Systems, Pleasanton, CA, United States) in peripheral plasma samples of NSCLC patients.

MATERIAL AND METHODS

Patients and Samples

Altogether 401 samples of 242 NSCLC patients, previously treated with first- or second-generation EGFR TKI therapy have been analyzed in the Molecular Pathology Laboratory of the National Institute of Oncology between 2019 and 2021. The number of cases in different sample types was as follows: 3 pleural effusions, 5 cell blocks, 6 cytology smears, 6 resection specimens, 17 lung biopsies and 364 blood samples. All the cytology and tissue samples contained viable tumor cells. The average number of blood samples per patient was 1.65; the maximum number was 6 blood samples per patient. Blood specimens and pleural effusions were collected and stored either in K2EDTA S-Monovette tubes (Sarstedt, Nümbrecht, Germany) at 4°C or in Cell-Free DNA BCT Streck tubes (Streck, La Vista, NE, United States) at room temperature, depending on the proximity of the sampling site. In the first case, liquid biopsies were processed within 2 h, while in the case of Streck tubes the time interval did not exceed 72 h.

The study was reviewed and approved by ETT-TUKEB, Health and Scientific Committee of Ministry of Human Resources of Hungary. Number of permission: IV/1792-4/2021/EKU.

DNA Extraction

For an optimal yield and purity of ctDNA, plasma separation was performed in a two-step centrifugation protocol with a first centrifugation step of 3000×g for 10 min and a second step of 12,000×g for 10 min (12, 13). The ctDNA isolation started immediately after the plasma separation or after a maximum of 3-day storage at −80°C. Plasma samples between 4 and 6 ml were processed with the cobas ctDNA Sample Preparation Kit (Roche) following the manufacturer's instructions. For preparation of pleural effusion samples, 9–17 ml of the samples were centrifuged at 1700×g for 10 min to remove cells and debris. The supernatant was used for the extraction of ctDNA

TABLE 1 | Average DNA concentration, number of samples and proportion of patients showing T790M mutation according to sample type.

Sample type (number of cases 397)	Average DNA concentration ng/µl (min-max)	Number and proportion of T790M positive samples	Proportion of patients with T790M mutation (%)
Pleural effusion (3)	11.6 (3.8–20)	2 (66.6%)	66.6
Cell blocks (5)	2.8 (1.3–4.6)	3 (60%)	60
Cytology smears (6)	11.9 (0.1–44.8)	2 (33.3%)	33.3
Biopsy (17)	16.6 (1.1–60)	15 (88%)	88
Resection (6)	56.9 (5.1–155)	4 (66.6%)	66.6
Plasma (360)	3.9 (0.1–65)	61 (16.9%)	29.5

with the same isolation protocol as for the plasma samples. For DNA extraction from small biopsies and cytological specimens with low tumor cell contents, we preferred the ReliaPrep DNA Clean-Up and Concentration System kit (Promega, Madison, WI, United States) to achieve a highly concentrated DNA yield. As this system contains only purifying reagents, the deparaffinization and lysis steps were performed with the corresponding reagents, according to the Maxwell RSC DNA FFPE protocol (Promega). The same kit was also used for formalin fixed paraffin embedded (FFPE) resection specimens. In each case, the tumor area was macro-dissected and one to three 5-µm sections of an FFPE specimen were processed. The concentration of the DNA samples was measured by the Qubit 4 fluorometer with the Qubit™ 1X dsDNA HS (High Sensitivity) Assay Kit (Thermo Fisher Scientific, Waltham, MA, United States) and stored at 4°C until further usage. For resection specimens, Promega, ReliaPrep DNA Clean-up and Concentration System kit was used.

T790M Mutation Detection Methods

EGFR mutation detection was performed with the cobas *EGFR* Mutation test v2 on cobas z480 analyzer (Roche) and with the Super-ARMS EGFR Mutation Detection Kit (AmoyDx) on LightCycler 480 II instrument (Roche). All kits and devices were used as recommended by the manufacturer's protocol. In the majority of cases, due to limited amount of DNA, only the AmoyDx kit was used as a standard method. When sufficient amount of ctDNA was available, we performed the test with both methods to compare the performances of the two cross-platform technologies.

Statistical Analysis

McNemar's test for paired proportions was used to calculate the differences of the concordance rates of the different methods. The correlation of DNA concentration and T790M mutation detection rate was calculated with the point-biserial correlation method. Significance was calculated with two-tailed t-tests or chi-square tests.

RESULTS

T790M Mutation Detection Results With AmoyDx Test

Four plasma samples were not suitable for ctDNA analysis due to hemolysis. The result of 17 plasma samples and one resection specimen was invalid. The average DNA concentration according to the sample type is shown in **Table 1**. There were 9 cases where the ctDNA concentration was higher than 10 ng/µl.

TABLE 2 | Results of T790 mutation analysis of the samples of all the patients, according to the sample type (chi-square $p < 0.0001$).

Sample type	T790 mutation analysis results (number of patients)	
	T790 wild type	T790M mutant
Non-plasma	11 (29.7%)	26 (70.3%)
Plasma	144 (70.2%)	61 (29.8%)

We also assessed if the activating *EGFR* mutation of the corresponding primary tumors, previously analyzed with cobas *EGFR* Mutation test v2, could be detected in the sample. With the AmoyDx kit, we detected the same activating *EGFR* mutation which was seen in the primary tumors in 181 of 397 samples (45.6%). Eighty-seven of these 181 samples (48.1%) contained T790M mutation. Out of these 87 cases, T790M mutation was detected with the AmoyDx kit in the first blood samples of the patients in 50 cases and in a subsequent second blood sample in a further 32 cases. In 4 cases, only the third blood sample was T790M positive and we had only 1 case when only the fourth blood sample showed a positive result. Further repetition of the sampling did not improve the detection rate, as we did not detect any T790M mutation after the fourth sample, when the previous samples were negative.

Considering the sample type, T790M mutation was detected at 70.3% of the patients if non-plasma samples were used, while it was detected at only 29.8% of the patients if only plasma samples were analyzed. Although the number of non-plasma samples was relatively low, the difference was significant ($p < 0.0001$) (**Table 2**). Theoretically, the lower T790M detection rate in the plasma samples could be explained by the absence of circulating tumor DNA in the sample. Nevertheless, when we included only those samples in the analysis, where the primary *EGFR* mutation was also identified, hence confirming the presence of ctDNA in the sample, the difference remained significant ($p = 0.002444$) (**Table 3**).

We also examined whether the T790M mutation detection rate of the AmoyDx kit correlated with the DNA concentration. **Figure 1** shows the T790M mutation frequency in relation to the DNA concentration. There was no significant correlation

TABLE 3 | Results of T790 mutation analysis when the primary activating *EGFR* mutation was also detected in the sample, according to the sample type (chi-square $p = 0.00244$).

Sample type	T790 mutation analysis results (number of cases)	
	T790 wild type	T790M mutant
Non-plasma	11 (29.7%)	26 (70.3%)
Plasma	83 (57.6%)	61 (42.4%)

between the DNA concentration and the detection rate ($p = 0.339$), and the proportion of positive cases did not depend on the DNA concentration.

The type of the primary *EGFR* mutations in relation to the presence of T790M mutation is shown in **Table 4**. T790M mutation was most frequent in exon 19 del and exon 21 mutant cases. Frequency of T790M mutation was roughly similar in *EGFR* exon 19 del and exon 21 mutant groups, 49 of 94 (52.1%) and 36 of 75 (48%), respectively.

Comparison of the results of cobas *EGFR* mutation test v2 and AmoyDx Super-ARMS test

Eighty-six plasma samples had sufficient amount of DNA for analysis with both methods. The same amount of DNA was used for comparison. These cases were also used to assess the concordance rate between the plasma samples and the previously obtained tissue samples from the same patient.

In 73 plasma samples, 85% of all cases, we obtained the same result with both tests. With the AmoyDx Super-ARMS test, 43 cases showed the same activating *EGFR* mutation, which was detected previously in the primary tumor (50.5%) and 20 out of these 43 *EGFR* mutant cases also showed T790M positivity. With cobas test, 40 cases (46%) showed the same activating *EGFR* mutation, which was previously detected in the primary tumor and T790M mutation was present in 14 out of these cases. Overall, 20/86 samples (23%) tested with the AmoyDx kit were T790M mutation positive vs. 14/86 (16%) with the cobas kit. The higher T790M mutation detection rate of the AmoyDx kit compared to the cobas kit was statistically significant ($p = 0.014$). In six samples, the T790M mutation was only detectable with the AmoyDx kit. The concordance rate of *EGFR* activating mutation detection between the two methods was 89%, while this was 93% for T790M mutation detection.

Seventy-one plasma samples analyzed by both AmoyDx and cobas tests had a previous tissue sample with an available *EGFR* mutation analysis result. Among these cases, four samples had an *EGFR* activating mutation detected only by the AmoyDx test, while cobas test showed a wild-type result in these cases. In one case, the same double mutation (exon 18 G719x, exon 20 S768I) was detected in the primary tumor and with AmoyDx test in the plasma sample, but the cobas test detected only the exon 20 S768I mutation. In one case, where the primary lung tumor showed exon 21 L858R mutation, the same mutation was detected with cobas test in the ctDNA, but the AmoyDx test showed an exon 20 ins. We interpreted the AmoyDx result as being false positive, since the primary tissue sample analysis showed an exon 21 L858R mutation only, although this could also be explained by tumor heterogeneity. In addition, in one case, we detected the same *EGFR* exon 19 del mutation with cobas test as in the primary tumor sample, but the AmoyDx gave a wild-type result. The concordance rate between the primary tissue samples and the ctDNA testing platforms is shown in **Table 5**. Although the AmoyDx test showed a slightly better performance in detecting the primary activating *EGFR* mutation in case of exon 19 del, exon 18 mut and exon 21 mut, the difference between the two platforms was not statistically significant ($p = 0.563$, $p = 0.317$, $p = 0.157$, respectively). The overall concordance rate with

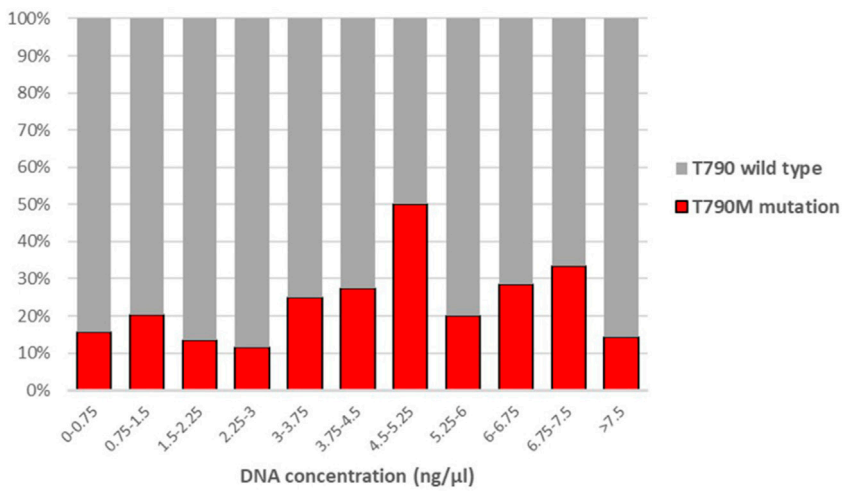

FIGURE 1 | Correlation between the proportion of T790M positive cases and DNA concentration. (Point-biserial correlation $p = 0.339$).

TABLE 4 | Occurrence of T790M mutation in different *EGFR* mutant groups.

Type of primary *EGFR* mutation	Number of T790M positive samples/total
Exon 19 del	49/94
Exon 20 ins	1/1
Exon 21 L858R	33/68
Exon 21 L861Q	2/4
Exon 21 L861Q and exon 20 S768I	1/3
Exon 18 G719X	0/7
Exon 18 G719X and exon 20 S768I	0/2
Exon 18 G719X and exon 21 L861Q	1/2

TABLE 5 | Concordance between the primary tissue samples and the plasma ctDNA results for *EGFR* activating mutations.

	Concordance		Probability of difference in concordance rates
	Cobas	AmoyDx	
exon 19 del	50/71 (70%)	52/71 (73%)	$p = 0.563$
exon 18 mut	67/71 (94%)	68/71 (96%)	$p = 0.317$
exon 21 mut	63/71 (89%)	65/71 (92%)	$p = 0.157$
exon 20 mut	64/71 (90%)	64/71 (90%)	n.a

the tissue sample result was 86% for the cobas and 88% for the AmoyDx kit, the difference of which was again not statistically significant ($p = 0.667$).

DISCUSSION

While T790M mutation occurs in less than 5% of untreated *EGFR* mutant lung adenocarcinomas, about 50%–70% of the *EGFR* mutated tumors develop T790M mutation as an acquired resistance if treated with first-generation TKIs (14). As a minimally invasive test, assessment of ctDNA in plasma samples is a valid and cost-effective alternative of tissue biopsies and identifies a large proportion of *EGFR* T790M mutations responsible for therapy resistance. In this study, we presented the results of *EGFR* T790M mutation testing in our laboratory over a 3-year period. Our results are in accordance with the literature data: as we detected T790M mutation in 48.1% of the samples, where the primary *EGFR* mutation could also be detected, confirming the presence of ctDNA in the sample (15). The AmoyDx test routinely used by us showed a higher detection rate of T790M mutation compared to the cobas test, and the difference was significant ($p = 0.014$). The concordance rate between the two tests was 93% in detecting T790M mutation and 89% in detecting the activating *EGFR* mutation. Compared to the previous tissue samples of the patients, the AmoyDx kit had a higher concordance rate than the cobas test kit in detecting activating *EGFR* mutations (86% vs. 88%), but this difference was not significant ($p = 0.667$). Overall, the detection rate of the AmoyDx test was slightly better than of the cobas test in our hands. However, cobas test is a very simple automated detection method with one of the widest *EGFR* mutation coverage among PCR based methods (42 mutations of exon 18, 19, 20, 21). Nevertheless, it was already shown previously that its sensitivity is inferior compared to ARMS techniques (allele specific polymerase chain reaction), like the AmoyDx test which also covers 42 mutations of exon 18, 19, 20 and 21, or digital PCR methods (16).

Our data suggest that plasma testing is useful in patients with *EGFR* T790M resistance mutations where continuous monitoring is recommended, especially if a tissue biopsy is not available. According to recent studies, in about 40% of relapsed cases it is not possible to obtain tumor tissue samples suitable for molecular analysis (17). In our hands with the AmoyDx test, T790M mutation frequency was 42.4% in those plasma samples where the activating *EGFR* mutation was detected. At the same time, we found that the detection of T790M mutation was not dependent on ctDNA concentration of the plasma samples. Furthermore, when multiple blood samples of a patient were sequentially taken at different points in time, the detection rate did not improve considerably after two repeated blood samples.

Although the number of non-plasma samples was very small in our study, comprising only 9.2% of the samples, the detection rate of T790M mutation was much higher than in non-plasma samples. This is in keeping with others studies on T790M testing. Tissue biopsy is still considered the gold standard for *EGFR* mutation analysis and up to 30% of the negative plasma samples for T790M mutation can have a positive result in a subsequent tissue biopsy (18). According to the results of Pereira et al, re-biopsy increased the detection rate of T790M mutation with 17% (19). The most probable cause of the higher detection rate of T790M in tissue samples is a higher tumor DNA content and a higher mutant allele frequency. Consequently, ctDNA mutational analysis could potentially be used as a triage test, where patients with a negative sample could undergo a further tissue biopsy. Recently, it has been demonstrated that using ctDNA as a triage test results in a superior T790M detection rate than tissue biopsy alone (20).

Re-biopsy rate can be considerably high in some practices. According to a recent Japanese publication on 120 patients with acquired resistance to EGFR-TKIs, re-biopsy was performed on 109 patients, with an implementation rate of 90.8%. However, re-biopsy is still very rare in our practice compared to the literature data. Although liquid biopsy alone is still less costly than tissue biopsy, considering its costs and effects directly relating to testing (20), re-biopsy should be considered more frequently in our practice in case of disease progression after first- and second-line *EGFR* TKI therapy.

DATA AVAILABILITY STATEMENT

The raw data supporting the conclusion of this article will be made available by the authors, without undue reservation.

ETHICS STATEMENT

The studies involving human participants were reviewed and approved by the ETT-TUKEB, Health and Scientific Committee

of Ministry of Human Resources of Hungary. Number of permission: IV/1792-4/2021/EKU. Written informed consent for participation was not required for this study in accordance with the national legislation and the institutional requirements.

AUTHOR CONTRIBUTIONS

ET, EC, NB, and LB-F designed the study, EB and AK performed the detection of T790M mutation, NB, VS, and KB took part in the collection of patients. ET, EC, KB, and ZM wrote the manuscript.

FUNDING

This work was supported by the Hungarian National Laboratory (under the National Tumor Biology Laboratory project (NLP-17)) and "Befektetés a jövőbe 2020-1.1.6-JÖVŐ-2021-0008. Számú pályázat".

CONFLICT OF INTEREST

The authors declare that the research was conducted in the absence of any commercial or financial relationships that could be construed as a potential conflict of interest.

REFERENCES

1. Bogos K, Kiss Z, Galffy G, Tamasi L, Ostoros G, Muller V, et al. Lung Cancer in Hungary. *J Thorac Oncol* (2020) 15(5):692–9. doi:10.1016/j.jtho.2019.11.001
2. Graham RP, Treece AL, Lindeman NI, Vasalos P, Shan M, Jennings LJ, et al. Worldwide Frequency of Commonly Detected EGFR Mutations. *Arch Pathol Lab Med* (2018) 142(2):163–7. doi:10.5858/arpa.2016-0579-CP
3. Foster SA, Whalen DM, Ozen A, Wongchenko MJ, Yin J, Yen I, et al. Activation Mechanism of Oncogenic Deletion Mutations in BRAF, EGFR, and HER2. *Cancer Cell* (2016) 29(4):477–93. doi:10.1016/j.ccell.2016.02.010
4. Morgillo F, Della Corte CM, Fasano M, Ciardiello F. Mechanisms of Resistance to EGFR-Targeted Drugs: Lung Cancer. *ESMO Open* (2016) 1(3):e000060. doi:10.1136/esmoopen-2016-000060
5. Tumbrink HL, Heimsoeth A, Sos ML. The Next Tier of EGFR Resistance Mutations in Lung Cancer. *Oncogene* (2021) 40(1):1–11. doi:10.1038/s41388-020-01510-w
6. Yun CH, Mengwasser KE, Toms AV, Woo MS, Greulich H, Wong KK, et al. The T790M Mutation in EGFR Kinase Causes Drug Resistance by Increasing the Affinity for ATP. *Proc Natl Acad Sci U S A* (2008) 105(6):2070–5. doi:10.1073/pnas.0709662105
7. Walter AO, Sjin RT, Haringsma HJ, Ohashi K, Sun J, Lee K, et al. Discovery of a Mutant-Selective Covalent Inhibitor of EGFR that Overcomes T790M-Mediated Resistance in NSCLC. *Cancer Discov* (2013) 3(12):1404–15. doi:10.1158/2159-8290.CD-13-0314
8. Diaz LA, Jr, Bardelli A. Liquid Biopsies: Genotyping Circulating Tumor DNA. *J Clin Oncol* (2014) 32(6):579–86. doi:10.1200/JCO.2012.45.2011
9. Fenizia F, De Luca A, Pasquale R, Sacco A, Forgione L, Lambiase M, et al. EGFR Mutations in Lung Cancer: from Tissue Testing to Liquid Biopsy. *Future Oncol* (2015) 11(11):1611–23. doi:10.2217/fon.15.23
10. Wang M, Huang X, Li X, Guo Q, Xu W, Zhao M, et al. Performance Comparison of Commercial Kits for Isolating and Detecting Circulating Tumor DNA. *Scand J Clin Lab Invest* (2021) 81(4):276–81. doi:10.1080/00365513.2020.1821394
11. Ho HL, Huang CC, Ku WH, Ho CL, Lin CH, Yu SL, et al. Liquid Biopsy for Detection of EGFR T790M Mutation in Nonsmall Cell Lung Cancer: An Experience of Proficiency Testing in Taiwan. *J Chin Med Assoc* (2019) 82(6):473–6. doi:10.1097/JCMA.0000000000000100
12. Maass KK, Schad PS, Finster AME, Puranachot P, Rosing F, Wedig T, et al. From Sampling to Sequencing: A Liquid Biopsy Pre-analytic Workflow to Maximize Multi-Layer Genomic Information from a Single Tube. *Cancers* (2021) 13(12):3002. doi:10.3390/cancers13123002
13. Sorber L, Zwaenepoel K, Jacobs J, De Winne K, Goethals S, Reclusa P, et al. Circulating Cell-free DNA and RNA Analysis as Liquid Biopsy: Optimal Centrifugation Protocol. *Cancers* (2019) 11(4):E458. doi:10.3390/cancers11040458
14. Oxnard GR, Thress KS, Alden RS, Lawrance R, Paweletz CP, Cantarini M, et al. Association between Plasma Genotyping and Outcomes of Treatment with Osimertinib (AZD9291) in Advanced Non-small-cell Lung Cancer. *J Clin Oncol* (2016) 34(28):3375–82. doi:10.1200/JCO.2016.66.7162
15. Jenkins S, Yang JC, Ramalingam SS, Yu K, Patel S, Weston S, et al. Plasma ctDNA Analysis for Detection of the EGFR T790M Mutation in Patients with Advanced Non-small Cell Lung Cancer. *J Thorac Oncol* (2017) 12(7):1061–70. doi:10.1016/j.jtho.2017.04.003
16. Li X, Zhou C. Comparison of Cross-Platform Technologies for EGFR T790M Testing in Patients with Non-small Cell Lung Cancer. *Oncotarget* (2017) 8(59):100801–18. doi:10.18632/oncotarget.19007
17. Chouaid C, Dujon C, Do P, Monnet I, Madroszyk A, Le Caer H, et al. Feasibility and Clinical Impact of Re-biopsy in Advanced Non Small-Cell Lung Cancer: a Prospective Multicenter Study in a Real-World Setting (GFPC Study 12-01). *Lung Cancer* (2014) 86(2):170–3. doi:10.1016/j.lungcan.2014.08.016
18. Stockley T, Souza CA, Cheema PK, Melosky B, Kamel-Reid S, Tsao MS, et al. Evidence-based Best Practices for EGFR T790M Testing in Lung Cancer in Canada. *Curr Oncol* (2018) 25(2):163–9. doi:10.3747/co.25.4044
19. Pereira I, Gaspar C, Pina M, Azevedo I, Rodrigues A. Real-World T790M Mutation Frequency and Impact of Rebiopsy in Patients with EGFR-Mutated Advanced Non-small Cell Lung Cancer. *Cureus* (2020) 12(12):e12128. doi:10.7759/cureus.12128
20. Ontario H. Cell-Free Circulating Tumour DNA Blood Testing to Detect EGFR T790M Mutation in People with Advanced Non-small Cell Lung Cancer: A Health Technology Assessment. *Ont Health Technol Assess Ser* (2020) 20(5):1–176.

Pathology & Oncology Research

frontiers

ORIGINAL RESEARCH
published: 12 April 2022
doi: 10.3389/pore.2022.1610024

Methodological Challenges of Digital PCR Detection of the Histone *H3* K27M Somatic Variant in Cerebrospinal Fluid

Margarita Zaytseva[1]*, *Natalia Usman*[1], *Ekaterina Salnikova*[1], *Agunda Sanakoeva*[1], *Andge Valiakhmetova*[1], *Almira Chervova*[1,2], *Ludmila Papusha*[1], *Galina Novichkova*[1] and *Alexander Druy*[1,3]

[1]Dmitry Rogachev National Medical Research Center of Pediatric Hematology, Oncology and Immunology, Moscow, Russia, [2]Epigenomics, Proliferation, and the Identity of Cells, Department of Developmental and Stem Cell Biology, Institut Pasteur, Paris, France, [3]Research Institute of Medical Cell Technologies, Yekaterinburg, Russia

Cell-free DNA (cfDNA) in body fluids is invaluable for cancer diagnostics. Despite the impressive potential of liquid biopsies for the diagnostics of central nervous system (CNS) tumors, a number of challenges prevent introducing this approach into routine laboratory practice. In this study, we adopt a protocol for sensitive detection of the *H3* K27M somatic variant in cerebrospinal fluid (CSF) by using digital polymerase chain reaction (dPCR). Optimization of the protocol was carried out stepwise, including preamplification of the *H3* target region and adjustment of dPCR conditions. The optimized protocol allowed detection of the mutant allele starting from DNA quantities as low as 9 picograms. Analytical specificity was tested using a representative group of tumor tissue samples with known *H3* K27M status, and no false-positive cases were detected. The protocol was applied to a series of CSF samples collected from patients with CNS tumors (n = 18) using two alternative dPCR platforms, QX200 Droplet Digital PCR system (Bio-Rad) and QIAcuity Digital PCR System (Qiagen). In three out of four CSF specimens collected from patients with *H3* K27M-positive diffuse midline glioma, both platforms allowed detection of the mutant allele. The use of ventricular access for CSF collection appears preferential, as lumbar CSF samples may produce ambiguous results. All CSF samples collected from patients with *H3* wild-type tumors were qualified as *H3* K27M-negative. High agreement of the quantitative data obtained with the two platforms demonstrates universality of the approach.

Keywords: cerebrospinal fluid, liquid biopsy, dPCR, cell-free DNA, CNS tumor, diffuse midline glioma, *H3* K27M

OPEN ACCESS

Edited by:
József Tímár,
Semmelweis University, Hungary

***Correspondence:**
Margarita Zaytseva
astice@list.ru

Received: *16 August 2021*
Accepted: *23 March 2022*
Published: *12 April 2022*

Citation:
Zaytseva M, Usman N, Salnikova E, Sanakoeva A, Valiakhmetova A, Chervova A, Papusha L, Novichkova G and Druy A (2022) Methodological Challenges of Digital PCR Detection of the Histone H3 K27M Somatic Variant in Cerebrospinal Fluid. Pathol. Oncol. Res. 28:1610024. doi: 10.3389/pore.2022.1610024

INTRODUCTION

High-grade gliomas are rare tumors which constitute 10%–15% of the central nervous system (CNS) neoplasms in pediatric patients [1]. Clinical characterization of midline gliomas with infiltrative growth is conventionally limited to a diagnosis based on neuroimaging data (including topography, relative signal intensity, and specific patterns of the contrast enhancement), whereas proper histological and molecular verification is complicated, given the tumor location [2]. However, in many cases, the analysis of clinical and radiological parameters cannot provide reliable grading of a CNS tumor.

Basic findings of the last decade have substantially advanced the understanding of molecular pathogenesis of glial tumors in pediatric patients. Wu et al. identified K27M[1] substitution in histone 3.3 in 60% of diffuse intrinsic pontine gliomas [3]. Further studies of molecular landscapes of high-grade gliomas confirmed the high prevalence of *H3* K27M variant in diffuse midline gliomas (DMG). This variant is observed in up to 94% of diffuse brainstem gliomas, 65% of thalamic gliomas, and 60% of spinal cord gliomas [4]. Moreover, the presence of *H3* K27M mutation is a very unfavorable prognostic factor. Accordingly, a distinct nosological entity 'Diffuse midline glioma *H3* K27M-mutant' was added to the 2016 update of the WHO classification of CNS tumors [5]. Verification of such diagnoses implies determination of the *H3F3A* mutational status. Importantly, the detection of *H3* K27M mutation in an infiltrating midline glioma implicates assignment of the tumor as WHO grade IV by definition.

Molecular profiling of malignant gliomas, enabled by modern advances in molecular oncology, allows ultimate specification of the diagnosis and selection of optimal therapies targeted at specific aberrations. Molecular inclusion criteria are increasingly used in clinical trials. The *H3* K27M substitution, in particular, is a prerequisite for the inclusion in currently running trials of anti-DRD2 agent ONC201 as a therapeutic option for *H3* K27M-mutant DMG (NCT03295396 and NCT02525692, both enrolling adult patients, and NCT03416530 enrolling pediatric patients). In this regard, the possibility of using liquid biopsy—an approach based on the presence of cell-free DNA (cfDNA) of tumor cells in biological fluids—is of particular interest. Repeated sampling of body fluids (plasma, serum, cerebrospinal fluid, etc.) provides access to the dynamics of genetic aberrations arising at different stages of tumorigenesis and allows monitoring of the therapy effectiveness [6].

Plasma is certainly the most common source of cfDNA for analysis. Representation of somatic mutations in plasma has been demonstrated for various solid tumors [7]. In 2016, determination of *EGFR* mutations in plasma specimens was approved by FDA as a companion diagnostic test in non-small cell lung cancer patients with poorly accessible tumors [8]. Liquid biopsies can be highly informative for molecular profiling. For instance, osimertinib recipients with *EGFR* mutations determined by using either liquid or conventional biopsy showed similar survival rates [9]. In 2019, FDA approved a diagnostic protocol involving determination of *PIK3CA* variants in cfDNA isolated from plasma of the patients with ER-positive HER2-negative locally advanced or metastatic breast cancer [10]. For patients with CNS tumors, penetration of tumor cfDNA into the blood circulation is hampered by the blood-brain barrier, which excludes the use of plasma for detection of somatic variants in CNS [11,12].

Examination of cerebrospinal fluid (CSF) samples is a promising diagnostic tool for neurooncology. However, the search for tumorigenic genetic aberrations in CSF is nontrivial due to the low concentrations of cfDNA [13,14]. The applicability is further limited by analytical sensitivity of the methods used for the analysis of somatic mutations in cfDNA. Mutations with extremely low allele burden are best identified with digital PCR (dPCR). Currently available dPCR platforms involve droplet- (RainDance Technologies and Bio-Rad), sealed chip- (Thermo Fisher), microfluidic chamber- (Fluidigm), or nanoplate-based workflows (Qiagen). To perform the experiments, we opted for one of the most common Droplet Digital™ PCR platform (Bio-Rad) and a new QIAcuity Digital PCR System (Qiagen).

The aim of this study was to develop a reliable cross-platform dPCR protocol for detection of *H3* K27M variant in cfDNA isolated from CSF of pediatric patients with CNS tumors.

PATIENTS AND METHODS

Study Design

Overall design of the study is presented in **Figure 1**. A retrospective cohort (n = 25) was intended for the protocol development and its analytical characterization on formalin fixed/paraffin embedded (FFPE) tumor tissues. For a prospective cohort (n = 18), FFPE and CSF samples were matched for diagnostic characterization and clinical validation of the protocol. All patients of the prospective cohort, presenting with newly diagnosed or recurrent radiographically-confirmed CNS tumors, were enrolled in the Molecular Diagnostics in Pediatric Neurooncology and Liquid Biopsies Project at the Dmitry Rogachev National Medical Research Center of Pediatric Hematology, Oncology and Immunology. An exclusion criterion was complete surgical resection (R0) determined on the basis of postoperative MRI data, unless CSF sampling has occurred during or before surgery. The Informed Consent for participation in the study was obtained from parents/guardians of all patients. The study was approved by the Institutional Review Board at the Dmitry Rogachev Center.

CSF Collection and Characterization

Clinical and analytical data for CSF donors (prospective cohort) are summarized in **Table 1**. CSF samples (1.0–13.3 ml, n = 19), collected either intraoperatively, or through a ventricular access device, or by lumbar puncture, were clarified by centrifugation at 1,100 g for 10 min and stored in 1 ml aliquots at −80°C. The samples were thawed immediately before cfDNA isolation. Cell-free DNA was isolated with the use of QIAmp Circulating Nucleic Acid Kit (Qiagen, the Netherlands). Concentrations of amplifiable fragments were measured by DNA Fragmentation Quantification Assay (EntroGen, United States). The cfDNA profiles were analyzed with the use of Cell-free DNA ScreenTape Assay Reagent Kit (Agilent Technologies).

Protocol Development

The protocol was adapted and optimized using the Droplet Digital™ PCR platform (Bio-Rad) for FFPE tumor tissues

[1]The H3 K27M substitution is designated in accordance with the nomenclature of histone modification sites established in scientific literature. In the HGVS sequence variant nomenclature (http//www.hgvs.org), this variant corresponds to *H3F3A*: c. 83A>T, p.(K28M).

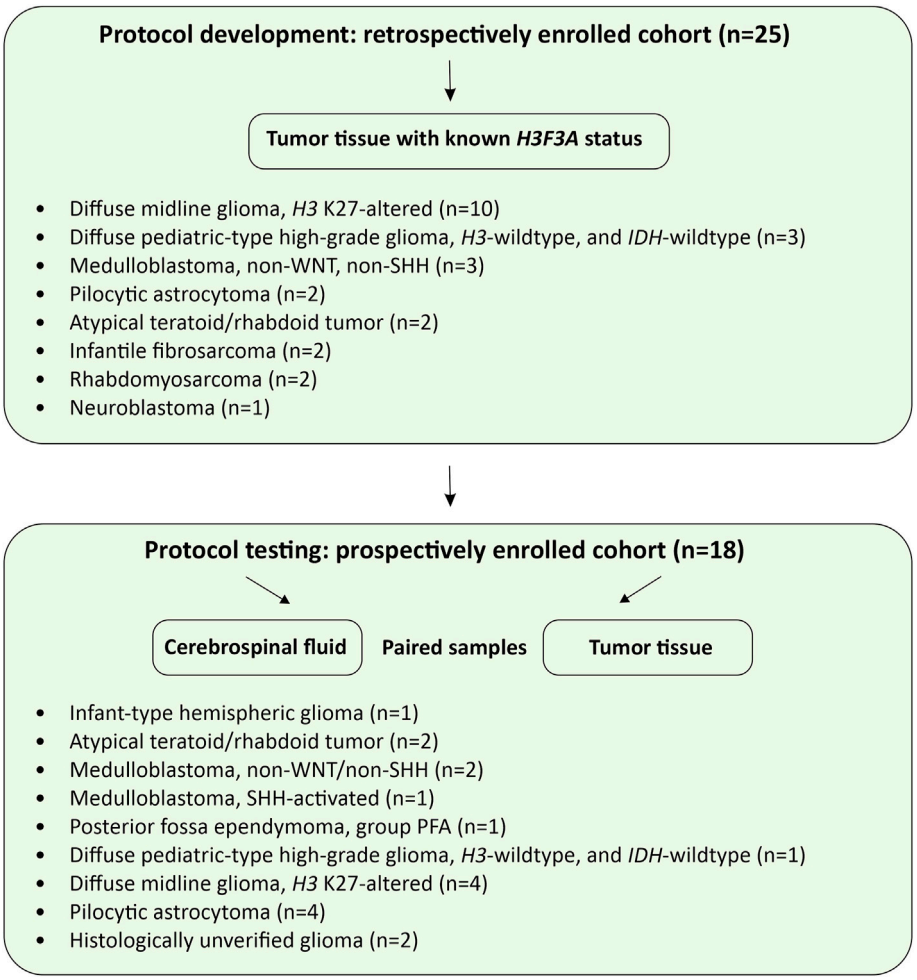

FIGURE 1 | Study design. The flow charts illustrate protocol development and pilot testing on CSF-derived cfDNA.

specimens of the retrospective cohort (n = 25, **Figure 1**) with the known *H3F3A* K27M status determined by Sanger sequencing (**Supplementary Table S1**). Genomic DNA was isolated from the tumor tissues using FFPE RNA/DNA Purification Plus Kit (Norgen Biotek, Canada). The degree of fragmentation corresponding to cfDNA was modeled by shearing in a Covaris M220 Focused-Ultrasonicator (Covaris, United States) in a standard 150 bp mode. The DNA was subsequently purified and concentrated with AMPure XP beads (Beckman Coulter, United States) and quantified on a Qubit 3.0 fluorometer (Thermo Fisher Scientific, United States) with Qubit dsDNA BR Assay Kit (Thermo Fisher Scientific). Representation of different fragment lengths (37 bp, 150 and 300 bp) was evaluated using DNA Fragmentation Quantification Assay (EntroGen, United States) and additionally by automated electrophoresis in a TapeStation 2200 system (Agilent Technologies, United States) with the use of High Sensitivity DNA ScreenTape Analysis Reagent Kit (Agilent Technologies).

Due to the expected low concentrations of the *H3F3A* target in cfDNA, the preamplification step was introduced to increase the sensitivity of dPCR assay. The reactions were set in 25 µl of 1× PCR buffer B (Syntol LLC, Russia) containing 50 nM of primers, 0.25 mM dNTPs, 2.5 mM $MgCl_2$ and 0.1 U/µl Taq polymerase (Syntol LLC) with 50–100 copies of 150 bp DNA fragments per reaction. Preamplification was run in a T100 thermal cycler (Bio-Rad) at 98°C for 1 min, followed by eight cycles of 98°C for 10 s, 58°C for 30 s and 72°C for 30 s, followed by 72°C for 2 min. The product was diluted 1:1 with TE buffer and used in dPCR with LNA-modified allele-specific probes. The reactions were set in duplicates, each comprising 20 µl of 1× ddPCR Supermix for Probes (No dUTP) (Bio-Rad, United States) with the primers and probes added to final concentrations of 1,800 nM and 500 nM, respectively. The process was run in a C1000 Touch Thermal Cycler (Bio-Rad) equipped with a QX200 Droplet Digital PCR (ddPCR) system (Bio-Rad) at 95°C for 10 min, followed by 40 cycles of 94°C for 30 s (ramp 2°C/s) and 57°C for 60 s (ramp 2 °C/s), followed by 98°C for 10 min. The data were processed and analyzed in

TABLE 1 | Patient data[a] with specification of tumors and cfDNA content in CSF.

#	Age of onset	Gender	Integrated diagnosis[b]	Tumor volume, cm^{3c}	Time of CSF collection	CSF collection procedure	CSF sample volume, ml	37 bp fragment concentration, copies/µl	150 bp fragment concentration, copies/µl	300 bp fragment concentration, copies/µl	*H3* K27M in tumor tissue	*H3* K27M in CSF
1	5 months	Female	Infant-type hemispheric glioma, *ETV6-NTRK3*-positive	345	Primary	VAD	3	16,793	15,170	8,583	-	-
2	3 months	Female	Atypical teratoid/rhabdoid tumor, *SMARCB1*-mutant	99.5	During therapy	VAD	2.4	2,972	1,486	546	-	-
3	2 years 10 months	Male	Atypical teratoid/rhabdoid tumor, NOS	9.5	During therapy	VAD	2.8	676	417	306	-	-
4	1 year 11 months	Female	Anaplastic medulloblastoma, non-WNT/non-SHH	12.2	During therapy	VAD	4	361	122	101	-	-
5	5 years 5 months	Male	Desmoplastic medulloblastoma, SHH-activated, *TP53*-wildtype, *PTCH1*-mutant	0.44	Metastatic relapse	VAD	2.5	53	35	20	-	-
6	11 years 5 months	Male	Medulloblastoma, non-WNT/non-SHH	26.3	Primary	IO	2	0	0	0	-	NA
7	5 years 2 months	Male	Posterior fossa ependymoma, group PFA	2.2	Local relapse	IO	4	973	683	669	-	-
8	10 years 8 months	Male	Diffuse pediatric-type high-grade glioma, *H3*-wildtype, and *IDH*-wildtype	140	Primary	IO	4	64	47	142	-	-
9	11 years 11 months	Female	Diffuse midline glioma, *H3* K27-altered	37.4	After surgery	LP	3	16	10	0	+	+
10	5 years 1 month	Male	Diffuse midline glioma, *H3* K27-altered	16	Primary	LP	2	1	3	4	+	?
11	5 years 7 months	Male	Diffuse midline glioma, *H3* K27-altered	14	Primary	IO	13.3	66 320	108 165	87 137	+	+
						LP	1	4	7	3		?
12	11 years 2 months	Male	Diffuse midline glioma, *H3* K27-altered	87	Primary	IO	10	27 19	14 8	6 9	+	+
13	6 years 9 months	Male	Optic chiasm pilocytic astrocytoma, NOS	10	Primary	VAD	5	106	81	51	NA	-
14	1 month	Male	Pilocytic astrocytoma, *KIAA1549* (exon 15)—*BRAF* (exon 9)—positive	134	During therapy	VAD	4.8	387	108	67	-	-
15	7 years 3 months	Male	Pilocytic astrocytoma, *KIAA1549* (exon 16)—*BRAF* (exon 9)—positive	2.9	Primary	LP	3.5	0	0	0	—	NA
16	9 months	Female	Pilocytic astrocytoma, *KIAA1549* (exon 15)—*BRAF* (exon 9)—positive	74	Local relapse	IO	1.2	0	0	0	—	NA
17	8 years 8 months	Female	Histologically unverified bilateral thalamic tumor with midbrain extension (suspected high-grade glioma)	142	Primary	VAD	2	9	6	0	NA	-
18	4 years 10 months	Female	Histologically unverified tumor of the right cerebral peduncle and basal ganglia on the right (suspected low-grade glioma)	16.4	Primary	LP	2	2	0	0	NA	NA

[a]*Sorted roughly by morphological assignment.*

[b]*Based on the 2021 WHO Classification of Tumors of the Central Nervous System [15].*

[c]*Tumor volume at the time of CSF collection.*

NA, no data available; VAD, ventricular access device; IO, intraoperatively; LP, lumbar puncture.

QuantaSoft Version 1.6.6.0320 (Bio-Rad). Fluorescence thresholds (respectively, 2,000 and 1,500 RFU for FAM and HEX) were set manually.

Oligonucleotide sequences of primers and probes previously published in [16] were as follows: forward *H3* K27M: 5′-GGTAAAGCACCCAGGAAG-3′; reverse *H3* K27M: 5′-CAAGAGAGACTTTGTCCC-3′; wild-type probe: 5′-HEX-TC^{+}GC^{+}A^{+}A^{+}GA^{+}GT^{+}GC-RTQ1-3′; K27M probe: 5′-6-FAM-TC^{+}GC^{+}A^{+}T^{+}GA^{+}GTGC-RTQ1-3′, with "locked" nucleic acid-modified (LNA) bases indicated by^{+}. LNA-modified allele-specific probes are known to increase dPCR specificity. Distinctive structural feature of LNA residues is the methylene bridge between atomic positions O2′ and C4′ of furanose, which locks the sugar in 3′-*endo* conformation thus enhancing hybridization of the probe with the template. Introducing LNA-monomers into oligonucleotide sequences significantly improves their discriminating capacity in the recognition of single-nucleotide substitutions [17].

Compatibility of the Developed Protocol With QIAcuity™ Digital PCR System

The optimized protocol was tested for compatibility with the nanoplate-based digital PCR system (Qiagen) technologically different from the water-oil emulsion droplet-based PCR platform (Bio-Rad). The mixtures were set up in duplicates with QIAcuity Probe PCR Kit in Nanoplate 8.5K 96-well plates (Qiagen). The reactions, containing 3 µl 4× Probe PCR Master Mix, 1.2 µl primer–probe mix, 5 µl DNA template, and 2.8 µl RNase-free water in 12 µl total volume each, were run in a QIAcuity One instrument (Qiagen). The analysis was carried out with the use of QIAcuity Software Suite (Qiagen). Fluorescence thresholds for optimal resolution and cloud clustering, selected manually to fit all reactions, constituted 40 and 20 RFU for FAM and HEX, respectively. To enhance the accuracy of concentration measurements, the Volume Precision Factor (VPF), adjusting for tiny variations in nanoplate geometry, was applied as recommended by the manufacturer.

Statistics

To quantitatively describe the dependence of dPCR outputs on reaction parameters (preamplification cycle number and template copy number), regression lines and determination coefficients were calculated in Microsoft Excel 2016. Bland–Altman test was used to assess quantitative agreement between the Droplet Digital™ PCR (Bio-Rad) and the QIAcuity™ Digital PCR System (Qiagen) based on the mean difference and standard deviation. The estimated concentrations of the target in starting samples were expressed in $\log_{10}$ copies/µl. Non-paired measurements (i.e., with missing value for an alternative platform) were excluded from the analysis.

RESULTS

Optimization of the Protocol

The *H3F3A* target preamplification protocol, as well as ddPCR settings and conditions, were optimized in order to increase the analytical sensitivity and specificity of the *H3* K27M variant determination. The optimality was defined as a combination of high number of positive droplets with robust cloud separation and minimal "rain" effects (a fraction of droplets showing sub-threshold fluorescence).

The optimization was carried out by varying preamplification cycle number (4, 6, 8, or 10), annealing temperatures and concentrations of the oligos, as well as the number of DNA copies at the start of the reaction. The exponential dependence of the ddPCR-detectable amount of DNA target on the preamplification cycle number (**Figures 2A,B**) allows significant boost in representation of the target. **Figure 2C** demonstrates the dependence of ddPCR outcomes on the number of DNA template copies at the start of the reaction when using eight cycles of preamplification of the *H3F3A* fragment. The analyses were set in duplicates for each sample. The data indicate that eight cycles of preamplification of the *H3F3A* gene fragment are necessary and sufficient for optimal cluster density and accurate interpretation of the results of ddPCR with 50–100 copies of the template at the start of preamplification. Representative examples of primary ddPCR data for different reaction conditions are shown in **Figure 3**.

The protocol was further optimized by adjusting annealing temperatures of ddPCR primers (within the range of 53–61°C) and final concentrations of the primers and probes in the reactions. Oligonucleotide concentrations were tested extensively within the range of 900–2,700 nM with a step of 300 nM for the primers and 250–750 nM with a step of 125 nM for the probes. Reducing the probe concentration to values below 500 nM resulted in the reporter fluorescence in HEX channel too low for reliable cloud separation. Elevated concentrations of oligonucleotides in the mixture increased the overall intensity of fluorescence but negatively affected specificity of the reaction. High concentration of the FAM-labeled fluorescence probe specific for the H3 K27M allele led to the non-specific annealing of the probe to the normal allele. This resulted in the ambiguous appearance of the small amount (less than 50 in two technical replicates) of positive droplets with fluorescence above 2,000 RFU in the FAM channel in samples with absence of the *H3* K27M substitution. Such results were considered as false positive (ambiguous sample). A sample containing at least 50 droplets with above-the-threshold fluorescence in the FAM channel and reproducible in two technical replicates was considered positive. In contrast, a sample containing more than 50 droplets with above-the-threshold fluorescence in the HEX channel and less than 50 droplets with above-the-threshold fluorescence in the FAM channel in the total number of duplicates and reproducible in two technical replicates was considered negative.

The optimal fluorescence levels and maximal ddPCR efficiency were achieved at eight cycles of preamplification with 50–100 copies of DNA template and annealing temperatures of 58°C and 57°C for preamplification and ddPCR, respectively. The clearest cluster separation efficiency was achieved with 1,800 nM of the primers and 500 nM of the probes. The uniform threshold values of the fluorescence intensity, above which the droplets were regarded as positive,

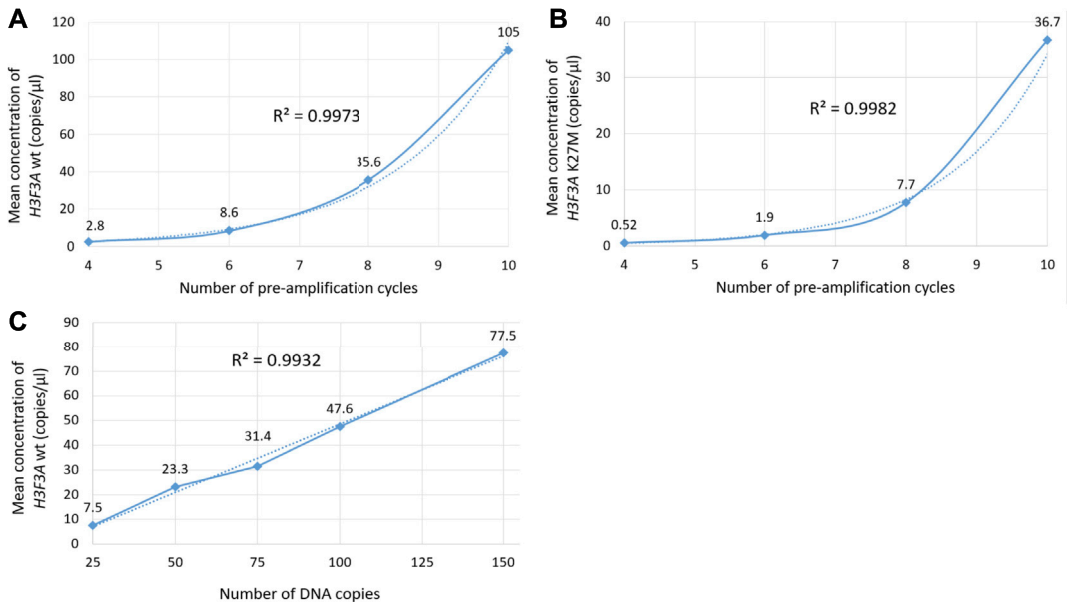

FIGURE 2 | Evaluation of ddPCR outputs for different reaction conditions. Plots **(A,B)** represent the dependence of the outputs of the *H3F3A* K27M mutant and *H3F3A* wild-type targets (for the samples with and without mutation, respectively) on the preamplification cycle number with 50 copies of DNA target at the start of the reaction. Plot **(C)** represents the dependence of the yields of wild-type target on the number of DNA copies at the start of preamplification (eight cycles). The dotted lines are estimated trends, R^2 are correlation coefficients.

were set manually. The thresholds for FAM and HEX signals constituted 2,000 and 1,500 RFU, respectively. Typical results of ddPCR obtained before and after the optimization experiments are shown in **Figure 4**. The optimized parameters of the developed ddPCR-based system are described in the Patients and Methods section.

Analytical Characterization of the Protocol

Analytical sensitivity of the modified ddPCR protocol was tested using a series of 10 sequential two-fold dilutions of genomic DNA comprising the studied *H3* K27M variant, with concentrations descending from 600 to 1 pg/µl of DNA at the start of preamplification. The reactions were carried out in two technical replicates. The sensitivity threshold was determined by minimal dilution affording at least 50 droplets with above-the-threshold fluorescence in at least one of the channels in total counts for the duplicates (**Figure 5**). The limit of detection for the *H3* K27M variant determined with the use of optimized ddPCR protocol was 9 pg of DNA (corresponding to 3 haploid genomes).

Analytical specificity of the developed ddPCR-based approach was tested using a selection of genomic DNA samples isolated from tumors with known *H3* K27M status determined by Sanger sequencing (the retrospective cohort, **Figure 1**). The lack of positive signals for *H3* K27M-negative samples confirmed full specificity of the developed protocol (see **Supplementary Table S1**).

Primary Validation for the Diagnostics

PCR-based assay of representation/integrity of amplifiable cfDNA in the studied samples revealed wide variation. For pts. 6, 15, 16, and 18, insufficient analytical quality of the isolates was indicated by the absence of ≥150 bp DNA fragments; these samples were excluded from further analysis as non-informative. In other samples, the concentrations ranged from 3 to 15,170 copies/µl with a median of 81 copies/µl for the working fragment length of 150 bp (**Table 1**).

The developed ddPCR-based system was applied for determination of the *H3* K27M somatic variant in cfDNA isolated from CSF. The analysis of CSF-derived cfDNA was validated against matching samples of FFPE tumor tissue by Sanger sequencing. The studied variant was identified in specimens #9–12 implicating the diagnosis of DMG *H3* K27-altered. FFPE specimens #1–8 and #14–16 were *H3* K27M-negative, and no solid bioptates were available for pts. 13, 17, and 18 (**Table 1**).

In sum, 14 ventricular (6 collected intraoperatively and eight from a ventricular access device), and 5 lumbar CSF samples were analyzed, corresponding to 18 patients with CNS tumors grade I–IV. In three out of four *H3* K27M-positive cases, the mutation was unequivocally identified in ventricular (pts. 11 and 12) or lumbar CSF (pt. 9). For pt. 11, both ventricular and lumbar CSF samples were available. Interpretation of the results for ventricular CSF was straightforward whereas analysis of the lumbar sample produced ambiguous results—solitary high-intensity signals in two channels (i.e., for both alleles) independently of dPCR platform. Comparative representation of these data is given in **Figure 6**. It is important to note that variant allele frequencies (VAFs) measured by these two platforms were identical and did not depend on the use of preamplification step. At the same time, VAFs in CSF were considerably lower compared with tumor tissue (37% vs. 51.3%).

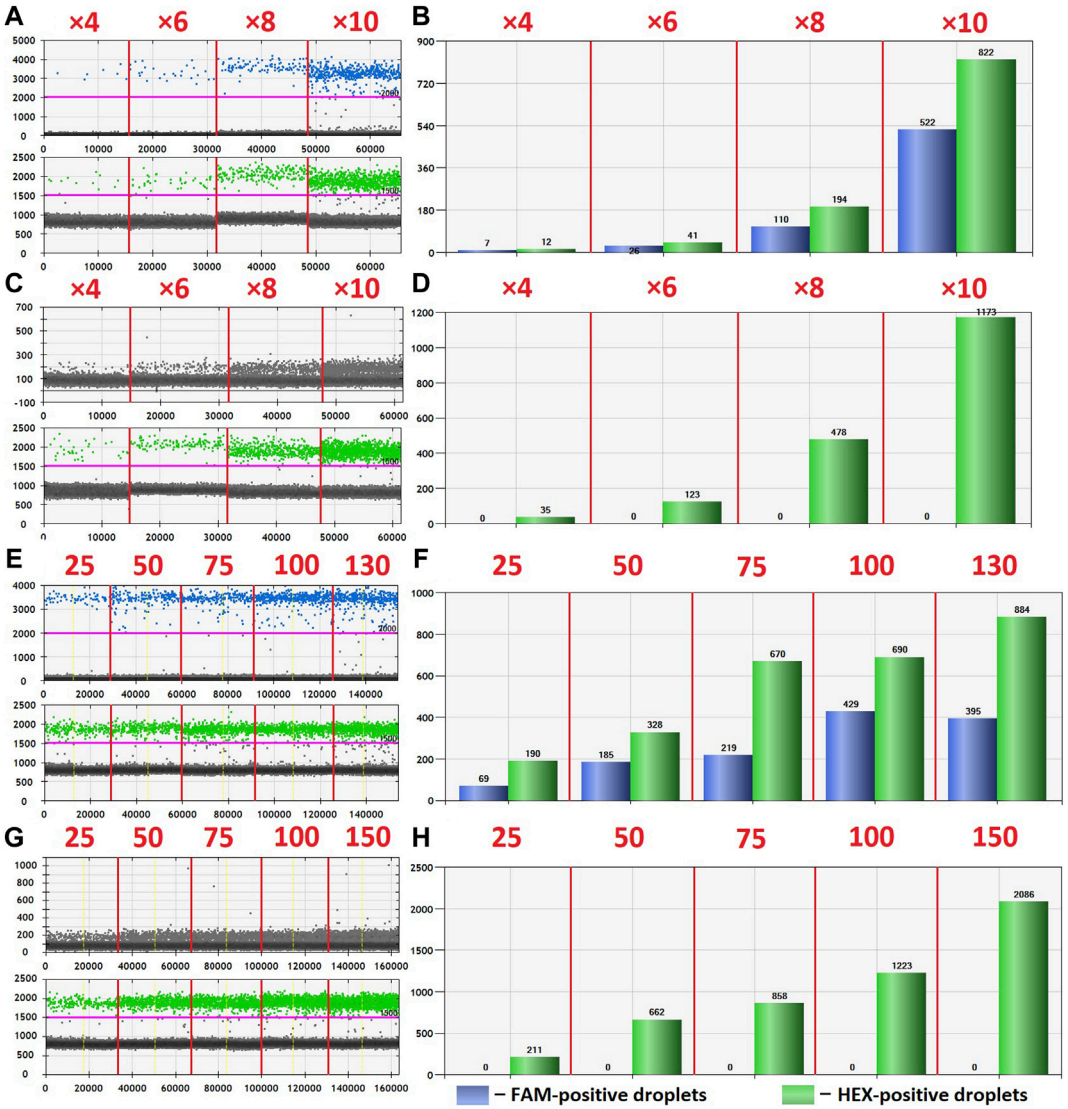

FIGURE 3 | Primary ddPCR data for different reaction conditions, visualized in QuantaSoft Version 1.6.6.0320 (Bio-Rad). Varying the preamplification cycle number with 50 copies of the target fragment at the start of the reaction: **(A,B)**—sample with *H3* K27M mutation; **(C,D)**—sample without *H3* K27M mutation (wild-type *H3F3A* allele); preamplification cycle numbers (4, 6, 8, or 10) are indicated at the top of the panels. Varying the number of target DNA copies at the start of the reaction with eight cycles of preamplification: **(E,F)**—sample with *H3* K27M mutation; copy numbers of the target at the start of the reaction (25, 50, 75, 100, or 130) are indicated at the top of the panel; **(G,H)**—sample without *H3* K27M mutation (wild-type *H3F3A* allele); copy numbers of the target at the start of the reaction (25, 50, 75, 100, or 150) are indicated at the top of the panel.

For pt. 10, only lumbar CSF with extremely low yields of cfDNA was available for the analysis, producing the same uninterpretable result despite preamplification.

All CSF samples from patients with *H3* K27M-negative tumors (n = 11) produced negative results in dPCR for *H3* K27M substitution, which indicates high diagnostic specificity of the developed protocol.

Diagnostic Sensitivity Assay

The accuracy of quantitative analysis for samples containing small amounts of genetic material (10–100 copies of DNA template) is limited by stochastic sampling. For small DNA copy numbers, the variation in the number of mutant alleles taken from the extracted volume of cfDNA and introduced into the preamplification reaction is described by the classical Bernoulli test scheme, and for copy numbers of 100 and above, according to the Moivre-Laplace limit theorem, by the Gaussian (normal) distribution [18]. In ordinary terms, with increasing concentrations of cfDNA, the probability of capturing the *H3* K27M mutant allele into the analyzed pool of molecules increases. To describe the influence of the initial abundance of the mutant allele on the ddPCR outcome, the *H3F3A* target was amplified from 65, 50, 25, or 12 copies of the template (sample #9) at the start of

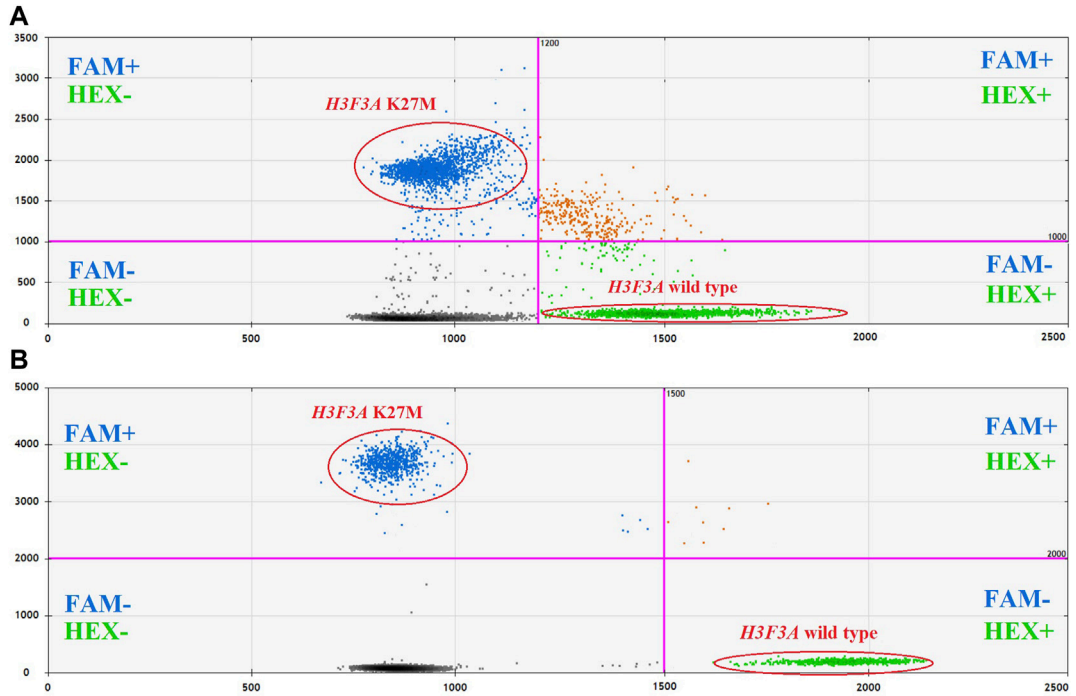

FIGURE 4 | 2D cluster plots of dual channel droplet fluorescence, Channel 1 (FAM) corresponding to *H3F3A* K27M vs. Channel 2 (HEX) corresponding to wild-type *H3F3A* (pt. 11, tumor DNA). Typical data obtained before **(A)** and after **(B)** optimization of the protocol.

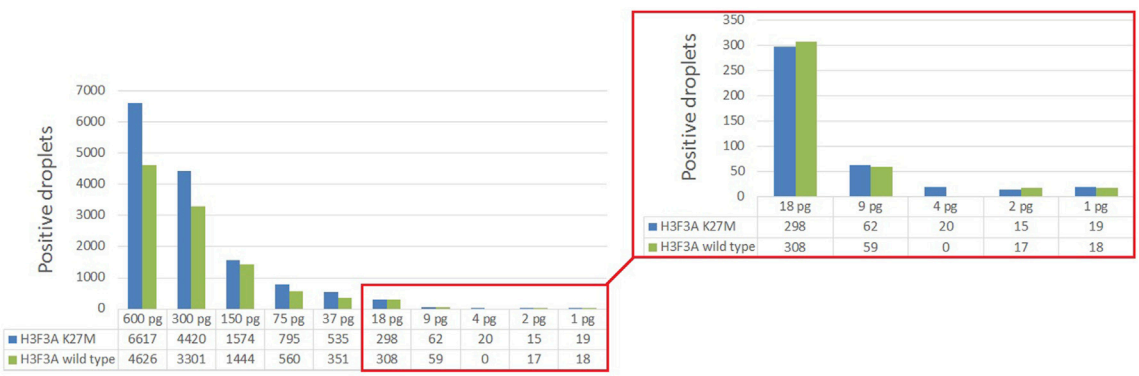

FIGURE 5 | Determining the lower limit of *H3* K27M detection by ddPCR.

preamplification. Comparative representation of the outcomes for different amounts of the template is given in **Figure 7**.

The number of copies of the DNA fragment-of-interest produced in the reaction at time t can be calculated as follows:

$$n = f(k)k\exp(tv),$$

where n is DNA copy number after PCR, k—DNA copy number at the start of the reaction, v—reaction rate, t—time, and $f(k)$ is a threshold function of k, $f(k) = \{0$ at $k < h$; 1 at $k \geq h\}$, with h regarded as the threshold value.

The known number of DNA copies at the start of the reaction enables estimation of the expected number of amplified DNA fragments. Considering that $k = 65$ DNA copies at the start of the reaction corresponds to $n = 1{,}574$ positive droplets in the FAM channel, we get $\exp(tv) = 24.2$. Accordingly, at $k = 50$, the expected number of amplified molecules will be $n = 1{,}210$, but only if k is not below the threshold value h; otherwise, $n = 0$. Thus, the empirical value of $n = 3$ is an artifact and should be replaced with a zero value. Similarly, at $k = 25$, the expected number of amplified copies will be $n = 605$, and at $k = 12$ it will be $n = 290$. In accordance with this model, the numbers of positive droplets

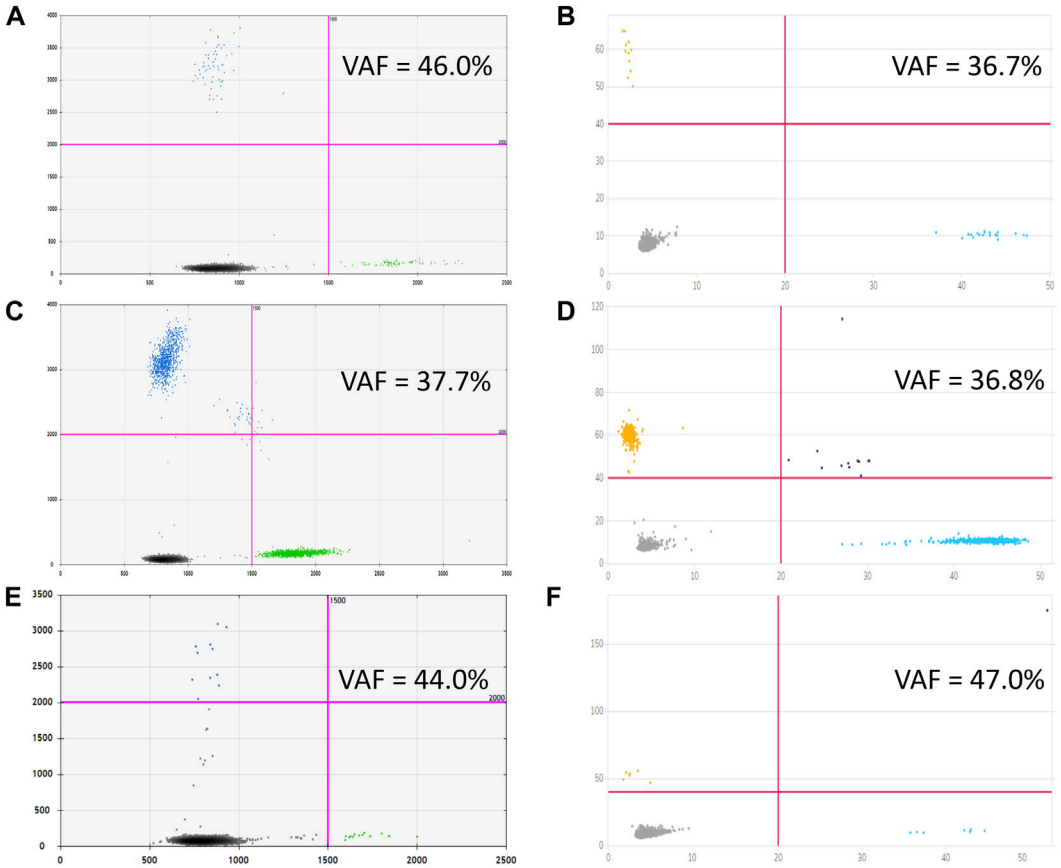

FIGURE 6 | Graphical outcomes of dPCR with **(C,D)** and without **(A,B)** preamplification step, performed on Droplet Digital™ PCR **(A,C)** and QIAcuity™ Digital PCR **(B,D)** platforms for ventricular CSF, to be compared with cumulative plots, comprising four reaction replicas each, obtained from lumbar CSF with preamplification [Droplet Digital™ PCR, **(E)**, and QIAcuity™ Digital PCR, **(F)**].

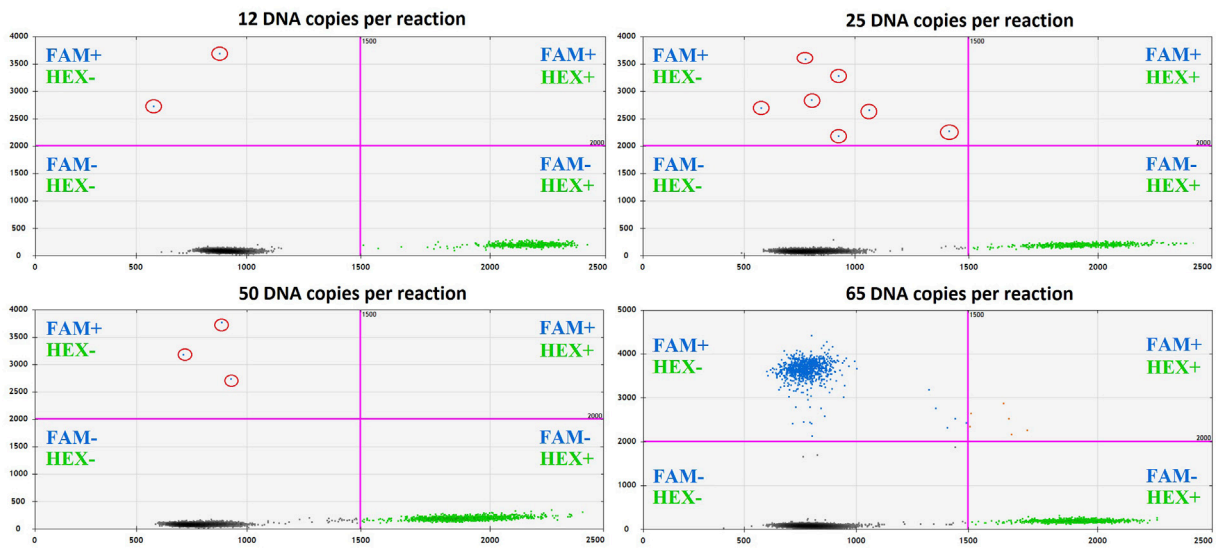

FIGURE 7 | The impact of cfDNA template load on the ddPCR result (sample #9).

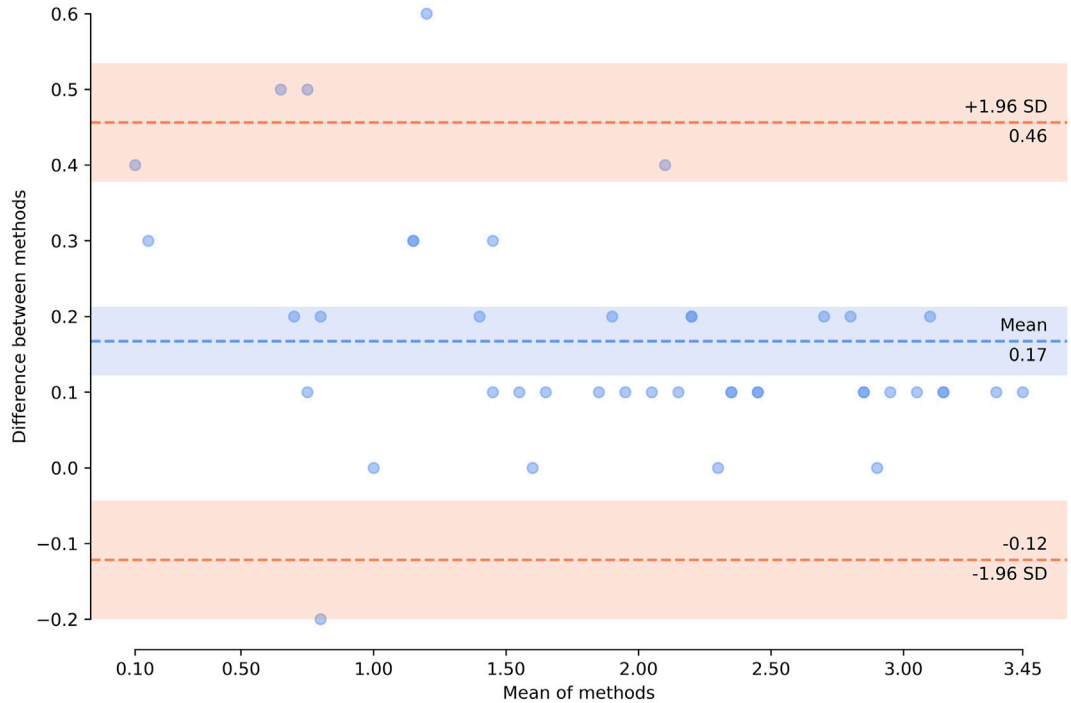

FIGURE 8 | Bland–Altman plot showing agreement of the results obtained by using two technological platforms—Droplet Digital™ PCR and QIAcuity™ Digital PCR System. Horizontal axis represents $\log_{10}$ (mean concentration of the target, copies/µl, in the starting sample). Vertical axis shows $\log_{10}$ (difference between the methods); blue dashed line represents the mean difference; red dashed lines represent the limits of agreement (mean difference ±1.96 × SD). Zero concentration values were excluded from the analysis. The plot was created using pyCompare (http://doi.org/10.5281/zenodo.1238915).

(measured in the FAM channel corresponding to the mutant allele) are valid only for the case of 65 copies of the template at the start of the reaction. However, this value could vary depending on VAF in the tumor and should not be considered as a threshold level, but only as the explanation for the appearance of single positive droplets. It's important to note that in the described case #9 *H3* K27M VAF was relatively low—14%.

The appearance of the low amount (<2) of the positive droplets has been seen after preamplification in several samples with confirmed H3 wild type status belonging to patients with the infant-type hemispheric glioma, *ETV6-NTRK3*-positive (sample #1), posterior fossa ependymoma, group A (sample #7), diffuse pediatric-type high-grade glioma, H3-wildtype, and IDH-wildtype (sample #8) and pilocytic astrocytoma, *KIAA1549* (exon 15)—*BRAF* (exon 9)—positive (sample #14). The presence of such droplets confirms their artefactual origin. The explanations of the appearance of the solitary droplets are either spontaneous cleavage of the fluorescence probe or its unspecific binding to the wild-type allele.

At the same time, CSF derived cfDNA samples from patients with *H3* K27M altered tumors provided adequate positive results beginning from significantly lower amounts of the input DNA (19 copies/µl, sample#11.1 and 31 copies/µL, sample#12.1) compared to 65 copies/µl. Remarkably, the VAF in both of this cases were higher (22 and 60%, respectively), comparing to the sample #9. Single mutant allele copies in the starting material could provide solitary positive droplets (samples#10 and 11.5), but extremely low overall cfDNA input prevents an unambiguous interpretation of the results.

Comparative Evaluation of Different Technological Platforms

The optimized protocol was tested using an alternative digital PCR technology platform (QIAcuity™) to evaluate its universality. Analytical consistency between the platforms was evaluated using Bland–Altman method. The analysis was performed on cfDNA with and without preamlification step. A total of 43 paired measurements were analyzed; four measurements, performed on a single dPCR platform, were excluded from the analysis given the lack of pairness. Due to high volume of CSF collected from patients 11 and 12, nucleic acids were isolated in quadruplicates and in duplicates, respectively (all included in the analysis); see **Supplementary Table S2** for the raw data.

Bland-Altman analysis (**Figure 8**) showed that the bias (mean difference) was 0.17 $\log_{10}$ copies/µl, with a standard deviation (SD) of 0.15 $\log_{10}$ copies/µl. For the vast majority of measurements (39 of 43, 90.7%), the results showed marked pairwise consistency of concentration values for mutant and wild-type alleles obtained with the two platforms, falling within the ±1.96 SD limit of agreement (−0.12. . .0.46 $\log_{10}$ copies/µl). The rest of the differences (4 of 43, 9.3%) were

outside the limits of agreement. For three of these outliers (two wild-type and one comprising the mutation), concentration values obtained with QIAcuity exceeded the differences, ranging from 0.52 to 0.60 $\log_{10}$ copies/μl. For one of the outliers, the concentration of mutant allele obtained with QX200 was higher (−0.22 $\log_{10}$ copies/μl). It should be noted that all differences falling outside the limits of agreement corresponded to non-preamplified cfDNA. Concentration values obtained with the use of preamplification had lower discrepancy between the platforms (−0.01. . .0.37 vs. −0.22. . .0.6 $\log_{10}$ copies/μl).

Overall, the results of *H3F3A* K27M mutant and *H3F3A* wild-type target quantification obtained with the QIAcuity dPCR system were comparable with those obtained with the QX200 ddPCR platform, which indicates universality of the developed protocol.

DISCUSSION

Current standards for the diagnosis and management of CNS tumors include histological examination of tumor tissue followed by search for molecular markers [2]. Cell-free DNA in biological fluids represents an invaluable source of information on mutational landscape of a tumor. In neurooncology, alternative ways of studying genetic aberrations are crucially important, as conventional biopsies are unfeasible due to specific localization and nature of the tumor.

However, the use of liquid biopsies for CNS tumors is challenging. Firstly, there are no clear indications for molecular examination of CSF. The efficacy depends on combinations of many factors, including tumor characteristics (histopathology, grade, type of growth in relation to surrounding tissues and liquor spaces, metastatic potential), as well as the methods for CSF collection (ventricular access or lumbar puncture) and its timing (at manifestation, at recurrence, or during treatment). Secondly, in connection with the low stability of cells and cell-free nucleic acids in *ex vivo* CSF, concentration and quality of CSF-derived cfDNA should be expertly evaluated prior to genetic testing. It should be noted that representation of mutant alleles in cfDNA is normally reduced due to 1) intra-tumor heterogeneity and 2) the admixture of non-tumor cfDNA. According to Pan et al., concentrations of cfDNA obtained from CSF of patients with CNS tumors fall within a wide range of 5.5–1,845.0 pg/μl with a median of 25 pg/μl; notably, for high-grade tumors, diagnostic sensitivity to somatic variants in cfDNA is significantly higher [13]. Wang et al. have also demonstrated that the use of CSF-derived cfDNA for molecular profiling of low-grade CNS tumors is non-informative [19]. In our setting, concentrations of 150 bp fragments, indicating cfDNA suitable for dPCR analysis, were 0–15,170 copies/μl (median 35 copies/μl), with a tendency towards higher values observed for high-grade tumors.

As reported by Zhao et al., patients with glial tumors invading ventricular cavities or bordering subarachnoid cisterns have significantly higher CSF levels of cfDNA than patients with similar tumors confined within the anatomical boundaries of nervous tissue [20]. Connolly et al. have demonstrated unfeasibility of using CSF liquid biopsies for patients with intramedullary spinal ependymomas and associated it with negligible cfDNA diffusion into CSF, as the tumor is localized inside the spinal cord, beneath the pia mater which effectively separates the tumor mass from subarachnoid space [21]. In our setting, for pt. 7 with aggressive posterior fossa ependymoma group A, the ventricular CSF-derived cfDNA concentration was high (683 copies/μl) due to the vicinity of the fourth ventricle, despite low volume of the tumor and the absence of metastatic spread.

In the context of liquid biopsies, the topography of CSF sampling matters. Undoubtedly, the use of CSF samples obtained by relatively non-invasive methods from patients with suspected brain tumors would be a preferable option. Presence a ventriculoperitoneal shunt enables CSF collection with the minimal invasive burden. However, a closer look at published evidence on liquid biopsies from CNS tumors reveals the predominance of intraoperative sampling [13,19-21]. Mean cfDNA concentrations for intracranial CSF samples are significantly higher than for preoperative lumbar samples (e.g., 73.33 *cf.* 7.31 pg/μl, respectively [22]), hence the higher efficacy of genotyping for CSF samples collected intraoperatively.

Despite the significantly reduced concentrations of cfDNA in CSF derived by lumbar puncture, Fujioka et al. detected mutations in *IDH1*, *TERT*, or *H3* genes in six of seven high-grade glioma cases [22]. At the same time, On et al. were able to unequivocally identify *H3* K27M mutation in only 1 of 10 CSF samples obtained by lumbar puncture from newly diagnosed DMG patients; for three other cases in this cohort, the result was ambiguous, as only 1-2 mutant droplets were observed in ddPCR charts [23]. In our experience, concentrations of lumbar CSF-derived cfDNA (0–10, median 3 copies/μl) were also lower compared with the isolates obtained from ventricular CSF (0–15,170, median 94.5 copies/μl). This situation reflects lower levels of wild-type positivity observed in dPCR with lumbar CSF-derived templates. We encountered two lumbar CSF samples from *H3* K27M-positive DMG patients, similar to those described by On et al. [23]—with low cfDNA concentrations and single positive signals in dPCR charts. For one of them, ventricular CSF was also available, and the result was interpreted unambiguously (**Figure 6**). Indeed, in cases of extremely low cfDNA concentrations, interpretation of dPCR results may be challenging, as distinguishing between the non-specific trace degradation of the probe (sporadic high-fluorescence droplets) and weak specific signals is impossible.

In addition to the difficulties in CSF sample collection and primary handling, their advanced molecular analysis is sophisticated. Modern strategies for analysis of somatic mutations in cfDNA are based on the use of targeted high-throughput sequencing [12-14,19-21] or dPCR [14,16,21,23,25]. Apart from being an established method for detecting extremely low allelic loads, dPCR provides the unique ability to quantify target DNA without external standards. A number of technological platforms for dPCR are available, each of which has been comprehensively characterized on its own, whereas studies involving their comparison are scarce [24,25]. Here we demonstrate comparability for the highly competitive Droplet Digital™ PCR platform (Bio-Rad) and the relatively novel QIAcuity Digital PCR System (Qiagen). Quantitation of target at the start of dPCR involves a Poisson-based computational model. The value depends on three parameters: number of positive signals, total number of signals, and the reaction compartment volume. The two

platforms used in this study operate under constant partition volume (droplet or plate cell). The total amount of signals (including both positive and negative) is defined by technical characteristics of the method—the counts of generated droplets for ddPCR™ or plate type (8.5k or 26k QIAcuity Nanoplate) for QIAcuity—and the number of replicates. The number of replicates, in turn, is limited by amount of cfDNA isolated from a CSF sample. The output of positive signals is determined solely by amount of target directly introduced in dPCR. Thus, increasing the absolute number of template molecules (as a sum total for all replicates) is the only means for enhancing the accuracy of analysis.

Preamplification step can be introduced in the protocol in order to increase representation of the target at the start of dPCR. This adjustment to the protocol is especially recommended for low quantities of starting material, as it ensures higher sensitivity of the analysis via target-specific enrichment. Increased numbers of target molecules at the start of the reaction allows it to outrun the background resulting from trace degradation of the probe [26]. The concentration measurements for the *H3* mutant and wild-type templates, obtained with alternative dPCR platforms by Bio-Rad and Qiagen, showed lower discrepancy upon the use of preamplification which, for its part, had no influence on the VAF estimates by dPCR.

Martínez-Ricarte et al. studied the mutational profile of CSF-derived cfDNA for a cohort of 20 patients with diffuse glioma. By using ddPCR, the authors identified *H3F3A* K27M in three patients with DMG, with VAFs within the range of 7.0–17.3% at cfDNA concentrations within the range of 4.8–37.5 pg/μl (with a median of 7.25 pg/μl) [14]. In a study by Stallard et al., a similar ddPCR-based approach afforded the detection of the *H3* K27M variant in liquid biopsies of high-grade glioma patients (n = 4) with significantly higher VAFs in cfDNA (18–65%) [16]. It should be noted that in the study by Martínez-Ricarte et al. CSF was collected by lumbar puncture, whereas in the study by Stallard et al. it was collected from liquor spaces of the brain. To emphasize the higher diagnostic value of ventricular CSF, Stallard et al. compared VAFs of *H3* K27M in lumbar and ventricular samples of CSF collected at autopsy from a patient with diffuse intrinsic pontine glioma. Indeed, concentration of target *H3* K27M variant in CSF collected from lateral ventricles was 2.5 times higher than in lumbar liquor (133 and 57 copies per ng cfDNA, respectively) [14,16].

CONCLUSION

The study provides a reliable tissue-validated technical basis for detection of *H3* K27M somatic variant in CSF of pediatric patients with CNS tumors. The optimized universal dPCR protocol allows detection of solitary copies of the mutant allele with excellent analytical sensitivity. Thorough analytical characterization of cfDNA pools in terms of fragment lengths and concentrations is required to diminish the risk of false negatives. This requirement, along with insufficient quality and low representation of tumor DNA in CSF, limit standardization of the approach and its clinical prospects. Altogether, ventricular CSF sampling is more informative compared with lumbar sampling. Multicenter study designs are needed to evaluate clinical relevance of CSF liquid biopsies for rare CNS tumors.

DATA AVAILABILITY STATEMENT

The original contributions presented in the study are included in the article/**Supplementary Material**, further inquiries can be directed to the corresponding author.

ETHICS STATEMENT

The studies involving human participants were reviewed and approved by the Institutional Review Board at the Dmitry Rogachev Center. Written informed consent to participate in this study was provided by the participants' legal guardian/next of kin.

AUTHOR CONTRIBUTIONS

MZ, LP, GN, and AD developed the concept; MZ and NU performed the analysis, carried out visualization, and drafted the manuscript; ES, AS, and AV collected the material and retrieved and formalized patient data; AC wrote Section *Diagnostic Sensitivity Assay* of the manuscript; LP and GN provided administrative support; AD expertly supervised the interpretation and writing. All authors have critically read the manuscript and approved the final version.

FUNDING

The study was supported by Foundation for support and development in the field of pediatric hematology, oncology and immunology "Science for Children" and Charity foundation Podari.Life.

CONFLICT OF INTEREST

The authors declare that the research was conducted in the absence of any commercial or financial relationships that could be construed as a potential conflict of interest.

ACKNOWLEDGMENTS

We acknowledge Alina Korovkina and Alexey Anikaev of QIAGEN Russia and CIS for informational support and provision of facilities for the study.

SUPPLEMENTARY MATERIAL

The Supplementary Material for this article can be found online at: https://www.por-journal.com/articles/10.3389/pore.2022.1610024/full#supplementary-material

REFERENCES

1. Ostrom QT, Gittleman H, Truitt G, Boscia A, Kruchko C, Barnholtz-Sloan JS CBTRUS Statistical Report: Primary Brain and Other Central Nervous System Tumors Diagnosed in the United States in 2011-2015. *Neuro Oncol* (2018) 20: iv1–iv86. doi:10.1093/neuonc/noy131
2. Walker DA, Liu J, Kieran M, Jabado N, Picton S, Packer R, et al. A Multi-Disciplinary Consensus Statement Concerning Surgical Approaches to Low-Grade, High-Grade Astrocytomas and Diffuse Intrinsic Pontine Gliomas in Childhood (CPN Paris 2011) Using the Delphi Method. *Neuro-Oncology* (2013) 15(4):462–8. doi:10.1093/neuonc/nos330
3. Wu G, Broniscer A, McEachron TA, Lu C, Paugh BS, Becksfort J, et al. Somatic Histone H3 Alterations in Pediatric Diffuse Intrinsic Pontine Gliomas and Non-brainstem Glioblastomas. *Nat Genet* (2012) 44(3):251–3. doi:10.1038/ng.1102
4. Zaytseva MA, Yasko LA, Papusha LI, Druy AE. Molecular Genetic Features of Pediatric Gliomas. *Pediatr Hematology/Oncology Immunopathology* (2019) 18(4):109–17. (In Russ.). doi:10.24287/1726-1708-2019-18-4-109-117
5. Louis DN, Perry A, Reifenberger G, von Deimling A, Figarella-Branger D, Cavenee WK, et al. The 2016 World Health Organization Classification of Tumors of the Central Nervous System: A Summary. *Acta Neuropathol* (2016) 131(6):803–20. doi:10.1007/s00401-016-1545-1
6. Nazarian J, Druy AE, Yasko LA, Papusha LI, Novichkova GA. Liquid Biopsy in Pediatric Brain Cancers: A Theragnostic Opportunity. *Pediatr Hematology/Oncology Immunopathology* (2018) 17(1):133–5. (In Russ.). doi:10.24287/1726-1708-2018-17-1-133-135
7. Scarlotta M, Simsek C, Kim AK. Liquid Biopsy in Solid Malignancy. *Genet Test Mol Biomarkers* (2019) 23(4):284–96. doi:10.1089/gtmb.2018.0237
8. Kwapisz D. The First Liquid Biopsy Test Approved. Is it a New Era of Mutation Testing for Non-small Cell Lung Cancer? *Ann Transl Med* (2017) 5(3):46. doi:10.21037/atm.2017.01.32
9. Oxnard GR, Thress KS, Alden RS, Lawrance R, Paweletz CP, Cantarini M, et al. Association between Plasma Genotyping and Outcomes of Treatment with Osimertinib (AZD9291) in Advanced Non–small-cell Lung Cancer. *J Clin Oncol* (2016) 34(28):3375–82. doi:10.1200/jco.2016.66.7162
10. Tzanikou E, Markou A, Politaki E, Koutsopoulos A, Psyrri A, Mavroudis D, et al. PIK3CA Hotspot Mutations in Circulating Tumor Cells and Paired Circulating Tumor DNA in Breast Cancer: A Direct Comparison Study. *Mol Oncol* (2019) 13(12):2515–30. doi:10.1002/1878-0261.12540
11. De Mattos-Arruda L, Mayor R, Ng CKY, Weigelt B, Martínez-Ricarte F, Torrejon D, et al. Cerebrospinal Fluid-Derived Circulating Tumour DNA Better Represents the Genomic Alterations of Brain Tumours Than Plasma. *Nat Commun* (2015) 6(1):8839. doi:10.1038/ncomms9839
12. Miller AM, Shah RH, Pentsova EI, Pourmaleki M, Briggs S, Distefano N, et al. Tracking Tumour Evolution in Glioma through Liquid Biopsies of Cerebrospinal Fluid. *Nature* (2019) 565(7741):654–8. doi:10.1038/s41586-019-0882-3
13. Pan C, Diplas BH, Chen X, Wu Y, Xiao X, Jiang L, et al. Molecular Profiling of Tumors of the Brainstem by Sequencing of CSF-Derived Circulating Tumor DNA. *Acta Neuropathol* (2019) 137(2):297–306. doi:10.1007/s00401-018-1936-6
14. Martínez-Ricarte F, Mayor R, Martínez-Sáez E, Rubio-Pérez C, Pineda E, Cordero E, et al. Molecular Diagnosis of Diffuse Gliomas through Sequencing of Cell-free Circulating Tumor DNA from Cerebrospinal Fluid. *Clin Cancer Res* (2018) 24(12):2812–9. doi:10.1158/1078-0432.CCR-17-3800
15. Louis DN, Perry A, Wesseling P, Brat DJ, Cree IA, Figarella-Branger D, et al. The 2021 WHO Classification of Tumors of the Central Nervous System: a Summary. *Neuro Oncol* (2021) 23(8):1231–51. doi:10.1093/neuonc/noab106
16. Stallard S, Savelieff MG, Wierzbicki K, Mullan B, Miklja Z, Bruzek A, et al. CSF H3F3A K27M Circulating Tumor DNA Copy Number Quantifies Tumor Growth and *In Vitro* Treatment Response. *Acta Neuropathol Commun* (2018) 6(1):80. doi:10.1186/s40478-018-0580-7
17. Watanabe K, Fukuhara T, Tsukita Y, Morita M, Suzuki A, Tanaka N, et al. EGFR Mutation Analysis of Circulating Tumor DNA Using an Improved PNA-LNA PCR Clamp Method. *Can Respir J* (2016) 2016:1–7. doi:10.1155/2016/5297329
18. Milbury CA, Zhong Q, Lin J, Williams M, Olson J, Link DR, et al. Determining Lower Limits of Detection of Digital PCR Assays for Cancer-Related Gene Mutations. *Biomol Detect Quantif* (2014) 1(1):8–22. doi:10.1016/j.bdq.2014.08.001
19. Wang Y, Springer S, Zhang M, McMahon KW, Kinde I, Dobbyn L, et al. Detection of Tumor-Derived DNA in Cerebrospinal Fluid of Patients with Primary Tumors of the Brain and Spinal Cord. *Proc Natl Acad Sci USA* (2015) 112(31):9704–9. doi:10.1073/pnas.1511694112
20. Zhao Z, Zhang C, Li M, Shen Y, Feng S, Liu J, et al. Applications of Cerebrospinal Fluid Circulating Tumor DNA in the Diagnosis of Gliomas. *Jpn J Clin Oncol* (2020) 50(3):325–32. doi:10.1093/jjco/hyz156
21. Connolly ID, Li Y, Pan W, Johnson E, You L, Vogel H, et al. A Pilot Study on the Use of Cerebrospinal Fluid Cell-free DNA in Intramedullary Spinal Ependymoma. *J Neurooncol* (2017) 135(1):29–36. doi:10.1007/s11060-017-2557-y
22. Fujioka Y, Hata N, Akagi Y, Kuga D, Hatae R, Sangatsuda Y, et al. Molecular Diagnosis of Diffuse Glioma Using a Chip-Based Digital PCR System to Analyze IDH, TERT, and H3 Mutations in the Cerebrospinal Fluid. *J Neurooncol* (2021) 152(1):47–54. doi:10.1007/s11060-020-03682-7
23. On J, Natsumeda M, Watanabe J, Saito S, Kanemaru Y, Abe H, et al. Low Detection Rate of H3K27M Mutations in Cerebrospinal Fluid Obtained from Lumbar Puncture in Newly Diagnosed Diffuse Midline Gliomas. *Diagnostics* (2021) 11(4):681. doi:10.3390/diagnostics11040681
24. Dong L, Meng Y, Sui Z, Wang J, Wu L, Fu B. Comparison of Four Digital PCR Platforms for Accurate Quantification of DNA Copy Number of a Certified Plasmid DNA Reference Material. *Sci Rep* (2015) 5:13174. doi:10.1038/srep13174
25. Li D, Bonner ER, Wierzbicki K, Panditharatna E, Huang T, Lulla R, et al. Standardization of the Liquid Biopsy for Pediatric Diffuse Midline Glioma Using DdPCR. *Sci Rep* (2021) 11(1):5098. doi:10.1038/s41598-021-84513-1
26. Jackson JB, Choi DS, Luketich JD, Pennathur A, Ståhlberg A, Godfrey TE. Multiplex Preamplification of Serum DNA to Facilitate Reliable Detection of Extremely Rare Cancer Mutations in Circulating DNA by Digital PCR. *J Mol Diagn* (2016) 18(2):235–43. doi:10.1016/j.jmoldx.2015.10.004

Pathology & Oncology Research

frontiers

REVIEW
published: 19 May 2022
doi: 10.3389/pore.2022.1610103

Blood, Toil, and Taxoteres: Biological Determinants of Treatment-Induced ctDNA Dynamics for Interpreting Tumor Response

Christopher T. Boniface[1,2]* *and Paul T. Spellman*[1,2]*

[1]*Knight Cancer Institute, Oregon Health & Science University, Portland, OR, United States,* [2]*Cancer Early Detection Advanced Research Center, Knight Cancer Institute, Oregon Health & Science University, Portland, OR, United States*

Collection and analysis of circulating tumor DNA (ctDNA) is one of the few methods of liquid biopsy that measures generalizable and tumor specific molecules, and is one of the most promising approaches in assessing the effectiveness of cancer care. Clinical assays that utilize ctDNA are commercially available for the identification of actionable mutations prior to treatment and to assess minimal residual disease after treatment. There is currently no clinical ctDNA assay specifically intended to monitor disease response during treatment, partially due to the complex challenge of understanding the biological sources of ctDNA and the underlying principles that govern its release. Although studies have shown pre- and post-treatment ctDNA levels can be prognostic, there is evidence that early, on-treatment changes in ctDNA levels are more accurate in predicting response. Yet, these results also vary widely among cohorts, cancer type, and treatment, likely due to the driving biology of tumor cell proliferation, cell death, and ctDNA clearance kinetics. To realize the full potential of ctDNA monitoring in cancer care, we may need to reorient our thinking toward the fundamental biological underpinnings of ctDNA release and dissemination from merely seeking convenient clinical correlates.

Keywords: biomarkers, liquid biopsy, circulating tumor DNA, ctDNA, tumor growth, treatment response

OPEN ACCESS

Edited by:
József Tímár,
Semmelweis University, Hungary

***Correspondence:**
Christopher T. Boniface
boniface@ohsu.edu
Paul T. Spellman
spellmap@ohsu.edu

Received: *02 October 2021*
Accepted: *29 April 2022*
Published: *19 May 2022*

Citation:
Boniface CT and Spellman PT (2022) Blood, Toil, and Taxoteres: Biological Determinants of Treatment-Induced ctDNA Dynamics for Interpreting Tumor Response. Pathol. Oncol. Res. 28:1610103. doi: 10.3389/pore.2022.1610103

BACKGROUND

Circulating tumor DNA (ctDNA) is extracellular DNA in plasma that originates from tumor cells and has emerged as a useful biomarker in non-invasive liquid biopsy (1-3). ctDNA abundance shows broad correlation with tumor burden and generally reflects the tumor DNA content such that clinical assays are commercially available for detection of molecular/minimal residual disease (MRD) and tumor mutational profiling (4–6). However, there are currently no ctDNA-based assays approved for serial monitoring during treatment to assess immediate tumor response and treatment efficacy.

Serial ctDNA monitoring during treatment can provide insight into underlying biological factors that can potentially be used to predict response, treatment efficacy, and long-term outcomes (7–11). In practice however, ctDNA levels can appear erratic across time points and are often inconsistent between patients with similar disease and treatment. This variability may be partially the result of disparate sampling frequency (often within the same study), extraction methods, and analytical approaches between studies. More likely, this variation is driven by factors that have yet to be elucidated and may vary between patients, such as individual host physiology, tumor location, tumor biology, and treatment modality.

Evidence that ctDNA concentration is more dependent on tumor cell replication rates than simply on tumor volume also suggests that understanding tumor biology and patient physiology are necessary to guide proper interpretation of ctDNA dynamics (12, 13). In some studies, early spikes in ctDNA shortly after treatment may predict a favorable clinical response, in keeping with the hypothesis that shedding is directly associated with treatment-induced tumor cell death (14–16). It is unclear however, how soon after treatment initiation this spike must occur in such cases, emphasizing the importance of collection timing. Nevertheless, early and rapid ctDNA clearance during treatment has consistently been shown to correlate with objective response and outcome (17–20). Evidence supports the idea that ctDNA release is clearly a byproduct of tumor cell proliferation, though whether this is through increased cell turnover and higher death rates or active release during cellular expansion is still an open question.

This review seeks to discuss the biological sources of variability in ctDNA abundance, with the hope that thoughtful analysis and a mechanistic understanding of ctDNA release will allow improved approaches to ctDNA interpretation in clinical response and progression.

A Note on Circulating Tumor DNA Detection and Its Implications for This Review

Typically, ctDNA is detected and characterized using methods such as droplet digital polymerase chain reaction (ddPCR) or next-generate sequencing (NGS) (reviewed by Heitzer et al. (2)) either targeting genomic positions based on *a priori* knowledge of tumor mutations or by calling mutations *de novo* at novel sites and recurrent hotspots. Although both *a priori* and *de novo* approaches to ctDNA detection assume that molecules harboring alternate alleles are tumor-derived, the later approach allows for ctDNA detection without *a priori* knowledge of tumor-specific mutations but is subject to much more uncertainty. The detection of tumor-derived copy-number aberrations in cell-free DNA is also possible and is dependent solely on read counts to detect gains or losses found in tumor cells (21). *De novo* mutations can be called from whole-genome and whole-exome sequencing, or smaller panels targeting just a few sites or genes known to harbor recurrent mutations. Panels intended to detect mutations at these canonical sites are often less informative about passenger mutations, secondary drivers, and subclonal populations. The same may be true for tumor-informed and patient-specific panels depending on the breadth of the panel used and the sampling bias of the original tumor tissue used to design the panel, particularly in the case of high intratumoral heterogeneity. These various approaches further confound our ability to compare results across studies, patient populations, and cancers. This problem is particularly true for studies where ctDNA was characterized by the prevalence of a single mutation in a single gene, where subclonal populations driven by other genetic aberrations may be under selective pressure during treatment. Of course, with a broader analytical space comes greater cost and complexity and additional challenges for implementation of accurate ctDNA assays in a clinical setting. For example, a simple ddPCR or amplicon-sequencing test to detect the presence of low-abundance EGFR mutations in the cell-free DNA of lung cancer patients is much cheaper and simpler to validate and execute in a diagnostic laboratory than a whole-exome or a multi-gene sequencing panel with similar accuracy and sensitivity. However, such an assay may not be representative of the entire tumor cell population, particularly if there are treatment-resistant subclones that harbor distinct genotypes. Consequently, careful evaluation of single-target vs. multi-target approaches is necessary.

Although the data available to assess ctDNA abundance as it relates to clinical observations, treatment response, and outcome consist primarily of mutant-allele detection and prevalence estimates, evidence suggests approaches like methylation profiling by whole-genome or targeted bisulfite sequencing may be more sensitive and are not dependent on the presence of genetic aberrations (5). A serial comparison of single-nucleotide variants (SNVs) and methylation profiles in EGFR T790M-positive advanced cancer patients found that methylation levels closely followed SNV mutant allele frequency and both were predictive of long-term treatment response (22). Silva et al. (23) reported changes in cell-free DNA methylation over time that were associated with therapy response and progression in prostate cancer patients. Few studies, however, have assessed methylation dynamics in cell-free DNA with high-frequency sample collection during early phases of treatment, and therefore the data presented here are biased toward somatic mutations as a means of ctDNA detection and characterization. It remains to be seen how broad the search space needs to be in order to effectively monitor tumor cell populations by ctDNA, and which reporter (i.e., mutations, methylation, etc.) will be the most informative, but may vary by patient, tumor, and treatment.

BIOLOGICAL FACTORS THAT MOST AFFECT CIRCULATING TUMOR DNA ABUNDANCE

In order to utilize ctDNA monitoring during treatment we must understand the various factors that impact ctDNA concentration over time. Multiple sources of ctDNA have been suggested including apoptosis, necrosis, and so called "active/passive release" (reviewed by Aucamp et al. (24)). Apoptosis, necrosis, and other forms of tumor cell death result in ctDNA release into interstitial space where it moves to the lymphatic system and blood circulation (8, 25). It is also hypothesized that extracellular DNA can be released from living cells in various contexts that are both energy-dependent and independent, and range in mechanism from shedding of mis-segregated DNA to intercellular signaling (26). Once ctDNA enters circulation, it is subject to further degradation by DNases in the blood and is putatively removed by the liver, spleen, and/or kidneys within 30–120 min (27). Changes in the balance of these processes due to treatment are assumed to be reflected in ctDNA dynamics, which, if correctly interpreted, may inform us about a patient's disease state and response to therapy (**Figure 1**). Furthermore, disruption of biological homeostasis resulting from disease and treatment can increase overall levels of cell-free DNA, decreasing the

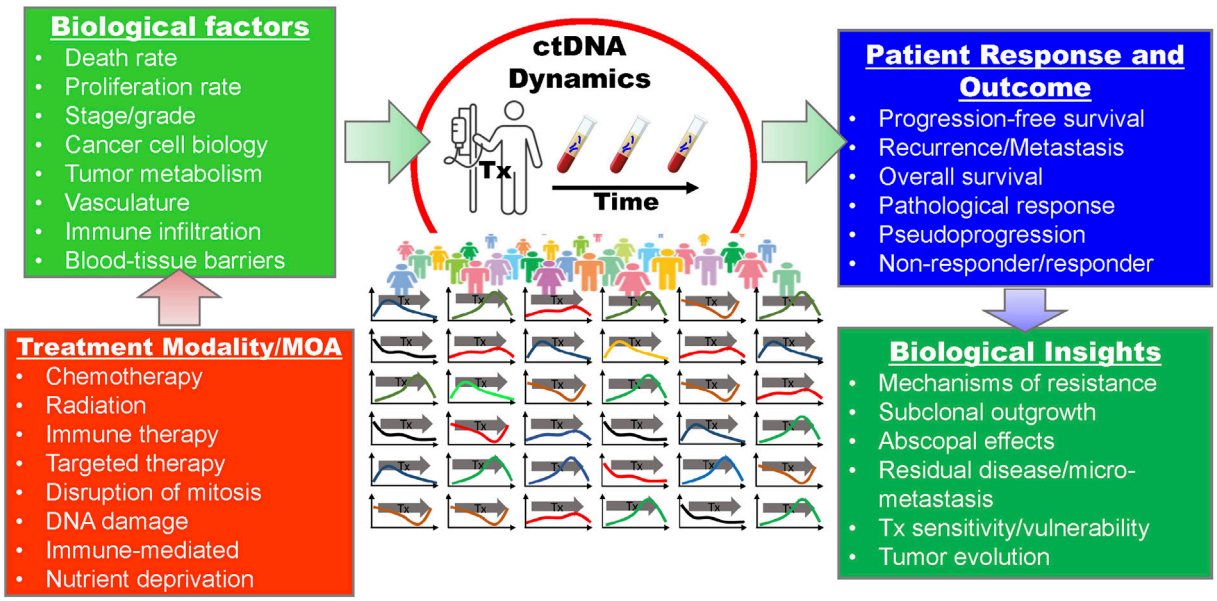

FIGURE 1 | The relationships between treatment, biological factors, clinical indicators and outcomes, and potential insights with regard to serial ctDNA monitoring during treatment. MOA, mechanism of action; Tx, treatment.

relative abundance of ctDNA and thus impacting assay sensitivity. This can also make interpreting data from studies that simply report mutant allele frequency challenging without accounting for such changes in total cell-free DNA. The following sections address how the unique biology of a cancer and host physiology influences ctDNA abundance in the blood stream.

Cancer Type and Biology

Even before our ability to distinguish ctDNA molecules amongst cell-free DNA, there appeared to be a clear relationship between cell-free DNA abundance and disease state. The more severe the patient's cancer, the more cell-free DNA present in their blood (reviewed by de Miranda et al. (28), Grabuschnig et al. (26), Aucamp et al. (24)), suggesting that disease burden impacts cell-free DNA homeostasis. Later work has shown that ctDNA levels, independent of non-tumor, cell-free DNA, vary dramatically across disease type, tumor location, and stage (29–33). *In vitro* assays have helped isolate the mechanistic variables involved in cell-free DNA release, particularly with regard to known apoptotic and necrotic processes. These experiments found that cell-free DNA release can vary significantly between cell-lines with different phenotypes and histologies (34–39).

Observations in human cohorts also correlate ctDNA with tumor histology, grade, and stage. Various studies in neoadjuvantly-treated breast cancer patients found that ctDNA levels and mutations were significantly different between breast cancer subtypes (9, 11, 40, 41). Expression levels of the proliferation-associated nuclear protein, Ki-67, have also been directly associated with ctDNA characteristics in breast and lung cancers (42–44). Studies assessing ctDNA in non-small cell lung cancer (NSCLC) patients found that ctDNA concentration was correlated with tumor stage, histology, and degree of cytological atypia (45–47).

Tumor Volume, Growth Rate, and Metabolism

Cell death has historically been considered the largest contributor to ctDNA and tumor volume the most reliable predictor of ctDNA abundance. More recently, various mechanisms and conditions have been proposed in which living tumor cells, particularly during mitosis, could shed DNA in both an energy-dependent and independent manner (26, 34). Therefore, it is likely the complex interplay between tumor cell proliferation and death that determines ctDNA abundance. This relationship has significant implications for how we should think about ctDNA measurements in the context of tumor volume, growth rate, and metabolism. For example, one can easily imagine a scenario where proliferation and death rates both increase but are in balance resulting in increased ctDNA shedding but no net change in tumor volume (48). Furthermore, although ctDNA may be hypothetically representative of the entire cancer cell population, it is likely subject to significant composition bias from differential cell turnover rates across subclones (3). Examining these variables *in vitro* and *in vivo* can shed light on which processes contribute more to ctDNA abundance.

Tumor growth rate and metabolism are often inferred by measuring tumor glucose uptake. Studies in metastatic melanoma patients found a strong correlation between the tumor PET avidity (a measure of cellular glucose uptake) and ctDNA abundance, independent of tumor volume (49). These results are supported by studies in resected NSCLC, where a correlation was found between increased mitotic rates and higher ctDNA levels measured 24 h prior to surgery, as well as increased levels of the proliferation marker Ki-67 (42–44, 47). Indeed, *in vitro* studies have consistently found that large amounts of cell-free

DNA can accumulate in the media of actively proliferating cell populations independent of apoptosis or necrosis (34, 50–53). DNA fragments resulting from mis-segregation events during mitosis were found to be released by actively proliferating cancer cells via the creation of micronuclei (54, 55), but their relative contribution to overall ctDNA abundance *in vivo* remains unclear. Similar to the DNA products of necrosis, it has been assumed that these fragments would appear distinct from apoptotic ctDNA given their larger size and that their contribution would therefore be obvious. However, evidence is emerging that cleavage of larger DNA fragments by extracellular DNases may also occur (51). These DNA fragments might have an apoptotic fragmentation pattern, yet be generated by non-apoptotic mechanisms, such as release during proliferative states.

The relationship between tumor cell proliferation and death is not independent. In healthy tissues, cell density homeostasis is achieved by compensating for cell death with an appropriate rate of cell proliferation. This process is known as "apoptosis-induced proliferation" (reviewed by Heitzer et al. (2) and Ryoo et al. (56)), but it is unclear how significant a role it plays in tumors. The consequences for ctDNA shedding could be straightforward, where increased cell death leads to increase cell birth and so on, and both processes result in increased ctDNA levels. However, positive feedback mechanisms like this may be tissue-dependent and could be dysregulated in cancer, complicating interpretation of ctDNA dynamics.

Tumor Vasculature, Blood Vessel Proximity, and Hypoxia

Tumor vascularization and proximity to major blood vessels are also features of tumor physiology that might be expected to significantly impact ctDNA levels. Blood flow to a tumor is the direct means by which ctDNA enters circulation and it affects the metabolic activity of a tumor by providing oxygen and nutrients (57). As a tumor grows its vasculature becomes more irregular and dysfunctional leading to reduced oxygen levels, hypoxia and necrosis. Necrosis, reduced nutrient levels, and limited accesses to wider blood circulation all potentially effect ctDNA abundance in unique ways. Vasculature can also impact drug delivery and efficacy, which may also affect ctDNA shedding. It is unclear how much ctDNA abundance is dependent on direct access to blood vessels. Interstitial ctDNA is assumed to passively enter circulation through nearby blood vessels, but other processes like macrophage clearance of dead and dying cells (see "*Immune Response*" and "*Immunotherapy*" sections below) may also play a role in transporting ctDNA from areas with poor vasculature to the bloodstream (8, 25, 27).

Results from studies directly comparing tumor vascularization, angiogenesis, and ctDNA abundance, are inconsistent between studies. Post-excision pathology by Abbosh et al. (4) found lymphovascular invasion to be predictive of ctDNA detection in early-stage lung cancer. Two other studies in lung cancer found vascular invasion to be marginally (47), or not at all (46), correlated with ctDNA detection. Interestingly, when only looking at patients with EGFR mutations, ctDNA was significantly correlated with vascular invasion in the former study by Cho et al. (47). In liver cancer, microvascular invasion was correlated with preoperative ctDNA levels (58). In recent preliminary data collected from a large cohort of colorectal cancer (CRC) patients, ctDNA was found to be strongly associated with lymphovascular invasion (59). In neurological malignancies, which typically have less detectable ctDNA, Nabavizadeh et al. (60) found that tumor vessel size was correlated with detectable ctDNA. Notably, previous work by the same group and others found that the amount of microvascular proliferation was not significantly correlated to ctDNA in glioblastoma (GBM) specifically (61, 62). The nature of such studies makes it challenging to discern if these correlations are independent of tumor stage and volume. Proving a causal link may only be possible with further evaluation of preclinical models, tumor pathology, and imaging.

Hypoxia is in many ways a measure of tumor cell access to functional vasculature (63). As a tumor grows, cells become more isolated from functional vasculature, despite upregulated angiogenesis that is characteristic of many cancers. This process selects for cells that are more tolerant of low-oxygen conditions while the remaining population become necrotic (64). There is a clear link between hypoxia and necrosis and some studies have suggested that ctDNA is primarily derived from necrotic processes (1, 35, 65, 66). This suggests that as a tumor grows and vasculature becomes more distant and dysfunctional, wider ctDNA abundance could either increase due to further necrosis, or decrease due to reduced access to that vasculature. Since both forces are not equal in all tumors, the overall effect on ctDNA levels from this process may not be neutral. *In vitro* experiments with CRC cells have found that hypoxic conditions induced cell-free DNA production during the first 24 h but decreased dramatically over the following 48–72 h (37). These results are also consistent with previous findings in both tumor-injected and tumor-free mice where hypoxia induced cell-free DNA release (67). Deprivation of the metabolite, folate, has been found to induced double-strand DNA breaks and mis-segregation events, which may also lead to ctDNA shedding in nutrient-starved tumors as well (68).

Organ Encapsulation

The free movement of cell-free DNA between tissue and blood may be restricted in some organs. Blood-tissue barriers have been identified throughout the body, such as the thymus, testes, retina, and intestines, but it is unclear what role they might play in cell-free DNA exchange (69). The blood-brain barrier (BBB) is often cited as the primary reason that neurological malignancies, particularly gliomas, produce less detectable ctDNA than other cancer types (29). In a 2018 review on ctDNA kinetics, Khier and Lohan speculate that physiological barriers, like the BBB, restrict the movement of cell-free DNA throughout the body while also acknowledging the exception of placental cell-free DNA, which has been shown to move quite freely throughout the mother (8, 70). Notably, disruption of the BBB that results in increased permeability and risk of metastasis also resulted in increased levels of ctDNA in patients with GBM (60).

Several studies have shown that disrupting the BBB in animal models using focused ultrasound techniques leads to increase blood levels of ctDNA and other biomarkers (71, 72). Therefore, it is possible that changes in tissue-blood barrier permeability, particularly during treatment, might significantly affect ctDNA dynamics.

Immune Response

Although there may be a significant role for inflammation and infection (e.g., sepsis) in cell-free DNA release, this review is primarily interested in the extent to which they directly impact ctDNA release from cancer cells. Early studies exploring the origins of cell-free DNA found that macrophages may play a significant role in cell-free DNA release though phagocytosis of dead and dying cells (73). Phagocytes have been shown to digest apoptotic cells and release the resulting cell debris and fragmented DNA (24, 73, 74). In the GBM study mentioned earlier, ctDNA levels were strongly associated with the density of macrophages around the tumor (60). In healthy individuals cell turnover is a tightly regulated process where apoptotic cells are quickly removed by phagocytes, however, this process appears to be dysfunctional in tumors resulting in excess cell debris (including DNA) that accumulates locally and in circulation (27, 66). The extent to which ctDNA levels might be directly affected by tumor cell targeting and/or clearance by immune cells is still an open question. Evidence for this phenomenon however, might be found in studies where ctDNA levels spike within 2 weeks of immune-therapy initiation in metastatic melanoma patients, if and only if, the tumors were responsive (75).

Cell-Free DNA Clearance

Cell-free DNA digestion and clearance, whether achieved locally *via* phagocytosis or in circulation via the liver, spleen, and kidneys, is influenced by a number of factors (8, 27, 76, 77). As described above, cell-free DNA clearance *in situ* is potentially dependent on interstitial diffusion and the presence of phagocytic cells, however, once it is in circulation its half-life is determined by extracellular DNase activity and organ function (8). ctDNA half-life in the blood ranges from 30 to 120 min (27) making blood collection timing critical. The decreased levels of DNase activity observed in the blood of cancer patients potentially explains the accompanying increase in cell-free DNA levels from disruption of homeostasis (78, 79). Studies have also suggested that cell-free DNA clearance and half-life is dependent on proper liver and kidney function suggesting that treatment toxicity in cancer patients could affect ctDNA clearance rates and abundance (80, 81). The role of renal function in ctDNA clearance is not well understood, however, based on experiments assessing cell-free DNA levels in urine (27). The presence of cell-free DNA in urine implies involvement of the kidneys in clearance from circulation, however, patients with chronic renal failure were found not to have increased levels of cell-free DNA in their plasma (82). Methylation profiling has suggested that cell-free DNA present in urine is derived from white blood cells, kidney cells and urinary tract cells, but data from stem cell transplant patients found that the majority of this DNA was from the renal system itself and not plasma (83, 84).

THE EFFECT OF TREATMENT ON CIRCULATING TUMOR DNA ABUNDANCE

The effect of treatment on tumor cell proliferation and death, and thus ctDNA dynamics, is dependent on its mechanism of action, efficacy, and tumor biology. Considering the factors described above that influence ctDNA abundance, it is not surprising that there are many discernable differences between the ctDNA dynamics of responders and non-responders during treatment. Predicting their timing and trajectories is not so simple, particularly when considering the short half-life of ctDNA. We might at least expect that ctDNA dynamics should reflect treatment response depending on the mechanism of action of a given treatment, but the timing of those effects is still unclear (**Figure 2**). The correlation between *in vitro* and *in vivo* models of treatment-induced cell death remains largely unclear, and is likely dependent on a variety of factors including the treatment and tissue of interest. Despite the paucity of data, it is possible that tumor cell death can occur within hours of treatment and therefore ctDNA levels may rapidly increase as well (36, 85–87). Serial ctDNA monitoring has been done with collection times ranging from minutes, hours or days after administration of treatment, to weeks and months. Some guidance may be gleaned from these studies, but the optimal time for sampling may be unique to cancer type and therapy and may need to be determined empirically. The following sections outline the expected effects of cancer treatment modalities on ctDNA dynamics, and what existing evidence, if any, tells about these hypotheses.

Chemotherapy and Radiation

Cytotoxic chemotherapies and radiation therapy (RT) are often used independently or in combination as first-line treatment in many cancers. Chemotherapy agents function by disrupting mitosis or causing DNA damage leading to cell-cycle arrest, mitotic catastrophe, and apoptosis. Radiation therapy kills cells by DNA damage as well, but it also elicits an immune response and vascular damage, which can result in subsequent rounds of tumor cell death. Mitotic arrests and DNA damage are thought to cause tumor cell death within 6–72 h of administration *in vivo*, so detecting ctDNA shedding in response to effective treatment may require immediate sampling (87). Unfortunately, very few studies sample ctDNA within the first 72 h of chemotherapy. It has also been suggested that treatment-induced mitotic catastrophe can cause delays in cell death from chemotherapy and RT for up to a week (36, 62, 88). These various mechanisms of action may result in multiple shedding events, where one may be more informative about treatment response over another.

Limited studies assessing ctDNA levels immediately after treatment are conflicting. In castration-resistant prostate cancer patients receiving docetaxel-based therapy, early ctDNA levels were found to increase rapidly within 1 h of administration with a corresponding decrease in total cell-free DNA (89). This observation is consistent with increased tumor cell sensitivity to cytotoxic agents compared to healthy tissue. Contrary to these findings, however, CRC patients receiving FOLFOX did not exhibit a spike in ctDNA at any point within the first 48 h of treatment, despite high-resolution sampling at 3, 9, 18, 23, 26, 42, and 47 h (90). Another study involving metastatic CRC patients receiving FOLFIRI looked at ctDNA levels before and 7 days after each of the first two

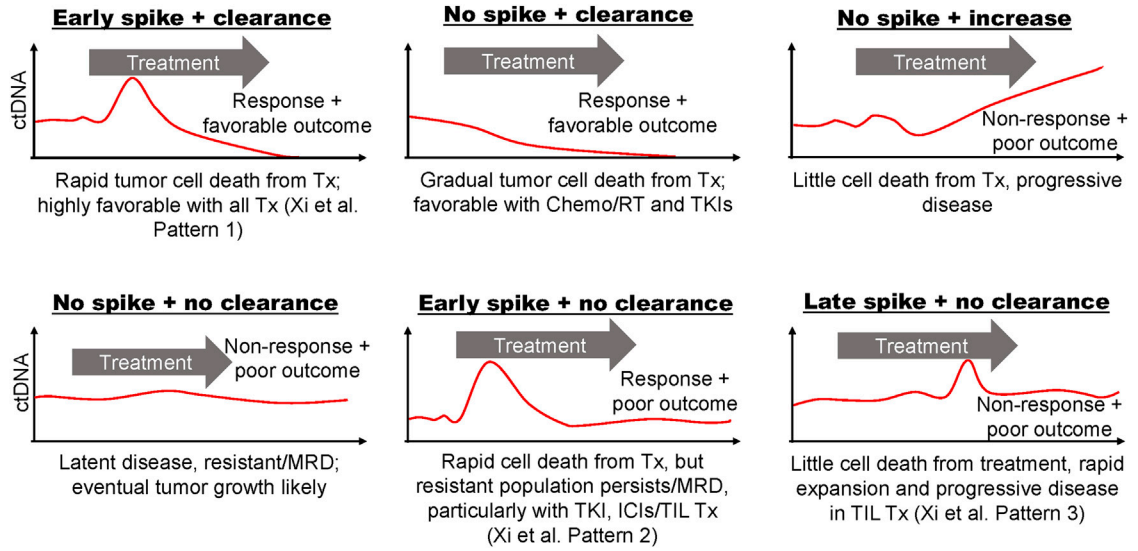

FIGURE 2 | Hypothetical ctDNA dynamics from blood sampled frequently before, during, and after treatment. Characteristic ctDNA dynamics are depicted as observed in various studies throughout the text or otherwise hypothesized. The speculated driving tumor biology is described for each plot and example outcomes are stated. Response patterns defined by Xi et al. (14) for metastatic melanoma patients undergoing tumor infiltrating lymphocyte (TIL) immunotherapy are indicated when relevant. Tx, treatment; TKI, tyrosine kinase inhibitors; ICI, immune checkpoint inhibitors; MRD, molecular/minimal residual disease; ChemoRT, chemoradiation therapy.

treatment cycles and again at progression (91). Interestingly, this study found that temporary increases in ctDNA while on treatment were predictive of progressive disease and worse survival rates, and suggested ctDNA monitoring within the first week of treatment to evaluate treatment efficacy. While ctDNA levels were decreased at the time of radiological assessment compared to baseline for all patient, patients with temporary spikes in ctDNA appeared to have more sustained ctDNA burden than those with favorable response (see **Figure 2**: "Early spike + no clearance"). Clonal composition was also found to vary during treatment suggesting a differential response to treatment among tumor cell subpopulations. Increases in cell-free DNA methylation levels of tumor suppressor genes (APC and RASSF1A) 24 h after receiving cisplatin-based chemotherapy were correlated with improved tumor response and overall outcome in advanced lung cancer patients (92). The same study showed that methylation levels of those genes in lung cancer cells also peaked 24 h after cisplatin exposure, however, it is unclear if the hypermethylated DNA was tumor-derived in patients. Notably, this study also found that elevated methylation of APC and/or RASSF1A in tumor-bearing mice were associated with tumor cell death as determined by biopsy shortly after treatment and blood collection. This finding might suggest that the methylated cell-free DNA originated from these dying tumor cells. In pancreatic cancer patients sampled for 4 weeks following treatment with gemcitabine, decreases in ctDNA were correlated with tumor response (93). In our work and others', decreases in or complete clearance of ctDNA levels during low-resolution sampling (i.e., weeks to months) of neoadjuvantly-treated breast cancer patients were associated with pathological complete response at the time of surgery (9–11).

In patient cohorts receiving combination chemoradiation therapy (CRT), decrease and clearance of ctDNA after 3–4 weeks was associated with tumor response in oropharyngeal and lung cancer (94, 95). Studies employing high-frequency sampling at time points within hours of treatment are sparse, however, recent data from Breadner et al. (96) found that ctDNA abundance increased in 77% of stage III/IV non-small cell lung cancer patients shortly after receiving CRT with peak abundance observed 7 h after chemotherapy initiation and 2 days after the first fraction of radiation. Early spikes in ctDNA were seen in some patients receiving CRT for treatment of locally advanced head and neck cancer, but were not correlated with response (16). Rather, overall decreases in ctDNA at later time points, which were not unique to patients who had early peaks, were more predictive of outcome.

Some of the earliest observations of cell-free DNA by Leon et al. (97) occurred in patients receiving RT alone, finding that general cell-free DNA levels decreased after treatment. Aucamp et al. (24) speculate that the reason for this may have been the coincident destruction of phagocytes needed to generate cell-free DNA. Another consideration that may confound ctDNA measurement from irradiated tumors is that, although mitotic arrest and catastrophe are the primary means by which RT is thought to kill cancer cells, they have also been found to result in mis-segregation events (98, 99). As discussed above, this process can result in releasing of DNA from living cells, providing another potential source of ctDNA that does not coincide with cell death. A recent study found that irradiation of head and neck cancer and NSCLC cell lines induced cell-free DNA shedding after 6–24 h in culture (36). The same study found that ctDNA levels increased within 24 h and peaked 96–144 h after 20 Gy of irradiation in xenograft mouse models. Interestingly, the authors found that treatment-induced senescence that was overcome with the

senolytic drug, Navitoclax, lead to apoptosis and increased ctDNA release. In human subjects, investigation of RT alone in NSCLC has shown mixed results. Walls et al. (100) found that 3 of 5 patients had decreased ctDNA levels 3-day after their first RT fraction, while the remaining 2 had increased levels of some tumor-derived variants, but not others. Preliminary data from our lab (101) and another study from Chen et al. (102) found that ctDNA levels were elevated 24–48 h after the first dose of stereotactic ablative radiotherapy. These three studies in NSCLC patients used varying doses of radiation per fraction (2.75, 12, and ~12.5 Gy, respectively), which along with sampling time differences, may account for the discrepancy. Chaudhuri et al. (103) also reported that mid-RT ctDNA levels in 13 NSCLC patients were correlated with outcomes at 2 years. A recently published study by our lab found that a metastatic breast cancer patient had increased ctDNA levels while receiving palliative radiation therapy. Deep sequencing using a 53-mutation panel representative of both clonal and subclonal mutations, which were previously identified from WES of multiple tumors, revealed differential response in ctDNA levels for various subclones with sample collection every 48-hour during RT (104). Differential response in subclonal ctDNA abundance is suggestive of varying sensitivity in irradiated tumor cell subpopulations and/or an abscopal response. First observed by Dr. R.H. Mole in 1953, the abscopal effect is the shrinkage of a distant, untreated tumor in response to RT of another tumor. It is thought that the destruction of cells in the irradiated tumor elicits an immune response that affects the non-radiated tumors elsewhere in the body (105). In our case, radiation of a single lesion may have induced immune-mediated responses and ctDNA shedding from distant metastatic sites that harbored subclonal tumor cell populations. It is also worth noting that CTCs may also be sources of ctDNA and CTC release timing may also be similar to tumor ctDNA shedding (106). In preliminary data in head and neck cancer patients treated with RT, 3 of 11 patients had increased circulating tumor cell (CTC) counts after the first fraction of RT, and 5 of 6 patients had increases CTCs after 2 weeks into therapy.(107).

Immunotherapy

ctDNA monitoring during treatment with immune checkpoint inhibitors (ICIs) has shown promise in multiple cancer types. A pan-cancer analysis done by Zhang et al. (17) found that changes in ctDNA levels during ICI treatment may be predictive of benefit. Patients in this study with increases in ctDNA levels during treatment had worse outcomes as compared to those that did not. Furthermore, patients with ctDNA clearance after detectable pre-treatment levels had the best progression-free and overall survival. A recent study by Herbretreau et al. (75) in patients with metastatic melanoma found that significant increases in ctDNA levels during the first 2–4 weeks of anti-PD1 (with or without anti-CTLA4) allowed early and highly-specific identification of treatment-resistant patients. Furthermore, ctDNA levels that rapidly decreased after starting PD-1 inhibitors were highly predictive of responses consistent with pseudoprogression (108, 109). When compared to changes in ctDNA levels later in treatment, regardless of early changes, increases beyond 12 weeks were not necessarily predictive of non-response, further suggesting that early sampling is more informative (110). In NSCLC patients treated with ICI, decreases in ctDNA 2 weeks after treatment initiation were strongly correlated with radiographic response and progression-free survival (111). A study investigating early response to tumor infiltrating lymphocyte (TIL) immunotherapy in metastatic melanoma patients identified three patterns of ctDNA dynamics that could be used to stratify patients by overall survival (14). Patients with an early spike in ctDNA within 5–10 days of treatment followed by clearance showed a statistically significant survival outcome over patients who had early peaks but latent ctDNA burden, or no peaks with or without clearing (see **Figure 2**). The study's authors speculate that early spike it ctDNA was in part due to the newly-transferred lymphocytes "identifying their targets and are effective in killing [them]."

Targeted Therapy

Given the clinical implications of tumor heterogeneity, one of the most significant unanswered questions in ctDNA analysis is whether ctDNA observed during therapy is more representative of resistant or responsive tumor cell populations. In a study of lung cancer patients undergoing EGFR tyrosine kinase inhibitor (TKI) therapy, ctDNA sampled 2 weeks after treatment initiation revealed activating mutations not previously detected in the tumor biopsies (112). Another study of lung cancer patients on TKIs found that clearing of ctDNA within days of treatment was associated with response, whereas sudden increases in ctDNA load later in treatment correlated with rapid tumor progression and poor outcome (113). In lung cancer patients receiving either anti-EGFR or HER2 therapies, increases in ctDNA abundance were observed within 4–12 h after initiation of treatment while total cell-free DNA was relatively constant (86). Phallen and coauthors point out that this timeframe is consistent with other studies in which apoptosis is observed *in vitro* within 6–48 h of treatment with EGFR TKIs. Patients in this study with an initial radiographic response all had ctDNA abundance eventually decrease by more than 95% within the first 19 days of treatment. Interestingly, baseline levels in a study of ALK-fusion positive lung cancer patients, pre-treatment ctDNA levels were not correlated with treatment response, yet changes in ctDNA during treatment with ALK TKIs were associated with progression (114).

Increases in ctDNA abundance of therapy-sensitive clones corresponds with response, however, increases in ctDNA abundance of therapy-resistant clones can also portend clinical progression (2). Outgrowth of subclonal tumor cell populations that are resistant to targeted therapy can be directly observed in allele-specific ctDNA dynamics. For example, genomic changes conferring resistance to targeted therapy in prostate cancer patients were detected by increasing fractions of the resistance-associated allele in several studies (115, 116).

DISCUSSION

Host physiology and tumor biology affect ctDNA abundance while changes in ctDNA levels during treatment may indicate disease response. Cancer type and stage appear to have the most

dramatic impact on ctDNA abundance, and significant decreases in, or clearance of ctDNA early in treatment seems to be predictive of response and improved outcomes. The association of treatment response and overall decreases in ctDNA levels during treatment is consistent with the hypothesis that tumor burden and tumor growth rate are reflected in ctDNA dynamics. Very early changes (1–3 h) in ctDNA levels have been hypothesized to reflect treatment response as well, but this appears to be less generalizable. For example, we might expect effective chemotherapy to induce ctDNA shedding immediately, and early, high-frequency sampling to detect it, yet observations between NSCLC, CRC and prostate cancer patients sampled within 1–3 h of chemotherapy were inconsistent (89, 90, 117). Unfortunately, there are a lack of studies sampling within this timeframe. Immunotherapy may be less fast-acting than chemotherapy given the time required for the body to prepare a successful immune response. PET/CT imaging has shown tumor responses with 4–6 weeks of treatment with ICIs in melanoma patients (118). Sample collection at 2 weeks following treatment found changes in ctDNA that correlated with outcome in ICI therapy of melanoma patients, but earlier time points were not collected (75). It possible that changes in ctDNA in response to treatment existed sooner, again, earlier, high-frequency sampling is needed to test such hypotheses. TKI-induced cell death appears to occur within 6–48 h of exposure *in vitro* (85); a similar timeframe as cell death from cytotoxic agents. Evidence presented in this review suggests that ctDNA dynamics might reflect TKI-induced cell death in this timeframe in NSCLC patients more consistently than during chemotherapy.

One potential use of ctDNA monitoring during treatment that has been explored by our lab and others (96, 101), is to induce ctDNA shedding from either inaccessible tumors or suspicious lesions for evaluation. Radiation treatment seems particularly suited for this task, however any method of perturbation that elicits ctDNA shedding could be used. For example, such approaches could improve the detection rates of ctDNA assays like CAPP-Seq and Lung-CLiP (45) in lung cancer patients or where low-dose CT is already in use for screening high-risk populations. Compression of breast tissue during mammography has been shown to temporarily increase ctDNA abundance, which could be leveraged for non-invasive biopsy or early detection (44). Other work has explored the use of ultrasound to elicit better movement of blood biomarkers across the BBB in preclinical brain tumor models (71, 72). Again, a clear understanding of early ctDNA dynamics in response to tumor perturbations is crucial before such approaches can be implemented in the clinic.

Variability in ctDNA measurements between patients and studies has been a challenge for serial monitoring. Efforts have been made to assess the biological variability of both cell-free DNA and ctDNA between measurements taken over short intervals (31, 119). Several groups have attempted to standardize criteria for evaluating differences between pre-treatment and on-treatment ctDNA levels. O'Leary et al. (120) created a "circulating tumor DNA ratio" or CDR, defined simply as the ratio of on-treatment to pre-treatment levels, to evaluate treatment response in metastatic breast cancer. Herbreteau, Kruger et al. (2018 and 2021) (75, 93) defined a "quantitative biological response and progression criteria" where patients were stratified by increases or decreases in ctDNA during treatment as compared to baseline. This approach also recognized the variability in accuracy at each time point when evaluating significance between measurements at different time points. Out of similar concern, our lab has also developed a Bayesian approach for testing statistical significance between ctDNA mutations in NGS data from serial collections (10). Given the variability in coverage of NGS data, which determines the limit of detection, the allele-specific background error rate, and the stochastic nature of mutant read detection by NGS, sophisticated methods may be required to account for these uncertainties in ctDNA evaluation.

Finally, attempts to model ctDNA shedding have shown promise in predicting ctDNA abundance based on tumor size and growth rate. Avanzini et al. (48) presented a stochastic mathematical framework based on observations in lung cancer patients which could extrapolate ctDNA copy counts using tumor cell proliferation rate, death rate, shedding probability, clearance rate, and starting tumor volume. Such modeling can reveal unexpected behavior that may be informative of real-world scenarios. For example, in simulations the authors unexpectedly found that a slow growing cancer generated more ctDNA molecules than a faster-growing cancer of the same size when the faster growth was achieved by proportional increases and decreases in birth and death rates, respectively. However, if a faster growth rate is achieved by increased birth rate and a stable death rate, the difference in ctDNA release was negligible. By integrating these variables over time, similar models might be useful in predicting changes in ctDNA abundance from changes in birth and death rates resulting from treatment.

CONCLUSION

The utilization of ctDNA in assessing treatment response will require a better understanding of the biological factors involved. We believe that ctDNA monitoring has the potential to truly revolutionize personal medicine in cancer care but there remain significant challenges that must first be overcome.

AUTHOR CONTRIBUTIONS

CB prepared and edited the text and figures; PS edited the text and figures.

CONFLICT OF INTEREST

PS has consulted for Natera.

The remaining author declares that the research was conducted in the absence of any commercial or financial relationships that could be construed as a potential conflict of interest.

REFERENCES

1. Wan JCM, Massie C, Garcia-Corbacho J, Mouliere F, Brenton JD, Caldas C, et al. Liquid Biopsies Come of Age: towards Implementation of Circulating Tumour DNA. *Nat Rev Cancer* (2017) 17(4):223–38. doi:10.1038/nrc.2017.7
2. Heitzer E, Auinger L, Speicher MR. Cell-Free DNA and Apoptosis: How Dead Cells Inform about the Living. *Trends Mol Med* (2020) 26(5):519–28. doi:10.1016/j.molmed.2020.01.012
3. Merker JD, Oxnard GR, Compton C, Diehn M, Hurley P, Lazar AJ, et al. Circulating Tumor DNA Analysis in Patients with Cancer: American Society of Clinical Oncology and College of American Pathologists Joint Review. *J Clin Oncol* (2018) 36(16):1631–41. doi:10.1200/jco.2017.76.8671
4. Abbosh C, Birkbak NJ, Wilson GA, Jamal-Hanjani M, Constantin T, Salari R, et al. Phylogenetic ctDNA Analysis Depicts Early-Stage Lung Cancer Evolution. *Nature* (2017) 545(7655):446–51. doi:10.1038/nature22364
5. Keller L, Belloum Y, Wikman H, Pantel K. Clinical Relevance of Blood-Based ctDNA Analysis: Mutation Detection and beyond. *Br J Cancer* (2021) 124(2): 345–58. doi:10.1038/s41416-020-01047-5
6. Adashek JJ, Janku F, Kurzrock R. Signed in Blood: Circulating Tumor DNA in Cancer Diagnosis, Treatment and Screening. *Cancers (Basel)* (2021) 13(14), 3600. doi:10.3390/cancers13143600
7. De Michino S, Aparnathi M, Rostami A, Lok BH, Bratman SV. The Utility of Liquid Biopsies in Radiation Oncology. *Int J Radiat Oncol Biol Phys* (2020) 107(5):873–86. doi:10.1016/j.ijrobp.2020.05.008
8. Khier S, Lohan L. Kinetics of Circulating Cell–free DNA for Biomedical Applications: Critical Appraisal of the Literature. *Future Sci OA* (2018) 4(4): FSO295. doi:10.4155/fsoa-2017-0140
9. Butler TM, Boniface CT, Johnson-Camacho K, Tabatabaei S, Melendez D, Kelley T, et al. Circulating Tumor DNA Dynamics Using Patient-Customized Assays are Associated with Outcome in Neoadjuvantly Treated Breast Cancer. *Cold Spring Harb Mol Case Stud* (2019) 5(2):a003772. doi:10.1101/mcs.a003772
10. Boniface C, Deig C, Halsey C, Kelley T, Heskett MB, Thomas CR Jr, et al. The Feasibility of Patient-specific Circulating Tumor DNA Monitoring throughout Multi-Modality Therapy for Locally Advanced Esophageal and Rectal Cancer: A Potential Biomarker for Early Detection of Subclinical Disease. *Diagnostics (Basel)* (2021) 11(1):73. doi:10.3390/diagnostics11010073
11. Magbanua MJM, Swigart LB, Wu H-T, Hirst GL, Yau C, Wolf DM, et al. Circulating Tumor DNA in Neoadjuvant-Treated Breast Cancer Reflects Response and Survival. *Ann Oncol* (2021) 32(2):229–39. doi:10.1016/j.annonc.2020.11.007
12. Morbelli S, Alama A, Ferrarazzo G, Coco S, Genova C, Rijavec E, et al. Circulating Tumor DNA Reflects Tumor Metabolism rather Than Tumor Burden in Chemotherapy-Naive Patients with Advanced Non-small Cell Lung Cancer: 18F-FDG PET/CT Study. *J Nucl Med* (2017) 58(11):1764–9. doi:10.2967/jnumed.117.193201
13. García-Olmo DC, Samos J, Picazo MG, Asensio AI, Toboso I, García-Olmo D. Release of Cell-free DNA into the Bloodstream Leads to High Levels of Non-tumor Plasma DNA during Tumor Progression in Rats. *Cancer Lett* (2008) 272(1):133–40. doi:10.1016/j.canlet.2008.07.003
14. Xi L, Pham TH-T, Payabyab EC, Sherry RM, Rosenberg SA, Raffeld M. Circulating Tumor DNA as an Early Indicator of Response to T-Cell Transfer Immunotherapy in Metastatic Melanoma. *Clin Cancer Res* (2016) 22(22): 5480–6. doi:10.1158/1078-0432.ccr-16-0613
15. Lo YM, Leung SF, Chan LY, Chan AT, Lo KW, Johnson PJ, et al. Kinetics of Plasma Epstein-Barr Virus DNA during Radiation Therapy for Nasopharyngeal Carcinoma. *Cancer Res* (2000) 60(9):2351–5.
16. Hilke FJ, Muyas F, Admard J, Kootz B, Nann D, Welz S, et al. Dynamics of Cell-free Tumour DNA Correlate with Treatment Response of Head and Neck Cancer Patients Receiving Radiochemotherapy. *Radiother Oncol* (2020) 151:182–9. doi:10.1016/j.radonc.2020.07.027
17. Zhang Q, Luo J, Wu S, Si H, Gao C, Xu W, et al. Prognostic and Predictive Impact of Circulating Tumor DNA in Patients with Advanced Cancers Treated with Immune Checkpoint Blockade. *Cancer Discov* (2020) 10(12): 1842–53. doi:10.1158/2159-8290.cd-20-0047
18. Song Y, Hu C, Hu C, Xie Z, Wu L, Zhu Z, et al. Circulating Tumor DNA Clearance Predicts Prognosis across Treatment Regimen in a Large Real-World Longitudinally Monitored Advanced Non-small Cell Lung Cancer Cohort. *Transl Lung Cancer Res* (2020) 9(2):269–79. doi:10.21037/tlcr.2020.03.17
19. Wang Y, Yang L, Bao H, Fan X, Xia F, Wan J, et al. Utility of ctDNA in Predicting Response to Neoadjuvant Chemoradiotherapy and Prognosis Assessment in Locally Advanced Rectal Cancer: A Prospective Cohort Study. *Plos Med* (2021) 18(8):e1003741. doi:10.1371/journal.pmed.1003741
20. Anagnostou V, Forde PM, White JR, Niknafs N, Hruban C, Naidoo J, et al. Dynamics of Tumor and Immune Responses during Immune Checkpoint Blockade in Non-small Cell Lung Cancer. *Cancer Res* (2019) 79(6):1214–25. doi:10.1158/0008-5472.can-18-1127
21. Adalsteinsson VA, Ha G, Freeman SS, Choudhury AD, Stover DG, Parsons HA, et al. Scalable Whole-Exome Sequencing of Cell-free DNA Reveals High Concordance with Metastatic Tumors. *Nat Commun* (2017) 8(1):1324. doi:10.1038/s41467-017-00965-y
22. Xia S, Ye J, Chen Y, Lizaso A, Huang L, Shi L, et al. Parallel Serial Assessment of Somatic Mutation and Methylation Profile from Circulating Tumor DNA Predicts Treatment Response and Impending Disease Progression in Osimertinib-Treated Lung Adenocarcinoma Patients. *Transl Lung Cancer Res* (2019) 8(6):1016–28. doi:10.21037/tlcr.2019.12.09
23. Silva R, Moran B, Baird A-M, O'Rourke CJ, Finn SP, McDermott R, et al. Longitudinal Analysis of Individual cfDNA Methylome Patterns in Metastatic Prostate Cancer. *Clin Epigenet* (2021) 13(1):168. doi:10.1186/s13148-021-01155-w
24. Aucamp J, Bronkhorst AJ, Badenhorst CPS, Pretorius PJ. The Diverse Origins of Circulating Cell-free DNA in the Human Body: A Critical Re-evaluation of the Literature. *Biol Rev* (2018) 93(3):1649–83. doi:10.1111/brv.12413
25. Gold B, Cankovic M, Furtado LV, Meier F, Gocke CD. Do circulating Tumor Cells, Exosomes, and Circulating Tumor Nucleic Acids Have Clinical Utility? A Report of the Association for Molecular Pathology. *J Mol Diagn* (2015) 17(3):209–24. doi:10.1016/j.jmoldx.2015.02.001
26. Grabuschnig S, Bronkhorst AJ, Holdenrieder S, Rosales Rodriguez I, Schliep KP, Schwendenwein D, et al. Putative Origins of Cell-free DNA in Humans: A Review of Active and Passive Nucleic Acid Release Mechanisms. *Int J Mol Sci* (2020) 21(21):8062. doi:10.3390/ijms21218062
27. Kustanovich A, Schwartz R, Peretz T, Grinshpun A. Life and Death of Circulating Cell-free DNA. *Cancer Biol Ther* (2019) 20(8):1057–67. doi:10.1080/15384047.2019.1598759
28. de Miranda FS, Barauna VG, Dos Santos L, Costa G, Vassallo PF, Campos LCG. Properties and Application of Cell-free DNA as a Clinical Biomarker. *Int J Mol Sci* (2021) 22(17):9110. doi:10.3390/ijms22179110
29. Bettegowda C, Sausen M, Leary RJ, Kinde I, Wang Y, Agrawal N, et al. Detection of Circulating Tumor DNA in Early- and Late-Stage Human Malignancies. *Sci Transl Med* (2014) 6(224):224ra24. doi:10.1126/scitranslmed.3007094
30. Phallen J, Sausen M, Adleff V, Leal A, Hruban C, White J, et al. Direct Detection of Early-Stage Cancers Using Circulating Tumor DNA. *Sci Transl Med* (2017) 9(403):eaan2415. doi:10.1126/scitranslmed.aan2415
31. Hojbjerg JA, Madsen AT, Schmidt HH, Sorensen SF, Stougaard M, Meldgaard P, et al. Intra-individual Variation of Circulating Tumour DNA in Lung Cancer Patients. *Mol Oncol* (2019) 13(10):2098–106. doi:10.1002/1878-0261.12546
32. Diehl F, Schmidt K, Choti MA, Romans K, Goodman S, Li M, et al. Circulating Mutant DNA to Assess Tumor Dynamics. *Nat Med* (2008) 14(9):985–90. doi:10.1038/nm.1789
33. Cheng ML, Pectasides E, Hanna GJ, Parsons HA, Choudhury AD, Oxnard GR. Circulating Tumor DNA in Advanced Solid Tumors: Clinical Relevance and Future Directions. *CA Cancer J Clin* (2021) 71(2):176–90. doi:10.3322/caac.21650
34. Aucamp J, Bronkhorst AJ, Peters DL, Van Dyk HC, Van der Westhuizen FH, Pretorius PJ. Kinetic Analysis, Size Profiling, and Bioenergetic Association of DNA Released by Selected Cell Lines *In Vitro*. *Cell. Mol. Life Sci.* (2017) 74(14):2689–707. doi:10.1007/s00018-017-2495-z

35. Wang W, Kong P, Ma G, Li L, Zhu J, Xia T, et al. Characterization of the Release and Biological Significance of Cell-free DNA from Breast Cancer Cell Lines. *Oncotarget* (2017) 8(26):43180–91. doi:10.18632/oncotarget.17858
36. Rostami A, Lambie M, Yu CW, Stambolic V, Waldron JN, Bratman SV. Senescence, Necrosis, and Apoptosis Govern Circulating Cell-free DNA Release Kinetics. *Cel Rep* (2020) 31(13):107830. doi:10.1016/j.celrep.2020.107830
37. Otandault A, Abraham J-D, Al Amir Dache Z, Khalyfa A, Jariel-Encontre I, Forné T, et al. Hypoxia Differently Modulates the Release of Mitochondrial and Nuclear DNA. *Br J Cancer* (2020) 122(5):715–25. doi:10.1038/s41416-019-0716-y
38. Bronkhorst AJ, Wentzel JF, Aucamp J, van Dyk E, du Plessis L, Pretorius PJ. Characterization of the Cell-free DNA Released by Cultured Cancer Cells. *Biochim Biophys Acta Mol Cel Res* (2016) 1863(1):157–65. doi:10.1016/j.bbamcr.2015.10.022
39. Bronkhorst AJ, Wentzel JF, Ungerer V, Peters DL, Aucamp J, de Villiers EP, et al. Sequence Analysis of Cell-free DNA Derived from Cultured Human Bone Osteosarcoma (143B) Cells. *Tumour Biol* (2018) 40(9):1010428318801190. doi:10.1177/1010428318801190
40. Hu Z-Y, Xie N, Tian C, Yang X, Liu L, Li J, et al. Identifying Circulating Tumor DNA Mutation Profiles in Metastatic Breast Cancer Patients with Multiline Resistance. *EBioMedicine* (2018) 32:111–8. doi:10.1016/j.ebiom.2018.05.015
41. Zhou Y, Xu Y, Gong Y, Zhang Y, Lu Y, Wang C, et al. Clinical Factors Associated with Circulating Tumor DNA (Ct DNA) in Primary Breast Cancer. *Mol Oncol* (2019) 13(5):1033–46. doi:10.1002/1878-0261.12456
42. Ortolan E, Appierto V, Silvestri M, Miceli R, Veneroni S, Folli S, et al. Blood-based Genomics of Triple-Negative Breast Cancer Progression in Patients Treated with Neoadjuvant Chemotherapy. *ESMO Open* (2021) 6(2):100086. doi:10.1016/j.esmoop.2021.100086
43. Abbosh C, Birkbak NJ, Wilson GA, Jamal-Hanjani M, Constantin T, Salari R, et al. Corrigendum: Phylogenetic ctDNA Analysis Depicts Early-Stage Lung Cancer Evolution. *Nature* (2018) 554(7691):264. doi:10.1038/nature25161
44. Förnvik D, Aaltonen KE, Chen Y, George AM, Brueffer C, Rigo R, et al. Detection of Circulating Tumor Cells and Circulating Tumor DNA before and after Mammographic Breast Compression in a Cohort of Breast Cancer Patients Scheduled for Neoadjuvant Treatment. *Breast Cancer Res Treat* (2019) 177(2):447–55. doi:10.1007/s10549-019-05326-5
45. Chabon JJ, Hamilton EG, Kurtz DM, Esfahani MS, Moding EJ, Stehr H, et al. Integrating Genomic Features for Non-invasive Early Lung Cancer Detection. *Nature* (2020) 580(7802):245–51. doi:10.1038/s41586-020-2140-0
46. Chen K-Z, Lou F, Yang F, Zhang J-B, Ye H, Chen W, et al. Circulating Tumor DNA Detection in Early-Stage Non-small Cell Lung Cancer Patients by Targeted Sequencing. *Sci Rep* (2016) 6:31985. doi:10.1038/srep31985
47. Cho M-S, Park CH, Lee S, Park HS. Clinicopathological Parameters for Circulating Tumor DNA Shedding in Surgically Resected Non-small Cell Lung Cancer with EGFR or KRAS Mutation. *PLoS One* (2020) 15(3):e0230622. doi:10.1371/journal.pone.0230622
48. Avanzini S, Kurtz DM, Chabon JJ, Moding EJ, Hori SS, Gambhir SS, et al. A Mathematical Model of ctDNA Shedding Predicts Tumor Detection Size. *Sci Adv* (2020) 6(50):eabc4308. doi:10.1126/sciadv.abc4308
49. McEvoy AC, Warburton L, Al-Ogaili Z, Celliers L, Calapre L, Pereira MR, et al. Correlation between Circulating Tumour DNA and Metabolic Tumour burden in Metastatic Melanoma Patients. *BMC Cancer* (2018) 18(1):726. doi:10.1186/s12885-018-4637-6
50. Chen Z, Fadiel A, Naftolin F, Eichenbaum KD, Xia Y. Circulation DNA: Biological Implications for Cancer Metastasis and Immunology. *Med Hypotheses* (2005) 65(5):956–61. doi:10.1016/j.mehy.2005.04.042
51. Ungerer V, Bronkhorst AJ, Van den Ackerveken P, Herzog M, Holdenrieder S. Serial Profiling of Cell-free DNA and Nucleosome Histone Modifications in Cell Cultures. *Sci Rep* (2021) 11(1):9460. doi:10.1038/s41598-021-88866-5
52. Fleischhacker M, Schmidt B. Circulating Nucleic Acids (CNAs) and Cancer-A Survey. *Biochim Biophys Acta Rev Cancer* (2007) 1775(1):181–232. doi:10.1016/j.bbcan.2006.10.001
53. Choi JJ, Reich CF, 3rd, Pisetsky DS. Release of DNA from Dead and Dying Lymphocyte and Monocyte Cell Lines *In Vitro*. *Scand J Immunol* (2004) 60(1-2):159–66. doi:10.1111/j.0300-9475.2004.01470.x
54. Utani K-i., Okamoto A, Shimizu N. Generation of Micronuclei during Interphase by Coupling between Cytoplasmic Membrane Blebbing and Nuclear Budding. *PLoS One* (2011) 6(11):e27233. doi:10.1371/journal.pone.0027233
55. Kisurina-Evgenieva OP, Sutiagina OI, Onishchenko GE. Biogenesis of Micronuclei. *Biochem Mosc* (2016) 81(5):453–64. doi:10.1134/s0006297916050035
56. Ryoo HD, Bergmann A. The Role of Apoptosis-Induced Proliferation for Regeneration and Cancer. *Cold Spring Harbor Perspect Biol* (2012) 4(8):a008797. doi:10.1101/cshperspect.a008797
57. Lugano R, Ramachandran M, Dimberg A. Tumor Angiogenesis: Causes, Consequences, Challenges and Opportunities. *Cel Mol. Life Sci.* (2020) 77(9):1745–70. doi:10.1007/s00018-019-03351-7
58. Wang J, Huang A, Wang Y-P, Yin Y, Fu P-Y, Zhang X, et al. Circulating Tumor DNA Correlates with Microvascular Invasion and Predicts Tumor Recurrence of Hepatocellular Carcinoma. *Ann Transl Med* (2020) 8(5):237. doi:10.21037/atm.2019.12.154
59. Shirasu H, Taniguchi H, Watanabe J, Kotaka M, Yamazaki K, Hirata K, et al. O-11 Monitoring Molecular Residual Disease by Circulating Tumor DNA in Resectable Colorectal Cancer: Molecular Subgroup Analyses of a Prospective Observational Study GALAXY in CIRCULATE-Japan. *Ann Oncol* (2021) 32:S222–S223. doi:10.1016/j.annonc.2021.05.015
60. Nabavizadeh SA, Ware JB, Guiry S, Nasrallah MP, Mays JJ, Till JE, et al. Imaging and Histopathologic Correlates of Plasma Cell-free DNA Concentration and Circulating Tumor DNA in Adult Patients with Newly Diagnosed Glioblastoma. *Neurooncol Adv* (2020) 2(1):vdaa016. doi:10.1093/noajnl/vdaa016
61. Bagley SJ, Nabavizadeh SA, Mays JJ, Till JE, Ware JB, Levy S, et al. Clinical Utility of Plasma Cell-free DNA in Adult Patients with Newly Diagnosed Glioblastoma: A Pilot Prospective Study. *Clin Cancer Res* (2020) 26(2):397–407. doi:10.1158/1078-0432.ccr-19-2533
62. Mair R, Mouliere F, Smith CG, Chandrananda D, Gale D, Marass F, et al. Measurement of Plasma Cell-free Mitochondrial Tumor DNA Improves Detection of Glioblastoma in Patient-Derived Orthotopic Xenograft Models. *Cancer Res* (2019) 79(1):220–30. doi:10.1158/0008-5472.can-18-0074
63. McKeown SR. Defining Normoxia, Physoxia and Hypoxia in Tumours-Implications for Treatment Response. *Br J Radiol* (2014) 87(1035):20130676. doi:10.1259/bjr.20130676
64. Harris AL. Hypoxia - A Key Regulatory Factor in Tumour Growth. *Nat Rev Cancer* (2002) 2(1):38–47. doi:10.1038/nrc704
65. Giacona MB, Ruben GC, Iczkowski KA, Roos TB, Porter DM, Sorenson GD. Cell-free DNA in Human Blood Plasma: Length Measurements in Patients with Pancreatic Cancer and Healthy Controls. *Pancreas* (1998) 17(1):89–97. doi:10.1097/00006676-199807000-00012
66. Jahr S, Hentze H, Englisch S, Hardt D, Fackelmayer FO, Hesch RD, et al. DNA Fragments in the Blood Plasma of Cancer Patients: Quantitations and Evidence for Their Origin from Apoptotic and Necrotic Cells. *Cancer Res* (2001) 61(4):1659–65.
67. Cortese R, Almendros I, Wang Y, Gozal D. Tumor Circulating DNA Profiling in Xenografted Mice Exposed to Intermittent Hypoxia. *Oncotarget* (2015) 6(1):556–69. doi:10.18632/oncotarget.2785
68. Lindberg HK, Wang X, Järventaus H, Falck GC, Norppa H, Fenech M. Origin of Nuclear Buds and Micronuclei in normal and Folate-Deprived Human Lymphocytes. *Mutat Res* (2007) 617(1-2):33–45. doi:10.1016/j.mrfmmm.2006.12.002
69. Al-Asmakh M, Hedin L. Microbiota and the Control of Blood-Tissue Barriers. *Tissue Barriers* (2015) 3(3):e1039691. doi:10.1080/21688370.2015.1039691
70. Lo YMD, Tein MSC, Lau TK, Haines CJ, Leung TN, Poon PMK, et al. Quantitative Analysis of Fetal DNA in Maternal Plasma and Serum: Implications for Noninvasive Prenatal Diagnosis. *Am J Hum Genet* (1998) 62(4):768–75. doi:10.1086/301800

71. Zhu L, Nazeri A, Pacia CP, Yue Y, Chen H. Focused Ultrasound for Safe and Effective Release of Brain Tumor Biomarkers into the Peripheral Circulation. *PLoS One* (2020) 15(6):e0234182. doi:10.1371/journal.pone.0234182
72. Pacia CP, Zhu L, Yang Y, Yue Y, Nazeri A, Michael Gach H, et al. Feasibility and Safety of Focused Ultrasound-Enabled Liquid Biopsy in the Brain of a Porcine Model. *Sci Rep* (2020) 10(1):7449. doi:10.1038/s41598-020-64440-3
73. Choi J-J, Reich CF, 3rd, Pisetsky DS. The Role of Macrophages in the *In Vitro* Generation of Extracellular DNA from Apoptotic and Necrotic Cells. *Immunology* (2005) 115(1):55–62. doi:10.1111/j.1365-2567.2005.02130.x
74. Jiang N, Reich CF, 3rd, Pisetsky DS. Role of Macrophages in the Generation of Circulating Blood Nucleosomes from Dead and Dying Cells. *Blood* (2003) 102(6):2243–50. doi:10.1182/blood-2002-10-3312
75. Herbreteau G, Vallee A, Knol AC, Theoleyre S, Quereux G, Varey E, et al. Circulating Tumor DNA Early Kinetics Predict Response of Metastatic Melanoma to Anti-PD1 Immunotherapy: Validation Study. *Cancers (Basel)* (2021) 13(8):1826. doi:10.3390/cancers13081826
76. Westman J, Grinstein S, Marques PE. Phagocytosis of Necrotic Debris at Sites of Injury and Inflammation. *Front Immunol* (2019) 10:3030. doi:10.3389/fimmu.2019.03030
77. Lo YMD, Zhang J, Leung TN, Lau TK, Chang AMZ, Hjelm NM. Rapid Clearance of Fetal DNA from Maternal Plasma. *Am J Hum Genet* (1999) 64(1):218–24. doi:10.1086/302205
78. Patel PS, Patel BP, Rawal RM, Raval GN, Patel MM, Patel JB, et al. Evaluation of Serum Alkaline DNase Activity in Treatment Monitoring of Head and Neck Cancer Patients. *Tumor Biol* (2000) 21(2):82–9. doi:10.1159/000030113
79. Martin M, Leffler J, Smoląg KI, Mytych J, Björk A, Chaves LD, et al. Factor H Uptake Regulates Intracellular C3 Activation during Apoptosis and Decreases the Inflammatory Potential of Nucleosomes. *Cell Death Differ* (2016) 23(5):903–11. doi:10.1038/cdd.2015.164
80. Kirsch C, Weickmann S, Schmidt B, Fleischhacker M. An Improved Method for the Isolation of Free-Circulating Plasma DNA and Cell-free DNA from Other Body Fluids. *Ann N Y Acad Sci* (2008) 1137:135–9. doi:10.1196/annals.1448.035
81. Gauthier VJ, Tyler LN, Mannik M. Blood Clearance Kinetics and Liver Uptake of Mononucleosomes in Mice. *J Immunol* (1996) 156(3):1151–6.
82. Korabecna M, Opatrna S, Wirth J, Rulcova K, Eiselt J, Sefrna F, et al. Cell-free Plasma DNA during Peritoneal Dialysis and Hemodialysis and in Patients with Chronic Kidney Disease. *Ann N Y Acad Sci* (2008) 1137:296–301. doi:10.1196/annals.1448.014
83. Cheng THT, Jiang P, Tam JCW, Sun X, Lee W-S, Yu SCY, et al. Genomewide Bisulfite Sequencing Reveals the Origin and Time-dependent Fragmentation of Urinary cfDNA. *Clin Biochem* (2017) 50(9):496–501. doi:10.1016/j.clinbiochem.2017.02.017
84. Hung ECW, Shing TKF, Chim SSC, Yeung PC, Chan RWY, Chik KW, et al. Presence of Donor-Derived DNA and Cells in the Urine of Sex-Mismatched Hematopoietic Stem Cell Transplant Recipients: Implication for the Transrenal Hypothesis. *Clin Chem* (2009) 55(4):715–22. doi:10.1373/clinchem.2008.113530
85. Costa DB, Halmos B, Kumar A, Schumer ST, Huberman MS, Boggon TJ, et al. BIM Mediates EGFR Tyrosine Kinase Inhibitor-Induced Apoptosis in Lung Cancers with Oncogenic EGFR Mutations. *Plos Med* (2007) 4(10):1669–80. doi:10.1371/journal.pmed.0040315
86. Phallen J, Leal A, Woodward BD, Forde PM, Naidoo J, Marrone KA, et al. Early Noninvasive Detection of Response to Targeted Therapy in Non-small Cell Lung Cancer. *Cancer Res* (2019) 79(6):1204–13. doi:10.1158/0008-5472.can-18-1082
87. Blankenberg FG. *In Vivo* imaging of Apoptosis. *Cancer Biol Ther* (2008) 7(10):1525–32. doi:10.4161/cbt.7.10.6934
88. Maier P, Hartmann L, Wenz F, Herskind C. Cellular Pathways in Response to Ionizing Radiation and Their Targetability for Tumor Radiosensitization. *Int J Mol Sci* (2016) 17(1):102. doi:10.3390/ijms17010102
89. Patsch K, Matasci N, Soundararajan A, Diaz P, Agus DB, Ruderman D, et al. Monitoring Dynamic Cytotoxic Chemotherapy Response in Castration-Resistant Prostate Cancer Using Plasma Cell-free DNA (cfDNA). *BMC Res Notes* (2019) 12(1):275. doi:10.1186/s13104-019-4312-2
90. Moser T, Waldispuehl-Geigl J, Belic J, Weber S, Zhou Q, Hasenleithner SO, et al. On-treatment Measurements of Circulating Tumor DNA during FOLFOX Therapy in Patients with Colorectal Cancer. *NPJ Precis Oncol* (2020) 4(1):30. doi:10.1038/s41698-020-00134-3
91. Lyskjær I, Kronborg CS, Rasmussen MH, Sørensen BS, Demuth C, Rosenkilde M, et al. Correlation between Early Dynamics in Circulating Tumour DNA and Outcome from FOLFIRI Treatment in Metastatic Colorectal Cancer. *Sci Rep* (2019) 9(1):11542. doi:10.1038/s41598-019-47708-1
92. Wang H, Zhang B, Chen D, Xia W, Zhang J, Wang F, et al. Real-time Monitoring Efficiency and Toxicity of Chemotherapy in Patients with Advanced Lung Cancer. *Clin Epigenet* (2015) 7:119. doi:10.1186/s13148-015-0150-9
93. Kruger S, Heinemann V, Ross C, Diehl F, Nagel D, Ormanns S, et al. Repeated mutKRAS ctDNA Measurements Represent a Novel and Promising Tool for Early Response Prediction and Therapy Monitoring in Advanced Pancreatic Cancer. *Ann Oncol* (2018) 29(12):2348–55. doi:10.1093/annonc/mdy417
94. Chera BS, Kumar S, Shen C, Amdur R, Dagan R, Green R, et al. Plasma Circulating Tumor HPV DNA for the Surveillance of Cancer Recurrence in HPV-Associated Oropharyngeal Cancer. *J Clin Oncol* (2020) 38(10):1050–8. doi:10.1200/jco.19.02444
95. Moding EJ, Liu Y, Hui AB, He J, Qiao Y, Xu T, et al. Abstract PO-069: Circulating Tumor DNA Kinetics to Identify Genomic Predictors of Rapid Response to Chemoradiation in Non-small Cell Lung Cancer. *Clin Cancer Res* (2021) 27(8 Suppl.):PO-069. doi:10.1158/1557-3265.radsci21-po-069
96. Breadner DA, Vincent MD, Correa R, Black M, Warner A, Sanatani M, et al. Exploitation of Treatment Induced Tumor Lysis to Enhance the Sensitivity of ctDNA Analysis: A First-In-Human Pilot Study. *Lung Cancer* (2022) 165:145–51. doi:10.1016/j.lungcan.2022.01.013
97. Leon SA, Shapiro B, Sklaroff DM, Yaros MJ. Free DNA in the Serum of Cancer Patients and the Effect of Therapy. *Cancer Res* (1977) 37(3):646–50.
98. Medvedeva NG, Panyutin IV, Panyutin IG, Neumann RD. Phosphorylation of Histone H2AX in Radiation-Induced Micronuclei. *Radiat Res* (2007) 168(4):493–8. doi:10.1667/rr0788.1
99. Durante M, Formenti SC. Radiation-Induced Chromosomal Aberrations and Immunotherapy: Micronuclei, Cytosolic DNA, and Interferon-Production Pathway. *Front Oncol* (2018) 8:192. doi:10.3389/fonc.2018.00192
100. Walls GM, McConnell L, McAleese J, Murray P, Lynch TB, Savage K, et al. Early Circulating Tumour DNA Kinetics Measured by Ultra-deep Next-Generation Sequencing during Radical Radiotherapy for Non-small Cell Lung Cancer: A Feasibility Study. *Radiat Oncol* (2020) 15(1):132. doi:10.1186/s13014-020-01583-7
101. Boniface C, Baker K, Dieg C, Halsey C, Rahmani R, Deffenbach M, et al. Abstract PR05: Radiation-Assisted Amplification Sequencing (RAMP-Seq): Evaluating the Use of Stereotactic Body Radiation Therapy (SBRT) for Enriching Circulating Tumor DNA in Liquid Biopsies. *Clin Cancer Res* (2020) 26(11 Suppl.):PR05. doi:10.1158/1557-3265.liqbiop20-pr05
102. Chen EL, Chaudhuri AA, Nabet BY, Chabon JJ, Merriott DJ, Loo BW, et al. Analysis of Circulating Tumor DNA Kinetics during Stereotactic Ablative Radiation Therapy for Non-small Cell Lung Cancer. *Int J Radiat Oncol Biol Phys* (2018) 102(3 Suppl.):e676. doi:10.1016/j.ijrobp.2018.07.1826
103. Chaudhuri AA, Lovejoy AF, Chabon JJ, Newman A, Stehr H, Merriott DJ, et al. Circulating Tumor DNA Analysis during Radiation Therapy for Localized Lung Cancer Predicts Treatment Outcome. *Int J Radiat Oncol Biol Phys* (2017) 99(2 Suppl.):S1–S2. doi:10.1016/j.ijrobp.2017.06.021
104. Johnson BE, Creason AL, Stommel JM, Keck JM, Parmar S, Betts CB, et al. An Omic and Multidimensional Spatial Atlas from Serial Biopsies of an Evolving Metastatic Breast Cancer. *Cel Rep Med* (2022) 3(2):100525. doi:10.1016/j.xcrm.2022.100525
105. Mole RH. Whole Body Irradiation-Radiobiology or Medicine? *Br J Radiol* (1953) 26(305):234–41. doi:10.1259/0007-1285-26-305-234
106. Neumann MHD, Bender S, Krahn T, Schlange T. ctDNA and CTCs in Liquid Biopsy - Current Status and where We Need to Progress. *Comput Struct Biotechnol J* (2018) 16:190–5. doi:10.1016/j.csbj.2018.05.002
107. Ng SP, Meas S, Bahig H, Skinner HD, Garden AS, Phan J, et al. Detection of Circulating Tumor Cells during Radiation Therapy in Patients with Head and Neck Cancer. *Int J Radiat Oncol Biol Phys* (2018) 102(3 Suppl.):e177. doi:10.1016/j.ijrobp.2018.07.657
108. Lee JH, Long GV, Menzies AM, Lo S, Guminski A, Whitbourne K, et al. Association between Circulating Tumor DNA and Pseudoprogression in

Patients with Metastatic Melanoma Treated with Anti-programmed Cell Death 1 Antibodies. *JAMA Oncol* (2018) 4(5):717–21. doi:10.1001/jamaoncol.2017.5332

109. Ma Y, Wang Q, Dong Q, Zhan L, Zhang J. How to Differentiate Pseudoprogression from True Progression in Cancer Patients Treated with Immunotherapy. *Am J Cancer Res* (2019) 9(8):1546–53.
110. Váraljai R, Elouali S, Lueong SS, Wistuba-Hamprecht K, Seremet T, Siveke JT, et al. The Predictive and Prognostic Significance of Cell-free DNA Concentration in Melanoma. *J Eur Acad Dermatol Venereol* (2021) 35(2): 387–95. doi:10.1111/jdv.16766
111. Goldberg SB, Narayan A, Kole AJ, Decker RH, Teysir J, Carriero NJ, et al. Early Assessment of Lung Cancer Immunotherapy Response via Circulating Tumor DNA. *Clin Cancer Res* (2018) 24(8):1872–80. doi:10.1158/1078-0432.ccr-17-1341
112. Kato K, Uchida J, Kukita Y, Kumagai T, Nishino K, Inoue T, et al. Transient Appearance of Circulating Tumor DNA Associated with De Novo Treatment. *Sci Rep* (2016) 6:38639. doi:10.1038/srep38639
113. Riediger AL, Dietz S, Schirmer U, Meister M, Heinzmann-Groth I, Schneider M, et al. Mutation Analysis of Circulating Plasma DNA to Determine Response to EGFR Tyrosine Kinase Inhibitor Therapy of Lung Adenocarcinoma Patients. *Sci Rep* (2016) 6:33505. doi:10.1038/srep33505
114. Horn L, Whisenant JG, Wakelee H, Reckamp KL, Qiao H, Leal TA, et al. Monitoring Therapeutic Response and Resistance: Analysis of Circulating Tumor DNA in Patients with ALK+ Lung Cancer. *J Thorac Oncol* (2019) 14(11):1901–11. doi:10.1016/j.jtho.2019.08.003
115. Wyatt AW, Azad AA, Volik SV, Annala M, Beja K, McConeghy B, et al. Genomic Alterations in Cell-free DNA and Enzalutamide Resistance in Castration-Resistant Prostate Cancer. *JAMA Oncol* (2016) 2(12):1598–606. doi:10.1001/jamaoncol.2016.0494
116. Romanel A, Gasi Tandefelt D, Conteduca V, Jayaram A, Casiraghi N, Wetterskog D, et al. Plasma AR and Abiraterone-Resistant Prostate Cancer. *Sci Transl Med* (2015) 7(312):312re10. doi:10.1126/scitranslmed.aac9511
117. Breadner DA, Vincent MD, Correa RJM, Black M, Warner A, Qu M, et al. Exploitation of Treatment Induced Tumor Lysis to Enhance Sensitivity of ctDNA Analysis: A First-In-Human Pilot Study. *J Clin Oncol* (2020) 38(15_Suppl. l):3530. doi:10.1200/jco.2020.38.15_suppl.3530
118. van de Donk PP, Kist de Ruijter L, Lub-de Hooge MN, Brouwers AH, van der Wekken AJ, Oosting SF, et al. Molecular Imaging Biomarkers for Immune Checkpoint Inhibitor Therapy. *Theranostics* (2020) 10(4):1708–18. doi:10.7150/thno.38339
119. Wagner JT, Kim HJ, Johnson-Camacho KC, Kelley T, Newell LF, Spellman PT, et al. Diurnal Stability of Cell-free DNA and Cell-free RNA in Human Plasma Samples. *Sci Rep* (2020) 10(1):16456. doi:10.1038/s41598-020-73350-3
120. O'Leary B, Hrebien S, Morden JP, Beaney M, Fribbens C, Huang X, et al. Early Circulating Tumor DNA Dynamics and Clonal Selection with Palbociclib and Fulvestrant for Breast Cancer. *Nat Commun* (2018) 9(1):896. doi:10.1038/s41467-018-03215-x

Pathology & Oncology Research | frontiers

HYPOTHESIS AND THEORY
published: 25 May 2022
doi: 10.3389/pore.2022.1610067

Single-Cell Transcriptome Profiling Signatures and Alterations of Microglia Associated With Glioblastoma Associate Microglia Contribution to Tumor Formation

Hailong Xia[1†], *Lei Deng*[2†], *Shu Meng*[3], *Xipeng Liu*[1] *and Chao Zheng*[1*]

[1]*Department of Neurosurgery, Chongqing Red Cross Hospital (Jiangbei District People's Hospital), Chongqing, China,* [2]*Department of Neurosurgery, Bishan District People's Hospital, Chongqing, China,* [3]*Internal Medicine, Chongqing Red Cross Hospital (Jiangbei District People's Hospital), Chongqing, China*

Glioblastoma (GBM), which occasionally occurs in pediatric patients, is the most common tumor of the central nervous system in adults. Clinically, GBM is classified as low-grade to high-grade (from 1 to 4) and is characterized by late discovery, limited effective treatment methods, and poor efficacy. With the development of immunotherapy technology, effective GBM treatment strategies are of great significance. The main immune cells found in the GBM tumor microenvironment are macrophages and microglia (MG). Both these monocytes play important roles in the occurrence and development of GBM. Macrophages are recruited during tumorigenesis, whereas MG is present in the brain during embryonic development. Interestingly, the accumulation of these monocytes is inversely proportional to the survival of adult GBM patients but not the pediatric GBM patients. This study used single-cell RNA-seq data to reveal the heterogeneity of MG in tumor lesions and to explore the role of different MG subtypes in the occurrence and development of GBM. The results may help find new targets for immunotherapy of GBM.

Keywords: GBM, single-sell RNA-seq, microglia, tumor immune microenvironment, aged microglia

OPEN ACCESS

Edited by:
József Tímár,
Semmelweis University, Hungary

***Correspondence:**
Chao Zheng
lemanarc@dreamway-china.com

[†]*These authors have contributed equally to this work*

Received: *08 September 2021*
Accepted: *05 May 2022*
Published: *25 May 2022*

Citation:
Xia H, Deng L, Meng S, Liu X and Zheng C (2022) Single-Cell Transcriptome Profiling Signatures and Alterations of Microglia Associated With Glioblastoma Associate Microglia Contribution to Tumor Formation. Pathol. Oncol. Res. 28:1610067. doi: 10.3389/pore.2022.1610067

INTRODUCTION

GBM is the most common and infiltrating type of primary brain tumor, with a global incidence of approximately 70,000–100,000 per year. It is characterized by hidden onset, high morbidity, high fatality, high recurrence, and low cure rates [1]. Even with active therapy, GBM is extremely prone to relapse and has poor prognosis. The median survival time of patients is usually between 15–19 months, and the 5-year survival rate is only 5%. Approximately 180,000–600,000 young and middle-aged people die of GBM worldwide each year [2, 3].

In the past decade, researchers have found that the tumor microenvironment has a notable impact on tumorigenesis and tumor development [4]. The interactions and mutual influence between non-

Abbreviations: CNS, the central nervous system; GBM, glioblastoma; HLA, human leukocyte antigen; MG, microglia; MHC-II, major histocompatibility complex classII; MMP, matrix metalloprotease; OS, overall survival; PCA, principal component analysis; TGF-β, transforming growth factor β; UMAP, uniform manifold approximation and projection.

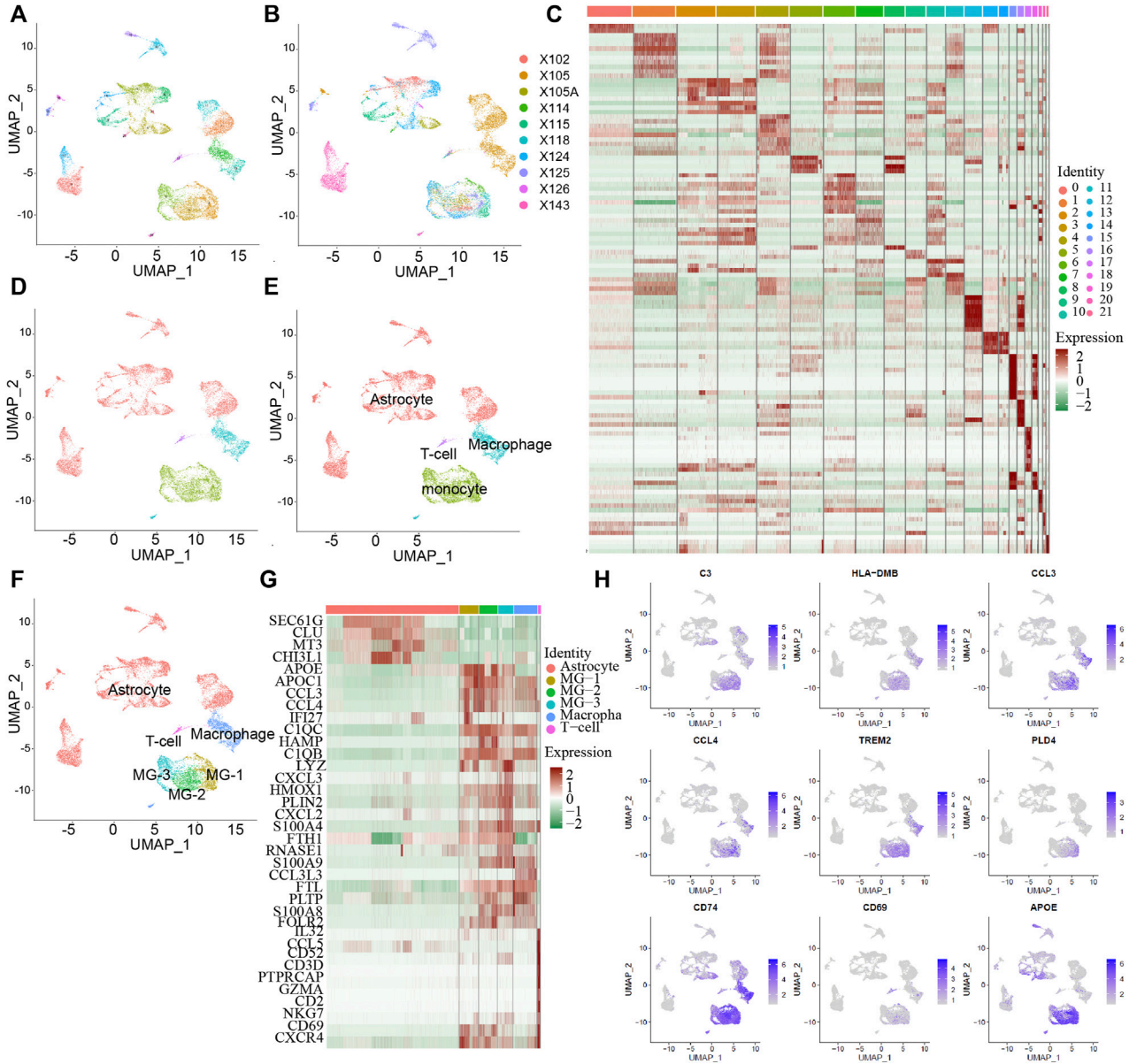

FIGURE 1 | The subtype of MG cells in GBM tumor microenvironment. Integrated single-cell RNA-Seq analysis of human GBM tumor cells. All ten samples were analyzed using canonical correlation analysis with the Seurat R package. Cells were clustered using a graph-based shared nearest neighbor clustering approach and visualized using a UMAP plot. **(A,B)** All cells were clustered in 21 clusters from 10 patients. **(C)** 21 cluster's marker genes expression heatmap. **(D)** All cells were characterized into 4 cell types. **(E)** Automatically identify cell types with the singleR package. **(F)** Combined with the GBM tumor microenvironment, identify the cell type and the MG cell subtype. **(G)** Heatmap of marker genes expressed in different cell types. **(H)** Some of MG cell associate genes are report by the previous studies and the current MG especially expressed genes.

tumor and tumor cells have gradually attracted attention and led to more in-depth discussions. Owing to the presence of the blood-brain barrier, the tissue environment in which GBM exists is very different from that of other tumors. Most GBM tumors are characterized by immune tolerance. MGs, macrophages, and T cells constitute the immune microenvironment [5, 6].

Malignant tumor and immune cells in the immune microenvironment are regulated. Inflammatory infiltrating cells, including macrophages and MG, account for more than half of the total immune cells in the GBM immune microenvironment [4]. They are considered important in inducing tumor invasion and growth by secreting CCL5, IL-113, TGF-β, EGF, IL-6, and platelet-derived growth factors [7, 8]. During its immune response to GBM, MG can also release soluble factors to promote tumor migration. It is believed that malignant tumor cells can secrete chemokines (CCL2 and CXCL2) [9, 10] to recruit macrophages and MG, which gather around tumor cells, thereby promoting tumor formation and evading immune cell attack. MG is a source of yolk sac myeloid precursor cells.

In GBM, the mechanism through which MG differentiates into subgroups with different roles is not fully understood. Previous studies have shown that the loss of MG induced in different ways can inhibit the growth of malignant gliomas [11–13]. *Gpnmb* and *Spp1* genes have also been implicated in the accumulation of disease-related MG and MG-related cancer cell proliferation, and they are associated with poor prognosis of human GBM [14]. The tetracycline analog minocycline can block the activation of MG and reduce tumor growth in a GBM mouse model [15, 16]. In a mouse brain tumor slice model, antibodies against the MG Toll-like receptors (TLRs) target the tumor size [17]. Unfortunately, human clinical trials targeting MGs have not yielded satisfactory results. At the same time, no markers have been identified that can distinguish tumor-associated MGs from other MG subgroups. Accordingly, analyzing single-cell sequencing data to explore the heterogeneity of MGs in the immune microenvironment of GBM can help determine the differentiation mechanism of tumor-related MG cells during tumor formation. This will provide a potential target for molecular diagnostics and clinical therapy of GBM.

MATERIALS AND METHODS

Data Collection

Single-cell RNA-seq data from 10 adult and pediatric patients with IDH-wildtype glioblastomas were downloaded from the Gene Expression Omnibus (GEO) database (dataset NO. GSE131928). The old and young mice brain single-cell RNA-seq data were also downloaded from the GEO database (dataset NO. GSE147693).

Single-Cell RNA-Seq Data Processing

The Cell Ranger software (v3.3.0) provided by 10x Genomics contains raw data with barcodes after single-cell sequencing. The STAR (v0.3.7) tool was used to map reads to the genome and transcriptome and aggregate the data in the samples to generate normalization data for generating a gene expression count matrix corresponding to the cell. We used the Seurat R package to process the unique molecular identifier (UMI) count matrix (v3.0) [18]. To remove low-quality cells and possible multiple captures, we filtered out cells with a limit of +/− 2 times the number of UMI/genes beyond the average value, assuming that the UMI/gene of each cell has a Gaussian standard deviation. After checking the cell distribution ratio for mitochondrial gene expression, Based on the distribution of mitochondrial gene expression, we further discarded >20% of the cells. After applying these quality control standards, we normalized the filtered matrix in Seurat to obtain normalized counts. Principal component analysis (PCA) was performed to reduce matrix dimensions. The cells are clustered based on the graph-based clustering method and visualized in two dimensions using Uniform Manifold Approximation and Projection (UMAP). Marker genes can simultaneously test the average expression and percentage of expressed cells to identify genes that are significantly differentially expressed between the clusters. For cell type identification, the singleR package (v1.4.1) [19] was used to assist in the determination based on the "HumanPrimaryCellAtlasData" parameter.

Pseudotime Analysis

We used Monocle and Monocle3 packages (http://cole-trapnell-lab.github.io/monocle-release/) to set a pseudo-chronological sequence of cell development [20]. First, we used the importCDS function in Monocle to convert the original count matrix in the Seurat object into the CellDataSet format and determine the differentiation trajectory between cells. Then, the Monocle3 package was used to infer the pseudo-time trajectory and differentiation direction of cell development.

Differential Expression Analysis

Differential expression analysis was performed using the MetaDE package (v1.30.1) [21]. Significantly differentially expressed genes were identified using the meta-analysis method and Bonferroni correction (adjusted *p*-value).

Gene Ontology Term and Pathway Enrichment Analysis

We took the significantly different genes obtained from the Single-cell RNA-seq analysis as the gene set and used the clusterProfile package (v3.18.1) [22] to perform GO and KEGG function and pathway enrichment analysis. The column chart displays the KEGG pathway enrichment results and the original chart displays the GO term enrichment analysis. The results show the enrichment results of the top ten enrichment scores and the presence of cross genes in the enriched set in the form of a network.

PPI-Network Analysis

The differentially expressed genes between the single-cell clusters were placed into the protein interaction database (STRING: functional protein association networks online analysis software), the differential gene interaction (from curated databases and experimentally determined) relationship network was extracted, and Cytoscape (v3.6.1) was used to perform protein interaction network analysis and find the key network nodes by combining GO and KEGG enrichment results.

TCGA Clinical and Sequencing Data Analysis

Connecting to the TCGA database through cBioPortal (www.cbioportal.org), we downloaded the RNA-seq data of 543 patients and the survival analysis data of 147 patients in the glioblastoma (TCGA, Cell 2013) gene set. We then performed mRNA co-expression analysis and analyzed the gene expression differences corresponding to the survival rate analysis.

RESULT

Single-Cell RNA-Seq Identifies Multiple Cell Population in 10 GBM Samples

To study the influence of MG in the tumor microenvironment of human GBM on tumorigenesis and development, we downloaded 10X single-cell RNA-seq data from 10 GBM samples (**Figure 1A**) from the GEO database. Among them,

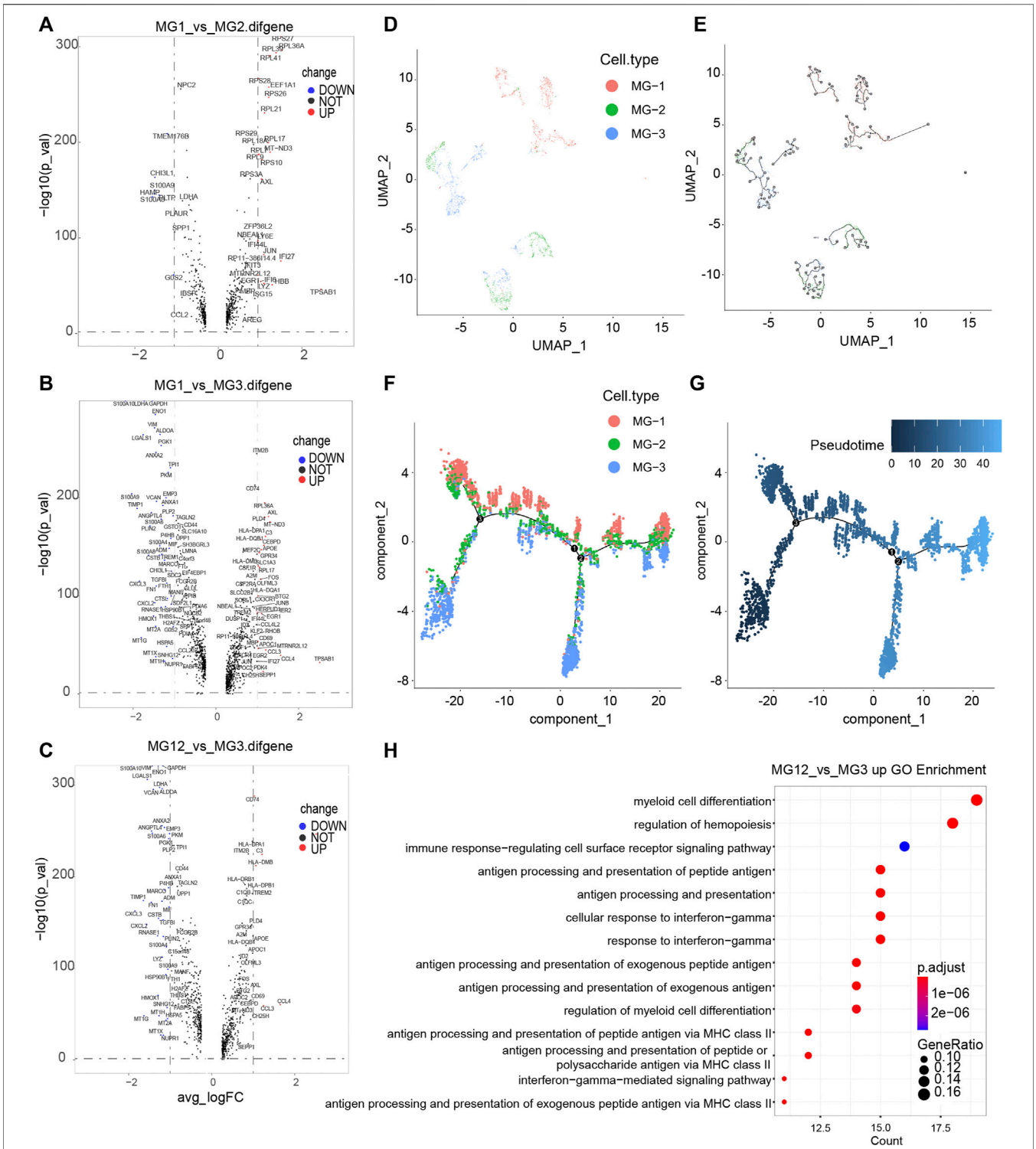

FIGURE 2 | Genetic analysis of differences among subtypes of MG cells in GBM tumor microenvironment. **(A–C)** Volcano plot of different genes between every two subtypes of MG cells. Significantly different genes (logFC > 1 and –log10 (p_val) > 20) are red dots (with gene names), while black dots represent those that are not significant; the x-axis represents the log2 (fold change) and the y axis is the –log10 (p_val). **(D,E)** Monocle relies on machine learning technology, Reversed Graph Embedding, to construct single-cell trajectories. **(F,G)** Trajectory inference by monocle3, the Pseudotime value of a cell, is the distance from its position along the branch to the root (relatively). **(H)** Functional enrichment analysis was performed using GO enrichment with the significantly upregulated genes in MG-12 compare to MG-3. The top 20 significantly enriched GO processes are shown.

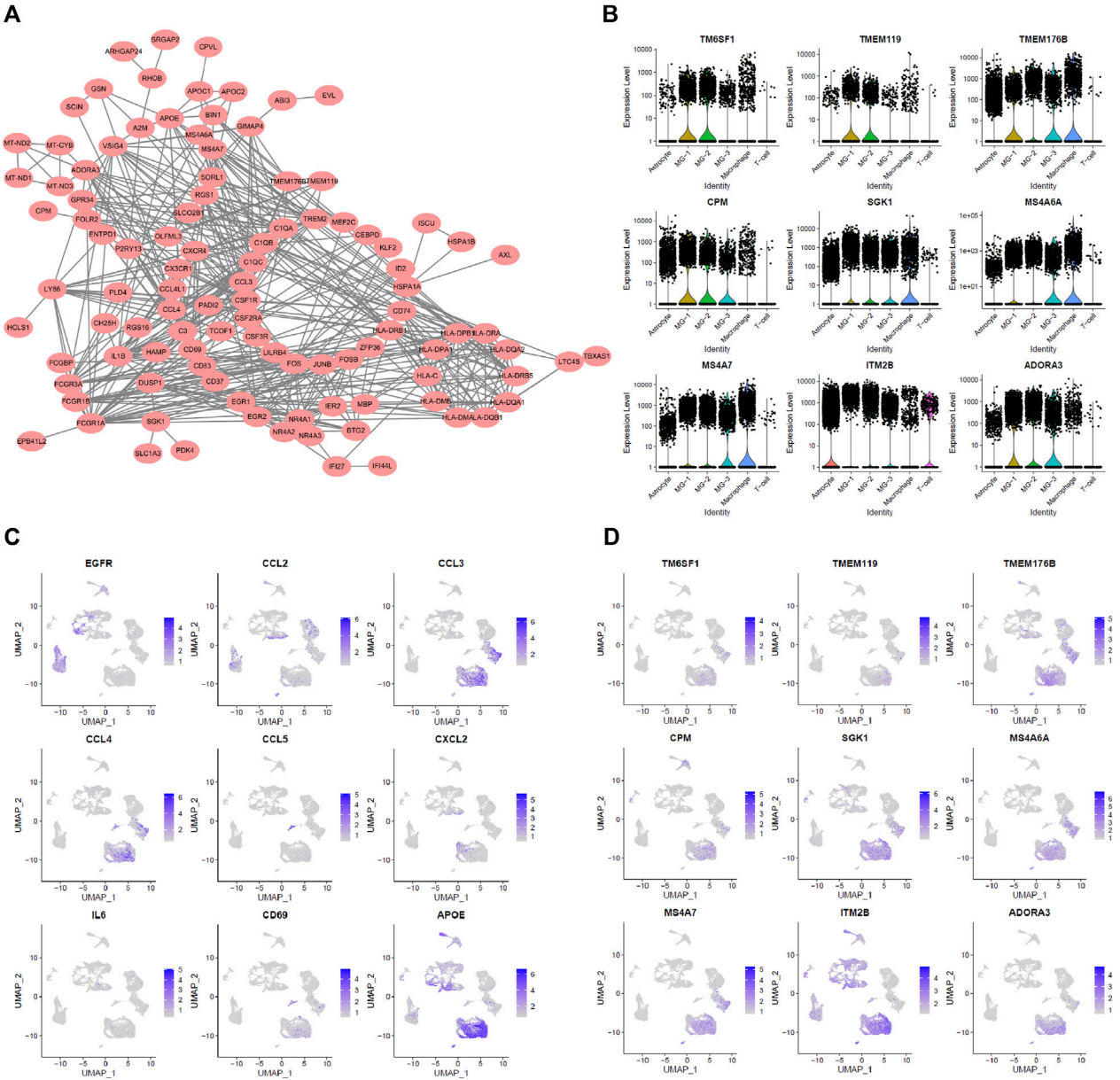

FIGURE 3 | Characteristic of MG-12 up-regulation genes. **(A)** PPI-Network representing related MG-12 up-regulation genes. **(B)** Cell chemotaxis-related genes. **(C,D)** Myeloid cell differentiation GO term genes expression in all cell types.

nine samples were from adults and one sample was from a minor. After data quality control and principal component analysis (PCA) (**Supplementary Figure S1**), all cells were classified into 21 clusters (**Figure 1A**), combined with the marker genes of cells in the HumanPrimaryCellAtlasData database, and they were divided into five cell types (**Figure 1D**). Malignant tumor cells accounted for the largest percentage of cells, followed by macrophages, monocytes, T cells, and endothelial cells. Based on previous studies on the microenvironment of GBM tumors and the marker gene of each cluster (**Figure 1C**), the monocyte cluster was further divided into three subsets of MGs (**Figure 1F**). Analysis of the marker genes (**Figure 1G**) of the final six cell types revealed that the three subsets of MG-1, MG-2, and MG-3 have the same markers (**Figure 1H**), including *CCL3*, *CCL4*, and *CXCL2*, which have been reported to be significantly elevated in MG.

GBM Associated MG Cells Transcriptomic Alteration Analysis

First, the three subsets of MG cells were analyzed for differential expression in pairs (**Figures 2A–C**; **Supplementary Figure S2**). The results showed that the overall difference between MG-1 and MG-3 was large, whereas the difference between MG-1 and MG-2

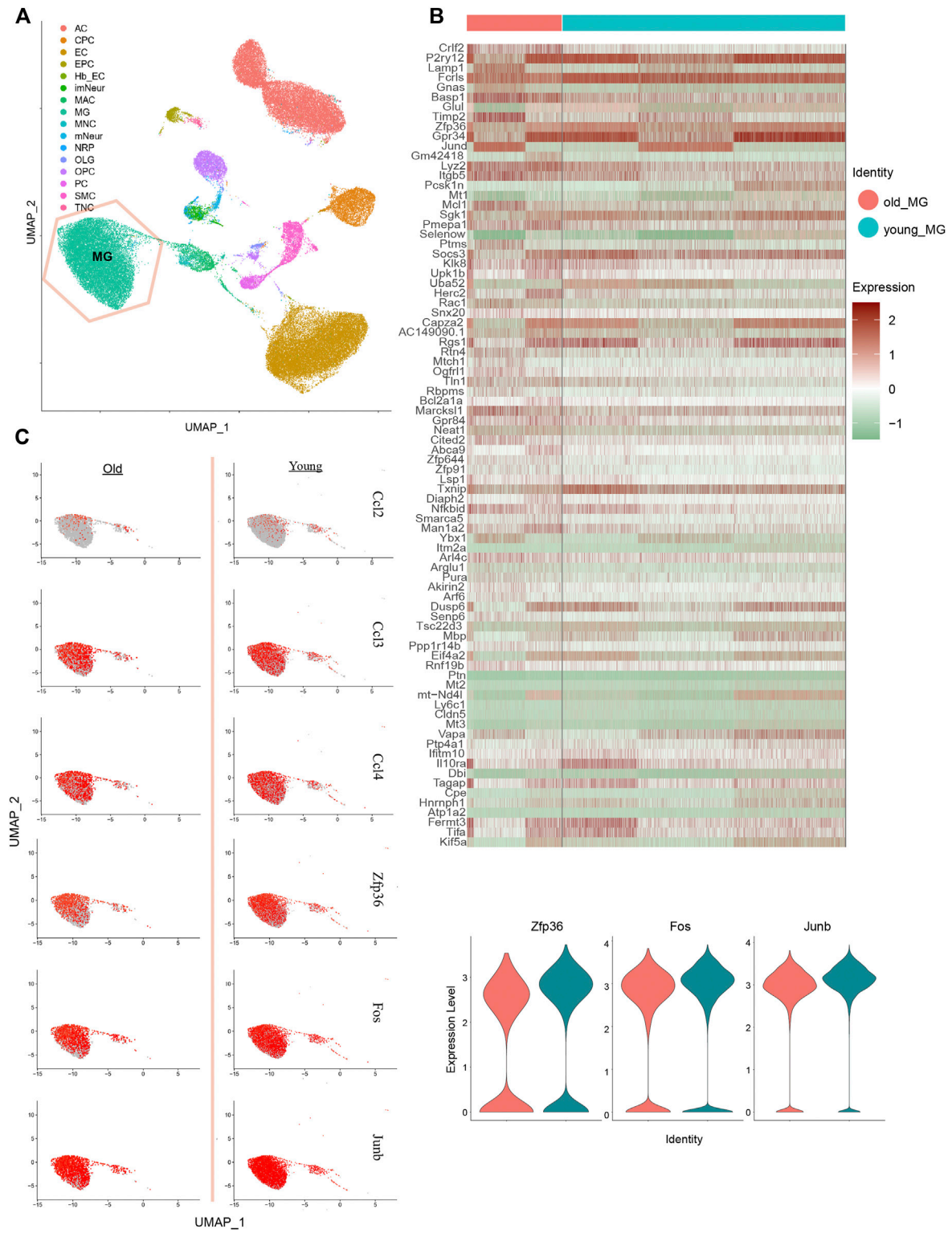

FIGURE 4 | Performance of MG-12 up-regulation genes in MG cells from old and young mice brain single-cell RNA-seq data. **(A)** Identification of cell types on UMAP plot. **(B)** Heatmap of the top 100 different genes between old and young MG cells. **(C)** UMAP plot and violin plot show the relative expressions of old and young MG cells in MG-12 up-regulation genes.

was small. In the analysis of intercellular development trajectory (**Figures 2D,E**), the distance between MG-1 and MG-3 was greater than that between MG-1 and MG-2. The pseudo-time trajectories (**Figures 2F,G**; **Supplementary Figures S3A,B**) showed that MG-2 may be the intermediate stage of MG-1 and MG-3. Finally, we performed GO and KEGG function and pathway enrichment analyses (**Figure 2H**; **Supplementary Figures S3C,D**) of the genes showing significant differential expression between the MG-1 and MG-2 combination and MG-3. The results showed that the most significant GO function terms were the myeloid cell chemotaxis-related genes (**Figures 2B**, **3A**) and many inflammatory and immune response pathways (**Supplementary Figures S3C,D**). In particular, the upregulated genes in MG-1 and MG-2, compared to those in MG-3 (**Figure 3A**), were significantly enriched in multiple genes related to myeloid cell chemotaxis, and the expression of these genes in MG cells was significantly higher than that in other cell types (**Figures 3B–D**). Integrating the results of MG cell heterogeneity and pseudo-time analysis, we hypothesize that MG in the GBM tumor microenvironment produces inflammatory pathways and activates immune response pathways (especially MHC-II). During the analysis, we found several significantly altered genes (*ZFP36*, *NFKBID*, *JUNB*, *FOS*, and *FOSB*) (**Figure 3B**), which are not only related to the chemotaxis of myeloid cells but are also closely related to cell senescence.

MG Cells Alteration Between Aged and Young Mouse Brain Single-Cell RNA-Seq

Based on the key differential genes and pathways we identified, we found that MG only has a cumulative effect in adult GBM; this is consistent with the study by Engler et al. We Further focused on what happens in MG cells during cell senescence. To compare the changes in MG cells during the aging process and those during the formation of GBM, we downloaded single-cell RNA-seq data of young and old mice whole brains from the GEO database. The MG cells were extracted based on cell typing, as in the original paper (**Figure 4A**). Further analysis of the differential genes in the expression profiles between old and young MG cells (**Figures 4B,C**), and the differential genes of GBM-related MG subsets, such as Zfp36 and Nfkbid, were found in the age differences of top 200 genes (**Figure 4B**). Changes in related genes were further verified in terms of the expression level and proportion of expressing cells (**Figure 4C**). ZFP36, as an inhibitor of the cellular senescence pathway, and NF-κB, as an activator, can directly regulate the expression of SASP-related 6 genes, thereby regulating cellular senescence. *ZFP36* and *NFKBID* decreased when MG cells aged, which is probably the key factor that causes only adult GBM to be affected by the number of MG cells.

Specific Manifestations of Genes Associated With MG Cell Heterogeneity in Clinical Data

To understand the important role of *ZFP36* and other key genes in the survival and prognosis of GBM, we analyzed the bulk RNA-seq data of tumor samples and their corresponding survival data by downloading the "Glioblastoma (TCGA, Cell 2013)" data. Among the 543 tumor samples, a considerable portion showed high mRNA levels of these genes (**Figure 5A**). Almost all the above genes were co-expressed with a significant positive correlation (**Figure 5B**; **Supplementary Figure S4**). Further analysis of the correlation between ZFP expression levels and GBM survival (**Figure 5C**) revealed significant difference ($p < 0.05$) between high and low ZFP expression levels. Analysis of clinical data further verified that *ZFP36* and other MG heterogeneity-related genes play an important role in the survival and prognosis of GBM.

DISCUSSION

The research for GBM therapy has been progressing slowly. Drugs against GBM are limited by the blood-brain barrier. Various studies have shown that the antitumor immune response of GBM is modulated. This indicates the feasibility of immunotherapy for GBM treatment. Like many other malignant tumors, GBM highly expresses typical immunosuppressive factors, such as *PD-L1*; A lot of progress has been made in immunotherapy targeting T cells [23–25]. However, owing to the blocking effect of the blood-brain barrier, the immune cell composition in the tumor microenvironment of GBM is significantly different from that of other tumors. This also suggests that it may be more meaningful to target GBM tumor-related macrophages and MG for immunotherapy of GBM.

The development of single-cell sequencing technology provides better methods and possibilities for studying cell heterogeneity and cell state transformation. In this study, we discovered a GM state identification method that is different from the traditional M1/M2 state model. In our cell state identification, we did not observe a difference in the expression of the typical features of M1/M2 (iNOS and Arginase1) [26]. Using the pseudo-time analysis method based on different algorithms, we found that MG-1 and MG-3 from our three classifications should be the two most distant populations. However, owing to the limitation of the depth of single-cell sequencing, we did not observe numerous differences between the two cell populations in the single-cell data. Fortunately, we are still exposed to a series of important differential genes, such as *ZNF36*, in gene set enrichment analysis. *ZNF36* is associated with the MAPK and TNF pathways and possesses complex negative feedback regulation mechanisms [27]. These two important pathways have been reported in many studies to be closely related to GBM [28–30], especially with respect to inflammation (MHC II) [31] and immune activation [25, 32]. In addition, we found that some genes such as *ZNF36*, *AP-1*, and *CCL3* are closely related to cell differentiation [33–36], especially the differentiation of myeloid monocytes as chemokines. This result suggests that chemotaxis between different types of MG cells is likely to be affected by the pathways in which genes such as *ZNF36* are located, and that this mechanism is affected by stress from the tumor environment, such as inflammatory factors.

Given the simultaneous appearance of key genes, such as *ZNF36*, *NFKBID*, and *IL-6*, we focused on the cellular senescence pathway [37]. There are large differences between adult and pediatric GBM, resulting in many therapy programs

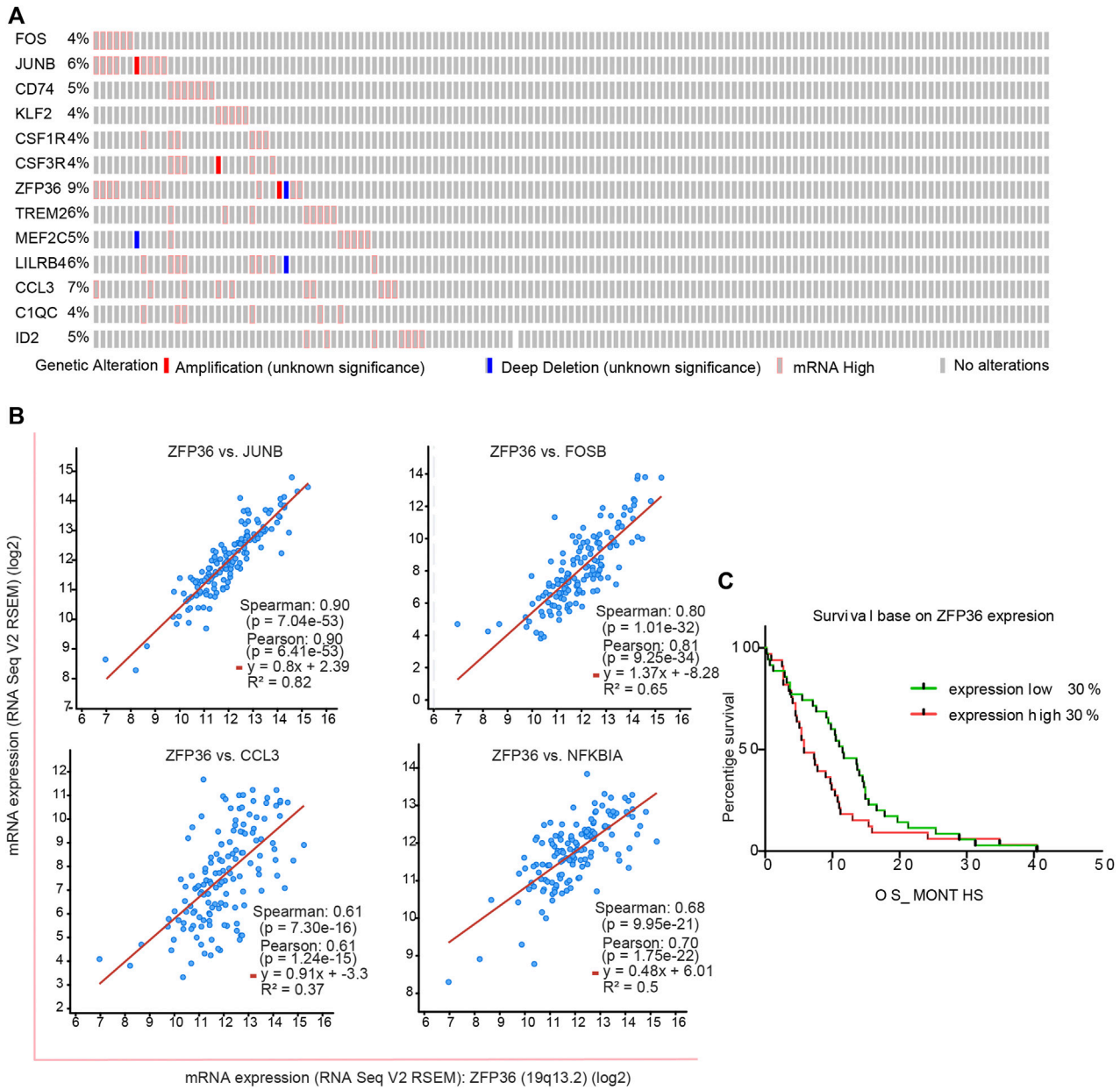

FIGURE 5 | Characteristic of MG-12 up-regulation genes in clinical data from TCGA database. **(A)** Comprehensive status of important genes in clinical samples. **(B)** The significance fitting curve of co-expression between genes. The red curve **(C)** The survival curve was significantly correlated with the expression of the *ZFP36* gene (p = 0.0398, Gehan-Breslow-Wilcoxon test).

for adult GBM that cannot be used for children. The enrichment of these genes related to the cellular senescence pathway may remind us that the difference between adult and pediatric patients is important for GBM tumor microenvironment. We identified MG cells in old and young mice through whole-brain single-cell sequencing data. Changes in MG cells during the aging process were analyzed. Perhaps because of the technical limitations of the depth of single-cell sequencing or the experimental protocol, we did not enrich the pathway in the aged and younger groups. It is worth noting that the main differential genes found in the tumor-related MG cell state differential gene set were still found to appear in the elderly related differential gene set. This result suggests that changes in MG cells during the aging process may have a huge impact on the tumor microenvironment of GBM.

To verify the criticality of the genes found in GBM, we performed co-expression analysis and survival analysis in the RNA-seq data of human GBM tumor samples. Except for these results, these genes not only showed very good consistent expression in tumor samples, the expression level of *ZFP36* was also significantly negatively correlated with patient survival.

DATA AVAILABILITY STATEMENT

Publicly available datasets were analyzed in this study. This data can be found here: dataset No. GSE131928, dataset No. GSE147693 Glioblastoma (TCGA, Cell 2013).

AUTHOR CONTRIBUTIONS

HX, LD, SM, XL, and CZ conceived and designed the experiments. HX and LD performed the analysis of the data and wrote the manuscript. SM, XL, and CZ reviewed and edited the manuscript. All authors read and approved the final manuscript.

CONFLICT OF INTEREST

The authors declare that the research was conducted in the absence of any commercial or financial relationships that could be construed as a potential conflict of interest.

SUPPLEMENTARY MATERIAL

The Supplementary Material for this article can be found online at: https://www.por-journal.com/articles/10.3389/pore.2022.1610067/full#supplementary-material

Supplementary Figure S1 | QC and PCA analysis of single-cell RNA-seq data. **(A)** Overview of all cell types of variable genes in the 10 samples highlighting the top-10 significant variable genes. **(B)** The top-20 principal components and their significance. **(C)** gene set that has greater influence in the top-9 principal components. **(D)** Heat-map based on a single principal component.

Supplementary Figure S2 | Marker genes of MG cell subtypes in GBM tumor microenvironment. **(A–C)** MG-1, MG-2, and MG-3 cluster marker genes are compared to each other.

Supplementary Figure S3 | Characteristic analysis of the subtypes of MG cells. **(A)** Genes with dispersion (variation) coefficients higher than the set value were selected for developmental trajectory analysis. **(B)** The stage of cells in **Figures 2F,G**. **(C,E)** Downregulated gene set KEGG pathway enrichment analysis result, top-10 pathway and their relationship (lines means that there are overlap genes between the two pathway). **(D,F)** Upregulated gene set KEGG pathway enrichment analysis result, top-10 pathway and their relationship (lines means that there are overlap genes between the two pathway).

Supplementary Figure S4 | ZFP36 signature co-expressed genes in TCGA GBM RNA-seq. **(A–F)** *CD83*, *CCL4*, *CCL4L1*, and *NFKB1* are co-expressed with *ZFP36* in clinical RNA-seq.

REFERENCES

1. Villa C, Miquel C, Mosses D, Bernier M, Di Stefano AL.The 2016 World Health Organization Classification of Tumours of the central Nervous System. *Presse Med* (2018) 47(11-12):E187–E200. doi:10.1016/j.lpm.2018.04.015
2. Stupp R, Mason WP, van den Bent MJ, Weller M, Fisher B, Taphoorn MJB, et al. Radiotherapy Plus Concomitant and Adjuvant Temozolomide for Glioblastoma. *N Engl J Med* (2005) 352(10):987–96. doi:10.1056/nejmoa043330
3. Wen PY, Kesari S Malignant Gliomas in Adults. *N Engl J Med* (2008) 359(17): 492–507. doi:10.1056/NEJMra0708126
4. Mukherjee S, Baidoo J, Fried A, Atwi D, Dolai S, Boockvar J, et al. Curcumin Changes the Polarity of Tumor-Associated Microglia and Eliminates Glioblastoma. *Int J Cancer* (2016) 139(12):2838–49. doi:10.1002/ijc.30398
5. Simmons GW, Pong WW, Emnett RJ, White CR, Gianino SM, Rodriguez FJ, et al. Neurofibromatosis-1 Heterozygosity Increases Microglia in a Spatially and Temporally Restricted Pattern Relevant to Mouse Optic Glioma Formation and Growth. *J Neuropathol Exp Neurol* (2011) 70(1):51–62. doi:10.1097/nen.0b013e3182032d37
6. Gutmann DH, Kettenmann H Microglia/Brain Macrophages as Central Drivers of Brain Tumor Pathobiology. *Neuron* (2019) 104(3):442–9. doi:10.1016/j.neuron.2019.08.028
7. Roesch S, Rapp C, Dettling S, Herold-Mende C When Immune Cells Turn Bad-Tumor-Associated Microglia/Macrophages in Glioma. *Int J Mol Sci* (2018) 19(2), 436. doi:10.3390/ijms19020436
8. Solga AC, Pong WW, Kim K-Y, Cimino PJ, Toonen JA, Walker J, et al. RNA Sequencing of Tumor-Associated Microglia Reveals Ccl5 as a Stromal Chemokine Critical for Neurofibromatosis-1 Glioma Growth. *Neoplasia* (2015) 17(10):776–88. doi:10.1016/j.neo.2015.10.002
9. Chen Z, Feng X, Herting CJ, Garcia VA, Nie K, Pong WW, et al. Cellular and Molecular Identity of Tumor-Associated Macrophages in Glioblastoma. *Cancer Res* (2017) 77(9):2266–78. doi:10.1158/0008-5472.can-16-2310
10. Guo X, Pan Y, Gutmann DH Genetic and Genomic Alterations Differentially Dictate Low-Grade Glioma Growth through Cancer Stem Cell-specific Chemokine Recruitment of T Cells and Microglia. *Neuro Oncol* (2019) 21(10):1250–62. doi:10.1093/neuonc/noz080
11. Hambardzumyan D, Gutmann DH, Kettenmann H The Role of Microglia and Macrophages in Glioma Maintenance and Progression. *Nat Neurosci* (2016) 19(1):20–7. doi:10.1038/nn.4185
12. Sørensen MD, Dahlrot RH, Boldt HB, Hansen S, Kristensen BW Tumour-associated Microglia/macrophages Predict Poor Prognosis in High-Grade Gliomas and Correlate with an Aggressive Tumour Subtype. *Neuropathol Appl Neurobiol* (2018) 44(2):185–206. doi:10.1111/nan.12428
13. Pyonteck SM, Akkari L, Schuhmacher AJ, Bowman RL, Sevenich L, Quail DF, et al. CSF-1R Inhibition Alters Macrophage Polarization and Blocks Glioma Progression. *Nat Med* (2013) 19(10):1264–72. doi:10.1038/nm.3337
14. Szulzewsky F, Pelz A, Feng X, Synowitz M, Markovic D, Langmann T, et al. Glioma-Associated Microglia/Macrophages Display an Expression Profile Different from M1 and M2 Polarization and Highly Express Gpnmb and Spp1. *Plos One* (2015) 10(2):e0116644. doi:10.1371/journal.pone.0116644
15. Daginakatte GC, Gutmann DH Neurofibromatosis-1 (Nf1) Heterozygous Brain Microglia Elaborate Paracrine Factors that Promote Nf1-Deficient Astrocyte and Glioma Growth. *Hum Mol Genet* (2007) 16(9):1098–112. doi:10.1093/hmg/ddm059
16. Markovic DS, Vinnakota K, van Rooijen N, Kiwit J, Synowitz M, Glass R, et al. Minocycline Reduces Glioma Expansion and Invasion by Attenuating Microglial MT1-MMP Expression. *Brain Behav Immun* (2011) 25(4):624–8. doi:10.1016/j.bbi.2011.01.015
17. Hu F, Dzaye OD, Hahn A, Yu Y, Scavetta RJ, Dittmar G, et al. Glioma-derived Versican Promotes Tumor Expansion via Glioma-Associated Microglial/macrophages Toll-like Receptor 2 Signaling. *Neuro Oncol* (2015) 17(2): 200–10. doi:10.1093/neuonc/nou324
18. Stuart T, Butler A, Hoffman P, Hafemeister C, Papalexi E, Mauck WM, et al. Comprehensive Integration of Single-Cell Data. *Cell* (2019) 177(7):1888–902. doi:10.1016/j.cell.2019.05.031
19. Aran D, Looney AP, Liu L, Wu E, Fong V, Hsu A, et al. Reference-based Analysis of Lung Single-Cell Sequencing Reveals a Transitional Profibrotic Macrophage. *Nat Immunol* (2019) 20(2):163–72. doi:10.1038/s41590-018-0276-y
20. Trapnell C, Cacchiarelli D, Grimsby J, Pokharel P, Li S, Morse M, et al. The Dynamics and Regulators of Cell Fate Decisions are Revealed by Pseudotemporal Ordering of Single Cells. *Nat Biotechnol* (2014) 32(4): 381–6. doi:10.1038/nbt.2859
21. Love MI, Huber W, Anders S Moderated Estimation of Fold Change and Dispersion for RNA-Seq Data with DESeq2. *Genome Biol* (2014) 15(12):550. doi:10.1186/s13059-014-0550-8
22. Yu G, Wang L-G, Han Y, He Q-Y clusterProfiler: An R Package for Comparing Biological Themes Among Gene Clusters. *OMICS: A J Integr Biol* (2012) 16(5): 284–7. doi:10.1089/omi.2011.0118

23. Wainwright DA, Balyasnikova IV, Chang AL, Ahmed AU, Moon K-S, Auffinger B, et al. IDO Expression in Brain Tumors Increases the Recruitment of Regulatory T Cells and Negatively Impacts Survival. *Clin Cancer Res* (2012) 18(22):6110–21. doi:10.1158/1078-0432.ccr-12-2130
24. Bloch O, Crane CA, Kaur R, Safaee M, Rutkowski MJ, Parsa AT Gliomas Promote Immunosuppression through Induction of B7-H1 Expression in Tumor-Associated Macrophages. *Clin Cancer Res* (2013) 19(12):3165–75. doi:10.1158/1078-0432.ccr-12-3314
25. Yu JS, Wheeler CJ, Zeltzer PM, Ying H, Finger DN, Lee PK, et al. Vaccination of Malignant Glioma Patients with Peptide-Pulsed Dendritic Cells Elicits Systemic Cytotoxicity and Intracranial T-Cell Infiltration. *Cancer Res* (2001) 61(3):842–7.
26. Mukherjee S, Fried A, Hussaini R, White R, Baidoo J, Yalamanchi S, et al. Phytosomal Curcumin Causes Natural Killer Cell-dependent Repolarization of Glioblastoma (GBM) Tumor-Associated Microglia/macrophages and Elimination of GBM and GBM Stem Cells. *J Exp Clin Cancer Res* (2018) 37:168. doi:10.1186/s13046-018-0792-5
27. Shah S, Mostafa MM, McWhae A, Traves SL, Newton R Negative Feed-Forward Control of Tumor Necrosis Factor (TNF) by Tristetraprolin (ZFP36) is Limited by the Mitogen-Activated Protein Kinase Phosphatase, Dual-Specificity Phosphatase 1 (DUSP1). *J Biol Chem* (2016) 291(1):110–25. doi:10.1074/jbc.m115.697599
28. Dranoff G Cytokines in Cancer Pathogenesis and Cancer Therapy. *Nat Rev Cancer* (2004) 4(1):11–22. doi:10.1038/nrc1252
29. Okada H, Lieberman FS, Walter KA, Lunsford LD, Kondziolka DS, Bejjani GK, et al. Autologous Glioma Cell Vaccine Admixed with Interleukin-4 Gene Transfected Fibroblasts in the Treatment of Patients with Malignant Gliomas. *J Transl Med* (2007) 5:67. doi:10.1186/1479-5876-5-67
30. Natsume A, Wakabayashi T, Ishii D, Maruta H, Fujii M, Shimato S, et al. A Combination of IFN-β and Temozolomide in Human Glioma Xenograft Models: Implication of P53-Mediated MGMT Downregulation. *Cancer Chemother Pharmacol* (2008) 61(4):653–9. doi:10.1007/s00280-007-0520-x
31. Qian J, Luo F, Yang J, Liu J, Liu R, Wang L, et al. TLR2 Promotes Glioma Immune Evasion by Downregulating MHC Class II Molecules in Microglia. *Cancer Immunol Res* (2018) 6(10):1220–33. doi:10.1158/2326-6066.CIR-18-0020
32. Kantoff PW, Higano CS, Shore ND, Berger ER, Small EJ, Penson DF, et al. Sipuleucel-T Immunotherapy for Castration-Resistant Prostate Cancer. *N Engl J Med* (2010) 363(5):411–22. doi:10.1056/nejmoa1001294
33. Pong WW, Higer SB, Gianino SM, Emnett RJ, Gutmann DH Reduced Microglial CX3CR1 Expression Delays Neurofibromatosis-1 Glioma Formation. *Ann Neurol* (2013) 73(2):303–8. doi:10.1002/ana.23813
34. Ntanasis-Stathopoulos I, Fotiou D, Terpos E CCL3 Signaling in the Tumor Microenvironment. *Tumor Microenviron Role of Chemokines Pt A* (2020) 1231:13–21. doi:10.1007/978-3-030-36667-4_2
35. Shaik S, Martin EC, Hayes DJ, Gimble JM, Devireddy RV Transcriptomic Profiling of Adipose Derived Stem Cells Undergoing Osteogenesis by RNA-Seq. *Sci Rep* (2019) 9:11800. doi:10.1038/s41598-019-48089-1
36. Caracciolo V, Young J, Gonzales D, Ni Y, Flowers SJ, Summer R, et al. Myeloid-specific Deletion of Zfp36 Protects against Insulin Resistance and Fatty Liver in Diet-Induced Obese Mice. *Am J Physiol Endocrinol Metab* (2018) 315(4):E676–E693. doi:10.1152/ajpendo.00224.2017
37. Calcinotto A, Kohli J, Zagato E, Pellegrini L, Demaria M, Alimonti A Cellular Senescence: Aging, Cancer, and Injury. *Physiol Rev* (2019) 99(2):1047–78. doi:10.1152/physrev.00020.2018

Pathology & Oncology Research

frontiers

ORIGINAL RESEARCH
published: 16 September 2022
doi: 10.3389/pore.2022.1610493

Identification of Diagnostic Exosomal LncRNA-miRNA-mRNA Biomarkers in Colorectal Cancer Based on the ceRNA Network

*Yajing Zhao, Xingguo Song, Xianrang Song and Li Xie**

Department of Clinical Laboratory, Shandong Cancer Hospital and Institute, Shandong First Medical University and Shandong Academy of Medical Sciences, Jinan, China

Background: Colorectal cancer (CRC) is currently the fourth most common cancer worldwide. The roles of exosomal competing endogenous RNAs (ceRNAs) in CRC remain unclear. In this study, we constructed an exosomal ceRNA network to identify the core ceRNAs and investigate the diagnostic biomarkers in CRC.

Methods and Patients: Serum exosomes were isolated from four CRC patients and two healthy donors by ultracentrifugation, and then subjected to RNA isolation, sequencing and microarray. Kyoto Encyclopedia of Genes and Genomes (KEGG) pathway and Gene Ontology (GO) analyses were performed to identify functional enrichment implications of differentially expressed exosomal mRNAs. TargetScan and miRanda were used for identifying the miRNA-mRNA and miRNA-LncRNA interactions. The predicted lncRNAs and mRNAs were intersected with the differentially expressed genes, for which the screening criterion was fold change >1.5 in the microarray. Differentially expressed exosomal miRNAs were identified in the GSE71008 dataset, and differentially expressed mRNAs (DEmRNAs) were further summarized from The Cancer Genome Atlas (TCGA) database.

Results: A total of 1186 exosomal DEmRNAs, 2088 exosomal DElncRNAs and 29 exosomal miRNAs were detected in CRC patients compared to the healthy donors. Functional enrichment analysis suggested that exosomal DEmRNAs might participate in pathways related to carcinogenesis and development of cancer. An exosomal ceRNA regulatory network of CRC was constructed based on 40 lncRNAs, two miRNAs, and five mRNAs. Exosomal miR-150-5p and miR-10b-5p expression levels were increased in healthy donors compared with CRC patients in the GSE71008 dataset, and five DEmRNAs (*TOMM70A*, *RBM48*, *BEND3*, *RHOBTB1*, and *ADAMTS2*) were significantly upregulated in TCGA database. Two potential exosomal regulatory axes of lncRNA G016261-miR-150-5p-*RBM48* and lncRNA XLOC_011677-miR-10b-5p-*BEND3* were identified from the network.

Conclusion: The current study revealed potential molecular biological regulation pathways and diagnostic biomarkers through the exosomal ceRNA regulatory network.

Keywords: colorectal cancer, lncRNA, miRNA, exosomes, diagnostic biomarker, mRNA

OPEN ACCESS

Edited by:
József Tímár,
Semmelweis University, Hungary

***Correspondence:**
Li Xie
l_xie2001@126.com

Received: *05 April 2022*
Accepted: *08 September 2022*
Published: *16 September 2022*

Citation:
Zhao Y, Song X, Song X and Xie L (2022) Identification of Diagnostic Exosomal LncRNA-miRNA-mRNA Biomarkers in Colorectal Cancer Based on the ceRNA Network. Pathol. Oncol. Res. 28:1610493. doi: 10.3389/pore.2022.1610493

INTRODUCTION

More than 1.8 million new cases of colorectal cancer (CRC) and 881,000 deaths were estimated to occur in 2018 [1]. CRC is the fourth most commonly diagnosed malignancy and the third leading cause of cancer-related mortality, which emphasizes the need for screening and early detection of CRC. Recently, non-invasive procedures have been developed for CRC pre-screening, such as liquid biopsy, which underlines new approaches for cancer detection, including circulating tumor nucleic acids (ctDNA and ctRNA), circulating tumor cells (CTCs), exosomes, etc [2].

Exosomes are 50–150 nm microvesicles that play a crucial role in cell–cell communication [3–5]. Through ligand-receptor interactions, endocytosis and phagocytosis, exosomes interact with the method by which plasma fusion transfers information to the adjacent target cell membrane. This exosomal crosstalk involves the transport of proteins, mRNAs, miRNAs and lncRNAs between donor and recipient cells [6, 7], leading to cancer initiation, progression and metastasis as well as epithelial–mesenchymal transition (EMT), angiogenesis, drug resistance and immune escape [8–10]. Many types of exosomal miRNAs, lncRNAs and mRNAs have been identified, and the underlying molecular mechanisms have been investigated, but their potential networks have not been fully elucidated.

The hypothesis of competing endogenous RNAs (ceRNAs) highlights a specific molecular biological regulatory mechanism for post-transcriptional regulation. Serving as ceRNAs, lncRNAs could indirectly regulate the expression of mRNAs through competitive binding response elements of miRNAs as endogenous molecular sponges, thereby regulating gene expression and cell function [11, 12]. Several studies have revealed that ceRNA networks play an important role in regulating tumor cell proliferation, differentiation, metastasis and chemo-resistance [13–15]. LncRNA-FAM225A binds to miR-1275 and miR-590-3p to regulate the expression of *ITGB3*, which is a potential ceRNA regulatory pathway that ultimately promotes tumorigenesis and metastasis in nasopharyngeal carcinoma [16]. LncRNA-KRTAP5-AS1 and lncRNA-TUBB2A could act as ceRNAs to affect the function of Claudin-4 by miR-596 and miR-3620-3p in gastric cancer [17]. Exosomal lncRNA-Sox2ot from Hs 766T-L2 cells transfers to BxPC-3 cells and modulates the expression of Sox2 by competitively binding to the miR-200 family, thus promoting invasion and metastasis of pancreatic ductal adenocarcinoma (PDAC) [18]. Exosomal lncRNA-UCA1 sequesters miR-135a, miR-143, miR-214 and miR-1271 to protect *ANLN*, *BIRC5*, *IP O 7*, *KIF2A*, and *KIF23* from miRNA-induced degradation in CRC [19]. Taken together, these findings suggested that exosomes could transfer RNAs, especially noncoding RNAs, to the recipient cells and participated in ceRNA network interactions to regulate specific aspects of tumor development, thereby indicating that exosomal ceRNA complex can act as excellent biomarkers for CRC diagnostics.

In this study, we first selected the differentially expressed exosomal lncRNAs between CRC patients and healthy donors using microarray and an integrated analysis, and then predicted and verified their combined miRNAs and mRNAs by bioinformatics prediction and correlation analysis using GEO and TCGA databases. Finally, we constructed the ceRNA network interactions in CRC and explored the potential role of exosomes involved in this network.

MATERIALS AND METHODS

Patients and Samples

Four CRC patients and two healthy donors, admitted at the Shandong Cancer Hospital between september 2017 and July 2018, were selected for this study. Written informed consent was obtained from all participants. The clinical stage of the CRC patients was determined, and one patient was classified as stage I, one as stage II, and two patients as stage IV according to the 8 AJCC Cancer Staging Handbook of the American Joint Committee on Cancer. The protocol was approved by the Shandong Cancer Hospital and Institute, Shandong First Medical University and Shandong Academy of Medical Sciences of committee. All subjects gave written informed consent in accordance with the Declaration of Helsinki.

CRC patients were not received any tumor treatment or suffered from any other immune, metabolic diseases or endocrine before serum collection, and all patients had clearly pathologically diagnosed as colorectal cancer, four of which were adenocarcinoma. Healthy donors do not have any underlying diseases, especially gastrointestinal diseases. Four CRC patients and two healthy donors were from 18 to 65 years old.

Isolation of Exosomes

The exosomes were isolated by ultracentrifugation, as previously described [20]. Briefly, the serum was centrifuged at 10000 ×g for 30 min at 4°C to remove the cellular debris, and then ultracentrifuged at 100,000 ×g (Beckman Coulter, Brea, CA, United States) at 4°C for 2 h to precipitate the exosomes. Trizol was added to the precipitate, and the samples were stored at −80°C.

Transmission Electron Microscopy

The exosome pellets were placed to the copper grids in a 50 μL drop of 1% glutaraldehyde for 5 min and transferred to a 100-μL drop of distilled water, after 2 min, the grids were stained with to a 50-μL drop of uranyl-oxalate solution (pH 7) for 5 min and placed a parafilm-covered glass dish covered anon ice. Subsequently, the exosome grids were cleaned using distilled water seven times for 2 min each. The TEM images were obtained using a JEM-1200EX transmission electron microscope (JEOL, Japan) operated at 100 kV.

Tunable Resistive Pulse Sensing

The size of the vesicles and the particle concentration of exosomes were measured by using TRPS (qNano; Izon Science Ltd.). The tunable nanopores with proprietary data capture and analysis using Izon Control Suite software v.3.3.2.2000 (Izon Science Ltd.).

Western Blotting Analysis

The extracted protein was resolved by 10% SDS-PAGE, transferred onto the PVDF membranes and placed in blocking buffer for 2 h, the membranes were incubated overnight with anti-CD63, anti-GM130, anti-TSG101 (CST, Danvers, United State) at 4°C, followed by incubation with HRP-coupled secondary Ab at room temperature for 1 h. The protein bands were detected through an ECL blot detection reagent.

Analysis of miRNA Sequence Datasets

The input material for the small RNA library was generated from 3 μg RNA in each sample. After the cluster was generated, the libraries were sequenced and 50 bp single-end reads were generated on the Illumina HiSeq 2500/2000 platform (Illumina, United States). After sequencing, coding potential analysis, quality control analysis, gene expression level quantification, transcriptome assembly, conservative analysis, target gene prediction, read mapping to the reference genome and differential expression analysis were carried out by Novogene Corporation.

Differential mRNA and LncRNA Expression of RNA-Microarray Datasets and Analysis

Global analysis of human lncRNA and protein-coding transcripts was conducted using human lncRNA microarray V4.0. Briefly, after the rRNA was removed using the mRNA-ONLY™ eukaryotic mRNA isolation kit (Epicentre), the mRNA was purified from the total RNA. Then, a random primer method (Arraystar flash RNA labeling kit) was used to amplify each sample and transcribe it into fluorescent cRNA along the entire length of the transcript without 3'bias. RNeasy mini kit (Qiagen) was used to purify the labeled cRNAs. The concentration and specific activity of the labeled cRNAs were measured by NanoDrop ND-1000. The labeled cRNA was diluted using 50 μl of hybridization solution, distributed on the spacer slides, and placed on the lncRNA expression microarray slides. The slides were incubated at 65°C for 17 h in an Agilent hybridization oven. After washing, the slides were fixed and scanned using Agilent DNA Microarray Scanner (Part No. G2505C).

Exosomal ceRNA Network Construction

To identify potential pairs among exosomal DEmRNAs, DElncRNAs, and DEmiRNAs between the CRC patients and healthy donors, data from two databases were retrieved. Arraystar's in-house miRNA target prediction software was applied based on TargetScan and miRanda algorithms. We intersected the predicted targets obtained from the database with miRNA sequencing and lncRNA, mRNA microarray. Fold-change of >1.5 and a p-value of <0.05 were set as the criteria.

Thereafter, the miRanda and TargetScan databases were used to predict potential miRNA targets, and Cytoscape software was used to delineate the ceRNA network of lncRNA-miRNA-mRNA.

Functional Annotation of the Exosomal ceRNA Network

The Gene Ontology (GO) project describes the attributes of genes and gene products in any organism (http://www.geneontology.org). The ontology includes three domains: Cellular Component, Molecular Function and Biological Process. The p-value indicates the importance of GO enrichment in the DE gene. The lower the p-value, the more significant is the GO term (p-value ≤0.05). The functional analysis of gene mapping to KEGG pathway is called pathway analysis. The p-value indicates the importance of disease-related pathways. Lower the p-value, more significant is the pathway. The recommended p-value cutoff is 0.05.

Statistical Analysis

GraphPad Prism 6.0 (San Diego, CA, United States) and SPSS 22.0 (IBM, Ehningen, Germany) were used for the statistical analyses. Mann–Whitney U or t-test were used to perform the comparisons. Receiver operating characteristic (ROC) curves with area under the curve (AUC) were used to determine the corresponding cutoff values, with pathological diagnosis as the "gold standard". A p-value <0.05 was considered to be statistically significant. In addition, each combination of miRNA and mRNA or mRNA was analyzed.

RESULTS

Identification of Isolated Exosomes

Exosomes isolated from CRC patients and healthy donors were characterized by qNano, TNM and western blotting analysis. The results suggested the typical exosome-like round morphology with 50–150 nm in diameter under TEM (**Figure 1A**), and the size range was in agreement with qNano (**Figure 1B**). Consistently, the characteristic protein markers of exosomes, CD63 and TSG101 were found in exosomes, but not in the whole cell lysates. whereas GM130 (the negative control) was not detected in the exosomal protein lysates (**Figure 1C**).

Identification of Exosomal DE mRNAs, DE lncRNAs, and DE miRNAs

Exosomal RNAs from four CRC patients and two healthy donors were isolated for RNA sequencing and microarray. A total of 28189 downregulated genes (10808 mRNAs, 16840 lncRNAs, and 541 miRNAs) and 28364 upregulated genes (8428 mRNAs, 19332 lncRNAs, and 604 miRNAs) were screened in CRC patients compared to healthy donors, of which 1182 DE mRNAs and 2092 DE lncRNAs were selected with the thresholds of p-value <0.05 and fold-change >1.5 (**Figure 2A**). Exosomal miRNAs have been reported in our previous study [21].

The GO and KEGG enrichment analyses of these 1182 exosomal DE mRNAs were further conducted to investigate the possible signaling mechanisms of CRC. Interestingly, exosomal DE mRNAs were mainly enriched in negative regulation of ATPase activity in the biological process

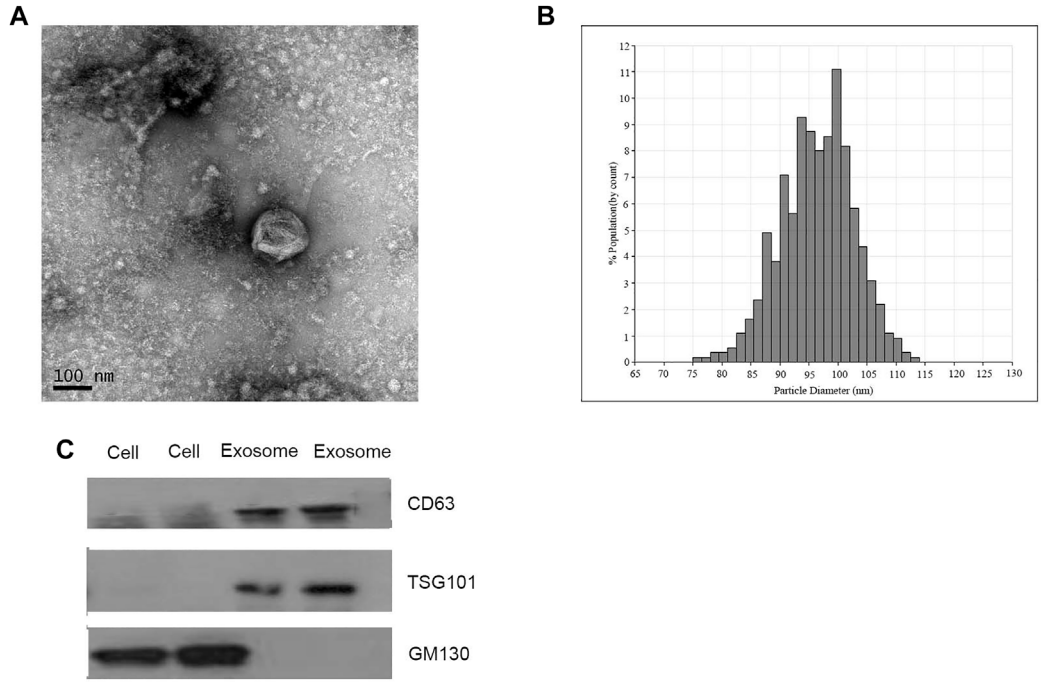

FIGURE 1 | Identification of isolated exosomes. **(A)** TEM image of exosomes from CRC patients with 50–150 nm diameter (scale bar: 100 nm; high voltage (HV) = 100 kV). **(B)** Size distribution of exosomes with 50–150 nm diameter were measured by qNano system. **(C)** Western blot analysis of CD63, TSG101, and GM130 as exosomal markers.

classification, and nucleic acid binding in the molecular function classification (**Figure 2B**). Additionally, KEGG pathway analysis showed that 207 pathways were significantly enriched. The top 10 significantly enriched pathways are shown in **Figure 2C**, including ECM-receptor interaction, adenosine monophosphate-activated protein kinase (AMPK) signaling pathway and mRNA surveillance pathway, which are closely correlated with the carcinogenesis and development of CRC. Therefore, these findings provided a resource for additional molecular participants in CRC.

Expression Analysis of Exosomal DE lncRNA-DE miRNA Pairs in Colorectal Cancer

To explore the relationship between exosomal DE lncRNAs and DE miRNAs in CRC, we predicted the target miRNAs of top 40 DE lncRNAs in the microarray expression profiles using TargetScan and miRanda databases. Finally, miRNA-150-5p and miRNA-10b-5p were selected since they could be targeted by the majority of exosomal DE lncRNAs (**Figure 3A**).

The two exosomal DE miRNAs were also analyzed using the GEO database, which includes exosomal RNA-sequence profiles from 100 CRC patients and 50 healthy donors (GSE71008). In the database, the exosomal miR-150-5p and miR-10b-5p expression levels were markedly downregulated in CRC patients ($p < 0.0125$ and $p < 0.0014$, respectively) compared to healthy donors (**Figures 3B,C**). In order to analyze the diagnostic performance of exosomal miR-150-5p and miR-10b-5p for CRC, a ROC curve was calculated. The AUC of miR-10b-5p was 0.625 (95% CI: 0.567–0.689), with specificity of 82% and sensitivity of 46%, while the AUC of miR-150-5p was 0.658 (95% CI: 0.571–0.745), with sensitivity of 56% and specificity of 58.8% (**Figures 3D,E**). Taken together, these data suggested that exosomal miR-150-5p and miR-10b-5p were significantly associated with CRC.

Expression Analysis of Exosomal DE miRNA-DE mRNA Interaction in Colorectal Cancer

The study flowchart was shown in **Figure 4A**. To identify targeted DE mRNA pairs, we predicted targeted mRNAs from the TargetScan and miRanda databases, followed by intersecting the predicted mRNAs with the exosomal DE mRNAs in the microarray, and finally constructed 27 mRNAs targeted by miR-10b-5p and miR-150-5p in the CRC regulatory network (**Figure 4B**). Due to lower complexity and more reliability, five significantly upregulated mRNAs (*TOMM70A*, *RBM48*, *BEND3*, *RHOBTB1* and *ADAMTS2*) in CRC patients ($n = 623$) compared to healthy donors ($n = 51$) were identified and analyzed using data from TCGA. As shown in **Figures 4C–G**, ROC curves were also calculated, and the AUCs of *BEND3*,

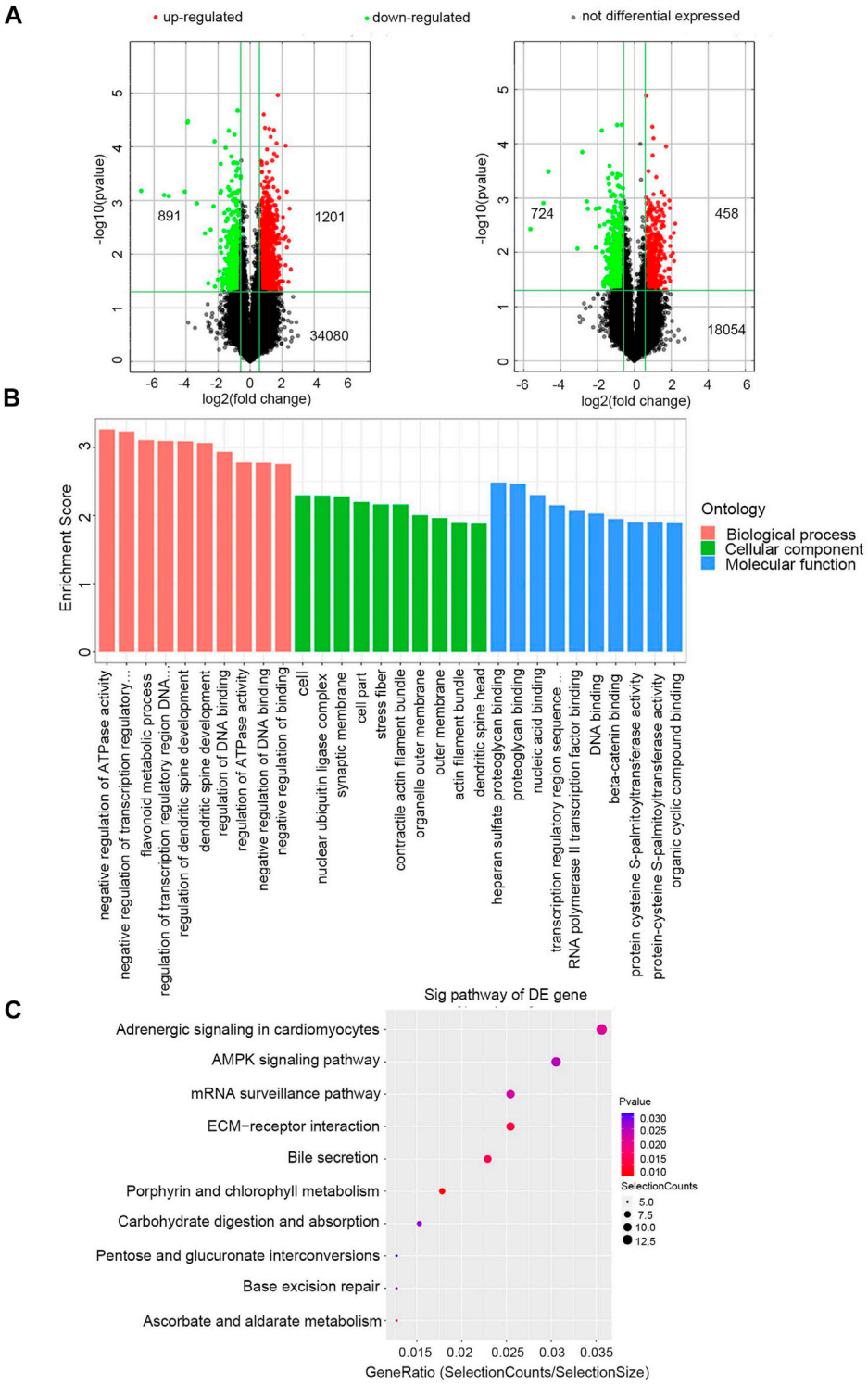

FIGURE 2 | Identification of exosomal DERNAs and Gene ontology and pathway analysis of DEmRNAs **(A)** Exosomal lncRNA and mRNA were compared by the volcano graph the expression fold changes in healthy donors and CRC patients. The green dots indicated the downregulated lncRNAs and mRNAs, the red dots indicated the upregulated lncRNAs and mRNAs and the black dots represent no differential expressed. **(B)** DE mRNAs were clustered in top 10 terms from a GO analysis of molecular function, biological process and cellular component. **(C)** DE mRNAs were clustered in Kyoto Encyclopedia ofGenes and Genomes (KEGG) pathways.

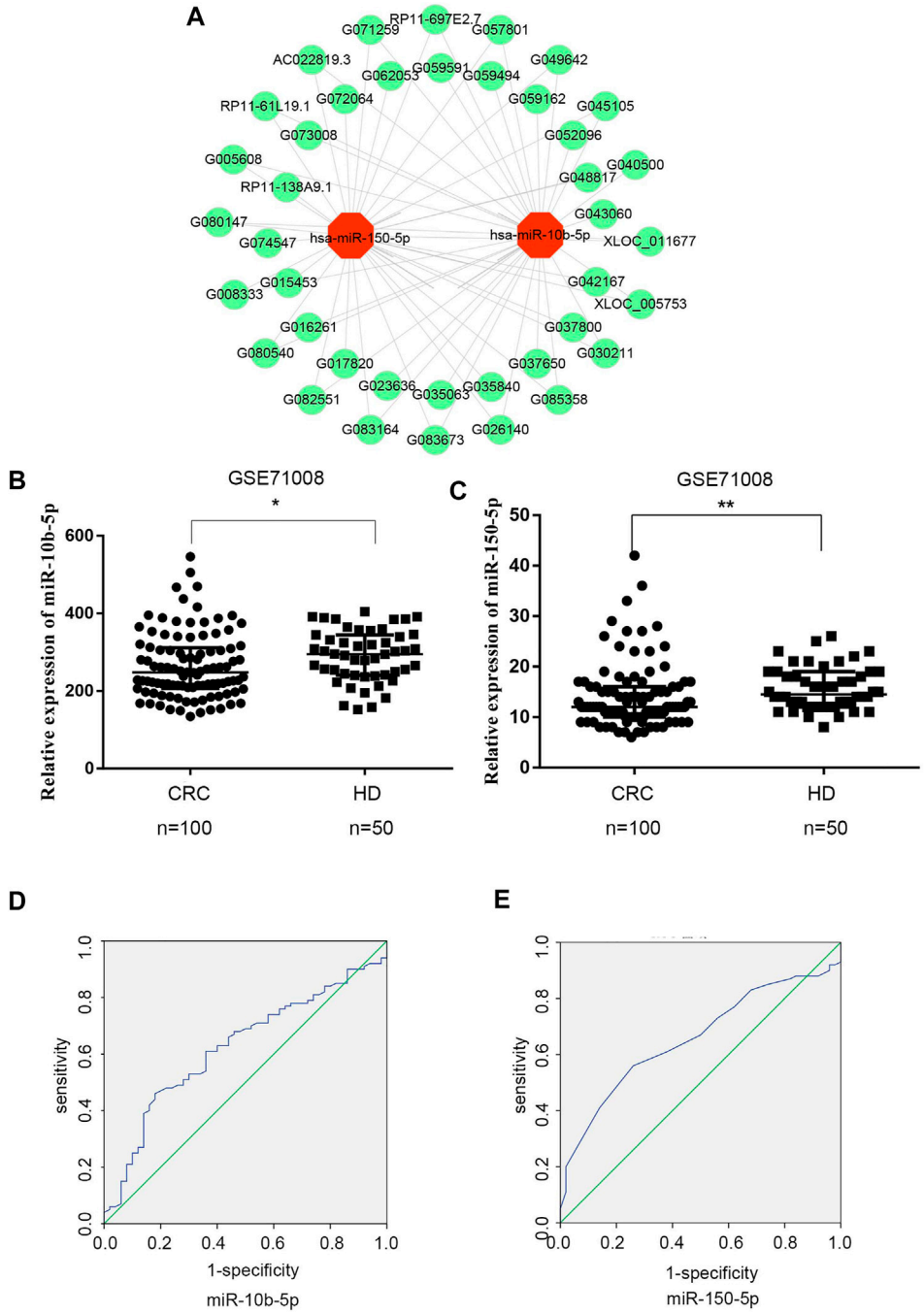

FIGURE 3 | Expression analysis of exosomal DElncRNA-DEmiRNAs pairs in CRC **(A)** Exosomal DElncRNA-DEmiRNAs pairs, the green dots represents up-regulated DElncRNAs, the red dots represents DEmiRNAs **(B)** Mann-Whitney U test shows that there is a significant differences in miR-10b-5p expression levels between CRC patients and healthy donors in GSE71008 dataset. Data were expressed as median with interquartile range (*p = 0.0125). **(C)** Mann-Whitney U test showed that there is a significant difference in miR-150-5p expression levels between CRC patients vs. healthy donors in GSE71008 dataset. Data were expressed as median with interquartile range (p = **0.0014). **(D,E)** The AUC of exosomal miR-10b-5p and exosomal miR-105-5p was 0.625 and 0.658 in 100 CRC patients vs. 50 healthy donors.

ADAMTS2, *TOMM70A*, *RBM48* and *RHOBTB1* were 0.887, 0.695, 0.73, 0.66 and 0.692, respectively. The study found that *BEND3*, *ADAMTS2*, *TOMM70A*, *RBM48* and *RHOBTB1* were significantly up-regulated in CRC tissues compared to the precancerous in the TCGA database (**Figure 4H**). Notably, the AUC of the combination of these five mRNAs was 0.925 (95% CI: 0.899-0.951), with specificity and sensitivity of 90.2% and 82.8%, respectively (**Figure 4I**).

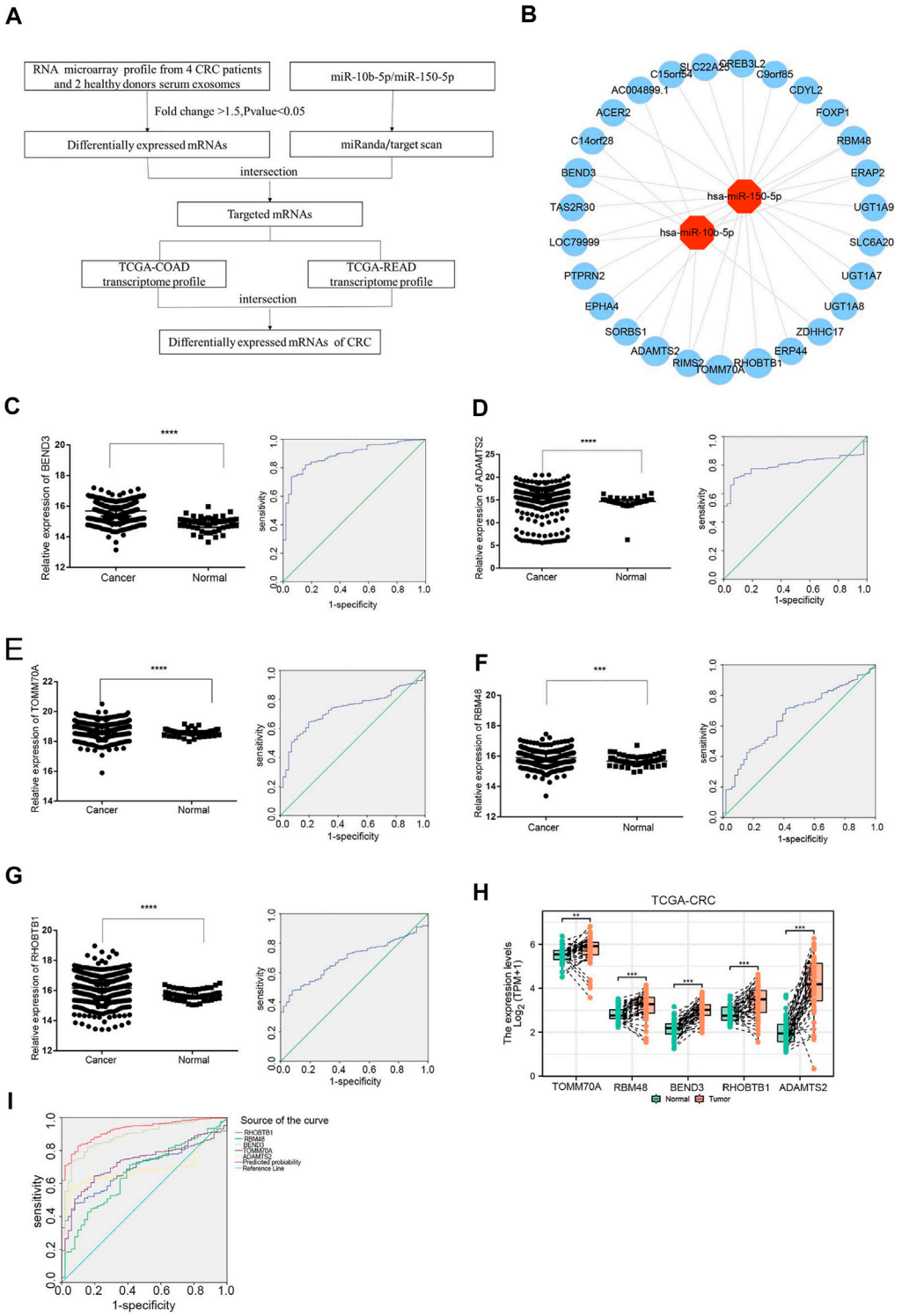

FIGURE 4 | Expression analysis of exosomal miRNA-mRNA internections in CRC **(A)** Flowchart of the DEmRNAs in CRC. TCGA-COAD: The Cancer Genome Atlas-colon adenocarcinoma, TCGA-READ: The Cancer Genome Atlas-rectal adenocarcinoma. **(B)** Analysis of exosomal miR-10b-5p and miR-150-5p targeted up-regulated DEmRNAs, red dots represent DEmiRNAs and the blue dots reprsent DEmRNAs. **(C–G)** The relative expression of *BEND3*, *ADAMTS2*, *TOMM70A*, *RBM48*, *RHOBTB1* from TCGA database (CRC patients *n* = 623, Healthy donors *n* = 51). The AUC of *BEND3*, *ADAMTS2*, *TOMM70A*, *RBM48*, *RHOBTB1* were 0.887, 0.695, 0.73, 0.66, 0.692 for CRC diagnostics, respectively. **(H)** *BEND3, ADAMTS2, TOMM70A, RBM48 and RHOBTB1* were significantly up-regulated in CRC tissues compared to the precancerous in the TCGA database. **(I)** The combination of five DEmRNAs had an AUC of 0.925 with a specificity of 90.2% and sensitivity of 82.8%.

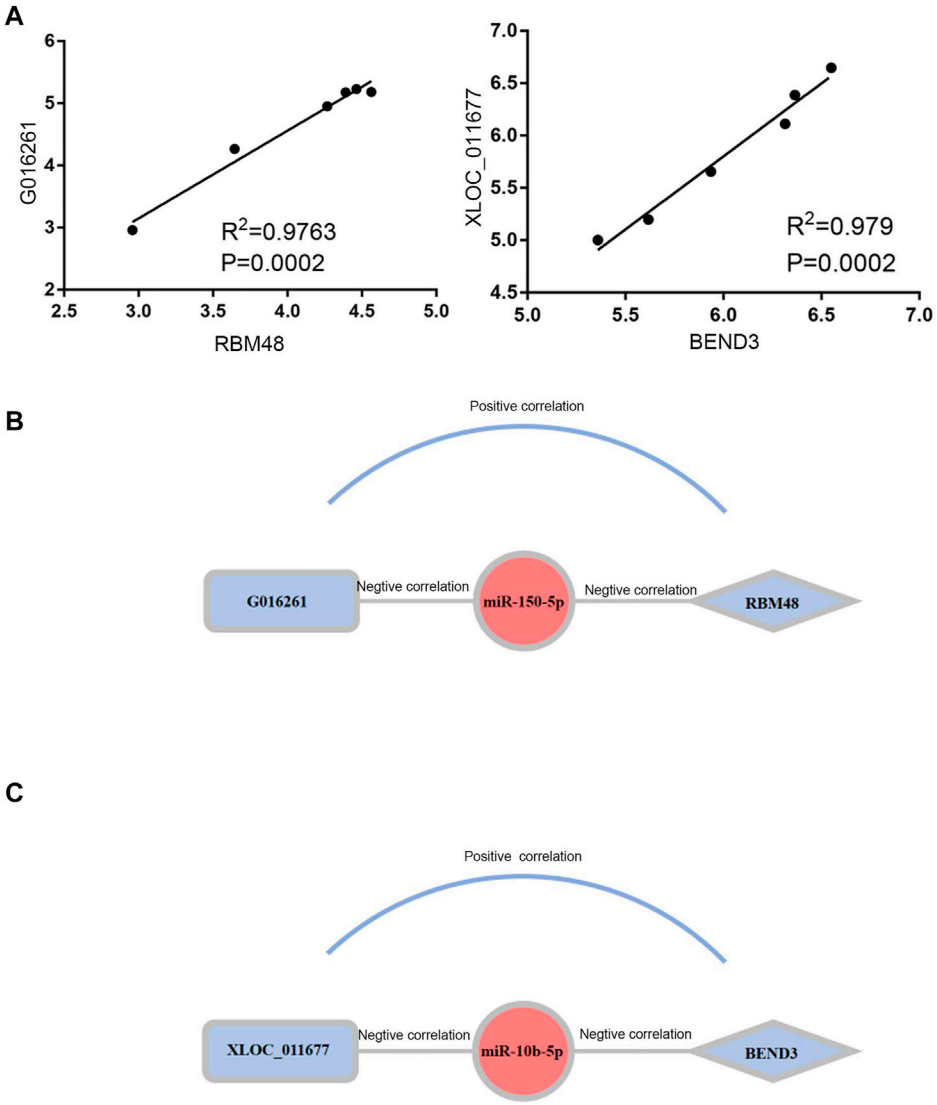

FIGURE 5 | Construction and Correlation analyses of exosomal ceRNA network in CRC. **(A)** Pearson correlation analysis for exosomal DElncRNAs and associated DEmRNAs. Horizontal axis indicates normalized exosomal DElncRNA expression levels; vertical axis indicates normalized exosomal DEmRNA expression levels (lncRNA xloc_011677 correlates to *BEND3*, lncRNA G016261 correlates to RBM48).**(B,C)**The exosomal lncRNA G016261-miR-150-5p-*RBM48* and exosomal lncRNA XLOC_01167-miR-10b-5p-*BEND3* regulatory axis, miRNAs, lncRNAs and mRNAs are represented by ellipse, round rectangle and diamonds, respectively.

Construction and Correlation Analyses of the Exosomal ceRNA Network

To elucidate the regulatory mechanism of CRC, an exosomal lncRNA-related ceRNA network of CRC was developed based on the above results. The ceRNA hypothesis states that exosomal lncRNAs harboring MREs can competitively bind to certain miRNAs, thus regulating miRNA-mediated downstream target gene silencing at the post-transcriptional level. We found that 40 exosomal DE lncRNAs might competitively bind to miR-10b-5p and miR-150-5p, and the latter might regulate 27 downstream targeted mRNAs (**Figure 4B**), which explained how mRNA expression was regulated by exosomal lncRNAs by combining with miRNAs. To confirm the possibility of indirect interactions between DE lncRNAs and DE mRNAs, a Pearson's correlation analysis was performed with R2 ≥0.95 and $p < 0.001$ as criteria, which revealed a positive correlation between the expression levels of ten DE lncRNA-DE mRNA pairs (**Figure 5A**). Among which exosomal lncRNA G016261/*RBM48* and lncRNA XLOC_011677/*BEND3* were better matched than others in binding sites, thus lncRNA G016261/*RBM48* and lncRNA XLOC_011677/*BEND3* were selected (**Tables 1**, **2**).

Finally, we predicted the exosomal ceRNA network in CRC. As shown in **Figure 5B**, lncRNA G016261 would function as ceRNA that interact with *RBM48*, serving as miRNA sponges to restrain miR-150-5p function, then inhibit its regulation of target gene *RBM48* expression; Meanwhile, lncRNA XLOC_011677 may also act as ceRNA to compete with

TABLE 1 | The targets mRNAs and lncRNAs of the miR-150-5p in targetsan and miRanda.

GeneSymbol	Type	8mer	7mer-m8	7mer-A1	6mer	Offset 6mer	Imperfect
RBM48	mRNA	1	0	0	0	0	1
TOMM70A	mRNA	0	1	0	0	0	0
BEND3	mRNA	0	1	0	0	0	0
G045105	lncRNA	0	1	0	0	0	0
XLOC_011677	lncRNA	0	2	0	0	0	0
G074547	lncRNA	0	1	0	0	0	0
G083164	lncRNA	0	1	0	0	0	0
RHOBTB1	mRNA	0	2	0	0	0	0
G016261	lncRNA	0	1	0	0	0	0
G059494	lncRNA	0	0	0	0	0	1
G005608	lncRNA	0	0	0	0	0	0

TABLE 2 | The targets mRNAs and lncRNAs of the miR-10b-5p in targetsan and miRanda.

GeneSymbol	Type	8mer	7mer-m8	7mer-A1	6mer	Offset 6mer	Imperfect
G045105	lncRNA	0	1	0	0	0	0
XLOC_011677	lncRNA	1	1	0	0	0	0
G016261	lncRNA	1	2	0	0	0	0
G059591	lncRNA	0	1	0	0	0	0
ADAMTS2	mRNA	0	1	0	0	0	0
G083164	lncRNA	0	1	0	0	0	0
BEND3	mRNA	1	0	0	0	1	0
RBM48	mRNA	0	1	0	0	0	0
G059494	lncRNA	0	1	0	0	1	0
G005608	lncRNA	0	0	0	0	0	0

8mer: 2-8 nucleic acid perfect matching, and the first nucleic acid was A. 7mer-m8: 2-8 nucleic acid perfect matching, and the first nucleic acid wasn't A. 7mer-A1: 2-7 nucleic acid perfect matching, and the first nucleic acid was A. 6mer: 2-7 nucleic acid perfect matching, and the first nucleic acid was A. Offset 6mer: 3-8 nucleic acid perfect matching. Imperfect: 2-7 nucleic acid was mismatch or deleted.

BEND3 transcripts for the miR-150-5p, thus mediating the interaction and regulation between miR-10b-5p and *BEND3* (**Figure 5C**).

DISCUSSION

Globally, colorectal cancer (CRC) is the third most commonly diagnosed malignancy and the second leading cause of cancer-related deaths [22]. Exosomes function as potent cell-cell transfer cargos for intercellular transfer of bioactive molecules, including lncRNA to the recipient cells and participate in ceRNA network. Recently, ceRNA hypothesis has been proposed to represent a class of RNAs with miRNA binding sites that competitively bind to miRNAs to inhibit their regulation of target genes, playing a crucial role in the underlying molecular mechanisms of CRC initiation and progression.

To verify the effectiveness and practicality of exosomal miRNAs, we compared them with another dataset, GSE71008, which includes exosomal RNA-sequence profiles from 100 CRC patients and 50 healthy donors. GSE71008 showed that compared with healthy donors, the expression of exosomal miR-150-5p and miR-10b-5p were markedly decreased in CRC patients. Previous studies reported that miR-10b-5p and miR-150-5p were associated with cancer progression, proliferation, and migration [23–25]. MiR-150-5p was significantly downregulated in both plasma and cancer tissue samples, and might be a biomarker in cancer [21, 26, 27]. Chen et al. showed that miR-150-5p inhibited CRC cell proliferation, migration, invasion and angiogenesis *in vitro* and *in vivo*, and its inhibitory effect could be reversed by vascular epithelial growth factor A (*VEGFA*) [28]. Other studies revealed a significantly lower expression of miR-10b-5p in renal cell carcinoma and triple-negative breast cancer [25, 29]. Jin et al. reported that exosomal miR-10b-5p may be a promising and effective candidate for the development of highly sensitive, non-invasive biomarkers for early NSCLC diagnosis [30]. MiR-10b-5p is related to proliferation, migration, and invasion of CRC cells [31].

MiRNA regulates gene expression at the post-transcriptional level by targeting mRNA 3′UTR. Based on microarray data and TCGA database analysis, we identified miR-10b-5p and miR-150-5p target mRNA pairs, which included *TOMM70A*, *RBM48*, *BEND3*, *RHOBTB1* and *ADAMTS2*. The five mRNAs were markedly upregulated in CRC patients compared with healthy donors from TCGA database. Bai et al. identified that RBM48 was a U12 splicing factor that promoted cell differentiation and repressed cell proliferation, and U12 was associated with the occurrence and development of cancer. BEND3 is a nuclear protein and transcriptional repressor that associates with the HP1-containing heterochromatin loci [32, 33], and might play a role in identifying the subgroup of breast carcinoma patients with potential to develop visceral metastasis [34]. *TOMM70A* localizes in the mitochondria of COS-7 cells [35], and is a new biomarker of resistance to hormonal

therapy in breast cancer [36, 37]. *RHOBTB1* is an atypical Rho GTPase with two BTB domains in addition to its Rho domain. Chemotherapy-induced fatigue may involve downregulation of *RHOBTB1* in peripheral blood mononuclear cells of patients with locoregional breast cancer [38]. Many studies have shown that tumor suppressor *RHOBTB1* contributes to the proliferation and invasion of cancer [39–41]. *ADAMTS*-2 is associated with tumor progression and invasion, metastasis and CRC-specific survival, and may serve as a potential biomarker to stratify CRC patients into low and high risk of tumor metastasis [42]. Jiang et al. reported that *ADAMTS*-2 protein expression was remarkably higher in gastric cancer cells than in normal tissues, therefore, *ADAMTS*-2 may be a potential biomarker for assessing the prognosis of gastric carcinoma [43].

In summary, a ceRNA regulatory network was successfully developed by identification of cancer-specific lncRNAs, miRNAs and mRNAs. We propose that this regulatory network centered on exosomal miR-10b-5p and miR-150-5p may play a critical role in the carcinogenesis of CRC. This study highlighted a novel ceRNA mechanism in which exosomal lncRNA G016261 and lncRNA XLOC_011677-sponging miR-10b-5p and miR-150-5p regulate the expression of *RBM48* and *BEND3*. A diagnostic model based on miRNAs in the ceRNA network might help in improving the diagnosis efficiency for CRC patients compared to miRNAs alone. However, exosomal lncRNA G016261-miR-150-5p-*RBM48* and lncRNA XLOC_011677-miR-10b-5p-*BEND3* regulatory axes should be further studied to fully elucidate their biological functions and confirm the molecular mechanisms.

DATA AVAILABILITY STATEMENT

The original contributions presented in the study are included in the article/**Supplementary Material**, further inquiries can be directed to the corresponding author.

ETHICS STATEMENT

The studies involving human participants were reviewed and approved by the Shandong Cancer Hospital and Institute, Shandong First Medical University and Shandong Academy of Medical Sciences of committee. The patients/participants provided their written informed consent to participate in this study.

AUTHOR CONTRIBUTIONS

All authors listed have made a substantial, direct, and intellectual contribution to the work and approved it for publication.

FUNDING

This work was supported by the Shandong Provincial Natural Science Foundation (ZR2020LZL017), National Natural Science Foundation of China (81773237).

CONFLICT OF INTEREST

The authors declare that the research was conducted in the absence of any commercial or financial relationships that could be construed as a potential conflict of interest.

SUPPLEMENTARY MATERIAL

The Supplementary Material for this article can be found online at: https://www.por-journal.com/articles/10.3389/pore.2022.1610493/full#supplementary-material

REFERENCES

1. Bray F, Ferlay J, Soerjomataram I, Siegel RL, Torre LA, Jemal A. Global Cancer Statistics 2018: GLOBOCAN Estimates of Incidence and Mortality Worldwide for 36 Cancers in 185 Countries. *CA Cancer J Clin* (2018) 68(6):394–424. doi:10.3322/caac.21492
2. De Rubis G, Rajeev Krishnan S, Bebawy M. Liquid Biopsies in Cancer Diagnosis, Monitoring, and Prognosis. *Trends Pharmacol Sci* (2019) 40(3): 172–86. doi:10.1016/j.tips.2019.01.006
3. Pegtel DM, Gould SJ. Exosomes. *Annu Rev Biochem* (2019) 88:487–514. doi:10.1146/annurev-biochem-013118-111902
4. Kulkarni B, Kirave P, Gondaliya P, Jash K, Jain A, Tekade RK, et al. Exosomal miRNA in Chemoresistance, Immune Evasion, Metastasis and Progression of Cancer. *Drug Discov Today* (2019) 24:2058–67. doi:10.1016/j.drudis.2019.06.010
5. Malla B, Zaugg K, Vassella E, Aebersold DM, Dal Pra A. Exosomes and Exosomal MicroRNAs in Prostate Cancer Radiation Therapy. *Int J Radiat Oncol Biol Phys* (2017) 98(5):982–95. doi:10.1016/j.ijrobp.2017.03.031
6. Zhang X, Yuan X, Shi H, Wu L, Qian H, Xu W. Exosomes in Cancer: Small Particle, Big Player. *J Hematol Oncol* (2015) 8:83. doi:10.1186/s13045-015-0181-x
7. Milman N, Ginini L, Gil Z. Exosomes and Their Role in Tumorigenesis and Anticancer Drug Resistance. *Drug Resist Updat* (2019) 45:1–12. doi:10.1016/j.drup.2019.07.003
8. Poggio M, Hu T, Pai CC, Chu B, Belair CD, Chang A, et al. Suppression of Exosomal PD-L1 Induces Systemic Anti-tumor Immunity and Memory. *Cell* (2019) 177(2):414–27. doi:10.1016/j.cell.2019.02.016
9. Kim J, Kim TY, Lee MS, Mun JY, Ihm C, Kim SA. Exosome Cargo Reflects TGF-β1-Mediated Epithelial-To-Mesenchymal Transition (EMT) Status in A549 Human Lung Adenocarcinoma Cells. *Biochem Biophys Res Commun* (2016) 478(2):643–8. doi:10.1016/j.bbrc.2016.07.124
10. Zhang W, Cai X, Yu J, Lu X, Qian Q, Qian W. Exosome-mediated Transfer of lncRNA RP11838N2.4 Promotes Erlotinib Resistance in Non-small Cell Lung Cancer. *Int J Oncol* (2018) 53(2):527–38. doi:10.3892/ijo.2018.4412
11. Salmena L, Poliseno L, Tay Y, Kats L, Pandolfi PP. A ceRNA Hypothesis: the Rosetta Stone of a Hidden RNA Language? *Cell* (2011) 146(3):353–8. doi:10.1016/j.cell.2011.07.014
12. Thomson DW, Dinger ME. Endogenous microRNA Sponges: Evidence and Controversy. *Nat Rev Genet* (2016) 17(5):272–83. doi:10.1038/nrg.2016.20
13. Xie C, Zhang LZ, Chen ZL, Zhong WJ, Fang JH, Zhu Y, et al. A Novel hMTR4-PDIA3P1-miR-125/124-TRAF6 Regulatory Axis and its Function in NF-K B Signaling and Chemoresistance. *Hepatology* (2020) 71(5):1660–77. doi:10.1002/hep.30931
14. Cheng Z, Yu C, Cui S, Wang H, Jin H, Wang C, et al. circTP63 Functions as a ceRNA to Promote Lung Squamous Cell Carcinoma Progression by Upregulating FOXM1. *Nat Commun* (2019) 10(1):3200. doi:10.1038/s41467-019-11162-4

15. Liu Y, Xue M, Du S, Feng W, Zhang K, Zhang L, et al. Competitive Endogenous RNA Is an Intrinsic Component of EMT Regulatory Circuits and Modulates EMT. *Nat Commun* (2019) 10(1):1637. doi:10.1038/s41467-019-09649-1
16. Zheng ZQ, Li ZX, Zhou GQ, Lin L, Zhang LL, Lv JW, et al. Long Noncoding RNA FAM225A Promotes Nasopharyngeal Carcinoma Tumorigenesis and Metastasis by Acting as ceRNA to Sponge miR-590-3p/miR-1275 and Upregulate ITGB3. *Cancer Res* (2019) 79(18):4612–26. doi:10.1158/0008-5472.CAN-19-0799
17. Song YX, Sun JX, Zhao JH, Yang YC, Shi JX, Wu ZH, et al. Non-coding RNAs Participate in the Regulatory Network of CLDN4 via ceRNA Mediated miRNA Evasion. *Nat Commun* (2017) 8(1):289. doi:10.1038/s41467-017-00304-1
18. Li Z, Jiang P, Li J, Peng M, Zhao X, Zhang X, et al. Tumor-derived Exosomal Lnc-Sox2ot Promotes EMT and Stemness by Acting as a ceRNA in Pancreatic Ductal Adenocarcinoma. *Oncogene* (2018) 37(28):3822–38. doi:10.1038/s41388-018-0237-9
19. Barbagallo C, Brex D, Caponnetto A, Cirnigliaro M, Scalia M, Magnano A, et al. LncRNA UCA1, Upregulated in CRC Biopsies and Downregulated in Serum Exosomes, Controls mRNA Expression by RNA-RNA Interactions. *Mol Ther Nucleic Acids* (2018) 12:229–41. doi:10.1016/j.omtn.2018.05.009
20. Wang N, Song X, Liu L, Niu L, Wang X, Song X, et al. Circulating Exosomes Contain Protein Biomarkers of Metastatic Non-small-cell Lung Cancer. *Cancer Sci* (2018) 109(5):1701–9. doi:10.1111/cas.13581
21. Zhao YJ, Song X, Niu L, Tang Y, Song X, Xie L. Circulating Exosomal miR-150-5p and miR-99b-5p as Diagnostic Biomarkers for Colorectal Cancer. *Front Oncol* (2019) 9:1129. doi:10.3389/fonc.2019.01129
22. Keum N, Giovannucci E. Global burden of Colorectal Cancer: Emerging Trends, Risk Factors and Prevention Strategies. *Nat Rev Gastroenterol Hepatol* (2019) 16:713–32. doi:10.1038/s41575-019-0189-8
23. Li X, Luo Y, Liu L, Cui S, Chen W, Zeng A, et al. The Long Noncoding RNA ZFAS1 Promotes the Progression of Glioma by Regulating the miR-150-5p/PLP2 axis. *J Cel Physiol* (2019) 235:2937–46. doi:10.1002/jcp.29199
24. Xiao G, Wang P, Zheng X, Liu D, Sun X. FAM83A-AS1 Promotes Lung Adenocarcinoma Cell Migration and Invasion by Targeting miR-150-5p and Modifying MMP14. *Cell Cycle* (2019) 18:2972–85. doi:10.1080/15384101.2019.1664225
25. Li Y, Chen D, Li Y, Jin L, Liu J, Su Z, et al. Oncogenic cAMP Responsive Element Binding Protein 1 Is Overexpressed upon Loss of Tumor Suppressive miR-10b-5p and miR-363-3p in Renal Cancer. *Oncol Rep* (2016) 35(4):1967–78. doi:10.3892/or.2016.4579
26. Paunescu IA, Bardan R, Marcu A, Nitusca D, Dema A, Negru S, et al. Biomarker Potential of Plasma MicroRNA-150-5p in Prostate Cancer. *Medicina (Kaunas)* (2019) 55(9):E564. doi:10.3390/medicina55090564
27. Zou SL, Chen YL, Ge ZZ, Qu YY, Cao Y, Kang ZX. Downregulation of Serum Exosomal miR-150-5p Is Associated with Poor Prognosis in Patients with Colorectal Cancer. *Cancer Biomark* (2019) 26(1):69–77. doi:10.3233/CBM-190156
28. Chen X, Xu X, Pan B, Zeng K, Xu M, Liu X, et al. miR-150-5p Suppresses Tumor Progression by Targeting VEGFA in Colorectal Cancer. *Aging (Albany NY)* (2018) 10(11):3421–37. doi:10.18632/aging.101656
29. Ouyang M, Li Y, Ye S, Ma J, Lu L, Lv W, et al. MicroRNA Profiling Implies New Markers of Chemoresistance of Triple-Negative Breast Cancer. *PLoS One* (2014) 9(5):e96228. doi:10.1371/journal.pone.0096228
30. Jin X, Chen Y, Chen H, Fei S, Chen D, Cai X, et al. Evaluation of Tumor-Derived Exosomal miRNA as Potential Diagnostic Biomarkers for Early-Stage Non-Small Cell Lung Cancer Using Next-Generation Sequencing. *Clin Cancer Res* (2017) 23(17):5311–9. doi:10.1158/1078-0432.CCR-17-0577
31. Lu C, Jiang W, Hui B, Rong D, Fu K, Dong C, et al. The circ_0021977/miR-10b-5p/P21 and P53 Regulatory axis Suppresses Proliferation, Migration, and Invasion in Colorectal Cancer. *J Cel Physiol* (2020) 235(3):2273–85. doi:10.1002/jcp.29135
32. Yuan L, Zhou M, Huang D, Wasan HS, Zhang K, Sun L, et al. Resveratrol Inhibits the Invasion and Metastasis of colon Cancer through Reversal of Epithelial- Mesenchymal Transition via the AKT/GSK-3β/Snail Signaling Pathway. *Mol Med Rep* (2019) 20(3):2783–95. doi:10.3892/mmr.2019.10528
33. Khan A, Prasanth SG. BEND3 Mediates Transcriptional Repression and Heterochromatin Organization. *Transcription* (2015) 6(5):102–5. doi:10.1080/21541264.2015.1100228
34. Savci-Heijink CD, Halfwerk H, Koster J, Horlings HM, van de Vijver MJ. A Specific Gene Expression Signature for Visceral Organ Metastasis in Breast Cancer. *BMC Cancer* (2019) 19(1):333. doi:10.1186/s12885-019-5554-z
35. Edmonson AM, Mayfield DK, Vervoort V, DuPont BR, Argyropoulos G. Characterization of a Human Import Component of the Mitochondrial Outer Membrane, TOMM70A. *Cell Commun Adhes* (2002) 9(1):15–27. doi:10.1080/15419060212186
36. Rangel R, Guzman-Rojas L, Kodama T, Kodama M, Newberg JY, Copeland NG, et al. Identification of New Tumor Suppressor Genes in Triple-Negative Breast Cancer. *Cancer Res* (2017) 77:4089–101. doi:10.1158/0008-5472.CAN-17-0785
37. Sotgia F, Fiorillo M, Lisanti MP. Mitochondrial Markers Predict Recurrence, Metastasis and Tamoxifen-Resistance in Breast Cancer Patients: Early Detection of Treatment Failure with Companion Diagnostics. *Oncotarget* (2017) 8(40):68730–45. doi:10.18632/oncotarget.19612
38. de Alcantara BBR, Cruz FM, Fonseca FLA, da Costa Aguiar Alves B, Perez MM, Varela P, et al. Chemotherapy-induced Fatigue Is Associated with Changes in Gene Expression in the Peripheral Blood Mononuclear Cell Fraction of Patients with Locoregional Breast Cancer. *Support Care Cancer* (2019) 27(7):2479–86. doi:10.1007/s00520-018-4519-0
39. Lin N, Zhou Y, Lian X, Tu Y. MicroRNA-31 Functions as an Oncogenic microRNA in Cutaneous Squamous Cell Carcinoma Cells by Targeting RhoTBT1. *Oncol Lett* (2017) 13(3):1078–82. doi:10.3892/ol.2017.5554
40. Xu RS, Wu XD, Zhang SQ, Li CF, Yang L, Li DD, et al. The Tumor Suppressor Gene RhoBTB1 Is a Novel Target of miR-31 in Human colon Cancer. *Int J Oncol* (2013) 42(2):676–82. doi:10.3892/ijo.2012.1746
41. Haga RB, Garg R, Collu F, Borda D'Agua B, Menendez ST, Colomba A, et al. RhoBTB1 Interacts with ROCKs and Inhibits Invasion. *Biochem J* (2019) 476(17):2499–514. doi:10.1042/BCJ20190203
42. Kirana C, Peng L, Miller R, Keating JP, Glenn C, Shi H, et al. Combination of Laser Microdissection, 2D-DIGE and MALDI-TOF MS to Identify Protein Biomarkers to Predict Colorectal Cancer Spread. *Clin Proteomics* (2019) 16:3. doi:10.1186/s12014-019-9223-7
43. Jiang C, Zhou Y, Huang Y, Wang Y, Wang W, Kuai X. Overexpression of ADAMTS-2 in Tumor Cells and Stroma Is Predictive of Poor Clinical Prognosis in Gastric Cancer. *Hum Pathol* (2019) 84:44–51. doi:10.1016/j.humpath.2018.08.030

Pathology & Oncology Research | frontiers

ORIGINAL RESEARCH
published: 09 June 2022
doi: 10.3389/pore.2022.1610446

Plasma Exosomal hsa_circ_0015286 as a Potential Diagnostic and Prognostic Biomarker for Gastric Cancer

Peiming Zheng[1], Huijie Gao[2], Xuanhu Xie[2] and Peipei Lu[2]*

[1]Department of Clinical Laboratory, Henan Provincial People's Hospital, People's Hospital of Zhengzhou University, People's Hospital of Henan University, Zhengzhou, China, [2]Department of Oncology, The First Affiliated Hospital of Henan University, Kaifeng, China

Circular RNA (circRNA) is stable and abundant in exosomes as a potential biomarker for the diagnosis and prognosis of tumor. In this study, cancer specific exosomal circRNAs were identified through circRNA microarray, and 58 circRNAs were significantly upregulated in cancer cells derived exosomes. Then 60 patients with newly diagnosed gastric cancer (GC), 30 chronic gastritis patients and 30 healthy subjects were enrolled for further clinical validation. We detected that hsa_circ_0015286 was remarkably highly expressed in GC tissue, plasma and cancer cells compared with normal controls. Results of ROC curve analysis showed that the area under curve (AUC) of hsa_circ_0015286, CEA and CA 19-9 was 0.778, 0.673, and 0.665, respectively. The combined detection of three indicators had the highest AUC (0.843). Exosomal hsa_circ_0015286 expression was closely associated with tumor size, TNM stage and lymph node metastasis. The expression level of exosomal hsa_circ_0015286 in GC patients decreased significantly after surgery. Overall survival of patients with low hsa_circ_0015286 expression was longer than those with high expression. Our data demonstrated that exosomal hsa_circ_0015286 might be a promising noninvasive biomarker for the diagnosis and prognosis evaluation of GC.

Keywords: biomarker, gastric cancer, diagnosis, CircRNA, exosomes

OPEN ACCESS

Edited by:
József Tímár,
Semmelweis University, Hungary

****Correspondence:***
Peiming Zheng
zpm8266@163.com

Received: *16 March 2022*
Accepted: *26 May 2022*
Published: *09 June 2022*

Citation:
Zheng P, Gao H, Xie X and Lu P (2022) Plasma Exosomal hsa_circ_0015286 as a Potential Diagnostic and Prognostic Biomarker for Gastric Cancer. Pathol. Oncol. Res. 28:1610446. doi: 10.3389/pore.2022.1610446

INTRODUCTION

Gastric cancer (GC) is the fifth most common malignant tumor and the third leading cause of cancer-related death worldwide, with over one million new cases in 2020 and an estimated 769,000 deaths globally [1]. GC remains the second most frequent cancer in China, and most patients are diagnosed at later stage with a lower five-year survival rate due to the finite early diagnosis [2, 3]. Therefore, it is urgent to find novel non-invasive biomarkers for diagnosing and prognosis monitoring of patients with GC.

Exosomes, one type of extracellular vesicles (EVs) with a diameter range of 30–150 nm, are secreted by almost all cells. More importantly, exosomes are widely existed in blood, urine, cerebrospinal fluid, saliva, and other common body fluids, comprising a variety of lipids, proteins, DNAs and noncoding RNAs (ncRNAs) derived from the original cells [4, 5]. Moreover, due to the protection of the lipid bilayer structure of exosomes, these disease-specific DNAs and RNAs in exosomes are stable and ideal biomarkers for diagnosis and prognosis

monitoring of most diseases [6, 7]. Circular RNA (circRNA) is a particular endogenous RNA with a covalently closed loop that is distinguished from the traditional linear RNA [8]. At present, circRNAs have been found to be stable and enriched in exosomes [9]. Recent studies have confirmed that circulating exosomal circRNAs can reflect the malignant characteristics and progression of cancer, implying their significant potential as novel diagnostic and prognostic biomarker for cancer [10, 11]. Therefore, we assumed that GC cells in the tumor microenvironment are able to produce and deliver exosomes, and the detection of plasma exosomal circRNAs might supply a noninvasive and convenient approach for the diagnosis and prognosis evaluation of GC.

In this study, based on the result of circRNA microarray in cancer cell-derived exosomes, hsa_circ_0015286 was selected and proved to be highly expressed in plasma and tissue of GC patients. The diagnostic and prognostic values were evaluated using receiver operating characteristic (ROC) curve and Kaplan-Meier survival curve. Then, the association between the expression level of plasma exosomal hsa_circ_0015286 and the clinicopathological parameters of GC patients was further analyzed. Our data illustrated the potential of exosomal hsa_circ_0015286 as a noninvasive biomarker for the diagnosis and prognosis evaluation of GC.

MATERIAL AND METHODS

Cell Culture

Human gastric epithelial cell line (GES-1) and four cancer cell lines (BGC823, SGC7901, MGC803, AGS) were purchased from the Chinese Academy of Sciences Cell Bank of Type Culture Collection. Three of the four cancer cell lines we commonly used (BGC823, SGC7901 and MGC803) are actually HeLa derivatives. Cells were cultured in high-glucose DMEM (HyClone) medium at 37°C with 5% CO_2, all media were supplemented with 100 μg/ml streptomycin, 100 U/ml penicillin and 10% exosome-depleted Foetal Bovine Serum (FBS, Gibco). For exosome extraction, culture medium (CM) was collected and centrifuged at 2,000 g for 10 min, then followed by 12,000 g for 10 min at 4°C. The supernatant was transferred and stored at −80°C.

Patients

Sixty newly diagnosed GC patients admitted to the First Affiliated Hospital of Henan University from October 2018 to December 2019 were selected. The average age of the GC patients was 63.7 (range from 38 to 81 years old), with 32 males and 28 females. The inclusion criteria were as follows: 1) all subjects were confirmed by gastroscopy or histopathology; 2) no any chemotherapy or surgical treatment before; 3) with complete clinicopathological features. The exclusion criteria were as follows: 1) together with heart, kidney, and liver dysfunction; 2) together with other cancer. Tumor clinical stages and histological grades were assessed according to the 8th AJCC/TNM staging system and National Comprehensive Cancer Network clinical practice guideline of oncology (V.1.2012), including 10 stage I patients, 17 stage II patients, 19 stage III patients and 14 stage IV patients. Lymph node metastasis was identified that metastasis to intraabdominal lymph nodes, including hepatoduodenal, retropancreatic, mesenteric, and para-aortic.

Besides, thirty of the above sixty patients received surgical treatment, 30 paired GC tissues and paracancerous tissues were collected from surgery before other treatments were initiated. The adjacent paracancerous tissues were 5 cm away from the margins of the tumor. In addition, 30 pure chronic gastritis patients (disease control group) and 30 healthy subjects (healthy control group) who underwent physical examination were also enrolled in the same period. The average age of chronic gastritis patients and healthy subjects were 59.5 and 61.2 years, respectively. This study was performed in accordance with the rules of the Declaration of Helsinki of 1975 (revised in 2013). The study was approved by the institutional ethics committee of the First Affiliated Hospital of Henan University (No.2019053), and all subjects signed informed consent.

Exosome Isolation

Preoperative fasting venous blood (4 ml) was collected using EDTA-anticoagulant tube and centrifuged at 3,000 g for 10 min within 2 h, then the plasma was further centrifuged at 12,000 g for 10 min at 4°C to remove cell debris. In addition, the second blood sample was collected 10 days after operation in twenty of the thirty patients who received surgical treatment. The processing method was the same as above. Subsequently, exosomes were isolated using ExoQuick solution (System Biosciences, United States) following the manufacturer's instructions.

Exosome Identification

The morphological characteristics of the purified exosomes were observed through transmission electron microscopy (TEM) and nanoparticle tracking analysis (NTA) as described previously [12]. Briefly, 10 μl of exosome suspension were absorbed onto carbon-coated cooper grids (200 mesh) for 1 min. Then the samples were washed with double-distilled water and negatively stained with 2% uranyl acetate solution for 1 min. Grids were visualized at 87000x in a Phillips Tecnai transmission electron microscope at 80 kV. The concentration and size distribution of the exosomes were determined using nanoparticle tracking analysis (NTA). Exosomes were diluted with PBS (1:1000) and then injected into the Zeta Potential/Particle Sizer NICOMPTM 380 ZLS analyzer (Santa Barbara, CA, United States). Particles were automatically tracked and sized based on brownian motion and the diffusion coefficient.

Circular RNA Microarray Analysis

Total RNA of cancer cells derived exosome was isolated through exoRNeasy Midi Kit (Qiagen) and then used for circRNA microarray assay. The RNA quality was evaluated by capillary electrophoresis on Agilent 2100 Bioanalyzer (Agilent Technologies, CA, United States). The circRNA microarray assay was conducted *via* the Agilent human circRNA V6 Microarray by Shanghai Biotechnology Corporation. The microarray data have been uploaded to the GEO database (GSE202538).

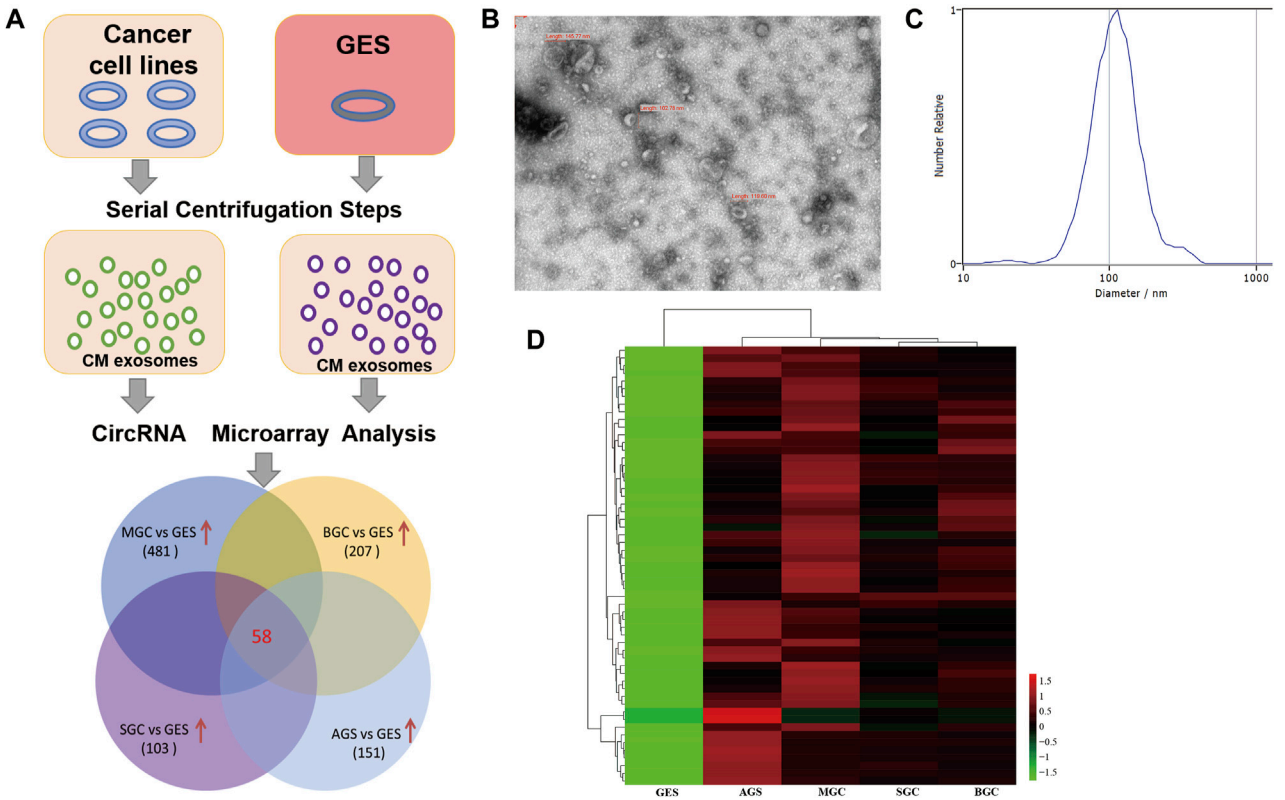

FIGURE 1 | Screening of cancer-specific exosomal circRNAs through circRNA microarray assay. **(A)**: Flow diagram of the screening strategy; **(B)**: Representative transmission electron microscopy image of purified exosomes; **(C)**: NTA of the size distribution and number of exosomes; **(D)**: Heatmap result of upregulated circRNAs based on circRNA microarray analysis.

RNA Extraction and Quantitative Real-Time PCR

RNA extraction and qRT-PCR analysis were performed as our previous description [12]. Briefly, the total RNA from tissues was extracted using TRIzol reagent (Invitrogen), and exosomal RNA was extracted using a miRNeasy Micro Kit (QIAGEN) according to the manufacturers' instructions. The quantity and quality of the RNA were evaluated using a NanoDrop spectrophotometer (Thermo Fisher Scientific). Five top upregulated circRNAs (hsa_circ_0028855, hsa_circ_0086471, hsa_circ_0049058, hsa_circ_0021091 and hsa_circ_0015286) were selected as candidate molecules for preliminary clinical validation. The primer sequences are shown in **Supplementary Table S1**. The relative expression levels of the target circRNA was calculated using the $2^{-\Delta\Delta CT}$ method. All results are expressed as the mean ± SD of three independent experiments.

Serum Tumor Marker Analysis

The traditional serum tumor markers CEA and CA19-9 were measured on Roche COBAS E602 Immunology Analyzer (Roche Diagnostics, China). The reference intervals of CEA and CA19-9 are 0–5.0 ng/ml and 0–35.0 U/ml respectively.

Statistical Analysis

SPSS 20.0 and GraphPad Prism 7.0 Software were used for all of the statistical analyses. Comparisons of hsa_circ_0015286 expression levels among different groups were analyzed using a Student's *t*-test or one-way ANOVA. ROC curve and Kaplan-Meier survival plot were established to evaluate diagnostic and prognostic capacity of exosomal hsa_circ_0015286. The relationships between hsa_circ_0015286 expression levels and clinicopathological parameters was further analyzed by t-tests. $p < 0.05$ was considered as statistically significant.

RESULTS

Screening of Cancer-Specific Exosomal circRNAs by Circular RNA Microarray Assay

The screening strategy for identification of cancer-specific exosomal circRNAs is illustrated in **Figure 1A**. Culture media from different cancer cell lines (MGC803, BGC823, SGC7901, and AGS) and GES-1 were collected, then exosomal RNA was isolated and circRNA microarray assay was conducted to detect differential circRNA expression. Transmission electron microscopy (TEM) and nanoparticle tracking analysis (NTA) were utilized to characterize and quantify the isolated exosomes, a typical teacup-like structure was observed with a diameter of 80–120 nm (**Figures 1B,C**). Based on the microarray data, the Venn diagram showed that 58 circRNAs were highly expressed (fold change of ≥2 and $p \leq 0.05$) in cancer cell derived exosomes

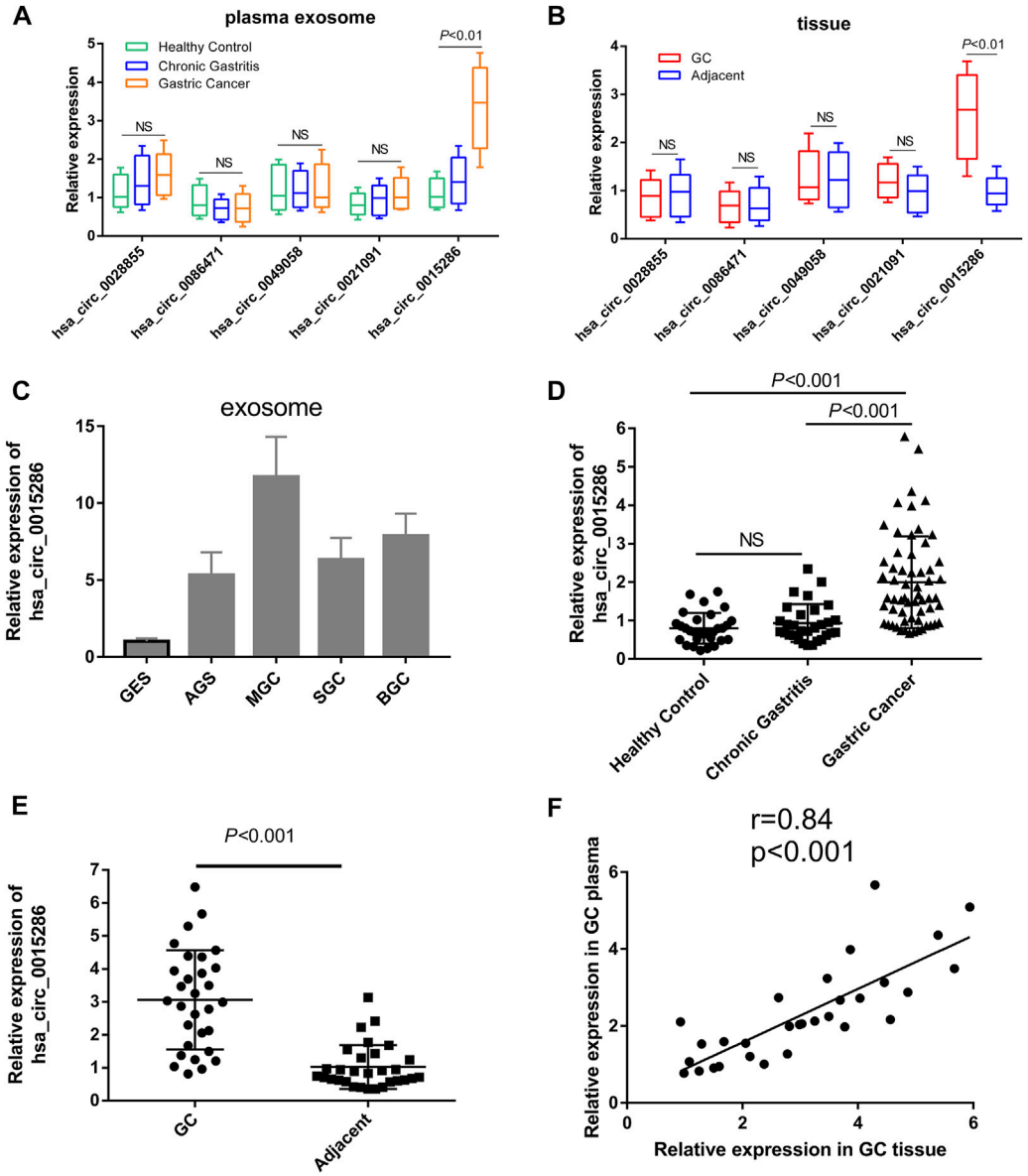

FIGURE 2 | Expression levels of candidate circRNAs in cancer cells and clinical specimens. **(A)** The relative expression of five upregulated circRNAs in plasma exosomes of preliminary clinical subjects; **(B)** The relative expression of five upregulated circRNAs in tissue samples of preliminary clinical subjects; **(C)**: Hsa_circ_0015286 expression levels in exosomes derived from cancer cell lines and control GES cell; **(D)**: Hsa_circ_0015286 expression levels in plasma exosomes of GC patients, chronic gastritis patients and healthy control; **(E)**: Hsa_circ_0015286 expression levels in 30 paired GC tissues and adjacent normal tissues; **(F)**: The relationship of hsa_circ_0015286 expression levels in GC tissues and plasma samples.

compared with those in GES-1. The heatmap showed the different expression levels of the 58 upregulated circRNAs (**Figure 1D**).

Exosomal hsa_circ_0015286 Expression Was Upregulated in Cancer Cells, GC Plasma and Tissues

Subsequently, in order to confirm the robustness of the circRNA microarray assay and investigate the clinical application value of candidate molecules, we detected the expression level of five top upregulated circRNAs using qRT-PCR in the plasma exosomes of 10 GC patients, 10 chronic gastritis patients and 10 healthy controls. Eight paired cancer tissue and paracancer tissue were also used for preliminary clinical validation. More interesting, besides the high expression in cancer cell derived exosomes, hsa_circ_0015286 was the uniquely upregulated circRNA in the plasma exosomes and tissues of GC patients compared with control groups. While there was no significant difference in the expression of four other molecules when validated with preliminary clinical specimens (**Figures 2A–C**). Thus, the following work was focused on this particular circRNA molecule.

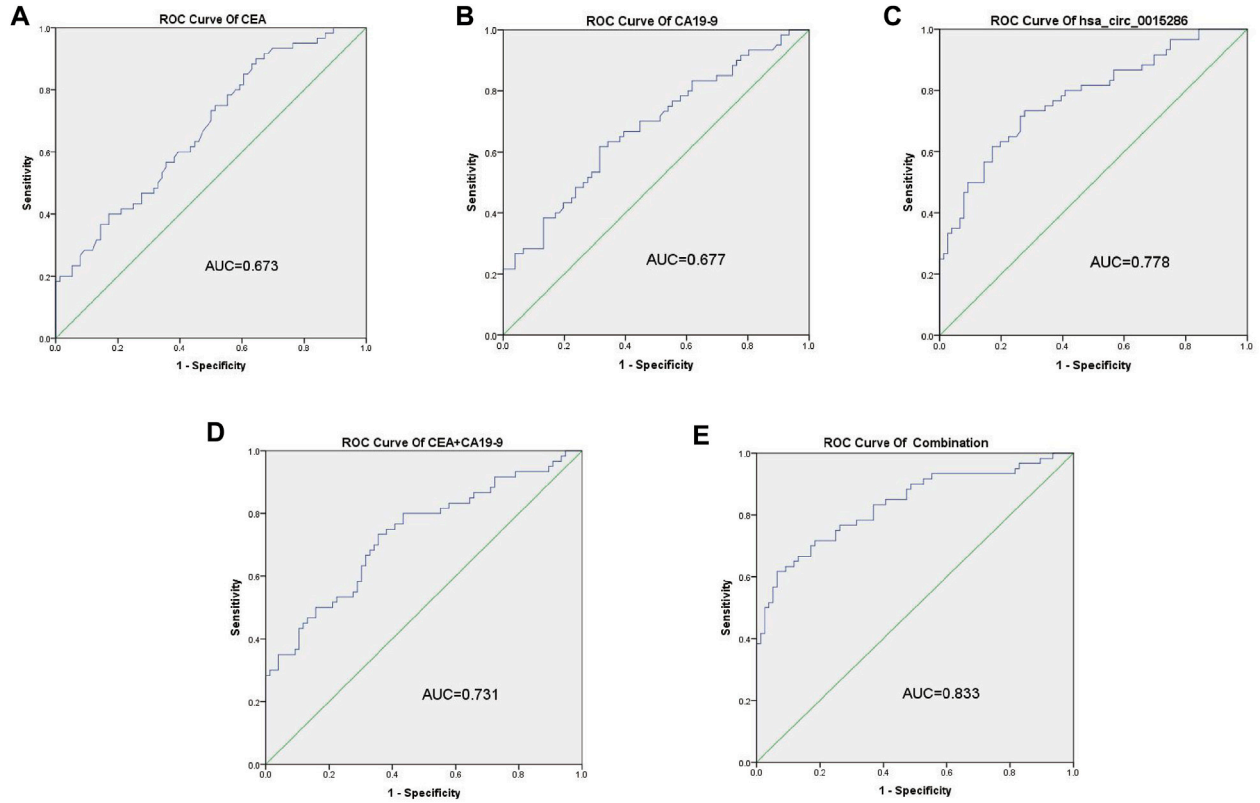

FIGURE 3 | ROC curve analysis of hsa_circ_0015286, CEA and CA19-9. **(A–C)**: ROC curve analysis of serum CEA, CA19-9 and exosomal hsa_circ_0015286 in GC patients versus controls, respectively; **(D)**: ROC curve analysis of the combination of CEA and CA19-9; **(E)**: ROC curve analysis of the combination of CEA, CA19-9 and exosomal hsa_circ_0015286 in GC patients versus controls.

Sixty patients with newly diagnosed GC, 30 chronic gastritis patients (disease control group) and 30 healthy subjects (healthy control group) were enrolled for further clinical validation. The RT-PCR results showed that plasma exosomal hsa_circ_0015286 level was significantly upregulated in the GC group compared with chronic gastritis patients and healthy control (**Figure 2D**, $p < 0.001$).

Then, the expression of hsa_circ_0015286 were tested in 30 paired GC tissues and paracancerous tissues. The expression levels of hsa_circ_0015286 in GC tissue were also substantially higher than that in paracancerous tissue (**Figure 2E**, $p < 0.001$). We further analyzed their relationship with plasma expression by Spearman correlation analysis, a significant positive correlation was observed between hsa_circ_0015286 expression in GC tissues and plasma samples (**Figure 2F**).

The Diagnostic Performance of Plasma Exosomal hsa_circ_0015286 in Gastric Cancer Patients

The potential diagnostic value of plasma exosomal hsa_circ_0015286 was evaluated through ROC curve, compared with the traditional tumor marker CEA and CA19-9. As shown in **Figure 3** A, B and C, the AUC value of exosomal hsa_circ_0015286 was 0.778 (CI = 0.699–0.857, $p < 0.001$), which was better than serum CEA (AUC = 0.673, CI = 0.583–0.763, $p < 0.01$) and CA 19–9 (AUC = 0.677, CI = 0.556–0.738, $p < 0.01$). At the optimal cut-off value, the sensitivity and specificity were 0.821 and 0.657, respectively. What is more, the AUC value was up to 0.833 (CI = 0.762–0.904, $p < 0.001$) when combined with CEA and CA 19–9, which was better than that of pairwise combination (**Figures 3D,E**). These results showed that exosomal hsa_circ_0015286 may serve as an effective diagnostic marker for GC.

Dynamic Monitoring and Potential Prognostic Value of Plasma Exosomal hsa_circ_0015286 in Gastric Cancer Patients

To further investigate whether the expression levels of circulating hsa_circ_0015286 are associated with tumor burden, we compared the difference of exosomal hsa_circ_0015286 levels in 20 GC patients' plasma before and after operation. As observed, the expression levels of exosomal hsa_circ_0015286 were remarkably downregulated 10 days post-surgery ($p < 0.01$, **Figure 4A**).

In addition, sixty GC patients were divided into high and low group based on the plasma expression levels of exosomal hsa_circ_0015286. Interestingly, the overall survival of GC patients in low expression group were longer than the high expression group ($p < 0.01$, **Figure 4B**). These results provided

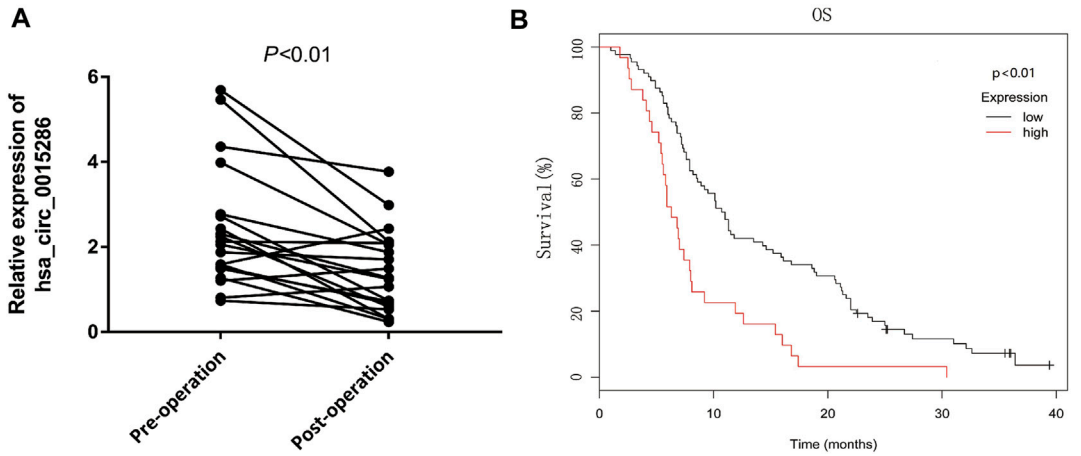

FIGURE 4 | Dynamic monitoring and potential prognostic value of plasma exosomal hsa_circ_0015286 in GC patients. **(A)**: Hsa_circ_0015286 expression levels in 20 paired GC patients before and after surgery; **(B)**: Kaplan-Meier survival curves for clinical outcomes of GC patients with different level of exosomal hsa_circ_0015286.

TABLE 1 | The relationship of plasma exosomal hsa_circ_0015286 expression levels and clinicopathologic features of GC patients.

Characteristics	Number	Mean ± SD	*p* value
Gender			0.286
Male	32	3.24 ± 1.23	
Female	28	2.92 ± 1.05	
Age, years			0.159
<60	23	3.07 ± 1.85	
≥60	37	3.72 ± 1.63	
Tumor size, cm			<0.001*
<5	31	1.76 ± 0.68	
≥5	29	4.19 ± 1.59	
Differentiation			0.247
Poor + Moderate	40	2.88 ± 1.71	
Well	20	3.45 ± 1.92	
T stage			<0.001*
T1+T2	27	2.57 ± 0.96	
T3+T4	33	3.93 ± 1.42	
Lymph node metastasis			<0.001*
No	34	2.05 ± 1.14	
Yes	26	4.36 ± 1.55	
CEA, ng/ml			0.603
<5	35	3.04 ± 1.63	
≥5	25	3.25 ± 1.39	
CA19-9, U/ml			0.162
<35	38	2.79 ± 1.48	
≥35	22	3.37 ± 1.61	

**Indicate significance at* p < *0.05.*
CEA, carcinoembryonic antigen; CA19-9, Carbohydrate antigen19-9.

evidence that exosomal hsa_circ_0015286 may be used for dynamic monitoring and prognosis prediction.

Correlation of Exosomal hsa_circ_0015286 With Clinicopathological Characteristics

The relationship of exosomal hsa_circ_0015286 expression levels with clinicopathological parameters of GC patients was summarized. As shown in **Table 1**, the expression levels of plasma exosomal hsa_circ_0015286 were closely related with tumor size ($p < 0.001$), T stage ($p < 0.001$) and lymph node metastasis ($p < 0.001$). Nevertheless, there was no correlation between its levels with age, gender, differentiation, CEA and CA19-9.

DISCUSSION

Early screening and diagnosis are pivotal to improve the 5-year survival rates of GC patients. However, traditional serum tumor biomarkers, such as CEA, CA 19–9, and CA 72–4, exhibit low sensitivity and specificity in GC diagnosis [13]. Meanwhile endoscopy detection, the gold standard for GC diagnosis, is invasive and uncomfortable for patients [14, 15]. As an important technique of liquid biopsy, accumulating evidence has demonstrated that tumor-specific proteins and RNA in exosomes exhibit an enormous potential in cancer diagnosis and prognosis judgment. Importantly, exosome detection has multiple advantages including non-invasiveness, convenient, rapid and higher sensitivity [16-19].

Li et al. first reported the existence and enrichment of circRNAs within cancer-derived exosomes *via* RNA-seq analysis [8, 9]. Moreover, previous studies showed that circRNAs are easy to be enriched in exosomes compared with linear RNA, and cancer-specific circRNAs can be transferred into the peripheral circulation *via* exosomes. Thus, the test of exosomal circRNA in peripheral blood as new biomarker may be feasible for tumor diagnosis [20, 21]. In this study, firstly cancer-specific exosomal circRNAs were identified by circRNA microarray assay. Next hsa_circ_0015286 was found that remarkably upregulated in GC tissue, plasma and cancer cells compared with normal controls. More importantly, a significant positive correlation was observed between its expression in GC tissues and plasma samples, which implying the preferable diagnostic and prognostic value for GC patients. ROC curve analysis demonstrated that exosomal hsa_circ_0015286 could be

used as an independent biomarker for GC diagnosis or combined with CEA and CA19-9 to improve the diagnostic efficacy. Similar to our results, several aberrant expressions of exosomal circRNAs have been found and represent potential biomarkers and therapeutic targets in various types of cancer, including GC [22-24]. For instance, researchers found that hsa_circ_0065149 and hsa_circ_0000419 were remarkably decreased in plasma exosomes and tissues of GC patients, showing better performence for early GC diagnosis than conventional tumor biomarkers [25, 26]. In addition, circ-KIAA1244 released from GC tissues derived exosomes could serve as novel circulating biomarker for GC screening [27]. Of course, most of these reports including ours are preliminary and exploratory, more clinical studies are required to validate the diagnostic performance in future.

Besides the diagnostic application, the abnormal expression of circulating exosomal circRNAs have been proved to be associated with the clinicopathological characteristics of patients. For example, circ-IARS was reported highly expressed in serum exosomes of patients with metastatic pancreatic cancer and was associated with TNM stage, liver metastasis and tumor vascular invasion [28]. The higher expression of exosomal circ-RanGAP1 in GC was significantly related to lymph node metastasis, TNM stage, and poor survival [29]. In addition, exosomal circFECR1 was also found upregulated in serum of small cell lung cancer (SCLC) patients, its expression can reflect the clinical reaction to chemotherapy and prognostic evaluation [30]. Our findings demonstrated that the upregulation of exosomal hsa_circ_0015286 was also positively associated with tumor size, T stage and lymph node metastasis. Moreover, the expression level of exosomal hsa_circ_0015286 dramatically reduced 10 days post-surgery. The overall survival of patients with low hsa_circ_0015286 expression was longer than those with high expression in Kaplan-Meier survival plot analysis. These indicate that exosomal hsa_circ_0015286 might be a useful prognostic biomarker and involve in the progression of GC. Next, it is necessary to carry out large-scale clinical verification, long-term follow-up and functional analysis to further confirm our conclusions.

In summary, our study indicates that exosomal hsa_circ_0015286 is highly expressed in GC patients and might be a promising noninvasive biomarker for the diagnosis and prognosis evaluation of GC.

DATA AVAILABILITY STATEMENT

The raw data supporting the conclusion of this article will be made available by the authors, without undue reservation.

ETHICS STATEMENT

The studies involving human participants were reviewed and approved by the Institutional Ethics Committee of the First Affiliated Hospital of Henan University. The patients/participants provided their written informed consent to participate in this study.

AUTHOR CONTRIBUTIONS

PZ, HG, and XX conceived and designed the study. PZ and HG did the main experiments, interpreted the data, and drafted the article. XX and PL did parts of the experiments and data analysis. PZ revised the article critically. All authors read and approved the final manuscript.

FUNDING

This work was supported by the National Natural Science Foundation of China (81802094) and the Key Project of Medical Science and Technology of Henan Province (LHGJ20200542, LHGJ20210017).

CONFLICT OF INTEREST

The authors declare that the research was conducted in the absence of any commercial or financial relationships that could be construed as a potential conflict of interest.

SUPPLEMENTARY MATERIAL

The Supplementary Material for this article can be found online at: https://www.por-journal.com/articles/10.3389/pore.2022.1610446/full#supplementary-material

REFERENCES

1. Sung H, Ferlay J, Siegel RL, Laversanne M, Soerjomataram I, Jemal A, et al. Global Cancer Statistics 2020: GLOBOCAN Estimates of Incidence and Mortality Worldwide for 36 Cancers in 185 Countries. *CA A Cancer J Clin* (2021) 71:209–49. doi:10.3322/caac.21660
2. Chen W, Zheng R, Baade PD, Zhang S, Zeng H, Bray F, et al. Cancer Statistics in China, 2015. *CA: A Cancer J Clinicians* (2016) 66:115–32. doi:10.3322/caac.21338
3. Smyth EC, Nilsson M, Grabsch HI, van Grieken NC, Lordick F. Gastric Cancer. *The Lancet* (2020) 396:635–48. doi:10.1016/s0140-6736(20)31288-5
4. Kalluri R, LeBleu VS. *The Biology, Function, and Biomedical Applications of Exosomes*. New York, N.Y.: Science (2020). p. 367.
5. Tkach M, Théry C. Communication by Extracellular Vesicles: Where We Are and where We Need to Go. *Cell* (2016) 164:1226–32. doi:10.1016/j.cell.2016.01.043
6. Ruivo CF, Adem B, Silva M, Melo SA. The Biology of Cancer Exosomes: Insights and New Perspectives. *Cancer Res* (2017) 77:6480–8. doi:10.1158/0008-5472.can-17-0994
7. Möhrmann L, Huang HJ, Hong DS, Tsimberidou AM, Fu S, Piha-Paul SA, et al. Liquid Biopsies Using Plasma Exosomal Nucleic Acids and Plasma Cell-free DNA Compared with Clinical Outcomes of Patients with Advanced Cancers. *Clin Cancer Res* (2018) 24:181–8. doi:10.1158/1078-0432.ccr-17-2007

8. Chen B, Huang S. Circular RNA: An Emerging Non-coding RNA as a Regulator and Biomarker in Cancer. *Cancer Lett* (2018) 418:41–50. doi:10.1016/j.canlet.2018.01.011
9. Li Y, Zheng Q, Bao C, Li S, Guo W, Zhao J, et al. Circular RNA Is Enriched and Stable in Exosomes: a Promising Biomarker for Cancer Diagnosis. *Cell Res* (2015) 25:981–4. doi:10.1038/cr.2015.82
10. Wang M, Yu F, Li P, Wang K. Emerging Function and Clinical Significance of Exosomal circRNAs in Cancer. *Mol Ther - Nucleic Acids* (2020) 21:367–83. doi:10.1016/j.omtn.2020.06.008
11. Wang S, Dong Y, Gong A, Kong H, Gao J, Hao X, et al. Exosomal circRNAs as Novel Cancer Biomarkers: Challenges and Opportunities. *Int J Biol Sci* (2021) 17:562–73. doi:10.7150/ijbs.48782
12. Zheng P, Zhang H, Gao H, Sun J, Li J, Zhang X, et al. Plasma Exosomal Long Noncoding RNA Lnc-Slc2a12-10:1 as a Novel Diagnostic Biomarker for Gastric Cancer. *Ott* (2020) 13:4009–18. doi:10.2147/ott.s253600
13. Shimada H, Noie T, Ohashi M, Oba K, Takahashi Y. Clinical Significance of Serum Tumor Markers for Gastric Cancer: a Systematic Review of Literature by the Task Force of the Japanese Gastric Cancer Association. *Gastric Cancer* (2014) 17:26–33. doi:10.1007/s10120-013-0259-5
14. Sawaki K, Kanda M, Kodera Y. Review of Recent Efforts to Discover Biomarkers for Early Detection, Monitoring, Prognosis, and Prediction of Treatment Responses of Patients with Gastric Cancer. *Expert Rev Gastroenterol Hepatol* (2018) 12:657–70. doi:10.1080/17474124.2018.1489233
15. Eusebi LH, Telese A, Marasco G, Bazzoli F, Zagari RM. Gastric Cancer Prevention Strategies: A Global Perspective. *J Gastroenterol Hepatol* (2020) 35:1495–502. doi:10.1111/jgh.15037
16. Siravegna G, Marsoni S, Siena S, Bardelli A. Integrating Liquid Biopsies into the Management of Cancer. *Nat Rev Clin Oncol* (2017) 14:531–48. doi:10.1038/nrclinonc.2017.14
17. Sorber L, Zwaenepoel K, Deschoolmeester V, Van Schil PEY, Van Meerbeeck J, Lardon F, et al. Circulating Cell-free Nucleic Acids and Platelets as a Liquid Biopsy in the Provision of Personalized Therapy for Lung Cancer Patients. *Lung Cancer* (2017) 107:100–7. doi:10.1016/j.lungcan.2016.04.026
18. Kalluri R. The Biology and Function of Exosomes in Cancer. *J Clin Invest* (2016) 126:1208–15. doi:10.1172/jci81135
19. Jiang L, Gu Y, Du Y, Liu J. Exosomes: Diagnostic Biomarkers and Therapeutic Delivery Vehicles for Cancer. *Mol Pharmaceutics* (2019) 16:3333–49. doi:10.1021/acs.molpharmaceut.9b00409
20. Lasda E, Parker R. Circular RNAs Co-precipitate with Extracellular Vesicles: A Possible Mechanism for circRNA Clearance. *PloS one* (2016) 11:e0148407. doi:10.1371/journal.pone.0148407
21. Bai H, Lei K, Huang F, Jiang Z, Zhou X. Exo-circRNAs: a New Paradigm for Anticancer Therapy. *Mol Cancer* (2019) 18:56. doi:10.1186/s12943-019-0986-2
22. Zhang H, Zhu L, Bai M, Liu Y, Zhan Y, Deng T, et al. Exosomal circRNA Derived from Gastric Tumor Promotes white Adipose browning by Targeting the miR-133/PRDM16 Pathway. *Int J Cancer* (2019) 144:2501–15. doi:10.1002/ijc.31977
23. Chen W, Quan Y, Fan S, Wang H, Liang J, Huang L, et al. Exosome-transmitted Circular RNA Hsa_circ_0051443 Suppresses Hepatocellular Carcinoma Progression. *Cancer Lett* (2020) 475:119–28. doi:10.1016/j.canlet.2020.01.022
24. Li T, Sun X, Chen L. Exosome Circ_0044516 Promotes Prostate Cancer Cell Proliferation and Metastasis as a Potential Biomarker. *J Cel Biochem* (2020) 121:2118–26. doi:10.1002/jcb.28239
25. Shao Y, Tao X, Lu R, Zhang H, Ge J, Xiao B, et al. Hsa_circ_0065149 Is an Indicator for Early Gastric Cancer Screening and Prognosis Prediction. *Pathol Oncol Res* (2020) 26:1475–82. doi:10.1007/s12253-019-00716-y
26. Tao X, Shao Y, Lu R, Ye Q, Xiao B, Ye G, et al. Clinical Significance of Hsa_circ_0000419 in Gastric Cancer Screening and Prognosis Estimation. *Pathol - Res Pract* (2020) 216:152763. doi:10.1016/j.prp.2019.152763
27. Tang W, Fu K, Sun H, Rong D, Wang H, Cao H. CircRNA Microarray Profiling Identifies a Novel Circulating Biomarker for Detection of Gastric Cancer. *Mol Cancer* (2018) 17:137. doi:10.1186/s12943-018-0888-8
28. Li J, Li Z, Jiang P, Peng M, Zhang X, Chen K, et al. Circular RNA IARS (Circ-IARS) Secreted by Pancreatic Cancer Cells and Located within Exosomes Regulates Endothelial Monolayer Permeability to Promote Tumor Metastasis. *J Exp Clin Cancer Res* (2018) 37:177. doi:10.1186/s13046-018-0822-3
29. Lu J, Wang Y-h., Yoon C, Huang X-y., Xu Y, Xie J-w., et al. Circular RNA Circ-RanGAP1 Regulates VEGFA Expression by Targeting miR-877-3p to Facilitate Gastric Cancer Invasion and Metastasis. *Cancer Lett* (2020) 471:38–48. doi:10.1016/j.canlet.2019.11.038
30. Li L, Li W, Chen N, Zhao H, Xu G, Zhao Y, et al. FLI1 Exonic Circular RNAs as a Novel Oncogenic Driver to Promote Tumor Metastasis in Small Cell Lung Cancer. *Clin Cancer Res* (2019) 25:1302–17. doi:10.1158/1078-0432.ccr-18-1447

Pathology & Oncology Research

frontiers

BRIEF RESEARCH REPORT
published: 05 April 2022
doi: 10.3389/pore.2022.1610096

Co-Detection of VEGF-A and Its Regulator, microRNA-181a, May Indicate Central Nervous System Involvement in Pediatric Leukemia

*Bálint Egyed[1,2,3], Anna Horváth[2], Ágnes F. Semsei[2], Csaba Szalai[2], Judit Müller[1], Dániel J. Erdélyi[1] and Gábor T. Kovács[1]**

[1]Hematology Unit, 2nd Department of Pediatrics, Semmelweis University, Budapest, Hungary, [2]Clinical Genomics Research Group, Department of Genetics, Cell- and Immunobiology, Semmelweis University, Budapest, Hungary, [3]HCEMM-SE Molecular Oncohematology Research Group, 1st Department of Pathology and Experimental Cancer Research, Semmelweis University, Budapest, Hungary

Central nervous system (CNS) involvement is a leading cause of therapy-refractory pediatric acute lymphoblastic leukemia (pALL), which is aggravated by underdiagnosing CNS disease with the currently used cell-based approach of cerebrospinal fluid (CSF) diagnostics. Our study focused on developing novel subcellular CNS leukemia indicators in the CSF and the bone marrow (BM) of patients with pALL. Serial liquid biopsy samples (n = 65) were analyzed by Elisas to measure the level of essential proteins associated with blast cell CNS trafficking, vascular endothelial growth factor A (VEGF-A) and integrin alpha 6 (ITGA6). In CSF samples from early induction chemotherapy, VEGF-A concentration were uniformly elevated in the CNS-positive group compared to those patients without unambiguous meningeal infiltration (9 vs Nine patients, Δc = 17.2 pg/ml, p = 0.016). Expression of miR-181a, a *VEGFA*-regulating microRNA which showed increased level in CNS leukemia in our previous experiments, was then paralleled with VEGF-A concentration. A slight correlation between the levels of miR-181a and VEGF-A indicators in CSF and BM samples was revealed (n = 46, Pearson's r = 0.36, p = 0.015). After validating in international cohorts, the joint quantification of miR-181a and VEGF-A might provide a novel tool to precisely diagnose CNS involvement and adjust CNS-directed therapy in pALL.

Keywords: cerebrospinal fluid, biomarkers, liquid biopsy, central nervous system involvement, pediatric leukemia, enzyme-linked immunosorbent assay

OPEN ACCESS

Edited by:
József Tímár,
Semmelweis University, Hungary

****Correspondence:***
Gábor T. Kovács
kovacs.gabor1@med.semmelweis-univ.hu

Received: *25 September 2021*
Accepted: *15 March 2022*
Published: *05 April 2022*

Citation:
Egyed B, Horváth A, Semsei ÁF, Szalai C, Müller J, Erdélyi DJ and Kovács GT (2022) Co-Detection of VEGF-A and Its Regulator, microRNA-181a, May Indicate Central Nervous System Involvement in Pediatric Leukemia. Pathol. Oncol. Res. 28:1610096. doi: 10.3389/pore.2022.1610096

INTRODUCTION

Pediatric acute lymphoblastic leukemia (ALL) is still the leading cause of cancer-related long-term disability influencing the quality of life not only in childhood but also in adulthood [1]. In ALL, a major clinical concern is to overcome central nervous system (CNS) infiltration which highly predisposes the patient to relapse with dismal prognosis [2]. Even then, we lack sensitive methods for diagnosing and monitoring CNS ALL as contemporary routine cytomorphology/cytometry/cytospin analysis of the cerebrospinal fluid (CSF) produce >40% false-negative reports. Risk-adapted CNS-directed therapy (intrathecal and intravenous chemotherapy plus craniospinal irradiation) is a considerable determinant of leukemia-free survival, even in patients without a detectable initial CNS

manifestation [3]. However, possible neurotoxic side effects of CNS-directed treatment, such as neurocognitive impairment or secondary brain tumor, limit therapy intensification opportunities. Finding the individualized balance of CNS-targeted therapy in order to reduce both toxic events and relapse rates is a clinical challenge. A gold standard method for CNS leukemia staging, which can identify and monitor occult, subclinical meningeal involvement as well, need to be urgently developed.

Previous studies suggest that subcellular biomarkers in the CSF may help to identify undiagnosed CNS leukemia cases. Earlier, more than 30 humoral factors and a set of molecular markers have been tested in the CSF, although, most of these candidate markers were proved not to be eligible for diagnostics in real clinical cohorts [4]. Recently, information gained by the thorough examination of molecular mechanisms and pathobiology of blast cell trafficking to the CNS compartment in mouse models open new perspectives, and refers to the central role of vascular endothelial growth factor A (VEGF-A) and integrin alpha 6 (ITGA6) proteins in neural invasion [5,6]. Independently, our group found markedly elevated level of microRNA-181a (miR-181a), a leukemia-related miR, in CSF samples of patients with CNS infiltration [7]. While the relationship between miR-181a and ITGA6 is only a possibility which is proposed by integrative miR target predictor databases, direct data suggest the regulative effect of miR-181a on VEGF-A level [8].

To establish a clinical diagnostics study on CNS leukemia with state-of-the-art candidate subcellular biomarkers, we analyzed serial liquid biopsies from the CNS and bone marrow (BM) niches in children with ALL by measuring VEGF-A and ITGA6 concentrations and correlating these data with miR-181a expressions.

METHODS

Patient Cohort and Samples

The study is based on patients (aged ≤ 18 years) diagnosed with ALL in two Hungarian pediatric hematology centers (Semmelweis University second Department of Pediatrics and Heim Pal National Pediatric Institute). We collected CSF and BM of patients at diagnosis and at day 15 of the induction cycle of the ALL IC-BFM 2009 trial protocol, between October 2015 and August 2019. Consecutive lumbar punctures are the standard of care for evaluating leukemic CNS involvement depending on cytomorphology of the CSF. In the treating centers mentioned above, CSF samples were analyzed by cell counting chamber and cytospin preparate to assess the initial CNS status of the patient (examination results are available in **Supplementary File S1**). Within 2 h of sampling, preparation platelet-free plasma (PFP) from BM samples were carried out by centrifugation at 2500 *g* for 15 min two times, while cell- and debris-free CSF samples were gained after centrifugation at 300 g for 10 min. Processed BM PFP and CSF samples were then stored at −80°C. In our study, we examined CNS-positive (CNS^+, i.e. unambiguously identified blasts by cytological techniques) ALL (n = 9) and matched CNS-negative (CNS^-, i.e. blast-free by cytological methods) patients (n = 9) based on sex, age at the diagnosis and immunophenotype. In addition, patients (n = 6) diagnosed with spinal muscular atrophy (SMA) were selected as CSF reference samples of non-cancerous origin. Further information about the patient cohort is available in **Table 1** and **Supplementary File S1**.

TABLE 1 | Baseline population characteristics according to central nervous system status.

	CNS^+ group	CNS^- group
Cases, *n*	9	9
Average age, *yr* (range)	6.9 (0.7–18.9)	10.7 (2.7–17.8)
Males, %	67	44
Disease progression state, *n*		
De novo ALL	7	8
Relapsed ALL	2	1
Immunophenotype, *n*		
Pre-B cell	4	1
Common (precursor B-cell)	3	6
Pre-T cell	1	1
Medullary T-cell	1	0
Mature T-cell	0	1
Sample type and sampling day, *n*		
CSF, day 0	8	9
CSF, day 15	8	8
BM PFP, day 0	7	9
BM PFP, day 15	7	9

CNS, central nervous system; ALL, acute lymphoblastic leukemia; CSF, cerebrospinal fluid; BM, bone marrow; PFP, platelet-free plasma.

Protein Concentration Measurements

ELISA was used for quantitative detection of VEGF-A (VEGF-A Human ELISA Kit, Thermo Fisher Scientific, Waltham, MA, United States) and ITGA6 (Human ITGa6 ELISA Kit, Biorbyt, St. Louis, MO, United States) in accordance with the manufacturer's guidelines. Due to the fact that we expected low protein concentrations, we transferred 75 µl of the samples to each well instead of the recommended 50 µl to assure a significant absorbance when performing the VEGF-A assay. The ITGA6 measurement was performed according to the manufacturer's instructions, with a volume of 100 µl per sample. Both ELISA kits contained standard samples which were serially diluted to generate a calibration curve. ELISA reactions were processed on pre-coated plates and spectrophotometry was applied to read the final optical density values.

Determination of microRNA-181a (miR-181a) Expression

In our previous study, we aimed to detect and quantify miR-181a levels in BM PFP and CSF samples of the same patient cohort [7]. After separating and pre-processing the miR fraction as detailed earlier [7], TaqMan Advanced miRNA Assays and TaqMan Fast Advanced Master Mix (Thermo Fisher Scientific, Waltham, MA, United States) were used to perform qPCR reactions. Measurements were carried out

TABLE 2 | Vascular endothelial growth factor A (VEGF-A) and microRNA-181a (miR-181a) concentrations measured in different sample types of patients with and without CNS leukemia.

	CNS positive group			CNS negative group		
VEGF-A	**c (pg/ml)**	**Avg. Δc (pg/ml)[a]**	***p* value[a]**	**c (pg/ml)**	**Avg. Δc (pg/ml)[a]**	***p* value[a]**
BM PFP d0	131.2 ± 43.4	—	—	130.6 ± 22.7	—	—
BM PFP d15	179.7 ± 93.0	—	—	145.6 ± 30.1	—	—
CSF d0	44.4 ± 4.0	47.9	0.030	24.8 ± 1.8	90.14	<0.001
CSF d15	45.2 ± 3.3	61.4	0.011	31.7 ± 3.7	86.7	0.001
miR-181a	**FC**	**Avg. ΔFC[a]**	***p* value[a]**	**FC**	**Avg. ΔFC[a]**	***p* value[a]**
BM PFP d0	34.8 ± 13.1	—	—	32.9 ± 13.2	—	—
BM PFP d15	1.5 ± 1.1	—	—	0.5 ± 0.1	—	—
CSF d0	14.9 ± 5.5	25.99	0.141	1.6 ± 0.8	33.1	0.018
CSF d15	3.1 ± 1.3	TLN	TLN	0.2 ± 0.2	TLN	TLN

Concentration and fold change data are displayed as mean ± standard error of the mean. CNS, central nervous system; BM, bone marrow; CSF, cerebrospinal fluid; PFP, platelet-free plasma; FC, fold change; Avg., average; TLN, too low number of patients to statistically analyze.

[a]In-patient VEGF-A concentration and miR-181a expression fold change differences between CSF and BM PFP samples (c_{BM}–c_{CSF} and FC_{BM}–FC_{CSF}, respectively) were averaged. p values were calculated by linear regression to compare CSF and BM PFP VEGF-A levels and miR-181a expressions.

on the 7900HT Fast Real-Time PCR System (Thermo Fisher Scientific, Waltham, MA, United States). Comparative cycle threshold algorithm was applied to estimate normalized miR-181a expression, in which non-leukemic SMA samples were used as reference specimen.

Statistical Analysis

All statistical analyses were performed using R version 4.0.3 (R Foundation for Statistical Computing, Vienna, Austria). In order to determine the concentration of the analyte within a sample, we used the non-linear 4-Parameter Logistic (4 PL) curve model. We fit the data obtained for the standard samples to the 4 PL curve by Levenberg-Marquardt algorithm (drc package). Concentration estimates were calculated as the natural logarithm of VEGF-A or ITGA6 absolute levels for each sample. Linear regression models were used to assess the statistical significance between each subgroup, where gender, age at diagnosis and ALL immunophenotype were considered as cofactors. The correlations between the expression level of miR-181a and the estimate of concentration was compared using Pearson's method and Student's t-test. Alpha level of 0.05 was used as criterion for statistical significance after false discovery rate correction, where it was relevant.

RESULTS

Patient Characteristics

ELISA measurements were performed on 33 CSF and 32 BM PFP samples collected from 18 children with ALL and on CSF reference samples from six SMA patients. The baseline characteristics for this cohort is described in **Table 1**. Briefly, the median age was 6.4, more than three-quarter of patients had precursor B-cell immunophenotype, and various genetic subgroups were involved (normal karyotype, hyperdiploid, high hyperdiploid, *KMT2A*-rearranged, *P2RY8-CRLF2* translocated, *CDKN2A* deleted and *ETV6* deleted).

Soluble VEGF-A and ITGA6 Levels in CSF and BM Samples of Children With ALL

To evaluate the VEGF-A and ITGA6 content of cell-free CSF and platelet-free BM plasma samples from both CNS^+ and CNS^- patients, two commercial ELISA tests were used. Due to the paucity of cell-derived material in CSF compared to other body fluids, we questioned whether these proteins can be detected in CSF supernatant. VEGF-A was measurable in all CSF samples in the CNS^+ as well as the CNS^- group, as seen in **Table 2**. However, the concentrations were markedly lower in the CSF relative to the

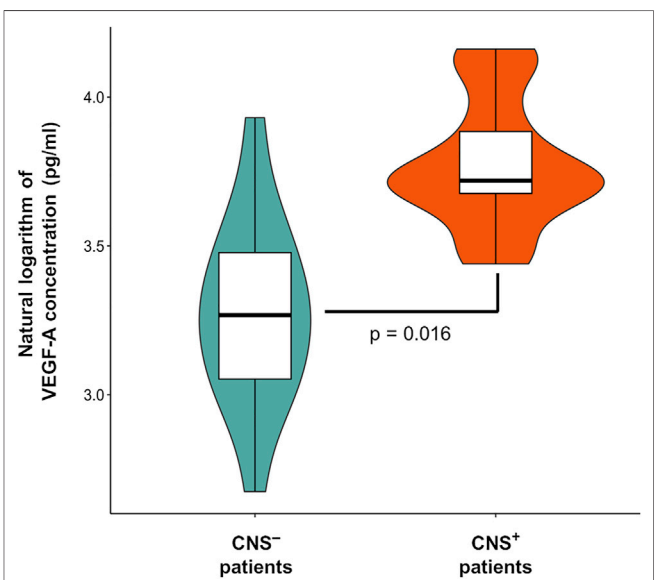

FIGURE 1 | Vascular endothelial growth factor A (VEGF-A) levels in the cerebrospinal fluid according to central nervous system (CNS) status in pediatric acute lymphoblastic leukemia. Violin plot describes the distribution of VEGF-A data. Box plot's box indicates mean ± SD, whiskers are means ± 3 SD.

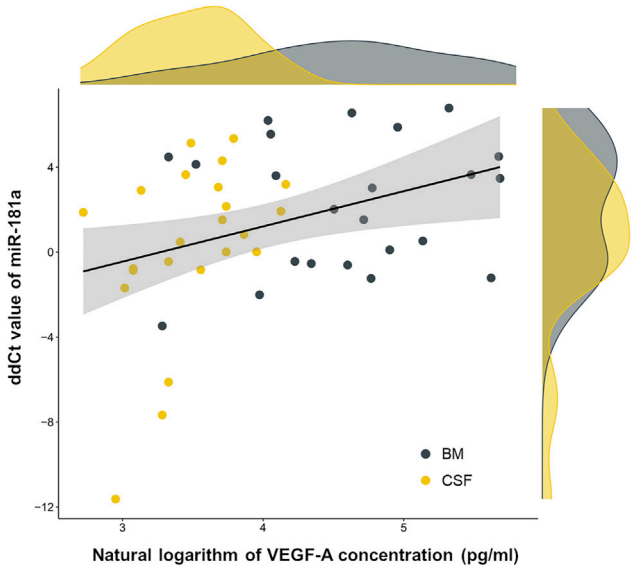

FIGURE 2 | Co-detection of two possible subcellular central nervous system leukemia indicators, microRNA-181a and vascular endothelial growth factor A (VEGF-A). Linear correlation (black line) was fitted on dots representing patient samples. Marginal density plots describe sample distributions. Yellow color represents cerebrospinal fluid (CSF) samples, grey color marks bone marrow (BM) platelet-free plasma samples. Abbreviation: miR, microRNA.

BM PFP, independent of CNS status (for detailed description, *see* **Table 2**). This CSF–BM gap in VEGF-A concentration was almost 2-fold greater in the CNS^- patients compared to the CNS^+ group. As opposed to these results, ITGA6 was not detectable in our CSF or BM samples using this method.

VEGF-A concentration estimates (natural logarithm values) were uniformly elevated in the CNS^+ ALL group compared to CNS^- patients when analyzing CSF samples from day 0 and day 15 of the induction chemotherapy ($\Delta c = 17.15$ pg/ml, $p = 0.016$). This means a mildly more than 1.5-fold difference in concentrations between the two subgroups (mean value in CNS^+ vs CNS^- patients: 43.61 vs 26.45 pg/ml), as seen in **Figure 1**. Gender, age at diagnosis and ALL immunophenotype were not significant contributors in the regression model. In this limited CNS^+ cohort, we were not able to demonstrate a change in VEGF-A level between d0 (rich in blasts) and d15 (paucity of blast cells) CSF samples. However, change in BM VEGF-A levels from d0 to d15 was not proportional to flow cytometry-based BM residual disease dynamics (**Supplementary File S1**), so the linear correlation between VEGF-A concentration and ALL cell burden remains unproven.

Correlation of VEGF-A Level and miR-181a Expression in Liquid Biopsy Samples From Leukemia Niches

After the identification of VEGF-A concentration gap between CSF samples of CNS^+ and CNS^- ALL patients, we addressed whether VEGF-A levels correlates with a previously proposed marker of CNS leukemia, miR-181a. Relative miR-181a expressions in the same patient cohort were determined by delta-delta cycle threshold (ddCt) algorithm as we previously published [7]. As of interest, miR-181a and VEGF-A indicators–i.e. ddCt value and natural logarithm of the concentration, respectively–in CSF and BM PFP samples from day 0 and day 15 of the treatment showed a slight correlation ($n = 46$, Pearson's $r = 0.36$, $p = 0.015$), as displayed in **Figure 2**.

DISCUSSION

As the identification and follow-up of pediatric ALL manifestation in the CNS compartment present difficulties in current clinical practice, sensitive and easy-to-measure novel markers are needed to develop. Our study proposes a subcellular approach of CNS leukemia diagnostics. We measured VEGF-A and ITGA6 concentrations in CSF samples of children with CNS^+ and CNS^- ALL defined based on cytomorphologic examinations. The CSF level of VEGF-A was significantly elevated in patients with meningeal disease compared to those without CNS involvement. The role of VEGF-A was previously investigated in preclinical models of CNS leukemia. Münch et al showed that patient derived ALL cells transplanted onto mice invaded the CNS niche by transmigrating through microvascular endothelial cells facilitated by VEGF-A signaling [5]. Similar mouse models were used in a report by Kato et al depicting the hypoxia-responsive gene *VEGFA* upregulation in the nutrient-poor CNS microenvironment [9]. However, clinical data are insufficient to draw conclusions regarding the CNS leukemia indicator role of VEGF-A. RNA sequencing of primary leukemic cells isolated from the cerebrospinal fluid of a small children cohort with CNS involvement revealed markedly elevated *VEGFA* expression in these cells [9], but CNS^- samples were not analyzed parallelly. In a study with pediatric and adult acute leukemia patients, levels of soluble VEGF-A receptors and their ratio to VEGF-A concentration in CSF and serum were proposed as a prognostic marker of leukemia and a contributor of CNS involvement evolution [10]. Nevertheless, our study provides the first description of the significance of VEGF-A ELISA measurements in leukemic CSF samples in CNS leukemia identification.

Our VEGF-A concentration results in BM PFP samples showed no difference between day 0 and day 15 of the treatment (**Table 1**), however, BM measurable residual disease uniformly decreased to the 15th day of chemotherapy (**Supplementary File S1**). This suggest that VEGF-A level is not an indicator of BM leukemic burden, while we propose CSF VEGF-A concentration as a marker of ALL expansion in the CNS compartment. This seemingly contradictory situation can be resolved by the above cited evidences claiming that VEGF-A production in ALL cells is predominantly evoked by the hypoxic environment, e.g. in the CSF niche. If we consider that higher initial CSF VEGF-A level may indicate a biological subtype of ALL with high risk for permanent meningeal blast deposits (and not circulating leukemic burden in the CSF), later relapses could

be expected and fueled by these dormant CNS clones. A long-term follow up of our patients for late BM and/or CNS relapses would be beneficial to analyze this question. Case reports confirming the clonal role of hidden, long-surviving CNS blasts behind later relapses in any of the main leukemic body compartments are available [11].

The positive correlation between VEGF-A level and regulatory RNA miR-181a expression in BM PFP and CSF samples of childhood ALL cases was also observed. MiR-181a seemed to be a sensitive subcellular marker of CNS disease in our previous study [7]. There is potential evidence explaining the relationship of miR-181a and VEGF-A in cancer. In human chondrosarcoma cell lines, miR-181a transfection raised the expression of VEGF messenger RNA and increased secreted VEGF protein quantity [12]. An in-depth study on how VEGF signaling is promoted by miR-181a in preclinical models of colorectal cancer identified SRC kinase signaling inhibitor 1 (SRCIN1), an angiogenesis suppressor, as a key target of miR-181a [8]. Studies investigating whether these mechanisms work in ALL as well are lacking. Interestingly, we did not see intra-patient reduction in BM or CSF VEGF-A concentrations to the 15th day of chemotherapy, while miR-181a levels significantly decreased in both body compartments in both CNS^+ and CNS^- groups [7]. If we suspect a direct miR-181a–VEGF-A regulatory relationship, a fall in VEGF-A levels would be expected as well. However, generally, miR expression level does not necessarily correlate with the target mRNA–protein levels since mRNA expression and protein translation may be regulated in several different molecular ways. Our data (**Figure 2**) show the same situation regarding the correlation of miR-181a expression and VEGF-A concentration as there was no straightforward reciprocity in the regulatory miR and protein levels. A hypothesis can be that miR-181a, an early marker of initial CNS leukemia burden, is produced when blasts recognize the nutrient-poor, hypoxic CSF microenvironment, and the consecutive increased excretion of VEGF-A is a prolonged phenomenon indicating persistent subclinical meningeal manifestation, but this approach definitely needs further and deeper investigation.

ITGA6 was not measurable in cell-free ALL samples by the ELISA method we used. ITGA6-expressing blasts are actively engaged in adhesion and migration on the abluminal side of vessels to the CNS as multiple studies suggest [6,13]. The absence of ITGA6 in BM and CSF supernatants gained by cell removal in our study claims that this cell surface protein of blast cells may not be likely to be involved in integrin shedding or such process allocating ITGA6 into the extracellular space. Previously, high ITGA6 expressions were measured inside the CNS-invading leukemic cells [14].

In summary, our data represents the first clinical observation of VEGF-A based CNS status evaluation and the identification of VEGF-A and miR-181a co-expression in ALL. However, several limitations should be considered when interpreting our results. The rarity of CNS involvement in childhood leukemia resulted in low patient numbers. Another bias is the selection of patients without CNS disease, which relied on insensitive conventional diagnostics and carries the risk of involving patients with occult CNS involvement in the CNS^- group. Yet, this study provides the rationale for future studies of subcellular elements, soluble proteins and miRs, in the diagnostics of CNS leukemia.

DATA AVAILABILITY STATEMENT

The original contributions presented in the study are included in the article, further inquiries can be directed to the corresponding author.

ETHICS STATEMENT

All procedures performed in this study, involving human participants were in accordance with the ethical standards of the Medical Research Council of Hungary and with the 1964 Helsinki declaration and its later amendments. The study was approved by the central ethical committee (institute: ETT-TUKEB; approval numbers: 60106-1/2015/EKU and 6886/2019/EKU). The study is compliant with all relevant ethical regulations for human research participants, and informed consent was obtained from all patients or legal guardians.

AUTHOR CONTRIBUTIONS

BE coordinated the sample banking, designed the study, performed the experiments as well as the statistical analysis and wrote the manuscript. AH performed laboratory as well as statistical work and wrote the manuscript. ÁS, CS, and DE revised the concept and interpreted the data. JM provided the samples. GK provided the samples, supervised the study and critically reviewed the manuscript. All authors have read and critically reviewed the final version of the manuscript.

FUNDING

This study was funded by the Hungarian National Research, Development and Innovation Office (NKFIH grant no. FK134253 and K139139). The study was highly supported and funded by the Hungarian Pediatric Oncology Network (03/MGYH-MGYGYT/2021). The study was also supported by the ÚNKP-20-3-II-SE-20 grant of the New National Excellence Program and the KDP-2020-1008491 grant of the Co-operative Doctoral Program of the Ministry for Innovation and Technology as well as by the Complementary Research Excellence Program of Semmelweis University (EFOP-3.6.3-VEKOP-16-2017-00009). The funders had no role in study design, data collection and analysis, decision to publish, or preparation of the manuscript.

CONFLICT OF INTEREST

The authors declare that the research was conducted in the absence of any commercial or financial relationships that could be construed as a potential conflict of interest.

ACKNOWLEDGMENTS

The authors would like to thank Mónika Sándorné Vángor for her enthusiastic and reliable work in the laboratory. We really appreciate the help of nurses in the sample collection.

SUPPLEMENTARY MATERIAL

The Supplementary Material for this article can be found online at: https://www.por-journal.com/articles/10.3389/pore.2022.1610096/full#supplementary-material

REFERENCES

1. Force LM, Abdollahpour I, Advani SM, Agius D, Ahmadian E, Alahdab F, et al. The Global burden of Childhood and Adolescent Cancer in 2017: an Analysis of the Global Burden of Disease Study 2017. *Lancet Oncol* (2019) 20(9): 1211–25. doi:10.1016/S1470-2045(19)30339-0
2. Nguyen K, Devidas M, Devidas M, Cheng S-C, La M, Raetz EA, et al. Factors Influencing Survival after Relapse from Acute Lymphoblastic Leukemia: a Children's Oncology Group Study. *Leukemia* (2008) 22(12):2142–50. doi:10.1038/leu.2008.251
3. Martínez-Laperche C, Gómez-García AM, Lassaletta Á, Moscardó C, Vivanco JL, Molina J, et al. Detection of Occult Cerebrospinal Fluid Involvement during Maintenance Therapy Identifies a Group of Children with Acute Lymphoblastic Leukemia at High Risk for Relapse. *Am J Hematol* (2013) 88(5):359–64. doi:10.1002/ajh.23407
4. Crespo-Solis E, López-Karpovitch X, Higuera J, Vega-Ramos B. Diagnosis of Acute Leukemia in Cerebrospinal Fluid (CSF-Acute Leukemia). *Curr Oncol Rep* (2012) 14(5):369–78. doi:10.1007/s11912-012-0248-6
5. Münch V, Trentin L, Herzig J, Demir S, Seyfried F, Kraus JM, et al. Central Nervous System Involvement in Acute Lymphoblastic Leukemia Is Mediated by Vascular Endothelial Growth Factor. *Blood* (2017) 130(5):643–54. doi:10.1182/blood-2017-03-769315
6. Yao H, Price TT, Cantelli G, Ngo B, Warner MJ, Olivere L, et al. Leukaemia Hijacks a Neural Mechanism to Invade the central Nervous System. *Nature* (2018) 560(7716):55–60. doi:10.1038/s41586-018-0342-5
7. Egyed B, Kutszegi N, Sági JC, Gézsi A, Rzepiel A, Visnovitz T, et al. MicroRNA-181a as Novel Liquid Biopsy Marker of central Nervous System Involvement in Pediatric Acute Lymphoblastic Leukemia. *J Transl Med* (2020) 18(1):250. doi:10.1186/s12967-020-02415-8
8. Sun W, Wang X, Li J, You C, Lu P, Feng H, et al. MicroRNA-181a Promotes Angiogenesis in Colorectal Cancer by Targeting SRCIN1 to Promote the SRC/VEGF Signaling Pathway. *Cell Death Dis* (2018) 9(4):438. doi:10.1038/s41419-018-0490-4
9. Kato I, Nishinaka Y, Nakamura M, Akarca AU, Niwa A, Ozawa H, et al. Hypoxic Adaptation of Leukemic Cells Infiltrating the CNS Affords a Therapeutic Strategy Targeting VEGFA. *Blood* (2017) 129(23):3126–9. doi:10.1182/BLOOD-2016-06-721712
10. Tang Y-T, Jiang F, Guo L, Si M-Y, Jiao X-Y. The Soluble VEGF Receptor 1 and 2 Expression in Cerebral Spinal Fluid as an Indicator for Leukemia central Nervous System Metastasis. *J Neurooncol* (2013) 112(3):329–38. doi:10.1007/S11060-013-1066-X
11. Bartram J, Goulden N, Wright G, Adams S, Brooks T, Edwards D, et al. High Throughput Sequencing in Acute Lymphoblastic Leukemia Reveals Clonal Architecture of central Nervous System and Bone Marrow Compartments. *Haematologica* (2018) 103(3):e110–e114. doi:10.3324/haematol.2017.174987
12. Sun X, Wei L, Chen Q, Terek RM. MicroRNA Regulates Vascular Endothelial Growth Factor Expression in Chondrosarcoma Cells. *Clin Orthop Relat Res* (2015) 473(3):907–13. doi:10.1007/S11999-014-3842-0
13. Shah Scharff BFS, Modvig S, Thastrup M, Levinsen M, Degn M, Ryder LP, et al. A Comprehensive Clinical Study of Integrins in Acute Lymphoblastic Leukemia Indicates a Role of α6/CD49f in Persistent Minimal Residual Disease and α5 in the Colonization of Cerebrospinal Fluid. *Leuk Lymphoma* (2020) 61(7):1714–8. doi:10.1080/10428194.2020.1731500
14. Yu X, Zhang H, Yuan M, Zhang P, Wang Y, Zheng M, et al. Identification and Characterization of a Murine Model of BCR-Abl1+ Acute B-Lymphoblastic Leukemia with central Nervous System Metastasis. *Oncol Rep* (2019) 42(2): 532. doi:10.3892/OR.2019.7184

Pathology & Oncology Research

POR is dedicated to keeping scientists informed of developments in its focused biomedical fields which span the gap between basic research and clinical medicine.

A special aim of POR is to promote publishing activity in pathology and oncology of colleagues in the Central and East European region. The journal will interest pathologists, and a broad range of experimental and clinical oncologists, and related experts.

Discover more of our Special Issues

See more →

fro.ntiers.in/Liquid-Biopsy
por-journal.com

Contact

por@por-journal.com
Editorial Office - Pathology & Oncology Research
Avenue du Tribunal Fédéral 34
1005 Lausanne, Switzerland
Tel + 41 21 510 17 00